

**Thermodynamic Property Models for Synthetic Lubricants
and their Mixtures with Working Fluids in ORCs**

Dissertation

zur

Erlangung des Grades

Doktor-Ingenieurin

der

Fakultät für Maschinenbau
der Ruhr-Universität Bochum

von

Theresa Eckermann

aus Witten

Bochum 2018

Dissertation eingereicht am: 13.11.2018

Tag der mündlichen Prüfung: 17.12.2018

Erstgutachter: Prof. Dr.-Ing. Roland Span

Zweitgutachter: Prof. Dr.-Ing. Marcus Petermann

Danksagung

Die vorliegende Arbeit entstand während meiner Tätigkeit als wissenschaftliche Mitarbeiterin am Lehrstuhl für Thermodynamik der Ruhr-Universität Bochum unter der Leitung von Herrn Prof. Dr.-Ing. Roland Span.

Daher gilt mein Dank zunächst Herrn Prof. Dr.-Ing. Roland Span, der mir bereits während des Studiums spannende Einblicke in die thermodynamische Forschung, und dann schließlich die Promotion an seinem Lehrstuhl ermöglicht hat. Als Doktorvater stand er mir stets mit seinem fundierten Fachwissen und einem offenen Ohr zur Seite. Besonders möchte ich ihm für seine vorbildliche Unterstützung bei einer familiengerechten Gestaltung meiner Promotionszeit danken! Herrn Prof. Dr.-Ing. Marcus Petermann danke ich für die Übernahme des Zweitgutachtens und sein Interesse an meiner Arbeit.

Weiterhin möchte ich besonders herzlich Herrn Dr. Eric W. Lemmon danken! Sein konstanter fachlicher und freundschaftlicher Beistand war stets von großem Wert, seine grenzenlose Begeisterung für dieses Fachgebiet ein unverzichtbarer Motivator für mich.

Neben allen aktuellen und ehemaligen Mitarbeiterinnen und Mitarbeitern des Lehrstuhls, denen ich für die immer angenehme Arbeitsatmosphäre danke, möchte ich das Team-Z ganz besonders hervorheben. Dr. Monika Thol, Dr. Stefan Herrig, Sebastian Hielscher, Dr. Johannes Gernert und Dr. Andreas Jäger danke ich besonders herzlich für die freundschaftliche und fachliche Unterstützung in all den Jahren! Lars Hüttermann danke ich für die stets unterhaltsame gemeinsame Zeit im Büro und seine wertvolle Funktion als Ruhepol im Endspurt! Außerdem möchte ich den „Muttis“ Ann-Christin Fler und Christine Wloka für ihre wertvolle mentale Unterstützung danken!

Zu guter Letzt gilt mein Dank meiner Familie, insbesondere meinem Mann sowie meinen Eltern und Schwiegereltern! Durch euch war es mir überhaupt möglich diese Mammutaufgabe zu bewältigen, sei es durch das Ertragen von Abwesenheit, das mentale Aufbauen, das offene Ohr oder wertvolle Unterstützung bei der Kinderbetreuung. Meinen Kindern danke ich für ihre Geduld mit mir und ihre absolut ansteckende Fröhlichkeit.

Vielen Dank!

Abstract

The potential of (Organic) Rankine Cycles for Exhaust Heat Recovery (EHR) in heavy-duty diesel engines for mobile applications was investigated in a joint research project. The EHR process design features ethanol as working fluid. Based on a parameter study, the potential benefit of ethanol-water mixtures was to be investigated. A new Helmholtz mixture model for ethanol-water was developed in this work, which is based on the most current pure fluid equations of state (EOS). The uncertainty of the new model with respect to the speed of sound was significantly improved compared to a preliminary model of Lemmon. This improvement is connected to the improved description of densities at elevated pressures. The uncertainties of other thermodynamic properties are in a comparable range with respect to the model of Lemmon.

A poly-alpha-olefin (PAO)-based synthetic lubricant containing several PAO base oils and an emulsifier was specially designed for the lubrication of the expansion machine used in this EHR process. The thermodynamic properties of the pseudo-pure lubricant and of its mixture with ethanol were required. Due to an insufficient data base, a generalized EOS (genEOS) based on the model of Alexandrov *et al.* was developed for the PAO, which requires less experimental data to develop than a fully optimized EOS. With the new genEOS, the available experimental data can be reproduced reasonably well. A new Helmholtz model describing ethanol-PAO mixtures was subsequently developed, which is based on the new genEOS for the PAO and the current ethanol EOS of Schroeder *et al.* General application of this method for the estimation of fluid properties was shown.

To validate the use of a genEOS in a mixture model with asymmetric components, the systems CO₂-PEC5 and CO₂-PEC7 were investigated. Therefore, new genEOS for the POE base lubricants PEC5 and PEC7 were fitted and mixture models for these lubricants with CO₂ were developed. It was shown that the genEOS reproduce the available experimental data within the AAD range claimed by Alexandrov *et al.* The new mixture model for CO₂-PEC5 represents the available phase-equilibrium and density data reasonably. Nevertheless, bubble lines calculated from the new model exhibit an unphysical oscillation that is not caused by the genEOS but by the mixture model itself. The new mixture model for CO₂-PEC5 was transferred to the CO₂-PEC7 system by a simple empirical conversion developed in this work, which is based on the critical pure-fluid parameters and the molar masses only. General applicability was shown with the restriction of $x_{\text{CO}_2} > 0.4$. For smaller CO₂ fractions, the bubble lines calculated from this model show an unphysical negative slope.

Table of Contents

| | |
|---|----|
| Table of Symbols | IV |
| 1 Introduction..... | 1 |
| 2 Exhaust Heat Recovery for an Automotive Application | 5 |
| 2.1 Fundamentals of Exhaust Heat Recovery | 5 |
| 2.2 Organic Rankine Cycles and Working Fluids..... | 6 |
| 2.3 Lubricants in Refrigeration and Organic Rankine Cycles | 11 |
| 2.4 Need for Thermophysical Properties..... | 13 |
| 3 Equations of State..... | 17 |
| 3.1 Historical Background..... | 17 |
| 3.1.1 Empirical and Semi-Empirical Pure Fluid Equations..... | 17 |
| 3.1.2 Empirical and Semi-empirical Mixture Models | 26 |
| 3.1.3 Physical Property Models | 29 |
| 3.2 PC-SAFT | 31 |
| 3.3 SRK..... | 38 |
| 3.4 Helmholtz Equations of State for Pure Fluids | 39 |
| 3.5 Generalized Empirical Equations of State for Pure Fluids..... | 44 |
| 3.6 Helmholtz Equations of State for Mixtures | 49 |
| 4 A New Model for Ethanol-Water Mixtures | 53 |
| 4.1 Available Experimental Data | 54 |
| 4.2 Fitting Process | 55 |
| 4.3 The New Mixture Model | 59 |
| 4.4 Comparison to Experimental Data..... | 62 |
| 4.4.1 Phase Equilibria..... | 63 |
| 4.4.2 Densities | 69 |
| 4.4.3 Excess Enthalpies | 79 |

| | | |
|-------|--|-----|
| 4.4.4 | Isobaric Heat Capacities | 83 |
| 4.4.5 | Speed of Sound | 85 |
| 4.5 | Summary | 87 |
| 5 | A New Generalized EOS for a PAO Lubricant and its Mixture with Ethanol..... | 89 |
| 5.1 | Pseudo Pure Fluid Equation for PAO | 89 |
| 5.1.1 | PAO: SRK | 90 |
| 5.1.2 | PAO: Generalized Helmholtz Equation | 92 |
| 5.2 | Mixture Model for Ethanol-PAO..... | 94 |
| 5.2.1 | Experimental Data | 94 |
| 5.2.2 | The New Mixture Model for Ethanol-PAO | 100 |
| 5.2.3 | Summary | 106 |
| 6 | New Generalized EOS for two POE Lubricants and their Mixtures with CO ₂ | 107 |
| 6.1 | Pure Fluid Equation for PEC5 | 107 |
| 6.1.1 | The New Generalized Equation of State | 108 |
| 6.1.2 | Comparison to <i>pρT</i> Data..... | 110 |
| 6.1.3 | Comparison to Vapor Pressure Data..... | 113 |
| 6.1.4 | Comparison to Caloric Data | 115 |
| 6.2 | Pure Fluid Equation for PEC7 | 119 |
| 6.2.1 | The New Generalized Equation of State | 120 |
| 6.2.2 | Comparison to <i>pρT</i> Data..... | 122 |
| 6.2.3 | Comparison to Vapor Pressure Data..... | 125 |
| 6.2.4 | Comparison to Caloric Data | 126 |
| 6.3 | Mixture Model for CO ₂ -PEC5 | 130 |
| 6.4 | Mixture Model for CO ₂ -PEC7 | 137 |
| 6.5 | Summary | 143 |
| 7 | Conclusions..... | 145 |
| | References..... | 149 |

| | |
|--|-----|
| Appendix A – Parameters of the Basic Generalized Equation of State..... | 175 |
| Appendix B – Parameters of the adjusted generalized equation of state..... | 177 |
| Appendix C – Density Deviations (Ethanol-Water)..... | 179 |

Table of Symbols

Latin Symbols

| | |
|-------------|--|
| a | Molar Helmholtz energy Cubic equation of state parameter Parameter of the Beattie and Bridgeman equation BWR parameter Parameter of NA terms |
| \tilde{a} | Reduced Helmholtz energy in PC-SAFT |
| a_i | Parameter of the PC-SAFT equation defined by equation (3.47) |
| A | 1 st virial coefficient Helmholtz energy |
| A_0 | Parameter of the Beattie and Bridgeman equation BWR parameter |
| A_i | Association site of component i |
| B | 2 nd virial coefficient |
| b | Cubic equation of state parameter Parameter of the Beattie and Bridgeman equation BWR parameter Parameter of NA terms |
| B_0 | Parameter of the Beattie and Bridgeman equation BWR parameter |
| b_i | Parameter of the PC-SAFT equation defined by equation (3.48) |
| B_i | Association site of component i |
| C | 3 rd virial coefficient |
| c | Heat capacity Parameter of the Beattie and Bridgeman equation BWR parameter Coefficient Integration constant of the equation for the ideal Helmholtz energy Parameter of NA terms |
| C_0 | BWR parameter |

| | |
|-----------|--|
| C_1 | Abbreviation defined by equation (3.42) |
| D | 4 th virial coefficient |
| d | Temperature-dependent segment diameter |
| | Density exponent |
| | Parameter of NA terms |
| e | Parameter of NA terms |
| E | 5 th virial coefficient |
| f | Parameter of NA terms |
| | Fugacity |
| F | 6 th virial coefficient |
| | Deviation between data point and value calculated from the equation of state |
| F_{ij} | Weighting factor for generalized departure function |
| g | Molar Gibbs enthalpy |
| | Radial distribution function |
| h | Molar enthalpy |
| I_1 | Power series in packing fraction |
| I_2 | Power series in packing fraction |
| k_{ij} | Binary adjustable interaction parameter |
| k_B | Boltzman's constant |
| M | Molar mass |
| m | Number of spherical segments forming one chain |
| | Coefficient |
| n | Coefficient |
| N | Number of experimental data points |
| | Generalized coefficient |
| N_C | Number of components in a mixture |
| N_s | Total number of segments |
| P | Power |
| p | Pressure |
| | Density exponent in the exponential function |
| \dot{Q} | Heat flow |
| R | Universal gas constant |
| r | Radial distance between two segments |

| | |
|--------------|--|
| s | Molar entropy |
| t | Temperature exponent |
| T | Temperature |
| u | Molar internal energy |
| | Pair potential function |
| v | Molar volume |
| w | Speed of sound |
| | Adjustable parameter |
| W | Weight assigned to a data point or constraint in the fitting process |
| X^{A_i} | Fraction of molecules of component i not bonded at site A |
| \mathbf{x} | Molar composition vector |
| x_i | Mole fraction of component i in a mixture |
| z | Arbitrary thermodynamic property |
| z_i | Overall mole fraction of component i in a mixture |
| Z | Compressibility factor |

Greek Symbols

| | |
|--------------------|---|
| α | Reduced Helmholtz energy |
| | Anisotropy parameter of hard body part in BACKONE |
| | BWR Parameter |
| | Temperature-dependent function in the SRK equation |
| β | Binary reducing function parameter |
| | Gaussian bell-shaped parameter |
| | Parameter of NA terms |
| γ | Binary reducing function parameter |
| | Gaussian bell-shaped parameter |
| | BWR Parameter |
| | Coefficient in the exponential function |
| δ | Reduced density |
| Δ | Variable of the NA terms |
| $\Delta^{A_i B_j}$ | Association strength |
| Δ_A | Parameter of the ideal gas isobaric heat capacity equation of Joback and Reid |

| | |
|----------------------|---|
| Δ_B | Parameter of the ideal gas isobaric heat capacity equation of Joback and Reid |
| Δ_C | Parameter of the ideal gas isobaric heat capacity equation of Joback and Reid |
| Δ_D | Parameter of the ideal gas isobaric heat capacity equation of Joback and Reid |
| $\epsilon^{A_i B_j}$ | Association energy between two sites A and B of two molecules of components i and j |
| ζ_n | Abbreviation defined by equation (3.33) with $n \in \{0; 1; 2; 3\}$ |
| η | Anisotropy parameter of attractive part in BACKONE models |
| | Packing fraction of segments |
| | Gaussian bell-shaped parameter |
| θ | Parameter in the equation for the isobaric heat capacity of the ideal gas |
| | Parameter of the NA terms |
| ϑ | Parameter in the equation for the isochoric heat capacity of the ideal gas |
| $\kappa^{A_i B_j}$ | Effective volume of an association interaction between two sites A and B of two molecules of components i and j |
| λ | Reduced well width of the square potential |
| σ | Temperature-independent segment diameter |
| ρ | Molar density |
| $\hat{\rho}$ | Total number density of molecules |
| τ | Inverse reduced temperature |
| φ | Fugacity coefficient |
| χ | Polar factor |
| ω | Acentric factor |

Subscripts

| | |
|------|---------------------------------------|
| 0 | Ideal gas state |
| b | Boiling point |
| c | Critical parameter |
| DATA | Experimental data point |
| EOS | Calculated from the equation of state |
| ETO | Ethanol |
| Exp | Exponential |
| GBS | Gaussian bell-shaped |
| i | Control variable |
| j | Control variable |

| | |
|----------|---|
| k | Control variable |
| NA | Non-analytic |
| p | At constant pressure |
| PE | Planck-Einstein |
| Pol | Polynomial |
| R | Reducing parameter |
| r | Reduced variable |
| | Reducing parameter |
| T | At constant temperature |
| v | Vapor state |
| v | At constant volume |
| δ | Partial derivative with respect to δ |
| ρ | At constant density |
| τ | Partial derivative with respect to τ |

Superscripts

| | |
|-------|------------------------------------|
| (0) | Simple fluid |
| (1) | Real fluid |
| a | Attractive force contribution |
| assoc | Association contribution |
| chain | Contribution of chain formation |
| disp | Dispersion contribution |
| E | Excess property |
| h | Hard-body contribution |
| hc | Hard chain contribution |
| hs | Hard-sphere contribution |
| I | 1 st integration |
| II | 2 nd integration |
| o | Ideal gas contribution |
| r | Residual contribution |
| rep | Repulsive force contribution |
| seg | Contribution of monomeric segments |

| | |
|---|------------------|
| ' | Saturated liquid |
| " | Saturated vapor |

Abbreviations

| | |
|-----------------|--|
| AAD | Average absolute relative deviation |
| AB | Alkyl benzene |
| API | American Petroleum Institute |
| BWR | Benedict-Webb-Rubin equation |
| CCSA | Classical corresponding states approach |
| CO ₂ | Carbon dioxide |
| eCSA | Extended corresponding states approach |
| EOM | Evolutionary optimization method |
| EOS | Equation of state |
| GBS | Gaussian bell-shaped |
| LLE | Liquid-liquid equilibrium |
| mBWR | Modified Benedict-Webb-Rubin equation |
| MCSA | Molecular corresponding states approach |
| ORC | Organic Rankine cycle |
| PAG | Polyalkylene glycol |
| PAO | Poly-alpha-olefin |
| PC-SAFT | Perturbed-chain statistical associating fluid theory |
| PE | Pentaerythritol esters |
| PFPE | Perfluoropolyether |
| POE | Polyol ester |
| PVE | Polyvinylether |
| RUB | Ruhr-Universität Bochum |
| SAFT | Statistical associating fluid theory |
| VLE | Vapor-liquid equilibrium |
| VLLE | Vapor-liquid-liquid equilibrium |

1 Introduction

With increasing awareness of the global change of climatic conditions due to increasing concentrations of atmospheric greenhouse gases, the efforts of minimizing relevant emissions have increased in the last decades. It is common understanding that the most relevant anthropogenic contribution to the increase of atmospheric greenhouse gases is related to carbon dioxide (CO₂) emissions. About 18% of the anthropogenic CO₂ emissions of Germany are generated by the transport sector, which is a major contributor next to the energy sector (38%) and industry (21%) [1]. The emissions of the transport sector are dominated by passenger cars, which account for 61%, followed by utility vehicles which account for 35% [2].

The significant power requirements of utility vehicles feature an immense requirement of expansive fuel. Consequently, the reduction of fuel consumption serves two interests: the reduction of CO₂ emissions and the reduction of cost. In the past, the engines of such vehicles have been optimized thoroughly. Therefore, the major potential of fuel savings and the respective reduction of emissions lies in the surrounding periphery. Lightweight bodies to reduce the weight and the driving resistance or the reduction of the energy demand of auxiliary units are possibilities to further reduce the fuel consumption. However, almost two thirds of the fuel-bound energy are rejected by the engine cooler or are purged with the exhaust gas on a rather high temperature level.

In a joint research project, the potential of (Organic) Rankine Cycles (ORC) for Exhaust Heat Recovery (EHR) in heavy-duty diesel engines for mobile applications was investigated. The industrial partners DAIMLER AG (on-road application) and MTU (off-road applications) contributed as well as the Chair of Fluidics of the TU Dortmund University. The knowledge of thermophysical properties of the involved fluids or fluid mixtures is essential for a safe design and optimization of the ORC process. The aim of this work is to provide the required thermodynamic properties of the relevant working fluids

The proposed process design includes ethanol as working fluid with the option of using ethanol-water mixtures for potentially following designs. The possible benefit of these mixtures should be investigated based on a parameter study. The required thermodynamic fluid properties are provided by equations of state. For ethanol, an equation of state was published by Schroeder *et al.* [3]. For the ethanol-water system, a preliminary

equation is available in REFPROP [4]¹, which is based on an outdated equation of state for ethanol. Therefore, a new mixture model for the ethanol-water system was developed in this work. Results are presented in chapter 4.

It was decided by all project partners to implement a screw expander with direct lubricant injection as expansion device in the ORC. Consequently, the working fluid ethanol will contain or entrain some of the lubricant. Therefore, a thermodynamic property model describing the lubricant and an additional model describing its mixture with ethanol are required. The lubricant was specially designed for this application and is commercially available. No information was given on the composition of this poly-alpha-olefin (PAO)-based fluid, which is treated as a pure fluid although it contains several compounds including an emulsifier, nor are any experimental data available in the literature. Today, it is state-of-the-art to develop a substance-specific Helmholtz equation of state based on a broad set of experimental data. However, for the adjustment of the new equation of state, only a few data points were provided by the producer. Consequently, no fluid-specific Helmholtz equation of state could be developed, but a generalized approach was employed. Results are shown in section 5.1. Subsequently, a mixture model for the binary system ethanol-PAO was adjusted to some experimental data points, which were measured by a project partner in the course of this project. Results are presented in section 5.2.

The description of such a complex mixture with a Helmholtz mixture model based on a generalized equation of state for the pseudo-pure lubricant is an innovative approach. Therefore, additional systems were chosen to prove the validity of this method. Due to the available experimental data in the literature, the systems CO₂-PEC5 and CO₂-PEC7 were selected. These pentaerythritol esters (PE) of different molecular length (C5 and C7) belong to the group of polyol esters (POE). New generalized equations of state for the base lubricants PEC5 and PEC7 were developed in this work, and a mixture model for CO₂-PEC5 was adjusted. Subsequently, this mixture model was scaled to the system CO₂-PEC7 without any adjustment. Results are shown in sections 6.1 to 6.4. The quality of the proposed pure fluid equations of state is evaluated with the help of fluid-specific Helmholtz equations of state. These equations, which are not part of this thesis,

¹ The preliminary mixture model for the ethanol-water system developed by Lemmon was never published in the literature but is available in REFPROP [4].

were collaboratively developed with the National Institute of Standards and Technologies (NIST) and are based on a significantly broader data set. For this purpose, new measurements were conducted at NIST to support the development of the EOS. These new data were not considered in the adjustment of this work in order to validate the predictive capabilities of the new generalized equations of state.

Finally, the results of this work are summarized in chapter 7 and recommendations for future investigations are given.

2 Exhaust Heat Recovery for an Automotive Application

In this chapter, general aspects of exhaust heat recovery (EHR) processes are discussed. Several technical applications and implementations are briefly introduced, and the basic thermodynamics behind organic Rankine cycles are presented. Requirements and restrictions concerning the choice of working fluid and lubricant are also discussed.

2.1 Fundamentals of Exhaust Heat Recovery

Aiming at an optimal process regarding the consumption of energy, two aspects need to be considered. On the one hand, the energy demand of the core process itself needs to be reduced. On the other hand, the utilization of the provided primary energy needs to be optimized, which means that exergetic losses in the entire process are to be minimized [5].

For an automotive application, the core process is represented by the engine. Over the last years, the engine efficiency has been thoroughly optimized. Ringler *et al.* [6] claim that it is reaching its technical limits and further investigations do not promise significant further energy savings. Consequently, the utilization of the provided primary energy regarding the surrounding process is gaining more attention.

Figure 2.1 shows a characteristic Sankey diagram for a typical modern heavy-duty diesel engine (OM457) at nominal load [7].

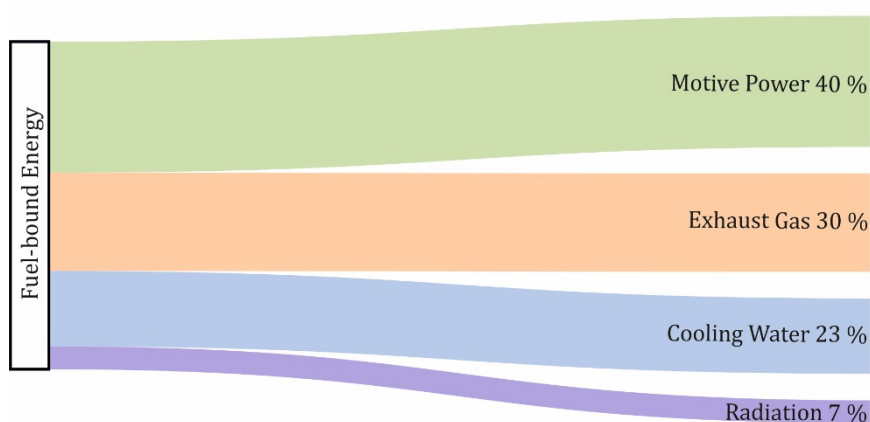


Figure 2.1: Sankey diagram of a modern heavy-duty diesel engine (OM457) at nominal load [7].

Only approximately 40% of the fuel-bound energy is converted into motive power. 23% is discharged with the cooling water, and another 7% is lost by radiation. These heat flows cannot be recycled by technical means. However, almost a third of the provided primary energy is lost with the exhaust gas, which has a rather high temperature level. Hence, there is an enormous potential to reduce the energy loss of this process. That is what exhaust heat recovery aims at.

In principle, there are several ways to use the exergy of the flue gas based on different physical effects. For example, turbomachines could be used to exploit the pressure gradient of the exhaust gas. However, the main potential lies in the high temperature and would remain largely unused. Nevertheless, a turbocharger could be implemented in combination with a process which profits from the high exhaust gas temperature.

Chemical reactions can be used to benefit from the available heat but are unfavorable. The heat recovery potential of thermo-acoustic and Stirling applications does not compensate for the high complexity of the required processes. A thermo-electric device or Joule process might profit from the provided heat, but they cannot reach the potential of a Rankine cycle.

So far, (organic) Rankine Cycles working with water or an organic fluid are the preferred technology to use the exhaust heat [8]. These cycles are explained in more detail in the following section.

2.2 Organic Rankine Cycles and Working Fluids

An Organic Rankine Cycle (ORC) is basically the same as a common steam process used in large scale power plants. The simplest process is based on four main components, as illustrated in Figure 2.2. First, the liquid working fluid (1) is compressed in a pump (2). Subsequently, it passes the first heat exchanger in which it is isobarically preheated (3) and then evaporated (4), changing its phase from liquid to gas. Depending on the working fluid and process design, it is beneficial to additionally superheat the fluid (5). The required heat input \dot{Q}_{EHR} is provided by the exhaust gas. In the following, the fluid pressure is reduced again driving the expansion machine (6). Finally, the working fluid is condensed (7) and subcooled (1) by heat removal in the second heat exchanger.

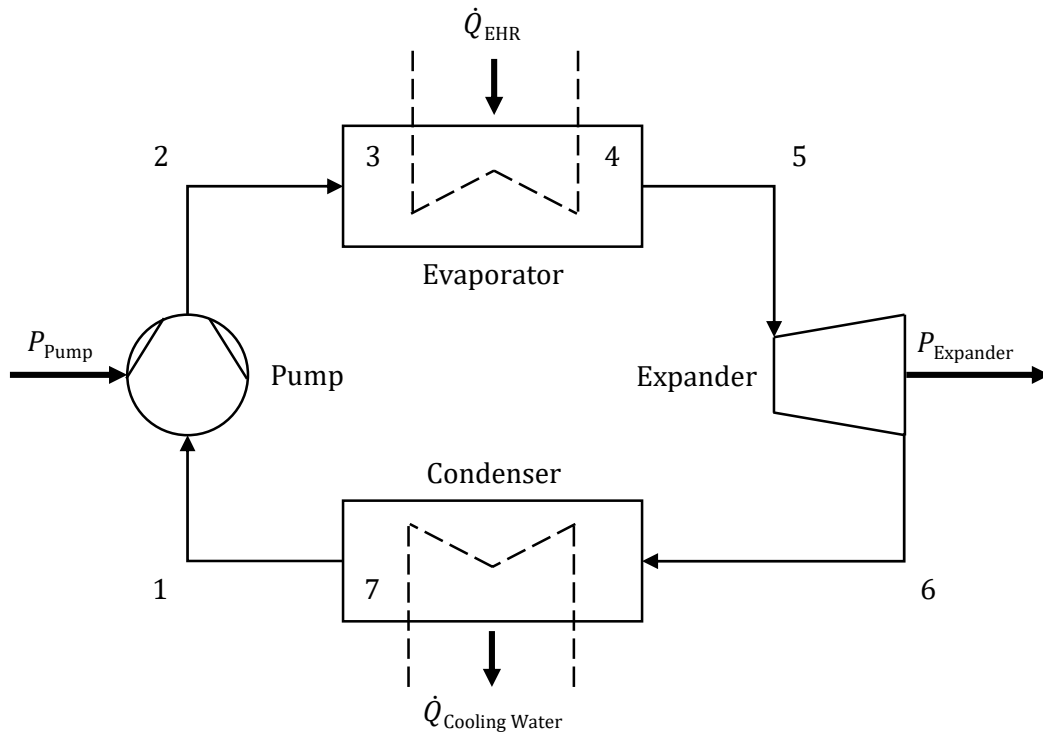


Figure 2.2: Schema of an exemplary basic ORC process.

In Figure 2.3, the exemplary process presented in Figure 2.2 is shown in a characteristic T,s -diagram for water as the working fluid.

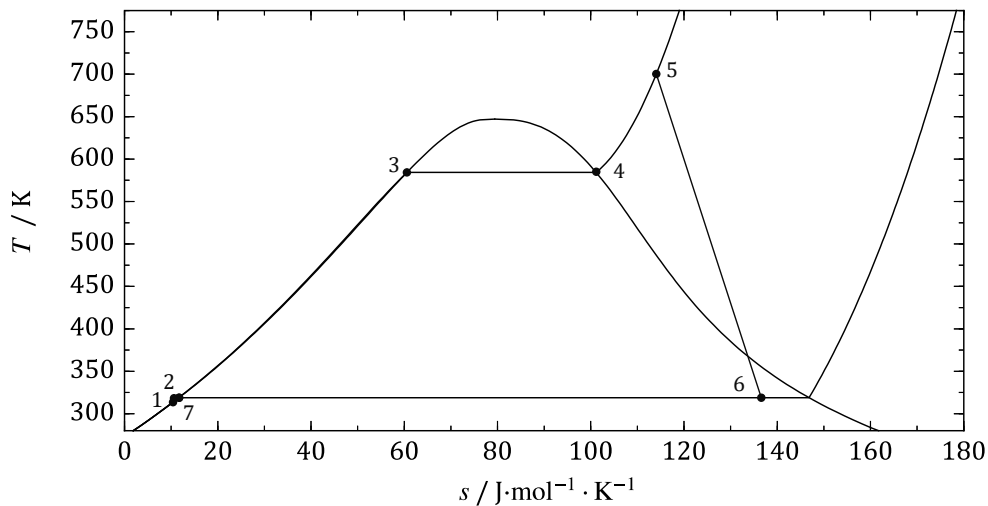


Figure 2.3: T,s -diagram for water with the state points of an exemplary Rankine Cycle.

As already mentioned, Rankine processes are state of the art for large scale power generation in steam power plants, nuclear power plants, and block-type thermal power stations. Despite many years of experience and despite of the successful transfer to smaller power outputs in block-type plants, there are a lot of challenges designing such a process for a mobile application. All components need to be optimized regarding volume and mass restrictions without degrading their efficiency significantly. Friction and

leakage have a much bigger impact when the size of a component is reduced drastically. Additionally, in contrast to stationary power plants, all components have to be designed to work optimally in transient states. For a further discussion of the general requirements of a mobile application see Jung [7].

In principle, there are several types of expanders available for usage in low power processes. There are micro-turbines, screw expanders, scroll expanders, and reciprocal piston expanders. Regarding the automotive ORC process, the volume-type expanders, screw and scroll, are more suitable due to the characteristically lower flow rates, higher pressure ratios, and much lower rotational speed compared with the other two expander types. [9]

While in large stationary Rankine processes water is commonly used as working fluid, there are many different fluids utilized in smaller applications on lower temperature level. Since these working fluids are usually organic compounds, the corresponding processes are called Organic Rankine Cycles (ORCs). Actually, the choice of the working fluid is part of the design and optimization process and depends on the expansion machine, heat input, and others. There are many publications dealing with the choice of an adequate working fluid for different applications, for example [10–12]. Working fluids can be categorized according to the slope of their dew line in a T,s -diagram, see Table 2.1.

Table 2.1: Categories of working fluids.

| $(\partial T / \partial s)_{\text{dew line}}$ | category |
|---|------------|
| > 0 | wet |
| = 0 | isentropic |
| < 0 | dry |

When the slope of the dew line is known, it is also known how the fluid expands in an isentropic ideal case. Starting from the dew line, the isentropic expansion of a wet fluid ends in the two-phase region, whereas it ends in the homogeneous vapor region for a dry fluid. An isentropic fluid would expand along the dew line. The knowledge of this characteristic feature of the working fluid is crucial for the choice and design of the expansion machine and for the modification of the ORC. In common steam processes for example, water is superheated after the evaporation to limit the amount of liquid

droplets formed during the expansion (see Figure 2.3). Otherwise, there would be damage in the turbine from impingement corrosion. For a dry fluid, superheating would not be necessary, and the heat exchanger could be designed in a simpler way. However, a screw expansion machine would profit from the formation of droplets, since they reduce the gap loss. Depending on the expander and the working fluid, even a power flash cycle might be favorable, where the fluid is only heated to the bubble line and evaporates during the pressure drop in the expansion machine. For a detailed discussion of potential ORC variants see Wiedemann [13].

As an alternative to water, organic working fluids usually have a larger vapor pressure close to ambient temperature and consequently higher vapor densities at the outlet of the expansion machine, which allow for lower volume flows in the process. In principle, there are numerous candidates for each ORC application, that fulfill the basic needs like a suitable vapor pressure in the relevant temperature range. But additionally, there are restrictions for the choice of working fluids besides availability and cost, which concern [5]

- flammability
- toxicity
- environmental compatibility
- chemical and thermal stability
- material compatibility
- heat transfer properties.

An earlier investigation by the Chair of Thermodynamics and the Chair of Combustion Engines of Ruhr University Bochum (RUB) [8] dealt with the choice of an optimal working fluid for a mobile ORC application. The study focused on the in advance selected fluids water, ethanol, methanol, hexamethyldisiloxan (MM), R245fa, and iso-pentane. Out of these six fluids, methanol, ethanol, and water were found to be most promising regarding the power output of the process. Water is the classical working fluid in commercial Rankine applications since it has the great advantage over most working fluids that it is neither flammable nor toxic. However, it is highly corrosive and has a rather high freezing point of $t = 0^{\circ}\text{C}$ at atmospheric pressure. The latter disqualifies pure water the working fluid in a mobile application. In comparison, ethanol has a very low freezing point of $t = -114^{\circ}\text{C}$ at atmospheric pressure while showing thermal stability up to temperatures of $t = 400^{\circ}\text{C}$. However, ethanol is easily flammable and has a low

ignition limit resulting in the need of absolute tightness of the system. Methanol shows qualities comparable to ethanol but is discarded due to its high toxicity. As a result, Span *et al.* [8] recommend ethanol, or ethanol-water mixtures as working fluid.

As already pointed out, a screw or scroll expander is the preferred expansion device for a mobile ORC. In order to determine which of these two is the best option for this application, the Chair of Fluidics of the TU Dortmund investigated the energetic and application-specific aspects of these expander types, based on computer simulations. According to earlier findings [8], ethanol was chosen as the working fluid. It was shown that due to comparatively small inlet openings, scroll expanders cause high throttling losses that lead to power losses at high rotational speeds. Given that screw expanders can be operated at higher rotational speeds, and higher pressure ratios, this type of expansion machine was chosen for further development. [14,15]

Subsequently, it was important to decide if the screw expander should be synchronized or not. Usually, there is no liquid found in the working chambers of unsynchronized screw expanders, which leads to an increased gap mass flow causing mass and energy losses. To minimize this effect, synchronized screw expanders are operated with significantly increased circumferential speeds at the crown circle. Apart from the energetic advantages of a smaller gap mass flow, unsynchronized screw expanders profit from a lighter and smaller constructional size, and a simpler assembly. Whether an unsynchronized design can be chosen depends on the lubricity of the fluid in the working chambers. There are several options to deal with this. Given that the lubricity is sufficient, liquid working fluid could be injected. Alternatively, a lubricant can be chosen and injected into the machine. Theoretically, it can be sufficient to have condensing working fluid in the working chambers. But since there is no secure way to predict how fast the working fluid nucleates and finally condensates, direct liquid injection is preferred. [15]

Within the framework of this project, it was decided to design an unsynchronized screw expander that is flooded with lubricant. Subsequently, the best machine geometry was investigated with regard to the maximum power output of the overall process [14].

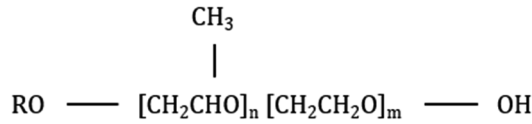
2.3 Lubricants in Refrigeration and Organic Rankine Cycles

With the decision to rely on direct oil injection into the screw expander, it is clear that there is lubricant in the entire ORC. Even if an oil separator is installed, the separation rates are limited. This effect is known from screw compressors in compressed-air or refrigeration applications. Installing an oil separator is still favored since it reduces the amount of oil that is heated and cooled cyclically with the working fluid. Hence, the provided exhaust heat would not be wasted on the lubricant that does not contribute to the expansion energy. Furthermore, the oil separator makes the lubricant directly available for lubrication of bearings and for injection into the working chambers. [15]

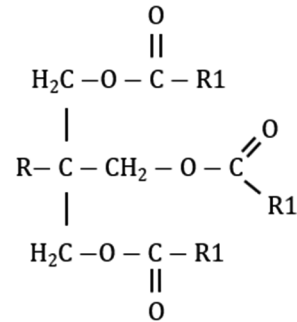
Depending on the miscibility of the present lubricant and working fluid over the relevant temperature range, the oil that escaped from the separator will return to the screw compressor or expander. However, if phase separation occurs, the lubricant can accumulate on the inside of heat exchanger tubes, which results in reduced heat transfer and reduced overall performance. This can even lead to compressor/expander oil starvation and potential breakdown. [16] Considering the accumulation of oil in the evaporator, thermal stability becomes even more an issue. Compared to the well-known refrigeration cycles, the maximum temperature of the working fluid is considerably higher in EHR processes. The solubility of the working fluid in the lubricant influences the viscosity and lubricity of the fluid mixture in the expansion machine. [17] Consequently, knowledge of the phase behavior of the complex working fluid–lubricant mixture is key for an effective and safe process design.

For the choice of a suitable lubricant, there are the same requirements concerning toxicity, flammability, environmental compatibility, and others, just as discussed for working fluids in section 2.2. The American Petroleum Institute (API) has categorized base oils into five categories (API 1509, Appendix E) from which the first three groups are exclusively refined from petroleum crude oil. Group IV base oils are fully synthetic Poly-alpha-olefins. All other base oils not included in Groups I through IV belong to Group V. So far, mineral-oil-based lubricating oils are widely used even though they are not readily biodegradable and are frequently toxic. However, environmental aspects gain more and more importance which leads to advances in green chemical technology. [18] Different synthetic lubricants have been developed, which are shortly presented here. They differ in their chemical structure, which allows a categorization in families:

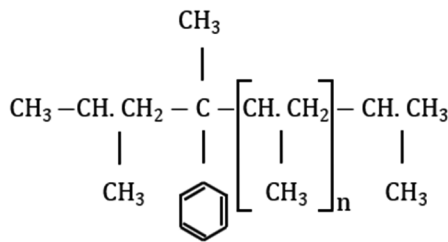
- a) Polyalkylene glycol (PAG)
- b) Polyol ester (POE)
- c) Alkyl benzene (AB)
- d) Poly-alpha-olefin (PAO)
- e) Polyvinylether (PVE).



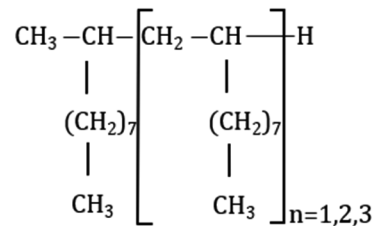
a) PAG



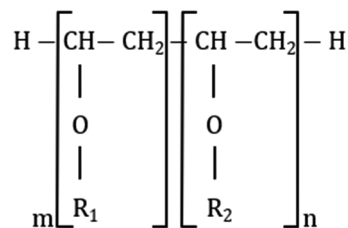
b) POE



c) AB



d) PAO



e) PVE

Figure 2.4: Chemical structure of the common synthetic lubricant families [16,19].

Figure 2.4 shows the different chemical structures of the synthetic lubricants used so far in ORCs. PAG lubricants are compatible with most elastomers, yet they are very hygroscopic. POEs have environmental benefits since they can be synthesized from renewable sources and are biodegradable. They are less hygroscopic than PAG lubricants, but if they adsorbed a considerable amount of moisture, the ester can break down at high temperatures. POEs are not compatible with common elastomers. Since

they are polar fluids and have high densities, they tend to dissolve many impurities. AB lubricants are synthetic aromatic hydrocarbon oils with seal compatibility and electrical insulating properties. PAOs are unsaturated hydrocarbon synthetic oils showing superior performance and stability. They are non-hygroscopic and show a high fluidity at low temperatures. Recently, PVE lubricants have been developed that are less dense and less polar than ester oils. Hence, they show a superior performance over ester oils with respect to blockage. Additionally, PVEs are less effected by moisture than POEs. [16]

A commercially available lubricant usually contains several base oils of the same or different API groups plus special additives to adapt its properties. Consequently, commercial lubricants are by no means pure fluids but mixtures of numerous compounds. In the framework of this joint project, the German company Fuchs Schmierstoffe GmbH was assigned to find the most suitable lubricant for an ORC with a screw expansion machine and ethanol as working fluid. They investigated a PAO, two different PAG formulations, and a Perfluoropolyether (PFPE). The latter describes a fully synthetic lubricant consisting exclusively of the elements fluorine, carbon, and oxygen. It was decided by the project partners to use a specially designed PAO, which builds a dispersive emulsion with ethanol. This oil guaranteed good lubricity and viscosity in the mixture with ethanol, which is crucial for an effective and safe operation of the proposed process.

2.4 Need for Thermophysical Properties

Prestudies showed that for an ORC in a mobile application, ethanol and ethanol-water mixtures are promising working fluids [8] and that a screw expander is the most promising expansion device [14]. Therefore, an ORC with ethanol as working fluid and a screw expander was assessed as the framework of this joint research project. Furthermore, it was agreed to use a flooded screw expander, assuring sufficient lubrication at all times.

The knowledge of thermophysical properties is crucial for a successful process design. Based on the agreed configuration, fluid properties of ethanol and ethanol-PAO mixtures are required. Furthermore, it was agreed to investigate ethanol-water mixtures as working fluids. Therefore, a mixture model for these components is required as well. For ethanol, an empirical multiparameter equation of state (EOS) explicit in the

Helmholtz energy is available in the literature [3] as is for water [20]. For mixtures of these two components, there is a preliminary model by Lemmon available in REFPROP [4], which is explicit in the Helmholtz energy. However, this model is based on the outdated pure fluid equation for ethanol by Dillon and Penoncello [21], which has been replaced by the new equation of Schroeder *et al.* [3], which was fitted to an updated, broader set of experimental data. Therefore, a new mixture model based on the most accurate pure fluid equations is required. Table 2.2 summarizes the models needed and shows which of them are developed in the course of this work. The models highlighted in grey are needed for the description of the desired EHR process. All mixture models are developed in this work.

Table 2.2: Matrix of the source of the thermodynamic property models for the discussed fluids and fluid mixtures. All mixture models are developed in this work. The models required for the description of the EHR process are highlighted in grey.

| Mixture (fluid 1 - fluid 2) | fluid 1 | fluid 2 |
|-----------------------------|-----------------------------|----------------------|
| ethanol-water | Schroeder <i>et al.</i> [3] | Wagner and Pruß [20] |
| ethanol-PAO | Schroeder <i>et al.</i> [3] | this work |
| CO ₂ -PEC5 | Span and Wagner [22] | this work |
| CO ₂ -PEC7 | Span and Wagner [22] | this work |

As already pointed out, the PAO employed here was specifically designed for this process. Consequently, there is no model available predicting its thermodynamic properties. The company Fuchs Schmierstoffe GmbH, which developed this product, insisted on keeping the oil's composition secret. However, they notified that it is a mixture of several different PAOs and further additives, resulting in an average molar mass of $M = 1773$ g/mol. Additionally, they provided some density, vapor pressure, and isobaric heat capacity data for the oil, which could be used to adjust a model. Despite the different compounds, the incorporated oil is treated as a pure fluid, and for simplicity it is referred to as PAO. Due to the very limited data base, no fluid-specific empirical Helmholtz energy model was developed but a generalized approach was applied. Further information on the corresponding theory is provided in chapter 3, and the results are shown in section 5.1.

For mixtures of ethanol and PAO, there is neither a model nor experimental data available in the literature. Therefore, the Chair of Process Technology of the RUB measured phase equilibria and some densities for ethanol-PAO mixtures, which were used for the

development of a new mixture model. This mixture model is based on the ethanol equation by Schroeder *et al.* [3] and the newly developed generalized equation for the PAO. Developing a mixture property model based on the Helmholtz energy for such different components, one even being described just by a generalized equation of state, is a challenging new path. Therefore, an additional model describing carbon dioxide (CO₂)-PEC5 mixtures, based on a newly developed generalized equation of state for PEC5, has been developed in this work. Additionally, a generalization of this mixture model to the similar system CO₂-PEC7 was investigated. Hence, an additional generalized equation of state describing PEC7 was developed. In contrast to PAO, PEC5 and PEC7 actually are pure fluids that might be mixed for commercial use. There are some data available in the literature for these lubricants that were used for the adjustment in this work. However, there has been a major investigation of the POEs PEC5, PEC7, and PEC9 at the National Institute for Standards and Technologies (NIST), including new measurements of the pure component properties, which all are to be published. Additionally, fluid-specific equations of state for these fluids [23] have been developed based on this new data, which are to be published as well. Despite the collaboration on the development of the new Helmholtz equations, the data set used for the adjustment of the generalized equations of state presented in this work was intentionally restricted to the data published in the literature. In this manner, the pure fluid equations of Lemmon and Eckermann [23] cannot only be used for a general validation of the generalized pure fluid equations of state developed in this work but rather for an evaluation of the prediction of caloric properties which the models have not been adjusted to.

CO₂ is one of the most promising alternative refrigerants. Due to rising concerns about the environmental impact of working fluids and lubricants, traditional chlorinated refrigerants are more and more replaced by hydrofluorocarbons (HFCs) and CO₂. [17] There are several publications dealing with density and solubility properties of CO₂ with POEs, e.g. [24–26].

Summing up, there are two main tasks to be addressed in the course of this work. A new mixture model for the experimentally well investigated ethanol-water system is required. Accurate pure fluid equations for these components have already been published. The theory is discussed in section 3.6, and results are shown in chapter 4.

Additionally, new property models for a new lubricant and its mixtures with the working fluid ethanol are required. There is very limited data available, so that a generalized

equation of state is used for the new pure fluid equation of state. This is explained in chapter 3 and results are presented in chapter 5. Since it is an innovative approach to model such an asymmetric mixture with multiparameter Helmholtz equations of state, an additional refrigerant-lubricant system, CO₂-PEC5, has been accordingly developed in order to verify this approach. Furthermore, the developed model for CO₂-PEC5 is transferred to mixtures of CO₂-PEC7. The results of this development are described in chapter 6.

3 Equations of State

The need for knowledge of thermophysical properties for design and optimization of technical processes is universal. If available, equations of state have replaced property tables as the source of information. Nevertheless, fitting a highly accurate multiparameter equation of state to a specific fluid or fluid mixture requires a considerable amount of reliable experimental data. Consequently, accurate empirical multiparameter property models are available in the literature for rather well measured fluids only. Water and CO₂ are very well and highly accurately measured fluids for which reference equations of state have been developed [20,22]. For ethanol, a multiparameter equation of state is available as well [3]. But since the experimental data set used for the adjustment of this equation of state is not as comprehensive and accurate as the data sets for CO₂ and water, the uncertainty of the equation is higher than the uncertainty of the reference equations of state. For the lubricants, there is little to no data available. This is a widespread problem throughout research and industry. For this reason, generalized equations of state, which are based on a physical background in a varying degree, are in wide use. As a matter of course, these models aren't as accurate as the multiparameter equations, but they allow for the prediction of properties depending on only a few fluid-specific parameters. Therefore, the usage of such models is somewhat independent of the experimental situation.

In the course of this chapter, the historical development of pure fluid and mixture property models is presented. Subsequently, the models that are used in this work are presented in more detail.

3.1 Historical Background

3.1.1 Empirical and Semi-Empirical Pure Fluid Equations

Generally, in equations of state, two independent state variables are used to describe another state variable. Most commonly, the pressure p or the Helmholtz energy a are formulated as a function of temperature T and molar volume v (or molar density ρ).

In 1834, Clapeyron [27] formulated the first equation of state describing the ideal gas behavior with

$$pv = RT, \quad (3.1)$$

R being the universal gas constant. The underlying assumptions of this model are molecules that are point particles without any extension, which exclusively interact with perfectly elastic collisions. For gases in the zero-density limit, particle volumes and interactions become negligible and the model is exact. At low pressures, this model is still quite accurate.

A few years later in 1873, van der Waals [28] proposed the first cubic equation that could describe not only the gaseous region but the liquid and supercritical regions as well as vapor-liquid equilibria. Van der Waals improved the ideal gas law by introducing two parameters, the attraction parameter a and the covolume of the molecules b . Thereby, he acknowledged that real molecules have an extension (b) and interact in a more complex way (a). Consequently, there is a contribution of attractive (a) as well as repulsive forces (rep):

$$p = \frac{RT}{v} \cdot \underbrace{\frac{v}{v-b}}_{\text{rep}} - \frac{a}{v^2}. \quad (3.2)$$

The two model parameters can be determined by evaluating the critical conditions $(\partial p / \partial v)_{T_c} = 0$ and $(\partial^2 p / \partial v^2)_{T_c} = 0$, which leads to

$$a = \frac{27R^2T_c^2}{64p_c}, \text{ and} \quad (3.3)$$

$$b = \frac{RT_c}{8p_c}. \quad (3.4)$$

The results show that based on two critical parameters, the complete phase behavior is determined. Applying the reduced variables $p_r = p/p_c$, $v_r = v/v_c$, and $T_r = T/T_c$ leads to the following reduced form of the van der Waals equation:

$$\left(p_r + \frac{3}{v_r^2}\right)(3v_r - 1) = 8T_r. \quad (3.5)$$

This equation yields the same results for every substance evaluated for a given set of reduced variables. Therefore, the van der Waals equation of state is the first corresponding states approach with two fluid-specific parameters. In the following, this is described by the classical corresponding states approach (CCSA) with two parameters. In 1913, van der

Waals discussed limitations of this approach [29]. He found the resulting relation $b = 1/3 v_c$ not suitable for many fluids. Experimental data proved this value to be too high. Van der Waals was aware that the two-parameter corresponding states approach reached its limitations.

In the 1930/1940s, Pitzer [30] and Guggenheim [31] discussed the physical assumptions that are necessary to apply this corresponding state principle correctly. Pitzer derived the theory of corresponding states for so called perfect liquids.

Redlich and Kwong [32] published another cubic formulation with a new description of the attractive pressure in 1948:

$$p = \frac{RT}{v - b} - \frac{a}{\sqrt{T}v(v + b)}. \quad (3.6)$$

The authors proposed a temperature-independent limiting value of $0.26 \cdot v_c$ for the volume of all gases at high pressures. Consequently, the equation has been constructed to satisfy the condition $b = 0.26V_c$. This model is based on the two-parameter CCSA as is the van der Waals equation.

In 1955, Pitzer *et al.* [33] proposed a third parameter that should help overcoming the shortcomings of the two-parameter CCSA. They introduced the so-called acentric factor ω . This new parameter accounts for intermolecular forces resulting from interactions between acentric parts of complex molecules with

$$\omega = -\log p_r - 1 \quad \text{and} \quad p_r = \frac{p_v(0.7 \cdot T_c)}{p_c}, \quad (3.7)$$

where p_v is the vapor pressure at a corresponding temperature. The theory postulates that any substances with the same acentric factor should behave equally according to the principle of corresponding states. However, the acentric factor is simply a measure for the slope of the vapor pressure curve with respect to reduced variables improving the description of phase equilibria.

In 1972, Soave [34] adapted the equation by Redlich and Kwong and incorporated the acentric factor in the description of the attractive pressure. This equation is discussed in detail in section 3.3. Another variation of the van der Waals equation was presented by Peng and Robinson in 1976 [35], who also incorporated the acentric factor in their new formulation of the attractive pressure. All cubic equations of state can be classified as

generalized equations since they only need the fluid-specific critical properties and potentially the acentric factor.

A completely different approach was used by Kamerlingh Onnes [36]. In 1902, he published an entirely new type of equation of state after having tried to empirically fit the two parameters of the van der Waals equation of state, a and b , to improve the representation of real fluids. He proposed a series formulation in molar volume with temperature-dependent coefficients, which he called virial coefficients. The first virial equation of state reads

$$pv = A(T) + \frac{B(T)}{v} + \frac{C(T)}{v^2} + \frac{D(T)}{v^4} + \frac{E(T)}{v^6} + \frac{F(T)}{v^8}, \quad (3.8)$$

where each virial coefficient A, B, C, D, E, F is a polynomial function of temperature. The coefficients of these equations were fitted to experimental pvT data of hydrogen, oxygen, nitrogen, and carbon dioxide. This is the first multiparameter equation of state developed and it is based on the corresponding states principle as well. The critical temperature and pressure are used as corresponding state parameters, so this is a two-parameter CCSA.

In 1928, Beattie and Bridgeman [37] proposed a different equation of state, that can be seen as an improvement of the van der Waals equation with

$$p = \frac{RT(1 - c/VT^3)}{V^2} [V + B_0(1 - b/V)] - \frac{A_0}{V^2} (1 - a/V). \quad (3.9)$$

where A_0, B_0, a, b , and c are adjustable parameters. Beattie and Bridgeman [37] aimed at a better physical description of real gases. Therefore, they analyzed limiting values as well as general relations and dependencies of temperature and density. Finally, they adjusted the equation parameters individually to several substances. This fact makes this equation the first not generalized empirical equation of state. Although this model is an improvement of the van der Waals equation based on physical considerations, it is no longer cubic with respect to the volume. Moreover, the authors converted the equation into the virial form following Kamerlingh Onnes [36] path.

In 1940, Benedict *et al.* [38] published the so called Benedict-Webb-Rubin equation (BWR) based on the work of Beattie and Bridgeman [37]. Among other things, they introduced an exponential correction term depending on the density into the virial expansion, which significantly improved the description of properties at high densities and low

temperatures. They fitted the empirical parameters to experimental data for methane, ethane, propane, and n-butane specifically for each substance. The BWR equation is given by

$$p = RT\rho + \left(B_0RT - A_0 - \frac{C_0}{T^2}\right)\rho^2 + (bRT - a)\rho^3 + a\alpha\rho^6 + \frac{c\rho^3(1 + \gamma\rho^2)\exp(-\gamma\rho^2)}{T^2}, \quad (3.10)$$

with the adjustable parameters A_0 , B_0 , C_0 , a , b , c , α , and γ .

The BWR equation is more commonly expressed in the compressibility factor

$$\frac{p(T, \rho)}{\rho RT} = Z(T, \rho) = 1 + \sum_{i=1}^6 n_i T^{t_i} \rho^{d_i} + \sum_{i=7}^8 n_i T^{t_i} \rho^{d_i} \exp\left(-\left(\frac{\rho}{\rho_r}\right)^2\right), \quad (3.11)$$

with the transformed coefficients n_i , and temperature and density exponents t_i and d_i , respectively.

In 1969, Carnahan and Starling [39] proposed an equation for non-attracting rigid spheres based on a virial series, that is still in use today, and has been introduced into other models that are presented later in this chapter. In 1973, Starling [40] published a variation of the BWR equation with the same density dependence. He fitted the parameters of the equation specifically for methane but proposed an additional generalized set of parameters that had been simultaneously fitted to multiple hydrocarbons. For this generalization, he also incorporated the three-parameter CCSA based on the acentric factor, the critical temperature T_c , and the critical density ρ_c .

In 1970, both Bender [41] and Wagner [42] developed algorithms to include vapor-liquid equilibrium (VLE) and pVT data simultaneously in the fitting process. Using this new multiproperty method, Bender [41] published virial-based equations for argon, nitrogen, oxygen, carbon dioxide, and methane with a new accuracy level concerning the description of saturated and caloric properties.

Jacobsen and Stewart [43] developed a virial-based equation of state for nitrogen with the help of a stepwise multiple regression analysis. As Bender, they included pVT data simultaneously with VLE data. They were able to reproduce the available experimental data within the uncertainty of the measurements. This type of equation (mBWR) has been widely used for other fluids.

In 1975, Lee and Kesler [44] developed a three-parameter CCSA model using two reference fluids. They applied the idea of Pitzer *et al.* [33] from 1955 of using a linear function in the acentric factor ω to calculate the compressibility factor of the desired fluid with

$$Z = Z^{(0)} + \omega Z^{(1)}, \quad (3.12)$$

where $Z^{(0)}$ is the compressibility factor of a simple fluid and $\omega Z^{(1)}$ is the deviation of the compressibility factor of the real fluid from $Z^{(0)}$. Lee and Kesler reformulated this expression for better convenience to the following form

$$Z = Z^{(0)} + \frac{\omega}{\omega^{(r)}} (Z^{(r)} - Z^{(0)}), \quad (3.13)$$

with $Z^{(1)} = (Z^{(r)} - Z^{(0)})/\omega^{(r)}$, and $Z^{(r)}$ being the compressibility factor of a reference fluid. This kind of generalization is referred to as extended corresponding states approach (eCSA) in the following. The simple and reference fluids were modeled with the BWR equation [38].

Platzer and Maurer [45] developed a four-parameter eCSA model especially designed for polar fluids. They additionally applied the polar factor χ , which was introduced by Halm and Stiel [46] with

$$\chi = \ln \left(\frac{p_v}{p_c} \right)_{\frac{T}{T_c}=0.6} + 1.7\omega + 1.552. \quad (3.14)$$

This builds the so called extended-Lee-Kesler-Bender method (eLKB). The interpolation is based on the acentric and polar factor using three reference fluids. The extension of the method by Pitzer *et al.* [33] by introducing a third reference fluid was developed by Stipp *et al.* [47]. In contrast to the model by Lee and Kesler [44], which incorporated BWR equations, the reference fluids are described by Bender-type equations.

So far, all introduced equations of state were explicit in pressure. These equations alone allow for the calculation of thermal properties. If caloric properties are to be calculated as well, thermal equations have to be transformed to a residual fundamental equation by integration and then be combined with an equation describing the ideal gas behavior. Fundamental equations of state formulated in the internal energy $u(v, s)$, enthalpy $h(p, s)$, Gibbs enthalpy $g(T, p)$, or Helmholtz energy $a(T, v)$ allow for the calculation of all thermodynamic properties. Of these four, the Helmholtz energy is the common standard in the development of equations of state today, since it is not depending on the not

measurable entropy, and in contrast to the Gibbs enthalpy, it is continuous through the two-phase region. The molar Helmholtz energy a is defined by

$$a(T, v) = u - Ts. \quad (3.15)$$

The Helmholtz energy is divided into two contributions, the ideal part a^0 and the residual part a^r . For a pure fluid, the Helmholtz energy can be written as

$$a(T, \rho) = a^0(T, \rho) + a^r(T, \rho). \quad (3.16)$$

The idea of simple corresponding states is applied to the Helmholtz energy as well. For that reason, a reduced formulation is utilized:

$$\alpha(\tau, \delta) = \frac{a(T, \rho)}{RT}, \quad (3.17)$$

with the reduced variables

$$\tau = \frac{T_r}{T} \quad \text{and} \quad \delta = \frac{\rho}{\rho_r}, \quad (3.18)$$

where usually $T_r = T_c$ and $\rho_r = \rho_c$ are used for pure fluids.

Pressure explicit equations of state are often expressed in the compression factor $Z = p/\rho RT$ or can easily be transferred to this form. This way, they can then be integrated to the reduced residual Helmholtz energy as follows:

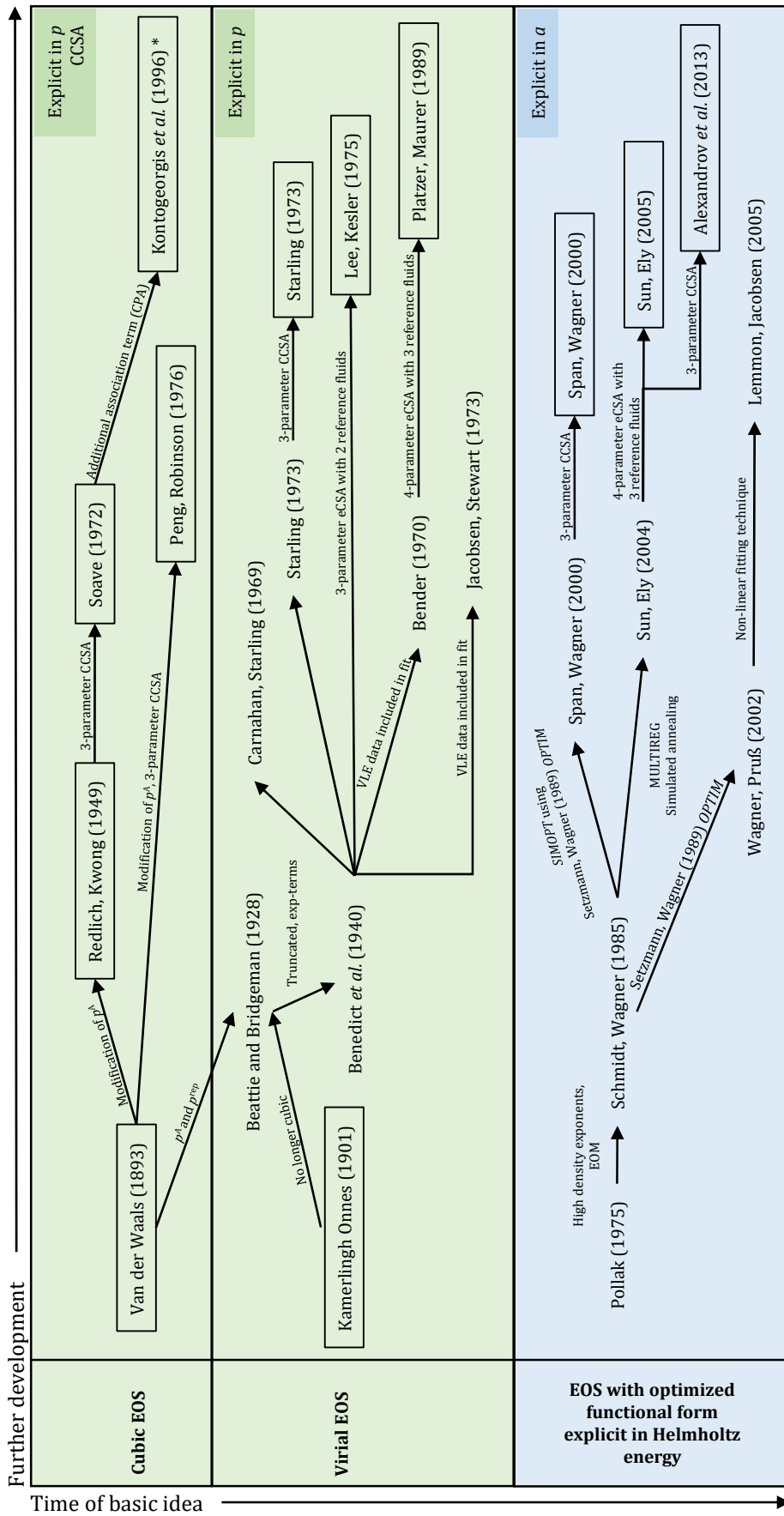
$$\alpha^r(\tau, \delta) = \int_0^\delta \frac{Z(\tau, \delta) - 1}{\delta} d\delta. \quad (3.19)$$

In combination with an equation describing the ideal gas behavior of the fluid, all thermo-physical properties, thermal and caloric, can be calculated from combinations of derivatives of these functions as well, see Table 3.3 in section 3.2.

Consequently, for equations of state explicit in pressure, terms that can be integrated to the reduced residual Helmholtz energy have exclusively been used. The required integration restricts the flexibility of chosen terms extremely. In 1969, Keenan *et al.* [48] published the first equation of state that was exclusively formulated in the free Helmholtz energy. However, it was Pollak in 1974 [49] who was the first to propose a functional form originally based on the Helmholtz energy including terms that could not have been used in a pressure explicit equation.

In 1985, Schmidt and Wagner [50] introduced exponential terms with density exponents higher than two, which are especially convenient for the description of the critical region. Even more important, the use of a powerful optimization algorithm led to an accurate equation with as few terms as possible. In 1974, Wagner [51] had proposed a stepwise regression analysis, which has the capability to select terms from a bank of terms, finding an optimized functional form based on mathematical analysis instead of the correlator's experience. This approach was improved in form of an evolutionary optimization method (EOM) by Ewers and Wagner in 1982 [52,53]. In 1989, Setzmann and Wagner [54] published a new optimization algorithm (OPTIM), which combines a modified stepwise regression analysis with elements of the evolutionary optimization method. Many powerful equations of state, that are still in use today, have been developed by means of this algorithm as are the reference equations for water [20] and CO₂ [22]. Recent equations of state have been developed with a different fitting technique, proposed and applied by Lemmon and Jacobsen [55] to develop an equation for R125 in 2005. This approach is also used in this work and is discussed further in section 4.2.

In 2003, Span and Wagner [56] published two technical equations of state, which are accurate but rather simple in structure, one for polar and another for non-polar fluids, that had been developed using an adapted optimization algorithm (SIMOPT). The difference to the classical approach is the simultaneous use of experimental data from multiple substances to determine the functional form of the equation. Like Starling [40], they published substance-specific coefficients [57,58] as well as a generalized version [59]. For the generalization, they applied the three-parameter CCSA but used the corresponding states parameter as adjustable parameters in order to reach the desired accuracy [59]. This model is further discussed in section 3.5. In 2004, Sun and Ely [60] published a universal equation of state explicit in the Helmholtz energy that had been adjusted to polar and non-polar fluids simultaneously using a simulated annealing method for the optimization. Lustig *et al.* [61] observed a high similarity between the universal equation of Sun and Ely [60] and the two original technical equations of Span and Wagner [56]. They showed that, except for one term, the Sun and Ely equation [60] is a linear combination of terms of the equations of Span and Wagner [56]. In 2005, Sun and Ely [60] proposed a generalization for their equation based on a four-parameter eCSA [62]. In 2013, Alexandrov *et al.* [63] used the universal equation of Sun and Ely and generalized it by means of the three-



*: No longer cubic in v , five pure fluid parameters are required. Framed references content generalized models that solely require the knowledge of the specific corresponding states parameters, and reference fluids if necessary .

Figure 3.1: Schematic overview of the historical development of empirical pure fluid models.

parameter CCSA in order to describe n -alkanes from n -pentane (C5) to n -pentacontane (C50). This equation is presented in detail in section 3.5. Figure 3.1 summarizes the most important pure fluid models presented so far and their interrelations.

3.1.2 Empirical and Semi-empirical Mixture Models

Evidently, the historical development of thermodynamic mixture models is strongly linked to the evolution of pure fluid equations of state. So far, the history of pure fluid equations of state explicit in pressure or reduced Helmholtz energy has been presented.

In 1873, van der Waals [64] proposed mixing rules for his two equation parameters a and b for a mixture consisting of N components with

$$a = \sum_{i=1}^N \sum_{j=1}^N x_i x_j a_{ij}, \quad (3.20)$$

and

$$b = \sum_{i=1}^N \sum_{j=1}^N x_i x_j b_{ij}, \quad (3.21)$$

x_i and x_j being the mole fraction of component i and j , respectively.

The unlike-interaction parameters can be determined by

$$a_{ij} = \sqrt{a_i a_j}, \quad (3.22)$$

and

$$b_{ij} = \frac{b_i + b_j}{2}, \quad (3.23)$$

leading to a simpler formulation of the parameter b with

$$b = \sum_i^N x_i b_i. \quad (3.24)$$

Since all mixture components are combined to one pseudo-pure fluid with the help of these mixing rules, this theory is widely referred to as the one-fluid theory.

Redlich and Kwong [32] incorporated the van der Waals mixing rules for their newly proposed cubic equation in 1949.

In the 1960s, Leland and co-workers [65–67] rederived these mixing rules based on statistical-mechanical theory of radial distribution functions. They were able to link van der Waals' equation parameters a and b to the molecular parameters ϵ and σ , which will be introduced in the context of SAFT theories in section 3.2. Based on this work, Kwak and Mansoori [68] stated that the mixing rules were used in a wrong way by Redlich and Kwong, since they changed the parameter dependency in a way that they no longer fulfilled the statistical mechanics behind the theory.

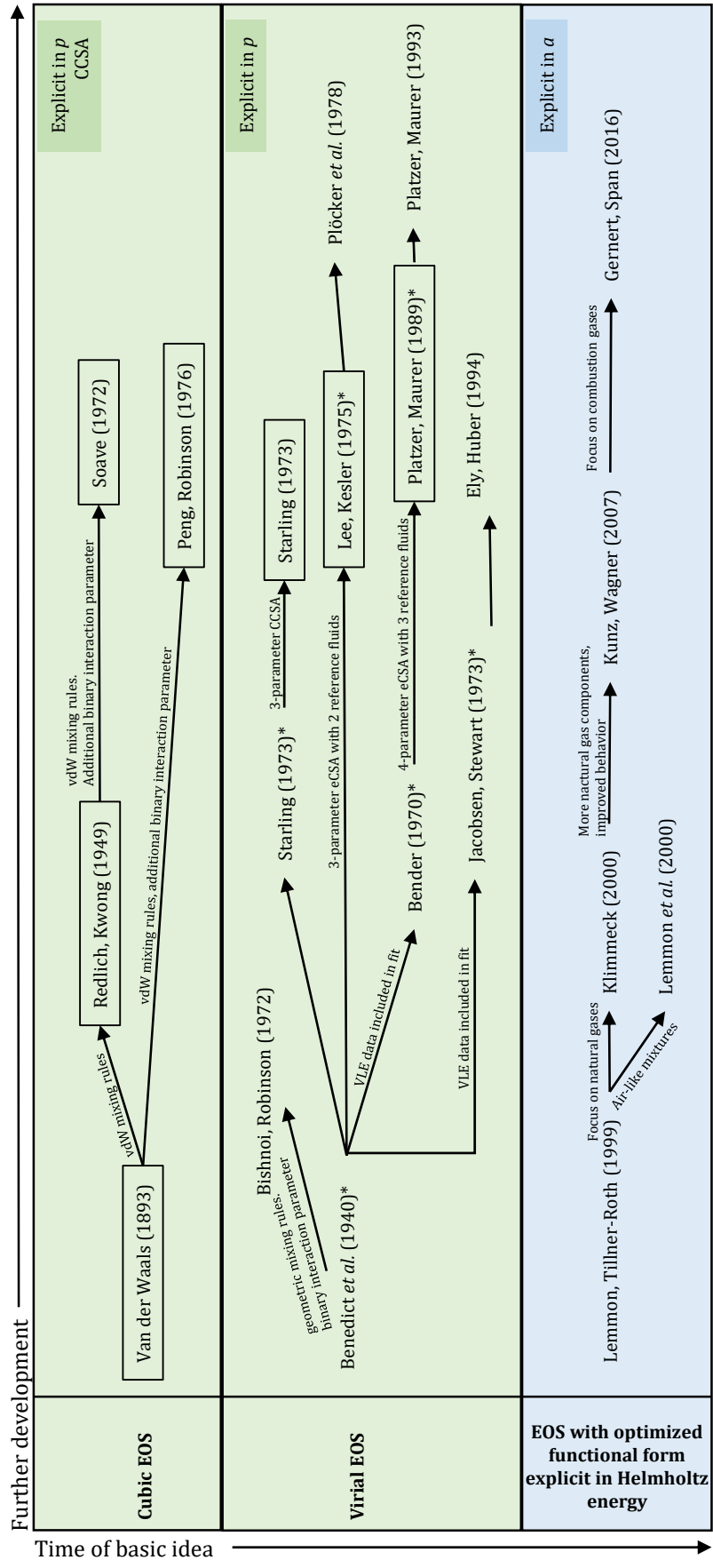
In 1970, Zudkevitch and David [69] introduced the adjustable binary interaction parameter k_{ij} representing the deviation of parameter a_{ij} from the classical geometric mean assumption leading to

$$a_{ij} = (1 - k_{ij})\sqrt{a_i a_j}. \quad (3.25)$$

Soave [34] as well as Peng and Robinson [35] introduced this binary interaction parameter in their description of mixtures using van der Waals' one-fluid theory.

In 1972, Bishnoi and Robinson [70] published mixing rules for the BWR equation parameters based on the one-fluid theory as proposed by van der Waals as well. They also introduced a binary interaction parameter into some of the mixing rules. Since his equation is a slight variance of the BWR, Starling [40] published analogous mixing rules in 1973, referring to Bishnoi and Robinson [70].

In 1978, Plöcker *et al.* [71] extended the generalized equation of state by Lee and Kesler [44] to mixtures. They proposed mixing rules to determine the pseudocritical properties of the mixture and introduced a binary interaction parameter in the formulation of the pseudocritical temperature. Plöcker *et al.* [71] introduced an additional constant exponent in the formulation of the pseudo-critical temperature accounting for asymmetric mixtures consisting of components of significantly different molecular size. If the value of this exponent is set to one, the mixing rules transfer to the van der Waals mixing rules. In 1993, Platzer and Maurer [72] extended their previously published generalized Bender equation [45] to predict properties of multicomponent mixtures. Therefore, they proposed three additional binary parameters for their mixing rules, two of them influencing the pseudo-critical temperature and one influencing the pseudo-critical density. In 1994, Huber and Ely [73] proposed an extended corresponding states model based on a wide-ranging modified BWR equation of state (mBWR). They chose density and temperature



*: Pure fluid model.
 Framed references content generalized models that solely require the knowledge of the specific corresponding states parameters, and reference fluids if necessary.

Figure 3.2: Schematic overview of the historical development of empirical mixture models.

dependent shape factors to transform results for a well-known reference fluid to the desired substance. To account for the composition dependence, they chose the van der Waals one-fluid mixing rules. In this model, there are two binary interaction parameters that can be adjusted.

The concept of pure fluid multiparameter Helmholtz energy equations was first extended to mixtures by Tillner-Roth [74] in 1993 and Lemmon [75] in 1996. They independently developed models, that describe a mixture's behavior in a very similar manner. In 1999, Lemmon and Tillner-Roth [76] revised and generalized the description of these mixture models based on highly accurate equations of state for the pure components, which are combined at the reduced temperature and density of the mixture. In 2000, Lemmon *et al.* [77] published a mixture model for air-like mixtures that was based on this work. In the same year, Klimeck [78] developed a preliminary multi-fluid mixture model for natural gas mixtures. This model was developed further by Kunz *et al.* [79]. It is known as the GERG-2004 equation of state. Considering up to 18 components, it sets new standards for the highly accurate description of multi-component natural gas mixtures. In 2012, this model was extended to 21 components and published as the GERG-2008 by Kunz and Wagner [80]. Recently, Gernert and Span [81] proposed a multi-fluid mixture model for combustion gases and combustion gas-like mixtures called EOS-CG. This model is designed in a similar way and can be seen as an extension of the GERG-2008 since it incorporates the already developed mixture models. This type of mixture models is presented in detail in section 3.6, since it is used for the development of the new model for ethanol-water mixtures. Figure 3.2 summarizes the so far presented mixture models.

3.1.3 Physical Property Models

A completely different approach of property modelling is the Statistical Associating Fluid Theory (SAFT) [82]. In contrast to the macroscopic point of view of the so far presented models, SAFT relates non-ideality to intermolecular forces. Therefore, it can be classified as a physical model even though its practical implementation contains empirical elements.

In 1989, Chapman *et al.* [82,83] published the original SAFT theory based on Wertheim's disturbance theory [84–87], which provides the basis for the description of a thermodynamic reference system. Wertheim expanded the Helmholtz energy in a series of integrals of molecular distribution functions and the association potential. Based on this approach,

Chapman *et al.* [82] divided the residual Helmholtz energy in three physical contributions: repulsion-dispersion contributions of segment-segment interactions, contributions resulting from the formation of chains, and site-site specific association interactions, for example hydrogen bonding. Consequently, the residual Helmholtz energy is given by

$$A^r = A^{\text{seg}} + A^{\text{chain}} + A^{\text{assoc}}, \quad (3.26)$$

where the superscripts *seg*, *chain*, and *assoc* refer to the contributions from the “monomeric” segments, from the formation of chains, and from the existence of association sites, respectively. [82] The original SAFT theory already accounts for mixtures using van der Waals’ one-fluid theory.

SAFT has been refined and adapted by many authors. One of the important changes was introduced by Huang and Radosz [88,89], who applied the dispersion term by Chen and Kreglewski [90] to the original SAFT theory [82,83]. This term was derived by adjusting a perturbation expansion to experimental data of argon [90].

In section 3.2, the perturbed-chain theory (PC-SAFT), which was published by Gross and Sadowski in 2001 [91], is presented more thoroughly since it will be used for comparison with the models developed in this work.

Another important semi-empirical generalized model is the Backone equation [92,93]. The authors adopt van der Waals’ approach and divide the residual behavior in a hard-body (*h*) and an attractive contribution (*a*)

$$A^r = A^h + A^a. \quad (3.27)$$

The ideal gas behavior, which is known quite well from statistical thermodynamics, describes a fluid’s behavior in the limit of zero-density. Recent perturbation theories allow for a good description of hard bodies, which is a good approximation of fluids in the limit of very high densities. Saager *et al.* [92] introduced the fluid-specific anisotropy parameter α to the hard-body contribution, which describes the shape of the molecule. For $\alpha = 1$, which means that the molecule is spherical, the contribution reduces to the Carnahan and Starling equation [39]. For the attractive contribution, a double polynomial equation dependent on a scaled temperature and a packing fraction with 24 universal parameters was fitted to experimental data of ethane. The anisotropy is described separately for both contributions with η being the anisotropy parameter of the attractive part. Additionally, a characteristic density ρ_0 and temperature T_0 are required as corresponding states

parameters. This makes this model a four-parameter CSA. For polar substances, the description of the Helmholtz energy is extended [93]. An additional parameter for the reduced dipole or quadrupole moment is required. These extended equations are called DI-BACK and QUABACK, respectively.

Müller *et al.* [94] changed the description of the attractive part by adjusting it to experimental data of methane, oxygen, and ethane using the optimization algorithm of Setzmann and Wagner [54]. In that manner, they found an optimized functional form that could use the anisotropy parameter α instead of the separate η , which was originally used in the hard-body contribution, as well as a scaled density instead of the packing fraction. The resulting equation for non-polar substances is called SIMBACKONE. For polar substances, they use the same additions published by Saager and Fischer [93]. It is important to notice that the additional equations for dipolar or quadrupolar substances cannot be used simultaneously, since they do not account for cross combinations. Weingerl *et al.* [95] published mixing rules for all equation parts of the BACKONE theory.

In the following, the models that are used in this work are presented in more detail.

3.2 PC-SAFT

The Perturbed-Chain Statistical Associating Fluid Theory (PC-SAFT) developed by Gross and Sadowski [91] is a modification of the SAFT version of Huang and Radosz [88,89], which is based on the original SAFT model of Chapman *et al.* [82]. Gross and Sadowski developed a new dispersion term by applying the perturbation theory to a hard-chain of spherical hard-sphere segments as reference instead of the hard-sphere molecules themselves. The resulting new model constants of the dispersion expression were adjusted to pVT and vapor pressure data of n -alkanes. Since the hard-chain is build-up of uniform hard-spheres, it knows only repulsive forces. All attractive chain interactions are modeled as perturbations in the dispersion term (disp). For associating fluids, the residual Helmholtz energy consists of the following contributions:

$$A^r = A^{\text{hc}} + A^{\text{disp}} + A^{\text{assoc}}. \quad (3.28)$$

The repulsive forces between the individual hard-chain molecules (hc) are modeled using the first order perturbation theory according to Wertheim [84–87]. The PC-SAFT model can be extended to describe the molecular behavior of the required substance more precisely. The extensions, for example extensions for dipolar or quadrupolar substances, can

simply be added to the existing Helmholtz equation as additional perturbations. Figure 3.3 illustrates the proposed molecular setup behind the PC-SAFT theory.

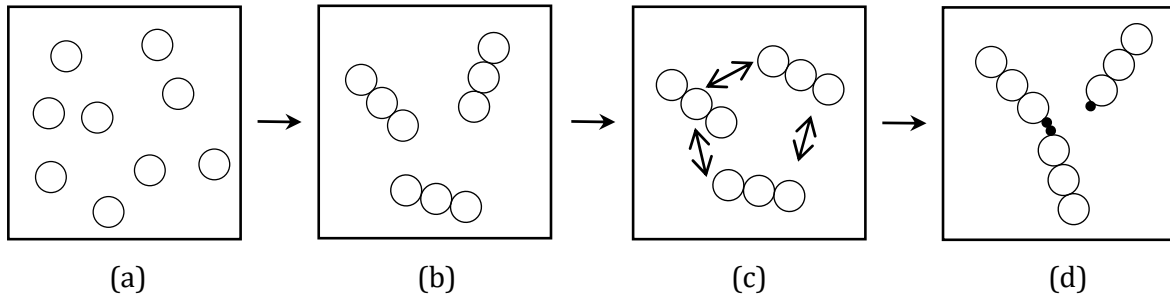


Figure 3.3: The molecular setup of PC-SAFT [91]. (a) An initial hard-sphere reference system of equally sized spherical segments. (b) Chain molecules are formed by bonding of m segments. (c) The hard-chains experience dispersive forces. (d) Association sites allow molecules to form hydrogen bonds. [96]

Molecular model

The molecular model underlying the PC-SAFT theory is a modified square well potential suggested by Chen and Kreglewski [90]:

$$u(r) = \begin{cases} \infty, & r < (\sigma - s_1) \\ 3\epsilon, & (\sigma - s_1) \leq r < \sigma \\ -\epsilon, & \sigma \leq r < \lambda\sigma \\ 0, & r \geq \lambda\sigma \end{cases}, \quad (3.29)$$

where $u(r)$ is the pair potential, r is the radial distance between two segments, σ is the temperature-independent segment diameter, ϵ is the depth of the potential well, and λ is the reduced well width. As suggested by Chen and Kreglewski [90], a ratio of $s_1/\sigma = 0.12$ is set. However, no additional temperature dependence of the potential depth is proposed.

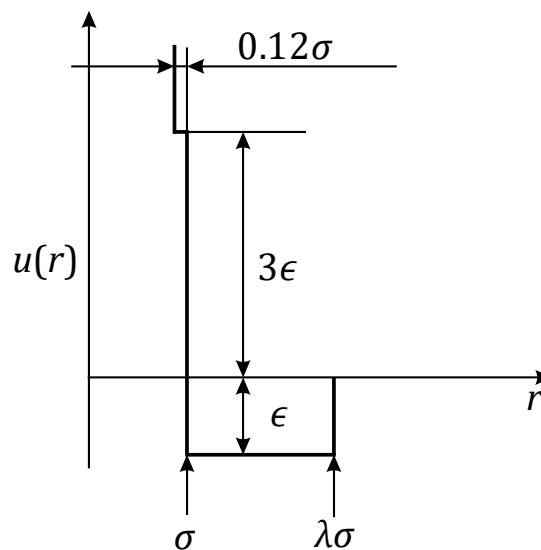


Figure 3.4: Modified square well potential by Chen and Kreglewski [90].

As a result, there are three substance specific parameters describing the molecule: σ , ϵ , m ; m being the number of spherical segments forming one chain. Figure 3.4 presents the applied potential model graphically.

Despite the simplicity of the molecular model, the step function accounts for the soft repulsion of molecules which is an essential feature of a real fluid's behavior. The validity of the temperature-independent segment diameter σ as the collision diameter is restricted to the zero-temperature limit. For higher temperatures, the collision diameter becomes smaller. Therefore, a temperature dependence of the collision diameter is introduced with

$$d(T) = \int_0^\sigma \left[1 - \exp\left(\frac{u(r)}{k_B T}\right) \right] dr. \quad (3.30)$$

The temperature-dependent segment diameter d for component i described by the proposed molecular model yields

$$d_i(T) = \sigma_i \left[1 - 0.12 \exp\left(-\frac{3\epsilon_i}{k_B T}\right) \right]. \quad (3.31)$$

Hard chain

As already pointed out, the innovation of the PC-SAFT model is the new hard-chain reference fluid consisting of hard-spheres. The reduced Helmholtz energy of the hard-sphere is defined in relation to the total number of segments N_s and is given by the expression of Mansoori *et al.* [97] reading

$$\tilde{a}^{\text{hs}} = \frac{A^{\text{hs}}}{N_s k_B T} = \frac{1}{\zeta_0} \left[\frac{3\zeta_1\zeta_2}{(1-\zeta_3)} + \frac{\zeta_2^3}{\zeta_3(1-\zeta_3)^2} + \left(\frac{\zeta_2^3}{\zeta_3^3} - \zeta_0 \right) \ln(1-\zeta_3) \right], \quad (3.32)$$

with the abbreviation

$$\zeta_n = \frac{\pi}{6} \hat{\rho} \sum_{i=0}^{N_c} x_i m_i d_i^n \quad \text{and} \quad n \in \{0, 1, 2, 3\}, \quad (3.33)$$

with x_i being the mole fraction of component i in the mixture with N_c components. The packing fraction or reduced segment density is defined as

$$\eta = \zeta_3 = \frac{\pi \hat{\rho}}{6} \sum_{i=1}^{N_c} x_i m_i d_i^3, \quad (3.34)$$

with $\hat{\rho}$ being the total number density of molecules

$$\hat{\rho} = \rho \cdot N_A \cdot 10^{-30} \frac{\text{m}^3}{\text{\AA}^3}. \quad (3.35)$$

The radial distribution function of the hard-sphere fluid according to Boublik [98] is given by the following relation:

$$g_{ii}^{\text{hs}} = \frac{1}{(1 - \zeta_3)} + \frac{1}{2} d_i \frac{3\zeta_2}{(1 - \zeta_3)^2} + \frac{1}{4} d_i^2 \frac{2\zeta_2^2}{(1 - \zeta_3)^3}. \quad (3.36)$$

As already pointed out, the repulsive forces between the individual chain molecules are modeled using the first order perturbation theory according to Wertheim [84–87]. The reduced Helmholtz energy of the hard-chain fluid is composed of the radial distribution function and the reduced Helmholtz energy of the hard-sphere fluid and can be determined from

$$\tilde{a}^{\text{hc}} = \frac{A^{\text{hc}}}{Nk_B T} = \bar{m} \tilde{a}^{\text{hs}} - \sum_{i=1}^{N_c} x_i (m_i - 1) \ln g_{ii}^{\text{hs}}(\sigma_{ii}), \quad (3.37)$$

with the average segment number

$$\bar{m} = \sum_{i=1}^{N_c} x_i m_i \quad (3.38)$$

to account for mixtures.

Dispersion

The dispersive interactions are modeled as second order perturbations based on the theory of Barker and Henderson [99,100] with

$$\tilde{a}^{\text{disp}} = \frac{A_1}{Nk_B T} + \frac{A_2}{Nk_B T} = -2\pi \hat{\rho} I_1 \overline{m^2 \epsilon \sigma^3} - \pi \hat{\rho} \bar{m} C_1 I_2 \overline{m^2 \epsilon^2 \sigma^3}. \quad (3.39)$$

For the utilization in mixtures, van der Waals' one-fluid theory is applied. Conventional Lorentz-Berthelot combining rules are proposed to obtain the mixture parameters

$$\sigma_{ij} = \frac{\sigma_{ii} + \sigma_{jj}}{2}, \quad (3.40)$$

and

$$\epsilon_{ij} = \sqrt{\epsilon_i \epsilon_j} (1 - k_{ij}), \quad (3.41)$$

with k_{ij} being the only binary interaction parameter.

The following abbreviations are introduced in equation (3.39):

$$C_1 = \left(1 + \bar{m} \frac{8\eta - 2\eta^2}{(1 - \eta)^4} + (1 - \bar{m}) \frac{20\eta - 27\eta^2 + 12\eta^3 - 2\eta^4}{[(1 - \eta)(2 - \eta)]^2} \right)^{-1}, \quad (3.42)$$

$$\overline{m^2 \epsilon \sigma^3} = \sum_{i=1}^{N_c} \sum_{j=1}^{N_c} x_i x_j m_i m_j \left(\frac{\epsilon_{ij}}{kT} \right) \sigma_{ij}^3, \quad (3.43)$$

and

$$\overline{m^2 \epsilon^2 \sigma^3} = \sum_{i=1}^{N_c} \sum_{j=1}^{N_c} x_i x_j m_i m_j \left(\frac{\epsilon_{ij}}{kT} \right)^2 \sigma_{ij}^3. \quad (3.44)$$

To shorten the volume integrals of Barker and Henderson [99,100], the following power series in the packing fraction are introduced:

$$I_1 = \sum_{j=0}^6 a_j(\bar{m}) \eta^j, \quad (3.45)$$

and

$$I_2 = \sum_{j=0}^6 b_j(\bar{m}) \eta^j, \quad (3.46)$$

with

$$a_j(\bar{m}) = a_{0j} + \frac{\bar{m} - 1}{\bar{m}} a_{1j} + \frac{\bar{m} - 1}{\bar{m}} \frac{\bar{m} - 2}{\bar{m}} a_{2j}, \quad (3.47)$$

and

$$b_j(\bar{m}) = b_{0j} + \frac{\bar{m} - 1}{\bar{m}} b_{1j} + \frac{\bar{m} - 1}{\bar{m}} \frac{\bar{m} - 2}{\bar{m}} b_{2j}. \quad (3.48)$$

Equations (3.47) and (3.48) account for the bonding of one segment to a nearest-neighbor segment and for the possible bonding of the neighbor segment to the next-nearest neighbor segment.

Association

If associating fluids are considered, there are two additional parameters that characterize the interactions between the association site A_i and B_i of a pure component i : the association energy $\varepsilon^{A_i B_i}/k$ and the effective association volume $\kappa^{A_i B_i}$. For mixtures, simple combining rules for the cross-association of substances by Wolbach and Sandler [101] are applied:

$$\kappa^{A_i B_j} = \sqrt{\kappa^{A_i B_i} \kappa^{A_j B_j}} \left(\frac{\sqrt{\sigma_{ii} \sigma_{jj}}}{1/2(\sigma_{ii} + \sigma_{jj})} \right)^3, \quad (3.49)$$

and

$$\varepsilon^{A_i B_j} = \frac{1}{2}(\varepsilon^{A_i B_i} + \varepsilon^{A_j B_j}). \quad (3.50)$$

There is no additional binary interaction parameter proposed. Therefore, only the dispersive interactions are corrected.

The contribution of association to the reduced Helmholtz energy according to Huang and Radosz [89] is defined as

$$\frac{\alpha^{\text{assoc}}}{RT} = \sum_{i=1}^N x_i \left[\sum_{A_i=1}^{M_i} \left(\ln X^{A_i} - \frac{X^{A_i}}{2} \right) + \frac{1}{2} M_i \right], \quad (3.51)$$

with A_i being the associating site A on component i , M_i the total number of associating sites of component i , and X^{A_i} the fraction of molecules of component i not bonded at site A . This fraction is determined from

$$X^{A_i} = \left(1 + \sum_{j=1}^N \sum_{B_j=1}^{M_j} \rho_j X^{B_j} \Delta^{A_i B_j} \right)^{-1} \quad (3.52)$$

with the associating strength

$$\Delta^{A_i B_j} = \sigma_{ij}^3 g_{ij}^{\text{seg}}(d_{ij}) \kappa^{A_i B_j} \left[\exp(\varepsilon^{A_i B_j}/kT) - 1 \right]. \quad (3.53)$$

The radial distribution function of the segment is approximated with that of the hard-sphere:

$$\begin{aligned}
g_{ij}^{\text{seg}}(d_{ij}) &\approx g_{ij}^{\text{hs}}(d_i, d_j) \\
&= \frac{1}{(1 - \zeta_3)} + \left(\frac{d_i d_j}{d_i + d_j} \right) \frac{3\zeta_2}{(1 - \zeta_3)^2} + \left(\frac{d_i d_j}{d_i + d_j} \right)^2 \frac{2\zeta_2^2}{(1 - \zeta_3)^3}.
\end{aligned} \tag{3.54}$$

Equation (3.54) resembles the Carnahan-Starling EOS [39] for a mixture of hard-spheres [102].

Huang and Radosz [88] published approximations for the fraction of sites not bonded to site A of a molecule. Table 3.1 presents an overview over the relevant bonding types for pure ethanol, and water. For any alcohol, the rigorous type is 3C since there are two lone pairs per oxygen atom (O), and one electron acceptor (H), which add to a total of three associating sites. In case of type 2B, both lone pairs are combined to one associating site. Consequently, the rigorous type of water is 4C, although it is often modeled as type 2B.

Table 3.1: Bonding types in alcohols and water, illustrating the basic associating schemes 2B, 3B, and 4C.

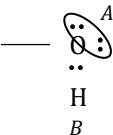
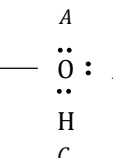
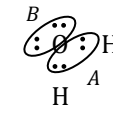
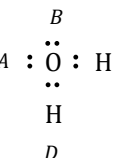
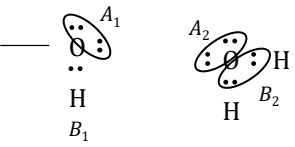
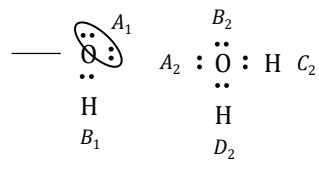
| Formula - Type | Δ approximations | X^A approximations | X^A site fractions |
|---|---|----------------------------------|---|
| Alcohol (2B)  | $\Delta^{AA} = \Delta^{BB} = 0;$ $\Delta^{AB} \neq 0$ | $X^A = X^B$ | $\frac{-1 + \sqrt{1 + 4\rho\Delta}}{2\rho\Delta}$ |
| Alcohol (3B)  | $\Delta^{AA} = \Delta^{AB}$ $= \Delta^{BB} = \Delta^{CC} = 0;$ $\Delta^{AC} = \Delta^{BC} \neq 0$ | $X^A = X^B;$ $X^C = 2X^A - 1$ | $\frac{-(1 - \rho\Delta) + \sqrt{(1 + \rho\Delta)^2 + 4\rho}}{4\rho\Delta}$ |
| Water (2B)  | $\Delta^{AA} = \Delta^{BB} = 0;$ $\Delta^{AB} \neq 0$ | $X^A = X^B$ | $\frac{-1 + \sqrt{1 + 4\rho\Delta}}{2\rho\Delta}$ |
| Water (4C)  | $\Delta^{AA} = \Delta^{AB} = \Delta^{BB} = \Delta^{CC}$ $= \Delta^{CD} = \Delta^{DD} = 0;$ $\Delta^{AC} = \Delta^{AD} = \Delta^{BC} = \Delta^{BD} \neq 0$ | $X^A = X^B = X^C = X^D$ | $\frac{-1 + \sqrt{1 + 8\rho\Delta}}{4\rho\Delta}$ |

Table 3.2 presents the association strength for the cross association of the components alcohol and water with the association schemes 2B, and 2B and 4C, respectively.

Table 3.2: Cross association of the basic associating schemes 2B - 2B, and 2B - 4C.

| Formula - Type | Δ approximations |
|--|--|
| Alcohol (2B) - Water (2B)  | $\Delta^{A_1A_2} = \Delta^{B_1B_2} = 0$ |
| Alcohol (2B) - Water (4C)  | $\Delta^{A_1A_2} = \Delta^{A_1B_2} = \Delta^{B_1C_2} = \Delta^{B_1D_2} = 0;$ |

3.3 SRK

In this section, Soave's [34] adaption of the model by Redlich and Kwong [32], the SRK, is presented. In the sense of the van der Waals equation, there are two contributions to the overall pressure, an attractive part as well as a repulsive part resulting from hard-body interactions. Soave changed the temperature dependence of the attractive part by simply turning the attraction parameter a into a function of temperature T . This new dependency leads to the following formulation:

$$p = \frac{RT}{v - b} - \frac{a(T)}{v(v + b)}. \quad (3.55)$$

For a pure component i , the attraction parameter a is now given by

$$a_i(T) = \alpha_i(T) \cdot a_{c,i}, \quad (3.56)$$

with $\alpha_i(T_{c,i}) = 1$, where subscript c denotes the critical condition. As introduced in section 3.1, both parameters $a_{c,i}$ and b_i are determined by evaluating the equation at the critical point of component i , which yields

$$a_{c,i} = 0.42747 \frac{R^2 T_{c,i}^2}{p_{c,i}}, \text{ and} \quad (3.57)$$

$$b_i = 0.08664 \frac{RT_{c,i}}{p_{c,i}}. \quad (3.58)$$

Soave investigated in the description of the vapor pressure. From plotting calculated vapor pressures of hydrocarbons, he found the following relation:

$$\alpha_i(T) = \left(1 + m_i \left(1 - \sqrt{T/T_{c,i}} \right) \right)^2. \quad (3.59)$$

As an improvement, Soave introduced the acentric factor as an additional corresponding states parameter. Therefore, he correlated the empirical parameter m_i against ω_i , to find

$$m_i = 0.48 + 1.57\omega_i - 0.176\omega_i^2. \quad (3.60)$$

The SRK can be used predictively if the critical properties $T_{c,i}$ and $p_{c,i}$ as well as the acentric factor ω_i are known. In section 5.1.1, this model is used to adjust the corresponding states parameters to a synthetic PAO lubricant based on a very limited data base since the critical parameters are not known.

As already presented, Soave incorporates the one-fluid mixing rules for the calculations of a mixture consistent of N components:

$$a = \sum_i^N \sum_j^N x_i x_j a_{ij}, \quad (3.20)$$

with

$$a_{ij} = (1 - k_{ij}) \sqrt{a_i a_j}, \quad (3.22)$$

k_{ij} being a binary adjustable parameter, and

$$b = \sum_i^N x_i b_i. \quad (3.24)$$

3.4 Helmholtz Equations of State for Pure Fluids

In this section, Helmholtz equations of state for pure fluids are presented. The corresponding mixture approach is shown separately in section 3.6. As already introduced in equation (3.16), the contribution of the ideal gas behavior to the reduced Helmholtz energy is modeled separately from the residual part.

Ideal part

For an ideal gas, the Helmholtz energy is defined by

$$a^{\circ}(T, \rho) = u^{\circ}(T) + Ts^{\circ}(T, \rho). \quad (3.61)$$

The internal energy of the ideal gas u° can be obtained by integrating the isochoric heat capacity of the ideal gas c_v° over the temperature as

$$u^{\circ}(T) = u_0^{\circ} + \int_{T_0}^T c_v^{\circ} dT. \quad (3.62)$$

The ideal gas entropy can be determined by

$$s^{\circ}(T, \rho) = s_0^{\circ} + \int_{T_0}^T \frac{c_v^{\circ}}{T} dT - R \ln\left(\frac{\rho}{\rho_0}\right). \quad (3.63)$$

The density at the reference point of the ideal gas is determined by the thermal equation of state for the ideal gas given in equation (3.1) and is calculated from the reference pressure p_0 and the reference temperature T_0 :

$$\rho_0 = \frac{p_0}{RT_0}. \quad (3.64)$$

The combination of equations (3.62) and (3.63) results in the following description of the ideal Helmholtz energy:

$$a^{\circ}(T, \rho) = u_0^{\circ} - Ts_0^{\circ} + \int_{T_0}^T c_v^{\circ} dT - RT - T \int_{T_0}^T \frac{c_v^{\circ}}{T} dT + RT \ln\left(\frac{\rho}{\rho_0}\right). \quad (3.65)$$

In contrast to the residual part, the ideal gas contribution can be modeled by physically meaningful equations based on statistical thermodynamics. Usually, an equation for the ideal gas isobaric heat capacity c_p° is formulated in the following form:

$$\frac{c_p^{\circ}}{R} = n_0^* + \sum_{i=1}^{I_{\text{Pol}}} n_i^* T^{t_i^*} + \sum_{i=I_{\text{Pol}}+1}^{I_{\text{Pol}}+I_{\text{PE}}} m_i \left(\frac{\theta_i}{T}\right)^2 \frac{\exp(\theta_i/T)}{(\exp(\theta_i/T) - 1)^2}. \quad (3.66)$$

Apart from the constant n_0^* , the common formulation may contain polynomial (Pol) and Planck-Einstein terms (PE). The constant n_0^* describes contributions from translation as well as external rotation of the molecules. The Planck-Einstein terms characterize the internal molecular vibrations and enable a description of the ideal gas isobaric heat capacity over a wide temperature range with good extrapolation behavior with the help of relatively few terms. Despite the underlying physical idea, the θ_i and m_i in these terms are used as adjustable parameters in this context. For many fluids, Planck-Einstein terms in

combination with the constant n_0^* suffice for a description of the ideal gas behavior. In case the individual modes interact, polynomial terms can be used additionally. Equation (3.66) can be fitted to either experimental or theoretical data. For further details on the ideal gas behavior see Span [59].

The ideal reduced Helmholtz energy α^0 is linked to the ideal isochoric heat capacity c_v^0 as follows:

$$\left(\frac{\partial \alpha^0}{\partial \tau^2}\right)_\delta = -\frac{c_v^0}{R\tau^2}. \quad (3.67)$$

Consequently, the ideal isobaric heat capacity c_p^0 is transformed to the ideal isochoric heat capacity c_v^0 according to $c_p^0/R = c_v^0/R + 1$, which finally leads to

$$\frac{c_v^0}{R} = n_0 + \sum_{i=1}^{I_{\text{Pol}}} n_i \tau^{t_i} + \sum_{i=I_{\text{Pol}}+1}^{I_{\text{Pol}}+I_{\text{PE}}} m_i (\vartheta_i \tau)^2 \frac{\exp(\vartheta_i \tau)}{(\exp(\vartheta_i \tau) - 1)^2}, \quad (3.68)$$

where $n_0 = n_0^* - 1$, $n_i = n_i^* \cdot T_r^{t_i^*}$, $t_i = -t_i^*$, and $\vartheta_i = \theta_i/T_r$.

This equation can then be integrated twice with respect to the inverse reduced temperature τ :

$$\alpha^0(\tau, \delta) = c^{\text{II}} + c^{\text{I}}\tau + c_0 \ln(\tau) + \sum_{i=1}^{I_{\text{Pol}}} c_i \tau^{t_i} + \sum_{i=I_{\text{Pol}}+1}^{I_{\text{Pol}}+I_{\text{PE}}} m_i \ln[1 - \exp(-\vartheta_i \tau)] + \ln(\delta), \quad (3.69)$$

with $c_0 = n_0 = n_0^* - 1$, and $c_i = -n_i^*/(t_i^*(t_i^* + 1)) \cdot T_r^{t_i^*}$. The integration constants c^{I} and c^{II} are defined by an arbitrary reference state.

Residual part

In contrast to the ideal part, the residual fluid behavior is modeled by a completely empirical formulation. Generally, four different types of terms can be used to describe the residual reduced Helmholtz energy: polynomial (Pol), exponential (Exp), Gaussian bell-shaped (GBS), and non-analytic (NA) terms:

$$\alpha^{\text{r}}(\tau, \delta) = \alpha_{\text{Pol}}^{\text{r}}(\tau, \delta) + \alpha_{\text{Exp}}^{\text{r}}(\tau, \delta) + \alpha_{\text{GBS}}^{\text{r}}(\tau, \delta) + \alpha_{\text{NA}}^{\text{r}}(\tau, \delta). \quad (3.70)$$

These types of terms differ in complexity and number of parameters, as can be seen below

$$\begin{aligned}
\alpha^r(\tau, \delta) = & \sum_{i=1}^{I_{\text{Pol}}} n_i \tau^{t_i} \delta^{d_i} + \sum_{i=I_{\text{Pol}}+1}^{I_{\text{Pol}}+I_{\text{Exp}}} n_i \tau^{t_i} \delta^{d_i} \exp(-\delta^{p_i}) \\
& + \sum_{i=I_{\text{Pol}}+I_{\text{Exp}}+I_{\text{GBS}}}^{I_{\text{Pol}}+I_{\text{Exp}}+I_{\text{GBS}}} n_i \tau^{t_i} \delta^{d_i} \exp(-\eta_i(\delta - \epsilon_i)^2 - \beta_i(\tau - \gamma_i)^2) \\
& + \sum_{i=I_{\text{Pol}}+I_{\text{Exp}}+I_{\text{GBS}}+I_{\text{NA}}}^{I_{\text{Pol}}+I_{\text{Exp}}+I_{\text{GBS}}+I_{\text{NA}}} n_i \delta \Delta^{b_i} \exp(-e_i(\delta - 1)^2 - f_i(\tau - 1)^2),
\end{aligned} \tag{3.71}$$

$$\text{with } \Delta = \{(1 - \tau) + c_i[(\delta - 1)^2]^{1/(2\beta_i)}\}^2 + d_i[(\delta - 1)^2]^{a_i}. \tag{3.72}$$

Amongst others, the polynomial and exponential terms have already been used by Schmidt and Wagner in 1975 [50]. In 1991, Setzmann and Wagner [103] applied for the first time Gaussian bell-shaped terms to a fundamental equation of state which were introduced by Haar *et al.* [104]. They are especially useful for the description of the critical region. However, depending on the parameters, they can improve the fluid's description in the entire fluid region [105]. Non-analytic terms are only in use in two reference equations of state, in the reference equation for water by Wagner and Pruß [20], and in the reference equation for CO₂ by Span and Wagner [22]. The non-analytic terms were introduced for the equations to show infinite heat capacities as well as zero speed of sound at the critical point, as proposed by theory. However, these terms are very sensitive and lead to numerical problems if used in mixtures. This is the reason why non-analytic terms are no longer found in current equations of state.

To calculate thermophysical properties, the derivatives of the reduced Helmholtz energy α with respect to the independent variables τ and δ are needed. The relations of the different properties to the reduced Helmholtz energy are given in Table 3.3. The following notations are applied:

$$\alpha_\tau = \left(\frac{\partial \alpha}{\partial \tau}\right)_\delta \tag{3.73}, \quad \alpha_{\tau\tau} = \left(\frac{\partial^2 \alpha}{\partial \tau^2}\right)_\delta \tag{3.74}, \quad \alpha_{\delta\tau} = \left(\frac{\partial^2 \alpha}{\partial \delta \partial \tau}\right) \tag{3.75},$$

$$\alpha_\delta = \left(\frac{\partial \alpha}{\partial \delta}\right)_\tau \tag{3.76}, \quad \alpha_{\delta\delta} = \left(\frac{\partial^2 \alpha}{\partial \delta^2}\right)_\tau \tag{3.77}.$$

Table 3.3: Definitions of common thermodynamic properties and their relation to the reduced Helmholtz energy.

| Property | Relation to reduced Helmholtz energy |
|--|--|
| Pressure | |
| $p(T, \rho) = -\left(\frac{\partial a}{\partial v}\right)_T$ (3.78) | $\frac{p}{\rho RT} = 1 + \delta\alpha_\delta^r$ (3.79) |
| Fugacity coefficient of component i | |
| $\ln \varphi_i(T, p, \mathbf{n}) = \int_0^p \left[\frac{v_i}{RT} - \frac{1}{p} \right] dp_{T,n}$ (3.80) | $\ln \varphi_i = \left(\frac{\partial n\alpha^r}{\partial n_i} \right)_{T,V,n_{j \neq i}} - \ln Z$ (3.81) |
| Fugacity of component i | |
| $f_i(T, p, \mathbf{x}) = x_i p \varphi_i(T, p, \mathbf{x})$ (3.82) | $f_i = x_i \rho RT \exp\left(\frac{\partial n\alpha^r}{\partial n_i} \right)_{T,V,n_{j \neq i}}$ (3.83) |
| Entropy | |
| $s(T, \rho) = -\left(\frac{\partial a}{\partial T}\right)_v$ (3.84) | $\frac{s}{R} = \tau(\alpha_\tau^o + \alpha_\tau^r) - \alpha^o - \alpha^r$ (3.85) |
| Internal energy | |
| $u(T, \rho) = a + Ts$ (3.86) | $\frac{u}{RT} = \tau(\alpha_\tau^o + \alpha_\tau^r)$ (3.87) |
| Enthalpy | |
| $h(T, \rho) = u + pv$ (3.88) | $\frac{h}{RT} = 1 + \tau(\alpha_\tau^o + \alpha_\tau^r) + \delta\alpha_\delta^r$ (3.89) |
| Isobaric heat capacity | |
| $c_p(T, \rho) = -\left(\frac{\partial h}{\partial T}\right)_p$ (3.90) | $\frac{c_p}{R} = -\tau^2(\alpha_{\tau\tau}^o + \alpha_{\tau\tau}^r) + \frac{(1 + \delta\alpha_\delta^r - \delta\tau\alpha_{\delta\tau}^r)^2}{1 + 2\delta\alpha_\delta^r + \delta^2\alpha_{\delta\delta}^r}$ (3.91) |
| Gibbs energy | |
| $g(T, p) = h - Ts$ (3.92) | $\frac{g}{RT} = 1 + \alpha^o + \alpha^r + \delta\alpha_\delta^r$ (3.93) |
| Speed of sound | |
| $w(p, T) = \sqrt{\left(\frac{\partial p}{\partial \rho}\right)_s}$ (3.94) | $\frac{w^2}{RT} = 1 + 2\delta\alpha_\delta^r + \delta^2\alpha_{\delta\delta}^r - \frac{(1 + \delta\alpha_\delta^r - \delta\tau\alpha_{\delta\tau}^r)}{\tau^2(\alpha_{\tau\tau}^o + \alpha_{\tau\tau}^r)}$ (3.95) |
| 2 nd thermal virial coefficient | |
| $B(T) = \lim_{\rho \rightarrow 0} \left(\frac{\partial \left(\frac{p}{\rho RT} \right)}{\partial \rho} \right)_T$ (3.96) | $B\rho_r = \lim_{\delta \rightarrow 0} \alpha_\delta^r$ (3.97) |

Table 3.3 continued.3rd thermal virial coefficient

$$C(T) = \frac{1}{2} \lim_{\rho \rightarrow 0} \left(\frac{\partial^2 \left(\frac{p}{\rho RT} \right)}{\partial \rho^2} \right)_T \quad (3.98)$$

$$C\rho_r^2 = \lim_{\delta \rightarrow 0} \alpha_{\delta\delta}^r \quad (3.99)$$

The relations presented in Table 3.3 are of a general kind. They do not depend on the type of model, which is used to describe α^o or α^r , nor on whether the equation was originally formulated in the Helmholtz energy or has been integrated from c_p^o or pressure. The derivatives of the Helmholtz equations presented in this section and relations for further properties can be found in Span [59].

3.5 Generalized Empirical Equations of State for Pure Fluids

As already introduced at the beginning of this chapter, there are different publications dealing with the generalization of an empirical equation of state. In this section, two such models are presented in more detail, including the model by Alexandrov *et al.* [63] that has been used in this work.

In 2003, Span and Wagner [56] published two technical equations of state, that had been optimized for multiple fluids simultaneously, one for polar and one for non-polar fluids. Subsequently, they proposed substance-specific coefficients for numerous fluids that had been adjusted to experimental data of the respective fluids [57,58].

Additionally, they were looking for a way to generalize the coefficients N_i using the acentric factor as corresponding states parameter. Their generalized equation finally reads [59]²

$$\alpha^r(\tau, \delta) = \sum_{i=1}^5 N_i \delta^{d_i} \tau^{t_i} + \sum_{i=6}^{10} N_i \delta^{d_i} \tau^{t_i} \exp(-\gamma_i \delta^{p_i}), \quad (3.100)$$

with

$$N_i = c_{1,i} + c_{2,i}W + c_{3,i}W^4. \quad (3.101)$$

² The generalized equation of Span and Wagner was only published in chapter 7.2.2 of Ref. [59] and never in a journal article.

The parameter w is introduced in order to distinguish between the adjusted value and the true acentric factor ω of the respective substance. The reducing temperature and density are used as adjustable parameters as well, which only resemble the critical properties. The values for d_i , t_i , and p_i of the generalized equation of state given in equation (3.100) and for $c_{1,i}$, $c_{2,i}$, and $c_{3,i}$ given in equation (3.101) can be taken from Ref. [59].

The numerical stability of such a generalization is crucial for a beneficial predictive use. In comparison to the model of Platzter and Maurer [45], which was shortly introduced in section 3.1.1 and which is based on a four-parameter eCSA with three reference fluids, the calculated coefficients in dependence of the acentric factor of the model by Span and Wagner [59] are better behaved as can be seen in Figure 3.5.

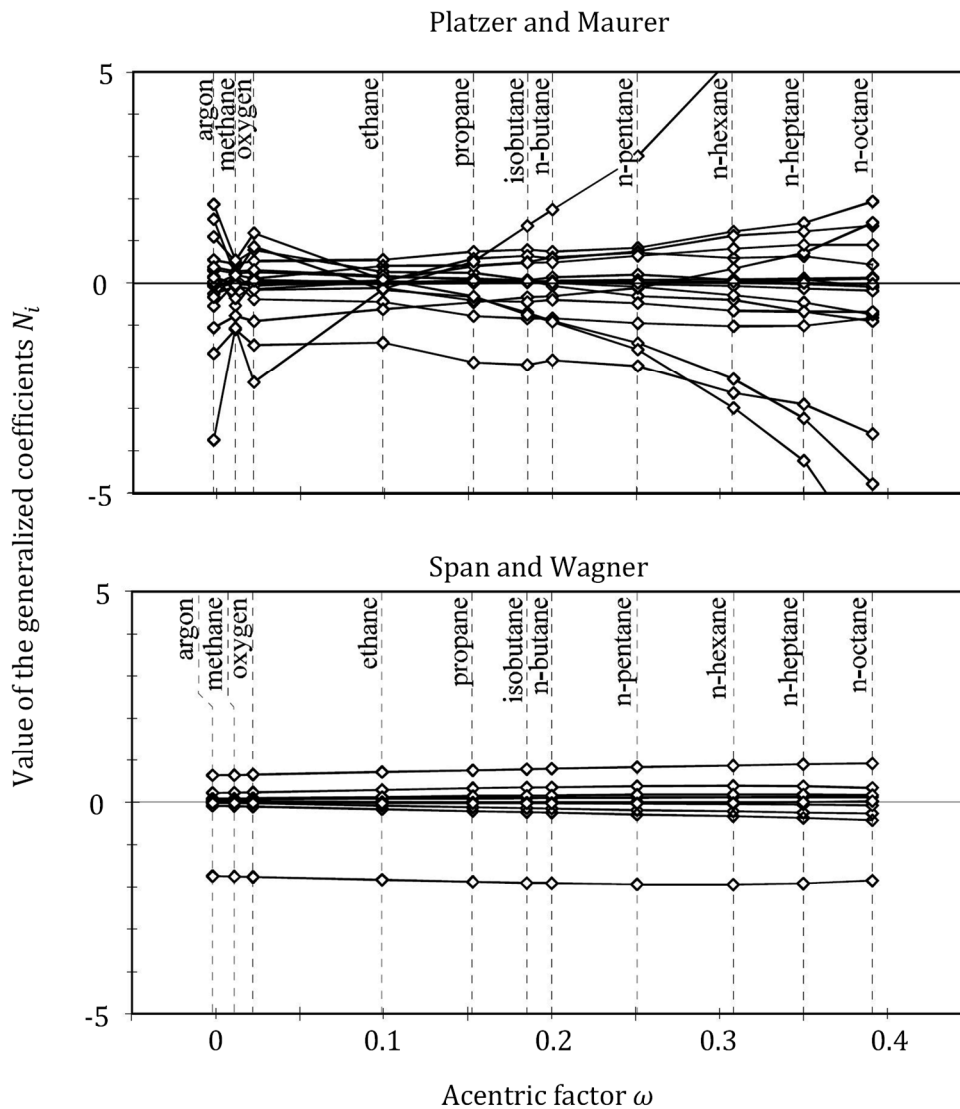


Figure 3.5: Values of the coefficients N_i which result from equation (3.101) and the generalization by Platzter and Maurer [45] for 11 nonpolar fluids. [59]

The model of Span and Wagner [59] presents a constant linearity over the acentric factor. In contrast, the coefficients of the model by Platzler and Maurer [45] show discontinuities, which can lead to numerical instabilities in the usage of this model. Figure 3.5 also illustrates the fluids relevant to the development of the model by Span and Wagner. It can be seen, that the highest acentric factor of a considered fluid was $\omega_{n\text{-octane}} \approx 0.4$. Theoretically, for a spherical fluid the acentric factor would be zero, as can be seen for argon with $\omega_{\text{argon}} \approx -0.00219$. With rising complexity of the molecule's form, the acentric factor deviates further from this ideal.

Alexandrov *et al.* [63] published a generalized empirical equation of state that was adjusted to long-chained *n*-alkanes and is valid for $\omega = 0.25$ to 1.8. The purpose of this model is to describe *n*-alkanes from *n*-pentane (C₅) to *n*-pentacontane (C₅₀). It is applicable over a temperature range from the triple point to 700K with pressures up to 100 MPa.

As a basis, Alexandrov *et al.* [63] used the universal equation developed by Sun and Ely [60], but chose a different generalization method than the authors in their following publication [62]. Sun and Ely proposed a four-parameter eCSA with three reference fluids, as used by Platzler and Maurer [45]. In contrast, Alexandrov *et al.* [63] presented a three-parameter CCSA based on the critical temperature and density as well as the acentric factor, as used by Span and Wagner [59]. This led to the following formulation:

$$\alpha^r(\tau, \delta) = \sum_{i=1}^6 N_i \delta^{d_i} \tau^{t_i} + \sum_{i=7}^{14} N_i \delta^{d_i} \tau^{t_i} \exp(-\gamma_i \delta^{p_i}), \quad (3.102)$$

with

$$N_i = c_{1,i} + c_{2,i} \omega + c_{3,i} \omega^{c_{4,i}}. \quad (3.103)$$

The coefficients of equation (3.103) and the temperature exponents t_i were simultaneously fitted. The values for d_i , t_i , and p_i of the generalized equation of state given in equation (3.102) and for $c_{1,i}$, $c_{2,i}$, $c_{3,i}$, and $c_{4,i}$ given in equation (3.103) can be taken from Appendix A.

Figure 3.6 shows the values of the generalized coefficients N_i of the model of Alexandrov *et al.* [63] for the full range of validity from $\omega = 0$ to 1.8 in comparison to the model of Span and Wagner [59].

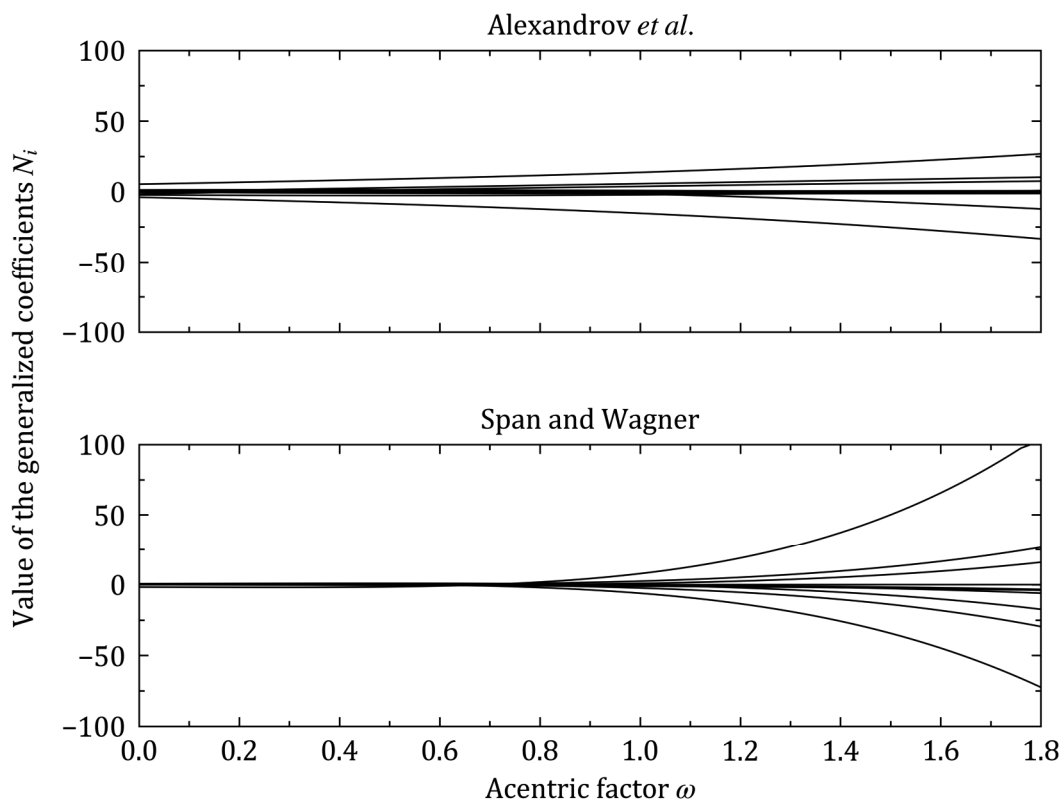


Figure 3.6: Values of the coefficients N_i which result from equation (3.101) and equation (3.103) for $\omega = 0$ to 1.8.

The individual coefficients of the model of Alexandrov *et al.* [63] show a linear course in the complete region of validity, whereas the coefficients of the model of Span and Wagner [59] do not extrapolate well for acentric factors higher than $\omega = 0.6$. Since the model has not been adjusted in this region, the values of the coefficients rapidly change, one coefficient even reaching a value over 100. Such high coefficients can have a strongly negative influence on the behavior of an equation. However, it can be seen from Figure 3.6 that the values of the coefficients of Alexandrov *et al.* [63] have a wider spread compared to the coefficients of Span and Wagner in their range of validity, and this spread expands with increasing acentric factor significantly. This leads to numerical problems of the model of Alexandrov *et al.* [63] as well. In Figure 3.7, p, ρ -diagrams for several fluids with varying acentric factors are presented, which were calculated with the model of Alexandrov *et al.* [63]. For pentane, decane, and pentadecane, the saturation lines show a steady course. However, already for decane, the curvature of the saturation lines descending from the critical point looks odd, whereas for pentadecane, a convexity of the saturation lines in the near-critical region becomes visible. The saturation lines of icosane, triacontane, and pentacontane show a discontinuity at elevated temperatures. This is caused by the presented course of the near-critical isotherms of these fluids. For icosane ($T_c = 768$ K), the

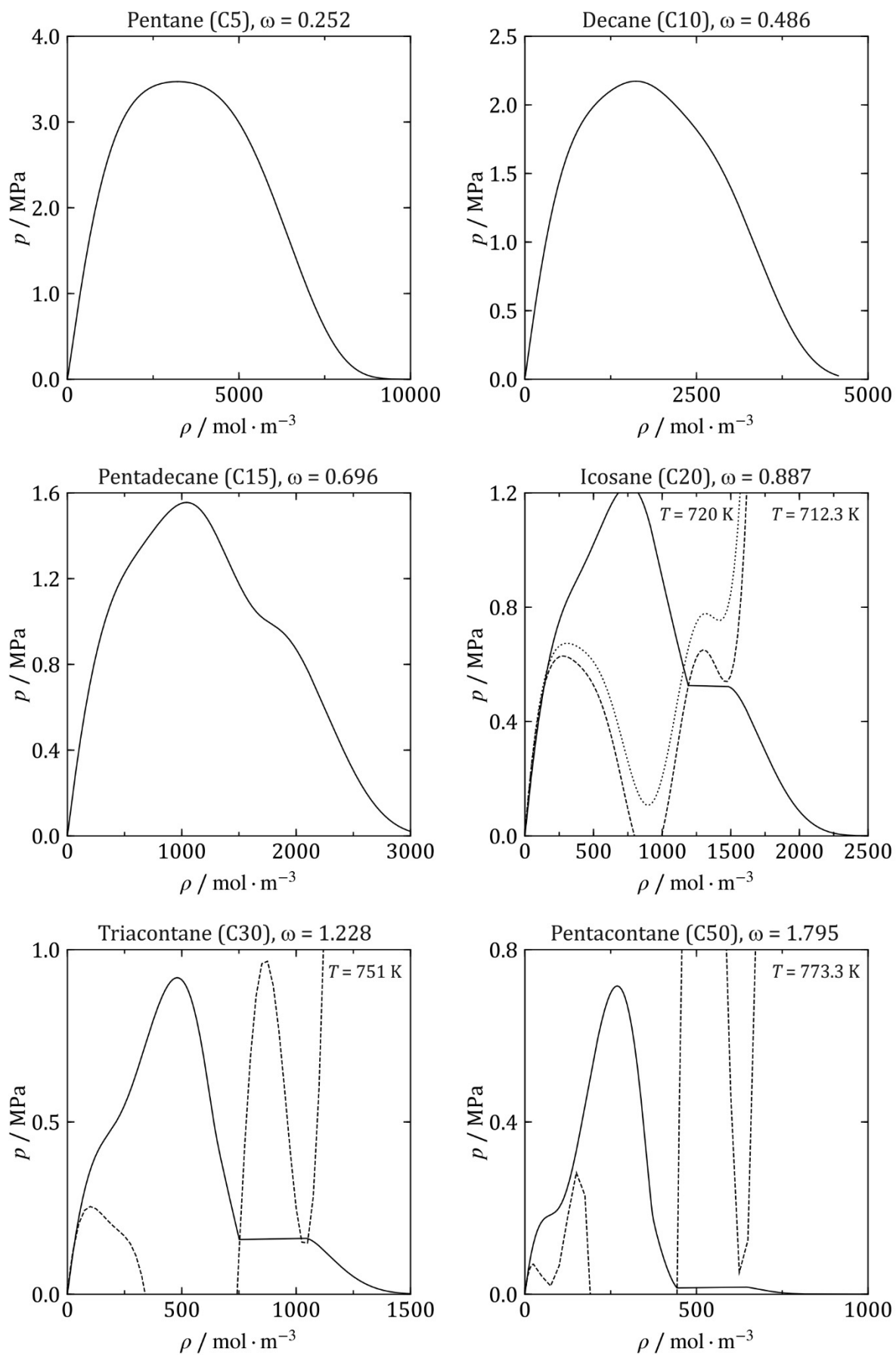


Figure 3.7: p, ρ -diagram for six exemplary fluids of different acentric factors containing the respective phase boundaries and a maximum of two isotherms, calculated with the model of Alexandrov *et al.* [63].

isotherm in the discontinuity ($T = 712.3$ K) as well as a higher isotherm of $T = 720$ K are illustrated. The outer extrema of the isotherm $T = 720$ K no longer overlap with respect to pressure. In order to find the coexisting densities as well as the vapor pressure of a two-phase equilibrium, the corresponding outer extrema are sought, and the pressure is varied until the areas between the individual extrema and the vapor pressure are of the same size in the vapor and liquid region. For icosane at $T = 712.3$ K and $T = 720$ K, a false solution is found, since the phase equilibrium cannot be solved with the outer extrema. Hence, Figure 3.7 shows numerical problems of the model of Alexandrov *et al.* [63] for acentric factors of $\omega > 0.7$ approximately. However, these numerical problems only occur in an elevated temperature region, probably beyond the thermal stability of the fluids. Nevertheless, the incorporation of such an equation of state in a mixture model can lead to the evaluation of the equation of state in this region, as will be explained in the next section.

Since the lubricants which are considered in this work are complex molecules, they are expected to have higher acentric factors than are allowed for use with the model of Span and Wagner [59]. For this reason, the model of Alexandrov *et al.* [63] is chosen for their description.

Alexandrov *et al.* [63] specify an average absolute relative deviation AAD of 0.5% to 1% for the representation of the collected density data in the development of their model. For the representation of vapor pressures, an AAD of 0.5% to 2.5% is given. The authors state an AAD of 1% for the isobaric heat capacity in the liquid, and an AAD of 1% to 4% for the speed of sound.

In sections 5.1.2, 6.1 and 6.2, the results of the adjustments for the lubricants considered in this work are presented.

3.6 Helmholtz Equations of State for Mixtures

In the following, the extension of the multiparameter Helmholtz energy approach for pure fluids presented in the previous section to mixtures is shown in detail.

The separation of the ideal gas behavior from the residual behavior can also be applied for mixtures. However, the molar composition vector \boldsymbol{x} is an additional independent variable which leads to the following expression:

$$a(T, \rho, \mathbf{x}) = a^o(T, \rho, \mathbf{x}) + a^r(T, \rho, \mathbf{x}). \quad (3.104)$$

Analogously to the pure fluid equation, the Helmholtz energy is reduced with the temperature T and the universal gas constant R

$$\alpha(\tau, \delta, \mathbf{x}) = \frac{a(T, \rho, \mathbf{x})}{RT}. \quad (3.105)$$

The ideal gas part can be calculated simply based on the knowledge of the pure fluid equations for the ideal gas behavior and an additional contribution due to ideal mixing with

$$\alpha^o(T, \rho, \mathbf{x}) = \sum_{i=1}^N x_i [\alpha_{o,i}^o(\tau_{o,i}, \delta_{o,i}) + \ln x_i], \quad (3.106)$$

where N is the number of components in the mixture, $\alpha_{o,i}^o$ is the dimensionless ideal-gas part of the Helmholtz free energy, and x_i is the mole fraction of component i in the mixture, respectively. The sum $x_i \ln x_i$ accounts for the entropy of mixing in the ideal mixture. The equations for the ideal part of the pure fluids are evaluated at the reduced variables of the pure fluids:

$$\tau_{o,i} = \frac{T_{c,i}}{T} \quad \text{and} \quad \delta_{o,i} = \frac{\rho}{\rho_{c,i}}. \quad (3.107)$$

The residual part of the mixture can be described as a combination of the pure fluids' residual parts evaluated at the reduced temperature and density of the mixture, which is referred to as an extended corresponding states approach, and possibly an additional departure function:

$$\alpha^r(\tau, \delta, \mathbf{x}) = \underbrace{\sum_{i=1}^N x_i \alpha_{oi}^r(\tau, \delta)}_{\text{residual part pure fluids}} + \underbrace{\sum_{i=1}^{N-1} \sum_{j=i+1}^N F_{ij} x_i x_j \alpha_{ij}^r(\tau, \delta)}_{\text{departure function}}. \quad (3.108)$$

The weighing factor F_{ij} was introduced by Lemmon and Jacobsen [106] for the use of generalized departure functions for a group of binary systems. For a binary case it follows:

$$\alpha^r(\tau, \delta, \mathbf{x}) = \sum_{i=1}^2 x_i \alpha_{oi}^r(\tau, \delta) + F_{12} x_1 x_2 \alpha_{12}^r(\tau, \delta). \quad (3.109)$$

According to the corresponding states principle for mixtures, the residual pure fluid equations are evaluated at the reduced temperature and density determined with the help of

the following equations. This approach leads to the evaluation of the individual pure fluid equations at different temperatures and densities. However, to determine the dimensionless variables τ and δ , reducing functions for the reducing temperature T_r and density ρ_r are required, which depend on the composition of the mixture with

$$\tau = \frac{T_r(\mathbf{x})}{T} \quad \text{and} \quad \delta = \frac{\rho}{\rho_r(\mathbf{x})}. \quad (3.110)$$

For a multicomponent mixture the reducing functions T_r and ρ_r are given by

$$\frac{1}{\rho_r(\mathbf{x})} = \sum_{i=1}^N x_i^2 \frac{1}{\rho_{c,i}} + \sum_{i=1}^{N-1} \sum_{j=i+1}^N 2x_i x_j \beta_{v,ij} \gamma_{v,ij} \frac{x_i + x_j}{\beta_{v,ij}^2 x_i + x_j} \frac{1}{8} \left(\frac{1}{\rho_{c,i}^{1/3}} + \frac{1}{\rho_{c,j}^{1/3}} \right)^3, \quad (3.111)$$

and

$$T_r(\mathbf{x}) = \sum_{i=1}^N x_i^2 T_{c,i} + \sum_{i=1}^{N-1} \sum_{j=i+1}^N 2x_i x_j \beta_{T,ij} \gamma_{T,ij} \frac{x_i + x_j}{\beta_{T,ij}^2 x_i + x_j} \frac{1}{8} \sqrt{T_{c,i} T_{c,j}}. \quad (3.112)$$

The adjustable parameters β_v , γ_v , β_T and γ_T are fitted to experimental data of each binary combination of the mixture's components. For a binary mixture, these functions reduce to

$$\frac{1}{\rho_r(\mathbf{x})} = \sum_{i=1}^2 x_i^2 \frac{1}{\rho_{c,i}} + 2x_1 x_2 \beta_{v,12} \gamma_{v,12} \frac{x_1 + x_2}{\beta_{v,12}^2 x_1 + x_2} \frac{1}{8} \left(\frac{1}{\rho_{c,1}^{1/3}} + \frac{1}{\rho_{c,2}^{1/3}} \right)^3, \quad (3.113)$$

and

$$T_r(\mathbf{x}) = \sum_{i=1}^2 x_i^2 T_{c,i} + 2x_1 x_2 \beta_{T,12} \gamma_{T,12} \frac{x_1 + x_2}{\beta_{T,12}^2 x_1 + x_2} \frac{1}{8} \sqrt{T_{c,1} T_{c,2}}. \quad (3.114)$$

The binary parameters β and γ allow for the description of arbitrary symmetric and asymmetric shapes of these functions which are derived from quadratic mixing rules. They form a composition-dependent surface between the critical parameters for the density and temperature of the pure components in the mixture. The binary parameters obey the following symmetry rules:

$$\beta_{T,ij} = \frac{1}{\beta_{T,ji}}, \quad \beta_{v,ij} = \frac{1}{\beta_{v,ji}}, \quad \gamma_{T,ij} = \gamma_{T,ji}, \quad \gamma_{v,ij} = \gamma_{v,ji} \quad (3.115)$$

If β_T , γ_T , β_v , and γ_v are set to unity, the equations merge into the combining rules by Lorentz and Berthelot as discussed in detail by Kunz *et al.* [79].

Very often, it is sufficient to fit the reducing functions to describe a mixture's non-ideal behavior. In case this is not enough, and more degrees of freedom are required, a departure function can be introduced. However, to fit this additional function, a good experimental data base concerning quality as well as quantity is mandatory.

A common functional form of the departure function is shown below:

$$\begin{aligned} \alpha_{ij}^{r(\tau,\delta)} = & \sum_{k=1}^{K_{\text{Pol},ij}} n_{k,ij} \tau^{t_{k,ij}} \delta^{d_{k,ij}} + \sum_{k=K_{\text{Pol},ij}+1}^{K_{\text{Pol},ij}+K_{\text{Exp},ij}} n_{k,ij} \tau^{t_{k,ij}} \delta^{d_{k,ij}} \exp(-\delta^{l_{k,ij}}) \\ & + \sum_{k=K_{\text{Pol},ij}+K_{\text{Exp},ij}+K_{\text{GBS},ij}}^{K_{\text{Pol},ij}+K_{\text{Exp},ij}+K_{\text{GBS},ij}} n_{k,ij} \tau^{t_{k,ij}} \delta^{d_{k,ij}} \exp\left(-\eta_{k,ij}(\delta - \epsilon_{k,ij})^2 - \beta_{k,ij}(\tau - \gamma_{k,ij})^2\right). \end{aligned} \quad (3.116)$$

These functions contain polynomial, exponential, and Gaussian-Bell shaped terms. The latter have just recently been introduced into these mixture models by Bell *et al.* [107]. The GERG [80] and EOS-CG [81] models both incorporate an additional type of exponential terms that has not been used in this work.

Theoretically, the mixture models based on this approach are independent of the utilized pure fluid equation, since the mixture model should exclusively describe the mixing behavior. The mixture model should not compensate shortcomings of the pure fluid equations, which in practice is impossible to ensure. Hence, if there is a new pure fluid equation available that seems superior to the original one, as is the case for ethanol and water, it is usually useful to refit an existing mixture model.

4 A New Model for Ethanol-Water Mixtures

In this chapter, a new model for ethanol-water mixtures is presented. It is based on the most current pure fluid equations of state, the equation of Wagner and Pruß [20] for water and the equation of Schroeder *et al.* [3] for ethanol. In 2008, Lemmon [4] developed a mixture model that utilizes the now outdated pure fluid equation of state for ethanol of Dillon *et al.* [21]. The equation of Schroeder *et al.* [3] was fitted to a broader experimental data base and has reduced uncertainties. Well-built pure fluid equations of state should be exchangeable, since a mixture model only describes the mixing behavior. Figure 4.1 illustrates relative density deviations of the mixture model of Lemmon [4] calculated with both ethanol equations of state from selected experimental data. On top, the mixture model is evaluated with the originally utilized pure fluid equation of state. At the bottom, the pure fluid equation describing ethanol has been exchanged and the equation of Schroeder *et al.* [3] is used instead of

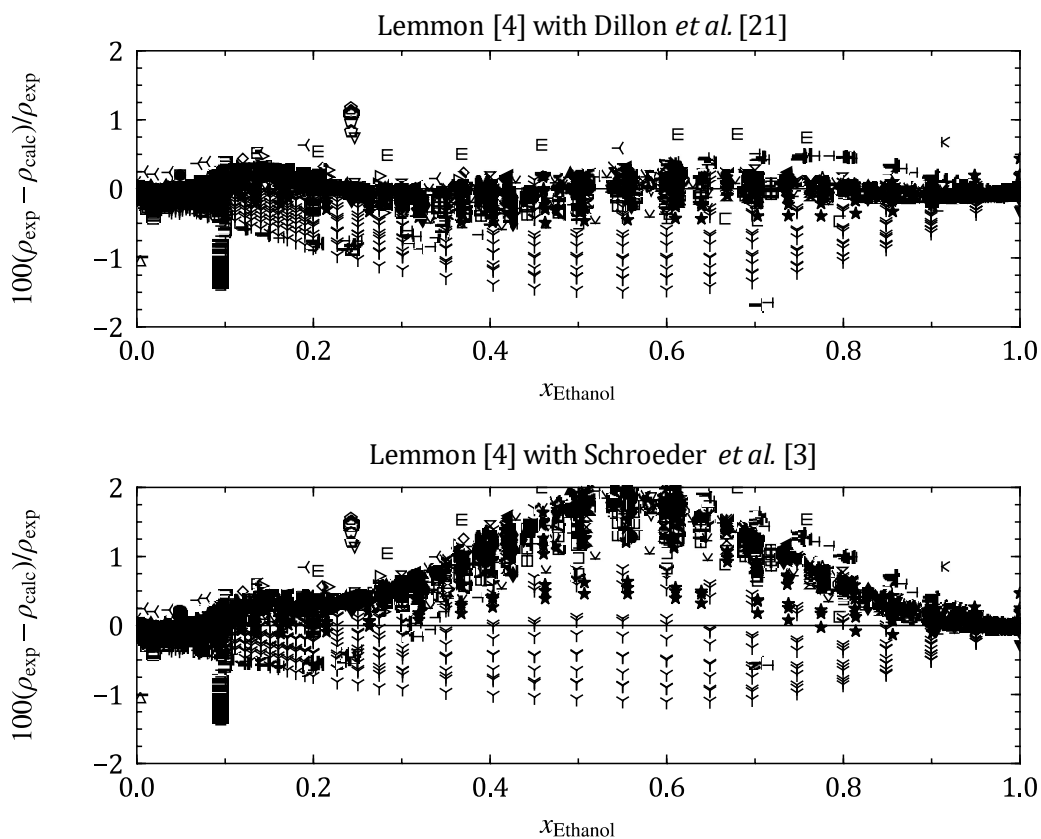


Figure 4.1: Relative density deviations of the mixture model of Lemmon [4] from selected exemplary experimental data. At the top, the original setup of the mixture model that uses the ethanol equation of state of Dillon *et al.* [21] is plotted. At the bottom, the ethanol equation of Schroeder *et al.* [3] was used instead.

the equation of Dillon *et al.* [21]. It is evident that the change of the pure fluid equation of state for this binary mixture has a strong, negative influence on the description of these mixture densities due to larger differences in the pure fluid equations than is typical with many other fluids.

A new mixture model, which incorporates the most accurate equations of state for the pure fluids involved, was developed in this work. In the following, the experimental data for ethanol-water mixtures found in the literature are presented. Subsequently, the fitting technique that was used to develop the new model is discussed. Finally, the new model is presented and evaluated based on the available experimental data. Additionally, the data and the new model are compared to the model of Lemmon [4].

4.1 Available Experimental Data

The development of an equation of a state depends on the availability of reliable experimental data for the thermodynamic properties of the fluid or fluid mixture. The knowledge of as many different properties as possible in a wide temperature, pressure, and composition range is desirable to describe the fluids behavior as accurately as possible. The quality of the equation strongly depends on the quality, quantity and location of the data.

There are many data sets for ethanol-water mixtures published in the literature including phase equilibria, density, speed of sound, isobaric heat capacity, and excess enthalpy. Table 4.1 gives an overview of the data published for ethanol-water mixtures.

Table 4.1: Available experimental data for ethanol-water mixtures.

| Data type | Data sets | Data points | T_{\min} / K | T_{\max} / K | p_{\min} / MPa | p_{\max} / MPa |
|------------------------|-----------|-------------|-----------------------|-----------------------|-------------------------|-------------------------|
| Phase equilibria | 81 | 2613 | 273.15 | 623.11 | <0.1 | 8.97 |
| Density | 56 | 5599 | 273.15 | 523.15 | 0.1 | 8.64 |
| Speed of sound | 7 | 68 | 293.12 | 606.3 | 0.1 | 0.1 |
| Isobaric heat capacity | 5 | 447 | 241.15 | 308.15 | 0.1 | 0.1 |
| Excess enthalpy | 24 | 1362 | 273.15 | 548 | 0.1 | 20 |

The phase behavior of this mixture has been investigated thoroughly throughout the last decades. There are many data sets available especially at atmospheric pressure. For elevated pressures, the quantity of data sets for phase equilibria of ethanol-water mixtures reduces drastically.

At first glance, the density of ethanol-water mixtures seems very well investigated. Unfortunately, this is only true for the liquid phase. Only Bazaev *et al.* [108] and Abdurashidova *et al.* [109] measured vapor phase densities and densities at high temperatures. In this region, there is only one further experimental data set by Safarov and Shakhverdiev [110] available.

Similar to the density, there are only homogeneous liquid speed-of-sound data available in the literature. Those few data sets are limited to atmospheric pressure. This also corresponds to the isobaric heat capacity. There are only homogeneous liquid phase data at atmospheric pressure available, which only cover a very narrow temperature range. Some of the authors published excess isobaric heat capacities. For fitting and comparison purposes, those values have been transferred to the full heat capacity of the mixture with the help of the pure fluid equations [3,20].

The excess enthalpy of ethanol-water mixtures has been well investigated. In contrast to the speed of sound and the isobaric heat capacity, there are many data sets available that agree well in the description of the mixture behavior. The available data sets cover a broad temperature and pressure range.

4.2 Fitting Process

Although the introduced empirical model is explicit in the Helmholtz energy as a function of temperature, density, and composition, there is no information on the shape of this thermodynamic surface. Since the Helmholtz energy cannot be measured experimentally, the energy surface is exclusively shaped by fitting the Helmholtz energy derivatives to experimental data. Therefore, it is crucial to ensure that derivatives with respect to all independent variables are included; the higher the order, the better. However, the uncertainty of the composition plays a major role in the fitting process. A significant error in composition can be problematic to fit several fluid properties.

The relations between the available experimental data and the derivatives are given in Table 4.2.

In principle, there are two ways to fit the parameters of empirical multiparameter models. They can either be fit linearly or non-linearly. Numerous Helmholtz equations of reference quality have been published by the Wagner group in the 1980s and 1990s that have been developed with a combination of linear and non-linear fitting techniques. Additionally, these equations were optimized with the help of a sophisticated

Table 4.2: Thermodynamic properties available as experimental data and the involved partial derivatives of the reduced Helmholtz free energy α .

| Thermodynamic property | Related derivatives of $\alpha(\tau, \delta, \mathbf{x})$ |
|---|--|
| p, ρ, T relation $p(T, \rho, \mathbf{x})$ | α_{δ}^r |
| Fugacity $f_i(T, \rho, \mathbf{x})$ for VLE calculation | $\alpha_{\delta}^r, \alpha_{\delta\delta}^r, \alpha_{\tau\delta}^r, \alpha_{\tau}^r, \alpha_{\tau\tau}^r, \alpha_x^r, \alpha_{xx}^r$ |
| Speed of sound $w(T, p, \mathbf{x})$ | $\alpha_{\delta}^r, \alpha_{\delta\delta}^r, \alpha_{\tau\delta}^r, \alpha_{\tau\tau}^r, \alpha_{\tau\tau}^o$ |
| Isobaric heat capacity $c_p(T, p, \mathbf{x})$ | $\alpha_{\delta}^r, \alpha_{\delta\delta}^r, \alpha_{\tau\delta}^r, \alpha_{\tau\tau}^r, \alpha_{\tau\tau}^o$ |
| Excess enthalpy $h^E(T, p, \mathbf{x})$ | $\alpha_{\delta}^r, \alpha_{\tau}^r, \alpha_{\tau}^o$ |

combinatory algorithm based on the work of Setzmann and Wagner [54]. This algorithm determines the optimal mathematical structure of the equation from a bank of terms. The bank of terms contains numerous terms that differ in temperature and density exponents and potentially the form of terms itself, e.g. polynomial or exponential. Only the coefficients are directly fitted to data. However, a precorrelation for the density is required since Setzmann and Wagner [54] used a linear optimization technique. Consuming significantly more time and resources, a non-linear method was applied in the last iteration only to refit the coefficients n_i non-linearly. The mixture model for natural gases (the GERG-2008 of Kunz and Wagner [80]) was developed with the optimization algorithm of Setzmann and Wagner [54]. For more details on this fitting method, see Wagner and Pruß [20] or Span [59].

The non-linear fitting algorithm that was used for the development of the mixture models in this work has been developed and was provided by Dr. Eric W. Lemmon at the National Institute of Standards and Technology (NIST) in Boulder, Colorado [55]. This algorithm has been used successfully for the development of many pure fluid equations as well as for the extensive mixture model EOS-CG of Gernert and Span [81].

By means of the non-linear algorithm, all thermophysical properties can directly be integrated in the fit in the original configuration of the experimental setup. Thus, the independent variables of the data sets do not need to be identical to those of the model. Another advantage of non-linear algorithms is the possibility to use flexible constraints based on inequalities instead of direct comparisons. With the help of such constraints, regions on the thermodynamic surface without experimental information can be forced to exhibit physically reasonable behavior. Additionally, the extrapolation behavior can be controlled to show reasonable trends.

There are numerous adjustable parameters simultaneously included in the fit: the parameters of the reducing functions (equations (3.113) and (3.114)), the coefficients of the departure function as well as the temperature exponents, and the Gaussian bell-shaped term parameters (equation (3.116)). It is important to mention that there are no density exponents included in the fit. These parameters are exclusively manipulated by hand to ensure that they always have positive integer values in order to maintain physical correct extrapolation behavior of the equation in the zero-density limit. Technically, density exponents can be considered in the fit, but the mandatory final rounding often leads to worse solutions. The flexibility of the equation is thus limited and depends on the correlator's experience. The temperature exponents are restricted to positive values of a considerate magnitude below ten to guarantee reasonable extrapolation behavior.

The development of a binary mixture model is an iterative procedure during which the deviation between the current equation and the selected experimental data as well as the physical constraints have to be evaluated repeatedly. As a measure of quality, the sum of square SSQ is introduced as

$$\text{SSQ} = \sum_{i=1}^I W_{\rho,i} F_{\rho,i}^2 + \sum_{j=1}^J W_{p,j} F_{p,j}^2 + \sum_{k=1}^K W_{w,k} F_{w,k}^2 + \dots, \quad (4.1)$$

with W being the assigned weight of the considered data point or constraint. The relative error F of an arbitrary property z is defined as

$$F_z = \frac{z_{\text{exp}} - z_{\text{EOS}}}{z_{\text{exp}}}, \quad (4.2)$$

where z_{exp} is the experimental data point and z_{EOS} is the calculated value from the equation of state. The different contributions to the SSQ of the selected and weighted experimental data are listed in Table 4.3.

The fitting algorithm minimizes the SSQ by adjusting the parameters of the mixture model. It is important to keep in mind that the absolute value of the SSQ depends on the weights assigned to the data points. Ideally, each data point would be weighted according to its experimental uncertainty. Unfortunately, many publications either do not contain a discussion of the uncertainty at all or underestimate it significantly. Therefore, the correlator has to observe not only the SSQ but also the relative change

of its value during the fit. Another important way to evaluate the fitting progress is to observe deviation plots and various property diagrams, e.g. p over ρ or p over x_i .

Table 4.3: Available experimental mixture data used to fit the mixture model, and their contribution to the sum of squares.

| Thermodynamic property | Contribution to SSQ |
|---|---|
| Density $\rho(p, T, \mathbf{x})$ | $F_{\rho}^2 = \left(\frac{p_{\text{exp}} - p_{\text{EOS}}(T, \rho, \mathbf{x})}{p_{\text{exp}}} \left(\frac{\partial p}{\partial \rho} \right)_{T, \mathbf{x}}^{-1} \right)^2$ |
| Pressure $p(\rho, T, \mathbf{x})$ | $F_p^2 = \left(\frac{p_{\text{exp}} - p_{\text{EOS}}(T, \rho, \mathbf{x})}{p_{\text{exp}}} \right)^2$ |
| VLE data $p, T, \mathbf{x}', \mathbf{x}''$ given | $F_{pT\mathbf{x}'\mathbf{x}''}^2 = \sum_{i=1}^2 \left(\frac{f_i'(p, T, \mathbf{x}') - f_i''(p, T, \mathbf{x}'')}{1 + f_i'(p, T, \mathbf{x}')} \right)^2$ |
| VLE data p, T, \mathbf{x}' or p, T, \mathbf{x}'' given | $F_{pT\mathbf{x}'}^2 = \sum_{i=1}^2 (x'_{i,\text{exp}} - x'_{i,\text{EOS}})^2 + \left(\frac{p_{\text{exp}} - p_{\text{EOS}}(\rho', T, \mathbf{x}')}{p_{\text{exp}}} \right)^2$ $F_{pT\mathbf{x}''}^2 = \sum_{i=1}^2 (x''_{i,\text{exp}} - x''_{i,\text{EOS}})^2 + \left(\frac{p_{\text{exp}} - p_{\text{EOS}}(\rho'', T, \mathbf{x}'')}{p_{\text{exp}}} \right)^2$ |
| Speed of sound $w(T, p, \mathbf{x})$ | $F_w^2 = \left(\frac{w_{\text{exp}} - w_{\text{EOS}}(T, p, \mathbf{x})}{w_{\text{exp}}} \right)^2$ |
| Isobaric heat capacity $c_p(T, p, \mathbf{x})$ | $F_{c_p}^2 = \left(\frac{c_{p,\text{exp}} - c_{p,\text{EOS}}(T, p, \mathbf{x})}{c_{p,\text{exp}}} \right)^2$ |
| Excess enthalpy $h^E(T, p, \mathbf{x})$ | $F_{h^E}^2 = \left(\frac{h^E_{\text{exp}} - h^E_{\text{EOS}}(T, p, \mathbf{x})}{h^E_{\text{exp}}} \right)^2$ |

The used non-linear fitting algorithm has the ability to adjust both coefficients and exponents of an equation of state at the same time. All types of thermodynamic data can be fit simultaneously without any previous linearization or pre-correlations. Additionally, the software allows for the use of a wide variety of constraints and control parameters. A detailed discussion of this minimization algorithm and its application on mixture models is given in Gernert [111].

Fitting ethanol-water mixtures is considerably challenging, since both components are complex fluids. Water shows a maximum in density in the liquid phase at $T \approx 277$ K. This phenomenon affects all kinds of properties and consequently many absolute property plots, which differ in shape from those of simpler fluids. Additionally, Wagner and Pruß [20] utilized non-analytic terms in their pure fluid equation, which are known to be challenging in mixture models. The very high temperature and density exponents of this equation can be problematic especially in the description of low temperatures and

high densities. Ethanol is strongly self-associating and cross-associates with water. As a result, some of the excess properties of the mixture change drastically with temperature and composition.

In the course of the adjustment of the newly developed mixture model, several constraints were used to enforce a specific behavior. Once the model became stable, the final fit used only one constraint. The isotherm $T = 800$ K was constrained to have positive curvature with respect to $(Z - 1)/\rho$ over density from vapor-like densities to liquid-like densities, as shown in Figure 4.2 in the following section.

4.3 The New Mixture Model

The new mixture model was developed with non-linear multiproperty fitting techniques. The model was fitted to selected experimental density data including phase equilibria, excess enthalpies, speeds of sound, and isobaric heat capacities. Additionally, constraints were added to control the qualitative behavior of the model.

Table 4.4 presents the parameters of the new reducing functions as described in equations (3.113) and (3.114).

Table 4.4: Parameters of the new reducing functions according to equations (3.113) and (3.114).

| β_T | γ_T | β_v | γ_v |
|-----------|------------|-----------|------------|
| 0.9866 | 0.9971 | 1.0124 | 0.9558 |

All four parameters are very close to unity. Table 4.5 gives the parameters of the newly fitted departure function, which contains polynomial, exponential, and Gaussian-bell shaped terms, as described in equation (3.116). All employed parameters show reasonable values.

Table 4.5: Parameters of the new departure function according to equation (3.116).

| i | n_i | t_i | d_i | l_i | η_i | β_i | ε_i | γ_i |
|-----|----------|-------|-------|-------|----------|-----------|-----------------|------------|
| 1 | -0.2726 | 1.68 | 1 | 0 | | | | |
| 2 | 0.027 | 0.73 | 4 | 0 | | | | |
| 3 | -0.01483 | 4.55 | 3 | 1 | | | | |
| 4 | 1.773 | 1.17 | 2 | | 0.585 | 0.19 | 1.11 | 1.08 |
| 5 | 6.9 | 0.15 | 1 | | 0.510 | 2.12 | 1.64 | 0.75 |
| 6 | -6.42 | 0.43 | 1 | | 0.700 | 1.22 | 1.64 | 1.34 |

For comparison the parameters of the preliminary mixture model of Lemmon are given in Table 4.6 and Table 4.7.

Table 4.6: Parameters of the reducing functions of Lemmon [4].

| β_T | γ_T | β_v | γ_v |
|-----------|------------|-----------|------------|
| 0.971761 | 0.93996768 | 1.0624092 | 0.8687762 |

The model of Lemmon [4] contains a generalized departure function with $F_{ij} = 0.3285109$ (see equation (3.109)). This departure function utilizes rather high temperature and density exponents and exclusively consists of exponential terms.

Table 4.7: Parameters of the departure function of Lemmon [4].

| n_i | t_i | d_i | l_i |
|-----------|-------|-------|-------|
| 1.09765 | 0.26 | 2 | 1 |
| 1.94679 | 7.3 | 3 | 2 |
| -2.16809 | 5.3 | 5 | 2 |
| -0.137077 | 2.3 | 5 | 1 |
| 0.0486690 | 0.7 | 7 | 1 |
| 1.04024 | 3.3 | 6 | 2 |

Figure 4.2 illustrates c_v^r over temperature, PIP over temperature, and $(Z - 1)/\rho$ over density for the pure fluid equations of state for ethanol [3] (a) and water [20] (b), and for the mixture model of Lemmon [4] (c) and the mixture model developed in this work (d). These properties are chosen, since they are often used to control the qualitative and extrapolation behavior of an equation of state as introduced by Gao *et al.* [112] as well as Thol and Lemmon [113]. It is important to consider the pure fluid equations of state incorporated in the development of a mixture model in order to not “correct” a special effect of a pure fluid equation that contributes to the mixture property.

For ethanol (a), there are several differences from the classical course of these graphs. The association occurring in the liquid phase enforces a maximum of the bubble line for c_v^r and the PIP at $T \approx 400$ K. In the vicinity of the critical point, the bubble line of the ethanol equation shows a little spike which has no physical explanation. The $(Z - 1)/\rho$ over density plot is shaped as expected [112]. For water (b), the c_v^r over temperature plot looks as expected as well. At the critical point, the non-analytic terms

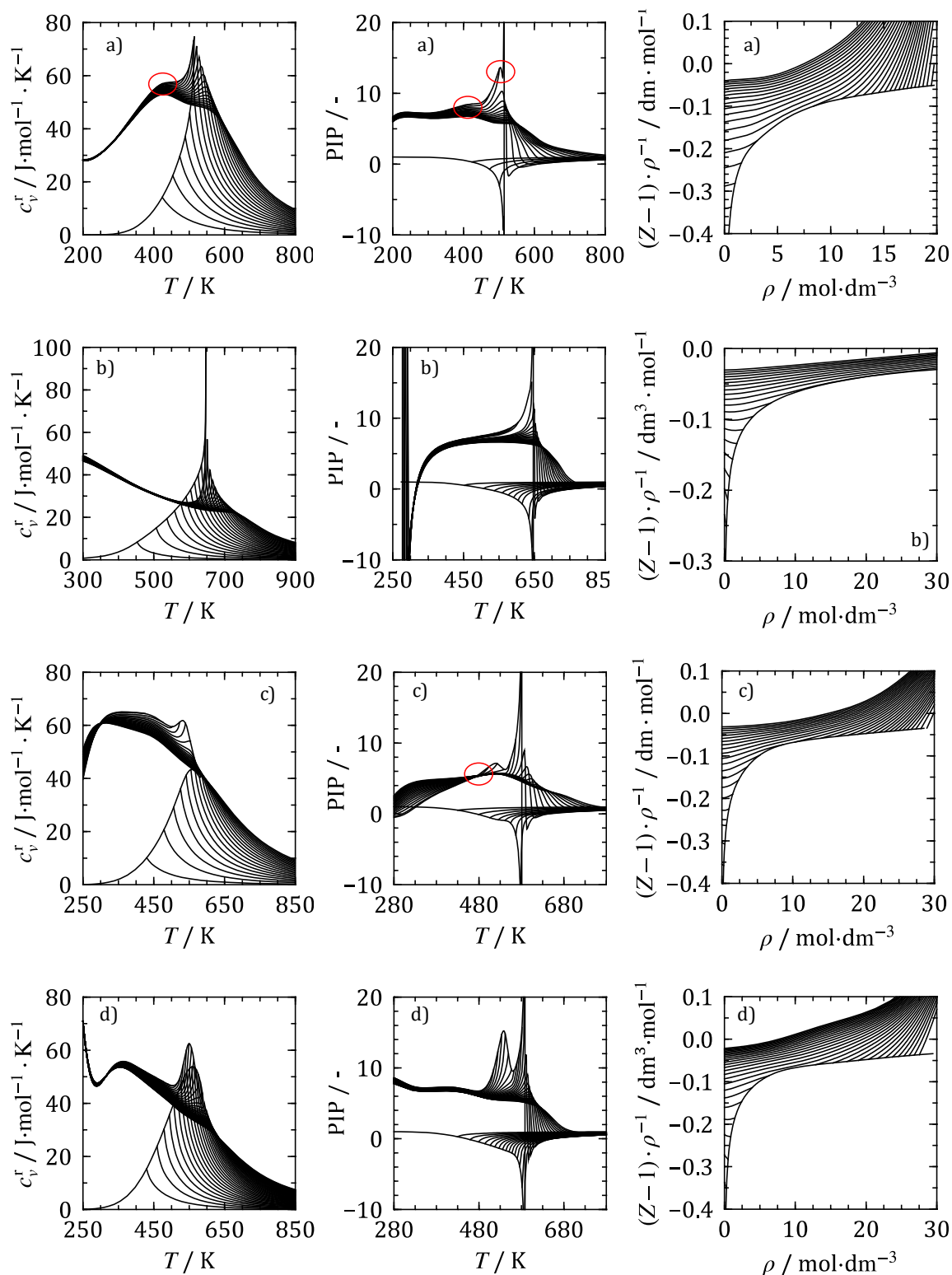


Figure 4.2: c_v^t over temperature including the saturation lines as well as several isobars, PIP over temperature including the saturation lines as well as several isobars, and $(Z-1)/\rho$ over density including the saturation lines as well as several isotherms calculated from the pure fluid equations for ethanol [3] (a) and water [20] (b), and from the mixture model of Lemmon [4] (c) and the mixture model developed in this work (d) for $x_{\text{Ethanol}} = 0.5$.

cause the maximum to go to infinity as proposed by theory. The PIP over temperature plot of the water equation of state reveals a pole in the low temperature region. The isotherms at a lower temperature level in the $(Z-1)/\rho$ over density plot show a

negative slope in the gaseous region, which is unusual. Both effects are also found for the current heavy water equation of state of Herrig *et al.* [114], which does not use as extensively high temperature and density exponents as are used in the water equation of state of Wagner and Pruß [20]. Hence, these effects seem to be caused by the properties of these fluids themselves.

For the model of Lemmon [4] (c), c_v^r shows a positive slope and negative curvature with respect to increasing temperature at low temperatures. The pressure dependence of the PIP is inverted at $T \approx 480$ K. The mixture model of Lemmon [4] includes very high temperature exponents that contribute heavily in the liquid region and might cause these effects. Similar to the water equation of state [20], both mixture models (c and d) show isotherms with negative slopes in the lower temperature region for $(Z - 1)/\rho$ over density. The PIP and c_v^r over temperature plots calculated from the new mixture model present a reasonable behavior.

4.4 Comparison to Experimental Data

Ideally, the new equation should be able to reproduce all experimental data within their uncertainty of measurement. To assess the representation with the aid of a statistical evaluation, the percentage deviation of a measuring point z of any thermodynamic property from the equation of state is calculated according to the following equation:

$$\Delta z = 100 \cdot \left(\frac{z_{\text{exp}} - z_{\text{EOS}}}{z_{\text{exp}}} \right). \quad (4.3)$$

For the comparison of complete data sets, the average absolute relative deviation (AAD) is calculated for each author and property individually:

$$\text{AAD} = \frac{1}{N} \sum_{i=1}^N |\Delta z_i|, \quad (4.4)$$

N being the amount of experimental data points of the respective author of the respective thermodynamic property.

However, potential systematic deviations of the model or a data set cannot be detected by an exclusively statistical evaluation. In contrast, graphical comparisons of the new model with the experimental data can reveal these effects. Therefore, both methods

are used in the following section. Depending on the property of interest, the plots illustrate deviations or absolute values.

4.4.1 Phase Equilibria

Numerous experimental data sets have been published that investigated the phase equilibria of ethanol-water mixtures. Unfortunately, most of them do not include a comprehensive and reasonable discussion of the experimental uncertainty. Therefore, deviations are presented either based on the saturation temperature or saturation pressure. Subsequently, the AAD of all data sets are evaluated in Table 4.8 with respect to the saturation temperature and saturation pressure.

Figure 4.3 presents a T, x -diagram with experimental data and values calculated from the new mixture model and from the model of Lemmon [4] for $p = 0.101325$ MPa as well as relative deviations between these data and the new mixture model. Many data sets are available that agree well with each other as well as with the new mixture model. The representation of these data by the model of Lemmon [4] is nearly identical to the representation by the new model. The experimental data on the bubble and dew line is depicted within $\pm 0.2\%$ with respect to the saturation temperature by the new model.

Figure 4.4 illustrates a p, x -diagram with experimental data and values calculated from both mixture model for $p = 0.101325$ MPa as well as relative deviations between these data and the new mixture model. As for the T, x -diagram at atmospheric pressure, there is no difference to be seen in the representation of these experimental data by the new model or the model of Lemmon [4]. The deviations between the data of Pemberton and Mash [115] and Kurihara *et al.* [116] with respect to the saturation pressure on the dew and bubble lines are lower than $\pm 0.5\%$.

Kurihara *et al.* [116] state individual uncertainties for their temperature, pressure, and composition measurements, as their technique involves the analysis of vapor and liquid samples. The combined uncertainty is estimated to be ± 0.003 with respect to the ethanol mole fraction in the vapor phase and ± 0.0045 in the liquid phase. Exemplary calculations prove that the new model represents these data within their estimated uncertainty (± 0.0021 and ± 0.0006 at $p = 0.023$ MPa). The same analysis could be pursued for the analogous data of Pemberton and Mash [115], which are also represented within their estimated uncertainty.

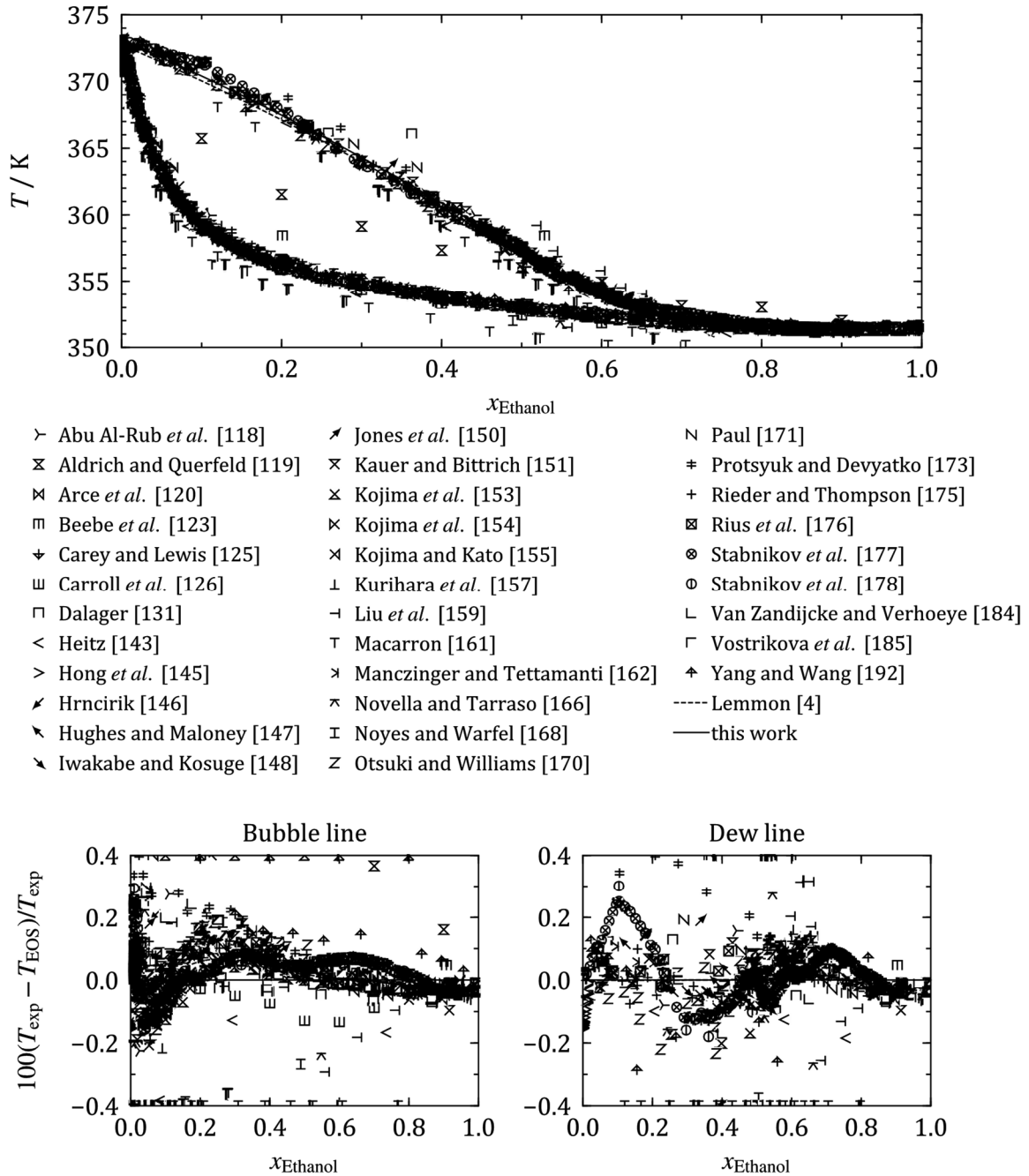


Figure 4.3: Experimental vapor-liquid equilibrium data at $p = 0.101325$ MPa and calculated values from the new model, and from the model of Lemmon [4] (dashed curve). Bottom: Relative dew and bubble point temperature deviations between experimental data and the new mixture model over the ethanol fraction.

In Figure 4.5, experimental data describing the phase equilibrium at $T = 523.15$ K as well as calculated values from the compared models are presented. The new model follows the data more accurately than the model of Lemmon [4], which overestimates the saturation pressure. The new model represents the available data within $\pm 2\%$ with respect to the saturation pressure. Barr-David and Dodge [117] published an extensive data set with high temperature phase equilibrium data. Their data at this isotherm agree well with the data published by other authors. However, the uncertainty of their

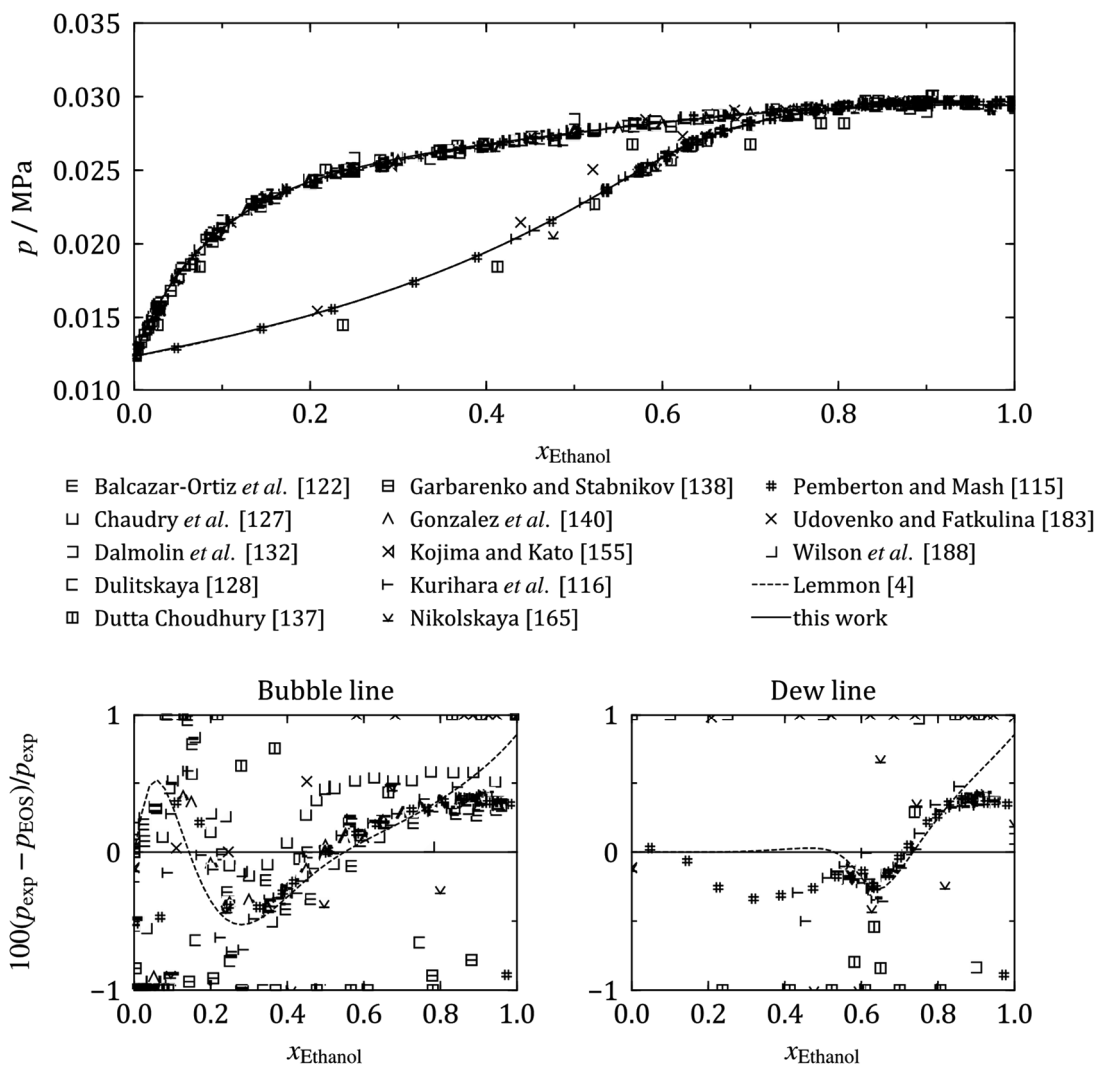


Figure 4.4: Experimental vapor–liquid equilibrium data at $T = 323.15$ K and calculated values from the new model, and from the model of Lemmon [4] (dashed curve). Bottom: Relative dew and bubble point pressure deviations between experimental data and the new mixture model over the ethanol fraction.

experimental technique is estimated to be of considerable magnitude. The analysis of the liquid and vapor samples was conducted by a determination of the respective liquid sample densities at $T = 298.15$ K and they do not further discuss the transformation to composition, which was based on a theoretical property model.

Figure 4.6 shows high temperature phase equilibria in a p - x -diagram for three isotherms. The absolute values are shown as well as relative deviations in the saturation pressure between the experimental data and the new model. Unfortunately, there are only few data sets available in this region which do not agree very well. The data of Barr-David and Dodge [117] were preferred in the fitting process, since they agree well with others in lower temperature regions. The model deviates from the data with -2% to $+3\%$, which is also assumed to be the approximate uncertainty of the data. The deviations do not increase significantly with increasing temperature but with increasing

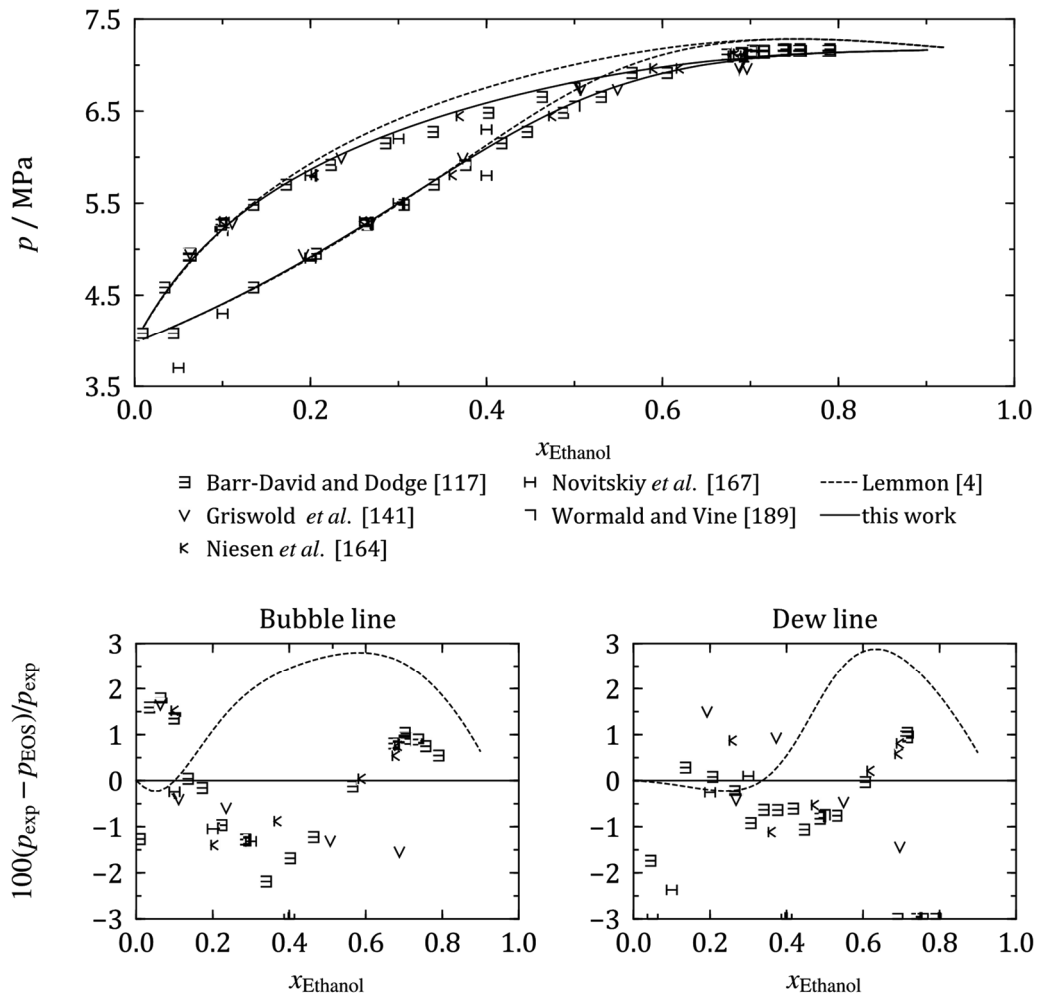


Figure 4.5: Experimental vapor–liquid equilibrium data at $T = 523.15$ K and calculated values from the new model, and from the model of Lemmon [4] (dashed curve). Bottom: Relative dew and bubble point pressure deviations between experimental data and the new mixture model over the ethanol fraction.

composition, which is caused by the tendency to prolong the phase boundaries of the new mixture model. The model of Lemmon [4] exhibits the same behavior. Due to slightly rotated saturation lines in the p, x diagram, the new model better represents the dew lines, whereas the model of Lemmon [4] agrees slightly better with the data on the bubble line.

The uncertainty of the new model is estimated to be $\pm 0.5\%$ in saturation pressure for temperatures $T \leq 400$ K. From $T > 400$ K to $T \leq 550$ K, these deviations are assessed with $\pm 2\%$ increasing to $\pm 3\%$ for higher temperatures.

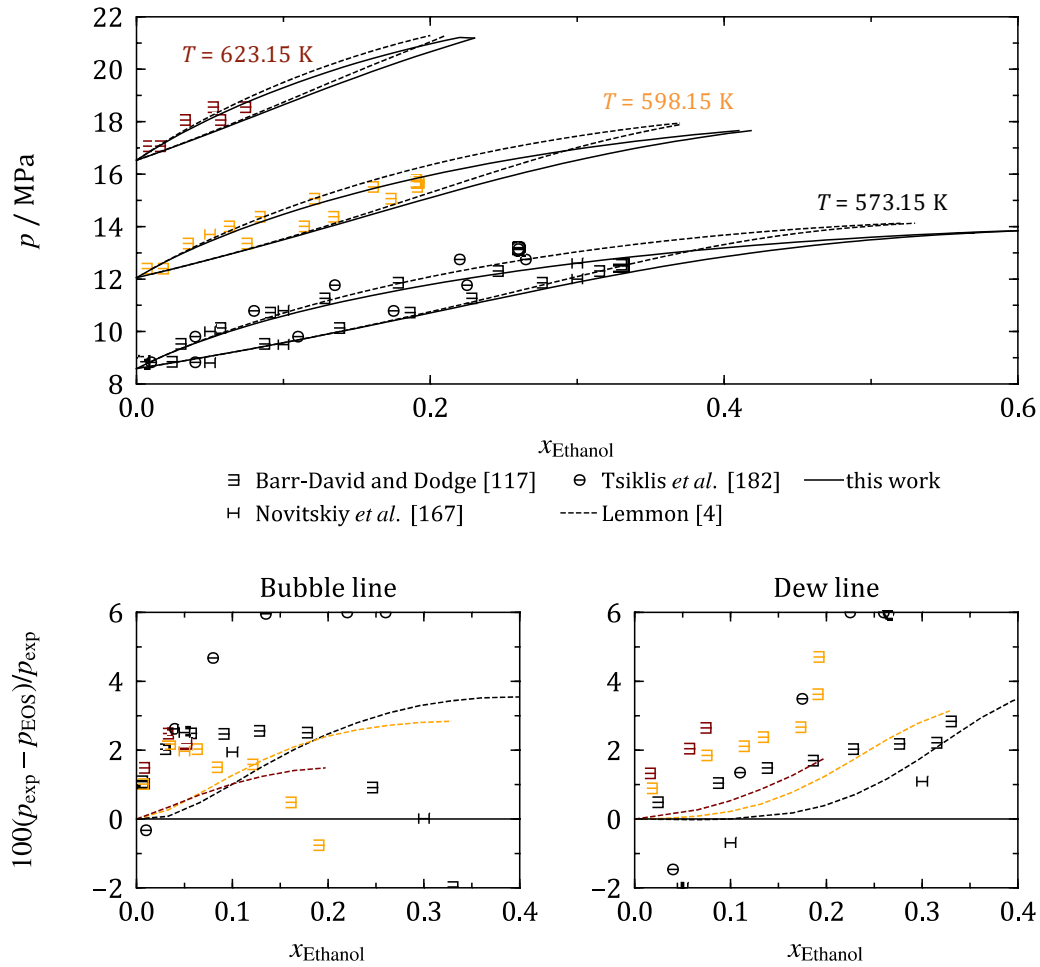


Figure 4.6: Experimental vapor–liquid equilibrium data at $T = 573.15 \text{ K}$, $T = 598.15 \text{ K}$, and $T = 623.15 \text{ K}$, and calculated values from the new model, and from the model of Lemmon [4] (dashed curve). Bottom: Relative dew and bubble point pressure deviations between experimental data and the new mixture model over the ethanol fraction.

Table 4.8: Absolute average deviation of the new mixture model from the experimental VLE data.

| Author | Nr- Pts | Pts-x | Pts-y | $(T_{\min} - T_{\max})$ / K | $(p_{\min} - p_{\max})$ / MPa | AAD(T_s) / % | | AAD(p_s) / % | |
|------------------------------------|------------|-------|-------|--------------------------------|----------------------------------|------------------|--------|------------------|--------|
| | | | | | | bub. | dew | bub. | dew |
| Abu Al-Rub <i>et al.</i> [118] | 11 | 11 | 9 | 351.27 - 373.14 | 0.1 | 0.64 | 0.05 | 6.191 | 0.648 |
| Aldrich and Querfeld [119] | 10 | 10 | 0 | 351.53 - 365.73 | 0.1 | 1.427 | 0 | 17.773 | 0 |
| Arce <i>et al.</i> [120] | 23 | 23 | 0 | 351.42 - 373.15 | 0.1 | 0.307 | 0 | 2.999 | 0 |
| Babinets <i>et al.</i> [121] | 4 | 0 | 4 | 351.53 - 351.93 | 0.1 | 0 | 0.195 | 0 | 2.766 |
| Balcazar-Ortiz <i>et al.</i> [122] | 26 | 26 | 0 | 323.14 - 323.14 | 0.01 - 0.03 | 0.243 | 0 | 2.558 | 0 |
| Barr-David and Dodge [117] | 82 | 79 | 77 | 423.11 - 623.11 | 0.56 - 18.55 | 0.197 | 0.174 | 1.768 | 1.585 |
| Beebe <i>et al.</i> [123] | 70 | 70 | 70 | 307.74 - 358.43 | 0.01 - 0.1 | 0.522 | 0.468 | 8.814 | 7.924 |
| Bloom <i>et al.</i> [124] | 36 | 18 | 18 | 351.33 - 367.43 | 0.1 | 0.061 | 0.932 | 0.828 | 11.284 |
| Carey and Lewis [125] | 14 | 14 | 14 | 293.25 - 295.59 | 0.1 | 20.95 | 20.965 | 94.971 | 95.111 |
| Carroll <i>et al.</i> [126] | 11 | 11 | 0 | 351.33 - 373.12 | 0.1 | 0.618 | 0 | 5.901 | 0 |
| Chaudhry <i>et al.</i> [127] | 24 | 24 | 0 | 323.14 | 0.01 - 0.03 | 0.268 | 0 | 2.836 | 0 |
| Dutta Choudhury [128] | 12 | 12 | 12 | 323.14 | 0.01 - 0.03 | 0.162 | 0.177 | 2.632 | 2.896 |

Table 4.8 continued.

| Author | Nr- | | | $(T_{\min} - T_{\max})$ / K | $(p_{\min} - p_{\max})$ / MPa | AAD(T_s) / % | | AAD(p_s) / % | |
|------------------------------------|-----|-------|-------|--------------------------------|----------------------------------|------------------|-------|------------------|--------|
| | Pts | Pts-x | Pts-y | | | bub. | dew | bub. | dew |
| Christensen [129] | 6 | 6 | 0 | 322.05 - 372.25 | 0.01 - 0.1 | 0.039 | 0 | 0.548 | 0 |
| Cristino <i>et al.</i> [130] | 74 | 74 | 74 | 363.3 - 423.7 | 0.13 - 0.99 | 0.137 | 0.087 | 1.619 | 1.041 |
| Dalager [131] | 27 | 27 | 27 | 351.33 - 373.12 | 0.1 | 0.034 | 0.079 | 0.471 | 1.129 |
| Dalmolin <i>et al.</i> [132] | 28 | 0 | 20 | 288 - 323 | 0 - 0.03 | 0 | 1.26 | 0 | 13.307 |
| D'Avila and Cotrim [133] | 10 | 10 | 10 | 303.14 - 308.14 | 0.01 - 0.01 | 0.082 | 0.074 | 1.382 | 1.261 |
| D'Avila and Silva [134] | 25 | 25 | 0 | 283.15 - 303.14 | 0 - 0.01 | 0.106 | 0 | 1.978 | 0 |
| Dobson [135] | 12 | 12 | 10 | 298.14 | 0 - 0.01 | 0.495 | 0.038 | 5.737 | 0.587 |
| Dornste [136] | 22 | 22 | 20 | 298.14 | 0 - 0.01 | 0.482 | 0.518 | 7.075 | 8.771 |
| Dulitskaya [137] | 8 | 8 | 0 | 323.15 - 323.15 | 0.01 - 0.03 | 0.768 | 0 | 8.026 | 0 |
| Garbarenko and Stabnikov [138] | 114 | 114 | 0 | 273.15 - 323.15 | 0 - 0.03 | 0.357 | 0 | 3.899 | 0 |
| Ghosh and Ghosal [139] | 12 | 11 | 10 | 273.15 - 361.33 | 0 - 0.07 | 0.066 | 0.106 | 0.948 | 1.497 |
| Gonzalez and Van Ness [140] | 20 | 20 | 0 | 323.14 - 323.14 | 0.02 - 0.03 | 0.018 | 0 | 0.29 | 0 |
| Griswold <i>et al.</i> [141] | 18 | 17 | 18 | 423.11 - 548.11 | 0.74 - 10.29 | 0.353 | 0.401 | 3.163 | 3.722 |
| Hall <i>et al.</i> [142] | 10 | 10 | 10 | 298.14 | 0 - 0.01 | 0.047 | 0.034 | 0.846 | 0.607 |
| Heitz [143] | 4 | 4 | 4 | 351.13 - 366.93 | 0.1 | 0.18 | 0.209 | 2.418 | 2.846 |
| Herraiz <i>et al.</i> [144] | 9 | 9 | 9 | 313.15 - 313.15 | 0.01 - 0.02 | 0.021 | 0.016 | 0.347 | 0.269 |
| Hong <i>et al.</i> [145] | 30 | 30 | 30 | 372.52 | 0.1 | 0.116 | 0.119 | 1.532 | 1.576 |
| Hrncirik [146] | 17 | 17 | 0 | 351.3 - 373.15 | 0.1 | 0.428 | 0 | 4.221 | 0 |
| Hughes and Maloney [147] | 19 | 19 | 19 | 351.29 - 372.05 | 0.1 | 0.093 | 0.083 | 1.319 | 1.191 |
| Iwakabe and Kosuge [148] | 28 | 28 | 28 | 351.39 - 364.23 | 0.1 | 0.059 | 0.031 | 0.802 | 0.432 |
| Johnson and Furter [149] | 15 | 15 | 13 | 351.43 - 373.12 | 0.1 | 0.494 | 0.061 | 4.951 | 0.867 |
| Jones <i>et al.</i> [150] | 13 | 13 | 11 | 351.39 - 373.12 | 0.1 | 0.545 | 0.078 | 5.313 | 0.961 |
| Kauer and Bittrich [151] | 9 | 9 | 8 | 351.13 - 368.02 | 0.1 | 0.777 | 0.063 | 7.485 | 0.833 |
| Kirschbaum and Gerstner [152] | 84 | 84 | 84 | 308.15 - 370.85 | 0.01 - 0.1 | 0.07 | 0.061 | 1.083 | 0.922 |
| Kojima and Kato [153] | 170 | 170 | 0 | 319.97 - 437.49 | 0.03 - 0.69 | 0.266 | 0 | 2.586 | 0 |
| Kojima <i>et al.</i> [154] | 21 | 21 | 19 | 351.35 - 373.12 | 0.1 | 0.326 | 0.046 | 3.142 | 0.575 |
| Kojima <i>et al.</i> [155] | 21 | 21 | 0 | 351.33 - 373.12 | 0.1 | 0.326 | 0 | 3.127 | 0 |
| Kolbe and Gmehling [156] | 122 | 122 | 0 | 363.23 - 423.61 | 0.07 - 1 | 0.273 | 0 | 2.422 | 0 |
| Kurihara <i>et al.</i> [157] | 107 | 107 | 107 | 323.15 - 333.15 | 0.02 - 0.05 | 0.022 | 0.028 | 0.341 | 0.426 |
| Kurihara <i>et al.</i> [116] | 18 | 18 | 18 | 351.33 - 362.19 | 0.1 | 0.053 | 0.057 | 0.73 | 0.798 |
| Linderstroem-Lang and Vaslow [158] | 20 | 20 | 0 | 298.16 | 0 - 0.01 | 0.381 | 0 | 4.989 | 0 |
| Liu <i>et al.</i> [159] | 15 | 15 | 13 | 351.2 - 373.1 | 0.1 | 0.487 | 0.265 | 4.764 | 3.4 |
| Lozovoi <i>et al.</i> [160] | 8 | 8 | 8 | 295.74 - 309.94 | 0.01 | 0.179 | 0.147 | 3.132 | 2.553 |
| Macarron [161] | 34 | 34 | 33 | 349.55 - 370.75 | 0.1 | 0.546 | 0.485 | 7.18 | 6.574 |
| Manczinger and Tettamanti [162] | 7 | 7 | 7 | 357.33 - 371.02 | 0.1 | 0.042 | 0.045 | 0.574 | 0.618 |
| Mertl [163] | 39 | 39 | 39 | 313.14 - 343.13 | 0.01 - 0.07 | 0.061 | 0.091 | 0.97 | 1.435 |
| Niesen <i>et al.</i> [164] | 21 | 19 | 19 | 423.11 - 523.11 | 0.74 - 7.12 | 0.121 | 0.073 | 1.168 | 0.723 |
| Nikolskaya [165] | 23 | 23 | 18 | 298.14 - 348.13 | 0 - 0.09 | 0.567 | 0.078 | 6.479 | 1.055 |

Table 4.8 continued.

| Author | Nr- | | | $(T_{\min} - T_{\max})$ | $(p_{\min} - p_{\max})$ | AAD(T_s) / % | | AAD(p_s) / % | |
|----------------------------------|-----|-------|-------|-------------------------|-------------------------|------------------|-------|------------------|--------|
| | Pts | Pts-x | Pts-y | / K | / MPa | bub. | dew | bub. | dew |
| Novella and Tarraso [166] | 17 | 17 | 17 | 351.33 - 368.32 | 0.1 | 0.109 | 0.098 | 1.494 | 1.363 |
| Novitskiy <i>et al.</i> [167] | 36 | 18 | 18 | 423.1 - 598.1 | 0.5 - 13.7 | 0.344 | 0.499 | 2.953 | 4.983 |
| Noyes and Warfel [168] | 60 | 60 | 0 | 351.32 - 372.8 | 0.1 | 0.159 | 0 | 1.715 | 0 |
| Othmer <i>et al.</i> [169] | 43 | 43 | 43 | 377.92 - 431.91 | 0.19 - 0.86 | 1.641 | 1.623 | 23.36 | 23.588 |
| Otsuki and Williams [170] | 127 | 127 | 127 | 351.33 - 481.61 | 0.1 - 2.07 | 0.165 | 0.146 | 2.23 | 2.051 |
| Paul [171] | 13 | 13 | 13 | 351.25 - 369.22 | 0.1 | 0.1 | 0.077 | 1.381 | 1.086 |
| Pemberton and Mash [115] | 95 | 95 | 95 | 303.14 - 363.13 | 0 - 0.16 | 0.037 | 0.072 | 0.568 | 0.808 |
| Phutela <i>et al.</i> [172] | 14 | 14 | 12 | 298.13 | 0 - 0.01 | 0.417 | 0.038 | 4.79 | 0.613 |
| Protsyuk and Devyatko [173] | 14 | 14 | 14 | 351.29 - 371.52 | 0.1 | 0.206 | 0.163 | 2.849 | 2.289 |
| Rarey and Gmehling [174] | 60 | 60 | 0 | 343.15 | 0.03 - 0.07 | 0.038 | 0 | 0.559 | 0 |
| Rieder and Thompson [175] | 36 | 36 | 34 | 351.43 - 373.12 | 0.1 | 0.238 | 0.05 | 2.483 | 0.667 |
| Rius Miro <i>et al.</i> [176] | 12 | 12 | 12 | 352.73 - 370.82 | 0.1 | 0.058 | 0.043 | 0.793 | 0.599 |
| Safarov and Shakhverdiev [110] | 21 | 20 | 0 | 373.15 - 523.15 | 0.14 - 8.96 | 0.794 | 0 | 8.117 | 0 |
| Stabnikov <i>et al.</i> [177] | 126 | 126 | 126 | 351.31 - 372.93 | 0.1 | 0.063 | 0.059 | 0.865 | 0.816 |
| Stabnikov <i>et al.</i> [178] | 27 | 27 | 27 | 334.68 - 371.42 | 0.05 - 0.1 | 0.064 | 0.063 | 0.902 | 0.885 |
| Svoboda <i>et al.</i> [179] | 12 | 12 | 12 | 350.83 - 369.82 | 0.1 | 0.091 | 0.08 | 1.247 | 1.112 |
| Takiguchi <i>et al.</i> [180] | 25 | 25 | 0 | 340 - 420 | 0.05 - 0.92 | 0.071 | 0 | 0.901 | 0 |
| Tochigi <i>et al.</i> [181] | 6 | 6 | 0 | 338.71 - 351.32 | 0.06 - 0.1 | 0.034 | 0 | 0.488 | 0 |
| Tsiklis <i>et al.</i> [182] | 6 | 6 | 6 | 573.11 - 573.11 | 8.83 - 13.14 | 0.611 | 0.783 | 4.338 | 5.992 |
| Udoenko and Fatkulina [183] | 36 | 36 | 30 | 313.14 - 333.13 | 0.01 - 0.05 | 0.553 | 0.18 | 5.94 | 2.387 |
| Van Zandijcke and Verhoeve [184] | 13 | 13 | 13 | 351.23 - 365.13 | 0.1 | 0.098 | 0.056 | 1.363 | 0.783 |
| Vostrikova <i>et al.</i> [185] | 8 | 8 | 8 | 351.33 - 351.53 | 0.1 | 0.047 | 0.047 | 0.653 | 0.651 |
| Vouostas <i>et al.</i> [186] | 51 | 51 | 45 | 307.44 - 344.57 | 0.01 - 0.03 | 0.367 | 0.033 | 3.998 | 0.563 |
| Vu <i>et al.</i> [187] | 28 | 28 | 26 | 313.15 | 0.01 - 0.02 | 0.258 | 0.044 | 3.001 | 0.713 |
| Wilson <i>et al.</i> [188] | 17 | 17 | 0 | 323.14 - 323.14 | 0.01 - 0.03 | 0.362 | 0 | 3.764 | 0 |
| Wormald and Vine [189] | 14 | 14 | 7 | 423.2 - 533.2 | 0.84 - 7.65 | 2.999 | 0.15 | 21.365 | 22.551 |
| Wrewsky [190] | 70 | 70 | 39 | 312.9 - 347.92 | 0.01 - 0.09 | 0.324 | 0.2 | 3.662 | 3.198 |
| Yamamoto <i>et al.</i> [191] | 11 | 11 | 11 | 298.15 - 298.15 | 0 - 0.01 | 0.049 | 0.067 | 0.888 | 1.202 |
| Yang and Wang [192] | 20 | 20 | 20 | 351.6 - 372.97 | 0.1 | 0.075 | 0.097 | 1.041 | 1.331 |
| Zielkiewicz and Konitz [193] | 23 | 23 | 23 | 313.15 - 313.15 | 0.01 - 0.02 | 0.021 | 0.022 | 0.356 | 0.373 |

4.4.2 Densities

Except for two data sets, only liquid or liquid-like densities are available in the literature for ethanol-water mixtures. For those experimental data that were published as excess volumes, the pure fluid volumes were calculated with the equation of state for water of Wagner and Pruß [20] and the equation of state for ethanol of Schroeder *et al.*

[3], weighted with their molar fraction, and added to the excess value to obtain the total volume that was subsequently converted to a density.

In Figure 4.7, comparisons of densities calculated from the new mixture model to selected experimental liquid data up to $T = 450$ K are presented. The mixture model of Lemmon [4] is evaluated at $p = 0.101325$ MPa for $T < 350$ K and $p = 5$ MPa for $T > 350$ K, and plotted for comparison. The data sets agree very well. The mixture model of Lemmon [4] follows the data well in this temperature range.

The new model oscillates around the data showing systematical deviations. This oscillation could be reduced in the fitting process at the cost of an inferior representation of the VLE and speed-of-sound data. Therefore, a compromise had to be found. Up to $T = 350$ K, the data can be represented within $\pm 0.5\%$. For very high pressures only, the deviations increase to $\pm 1\%$.

A few selected data sets, which are considered to be the most accurate, are discussed in more detail. Zarei *et al.* [194] (Anton Paar oscillating u-tube) measured over a temperature range from $T = 283.15$ K to $T = 313.15$ K at atmospheric pressure and over the complete composition range. The combined uncertainty of their experimental setup is estimated to be within 0.05% in molar density, which seems rather optimistic regarding the use of a flexural resonator. The new model represents these data with a maximum deviation of $\pm 0.5\%$ and an AAD of 0.254%. Hervello and Sánchez [195] (Anton Paar vibrating-tube) conducted their experiments from $T = 283.15$ K to $T = 298.15$ K also at atmospheric pressure over the complete composition range. The uncertainty of their data is estimated to be within 0.025% in molar density without including the uncertainty in composition, which is again considered to be an underestimation. The new mixture model depicts these data with a maximum deviation of $\pm 0.46\%$ and an AAD of 0.21%. An extensive data set with pressures up to 40 MPa was published by Pečar and Doleček [196] (vibrating tube densimeter). Their data cover a range from $T = 298.15$ K to $T = 348.15$ K and over the complete composition range. The combined uncertainty has been determined to be 0.04% in molar density, which is considered to be underestimated regarding the experimental method used. The data are represented with a maximum deviation of $\pm 0.5\%$ and an AAD of 0.16%.

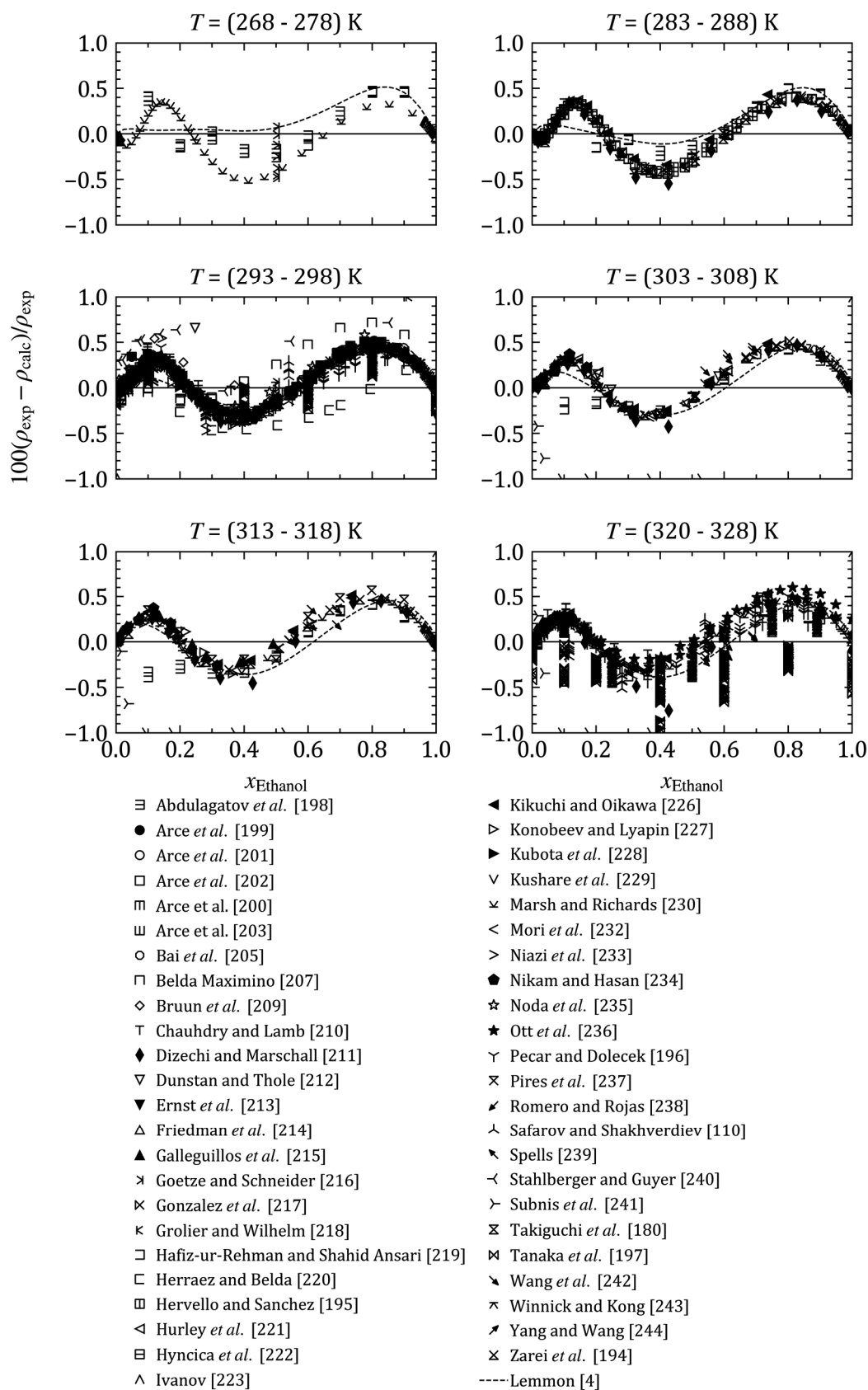


Figure 4.7: Relative deviations of selected experimental liquid densities over the molar ethanol fraction from the new mixture model. Results from the model of Lemmon [4] (dashed curve) evaluated at $p = 0.101325$ MPa for $T < 350$ K and $p = 5$ MPa for $T > 350$ K are plotted for comparison.

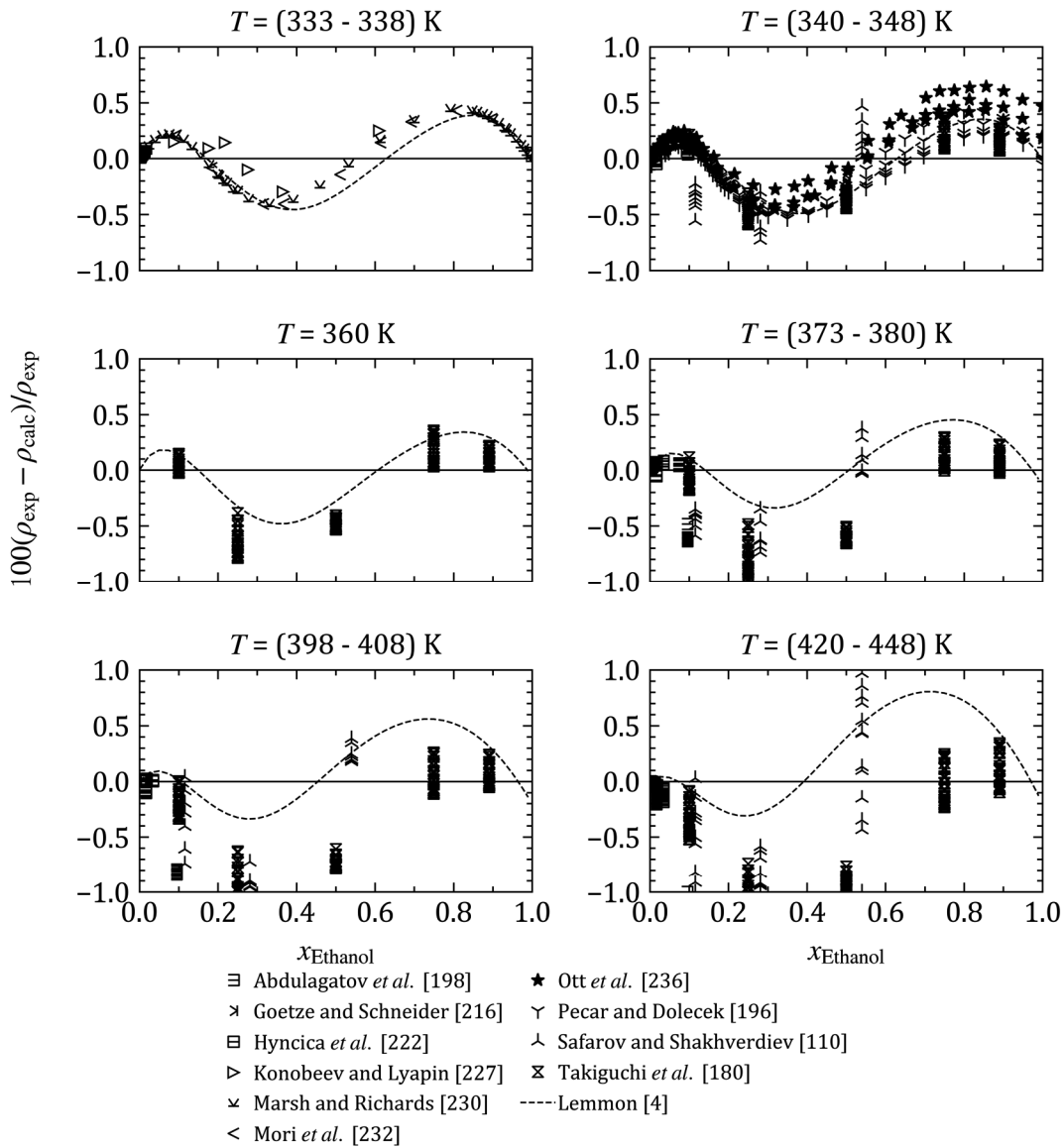


Figure 4.7 continued.

The measurements of Tanaka *et al.* [197] (Adam piezometer), which were conducted over the complete composition range, included pressures up to $p = 350$ MPa. The temperature range went from $T = 298$ K to $T = 323$ K. The authors claim a combined uncertainty of 0.05% in molar density for their experimental setup. The new model deviates by a maximum of +0.4% to -0.95% from these data with an AAD of 0.23%.

One major improvement of the new mixture model over the model of Lemmon [4] is the representation of densities at high pressures. This feature is illustrated in Figure 4.8, where selected experimental data containing measurements conducted at higher pressures are shown. At the top, deviations of the model of Lemmon [4] from the experimental data are presented. With increasing pressure, the absolute deviations

increase to over 4%. Whereas at the bottom, the deviations of the new model never exceed $\pm 1\%$.

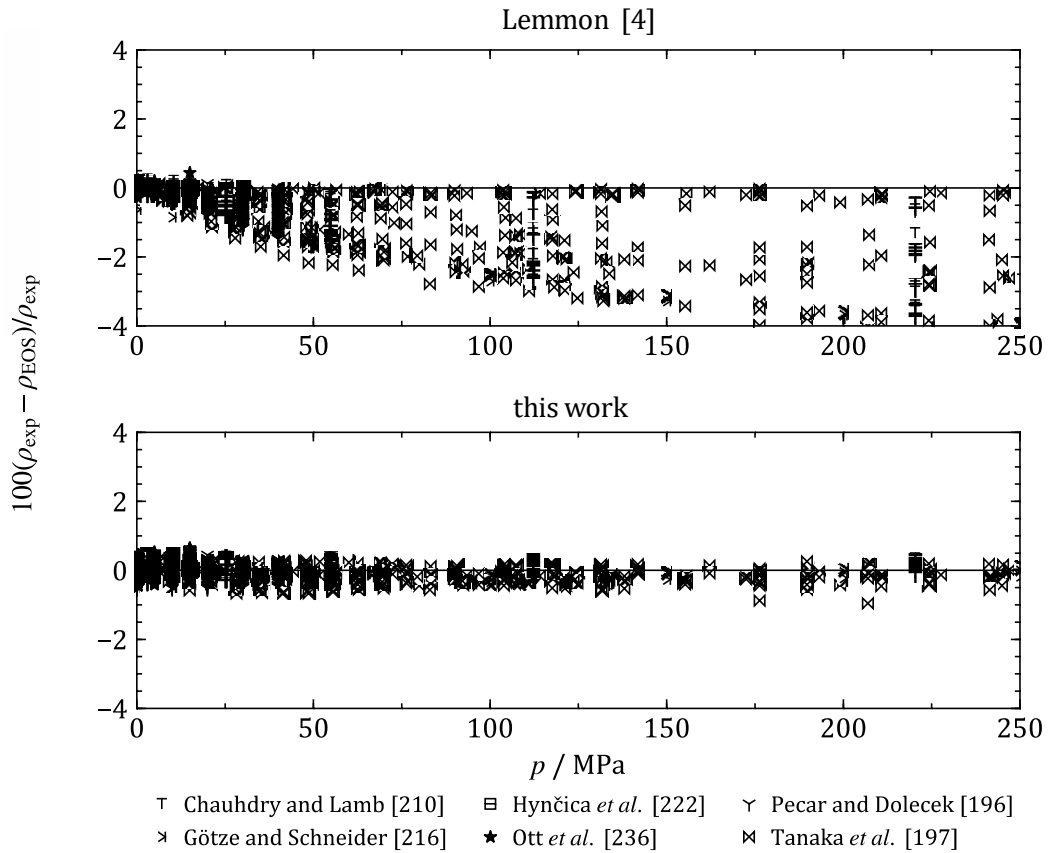


Figure 4.8: Relative deviations of selected experimental densities over pressure with $273\text{ K} < T < 450\text{ K}$ from the model of Lemmon [4] (top) and from the new mixture model. (bottom).

The experimental data at high temperatures with $x_{\text{Ethanol}} = 0.5$, which also cover the vapor phase, and their representation by the new mixture model are illustrated in Figure 4.9. The representation by the model of Lemmon [4] is given in Figure 4.10. Abdurashidova *et al.* [109] and Bazaev *et al.* [108] claim an uncertainty of 0.15% of their partly identical experimental data that have been conducted with a constant-volume piezometer. Since these data were measured along isochores, they are presented accordingly. The respective plots for the isopleths $x_{\text{Ethanol}} = 0.2$ and $x_{\text{Ethanol}} = 0.8$ are presented in Appendix C. Safarov and Shakhverdiev [110] estimate the uncertainty of their measurements to be within 0.15%. They also used a constant-volume piezometer for their investigations.

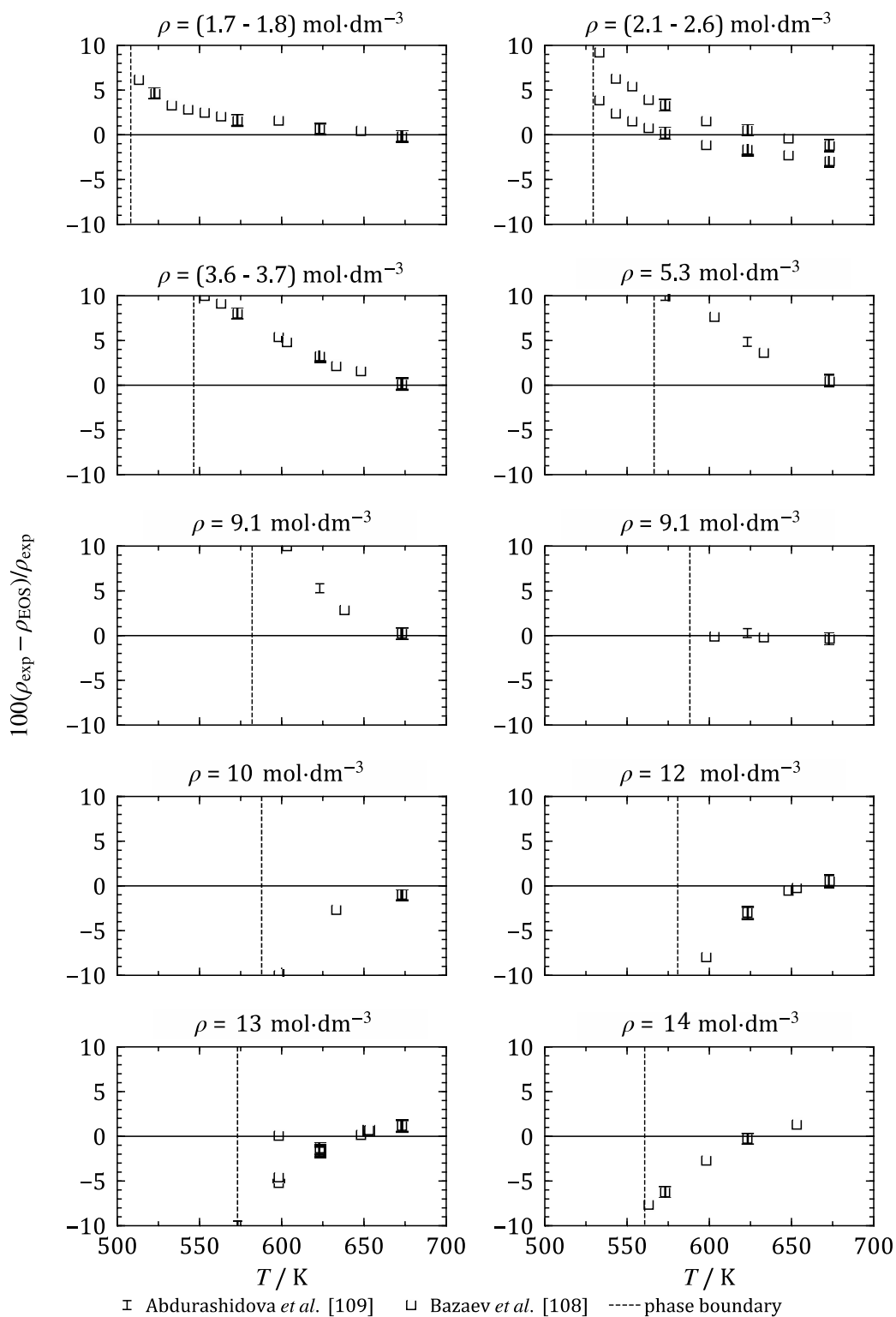


Figure 4.9: Relative deviations of the high temperature experimental densities along isochores over pressure from the new mixture model with $x_{\text{Ethanol}} = 0.5$.

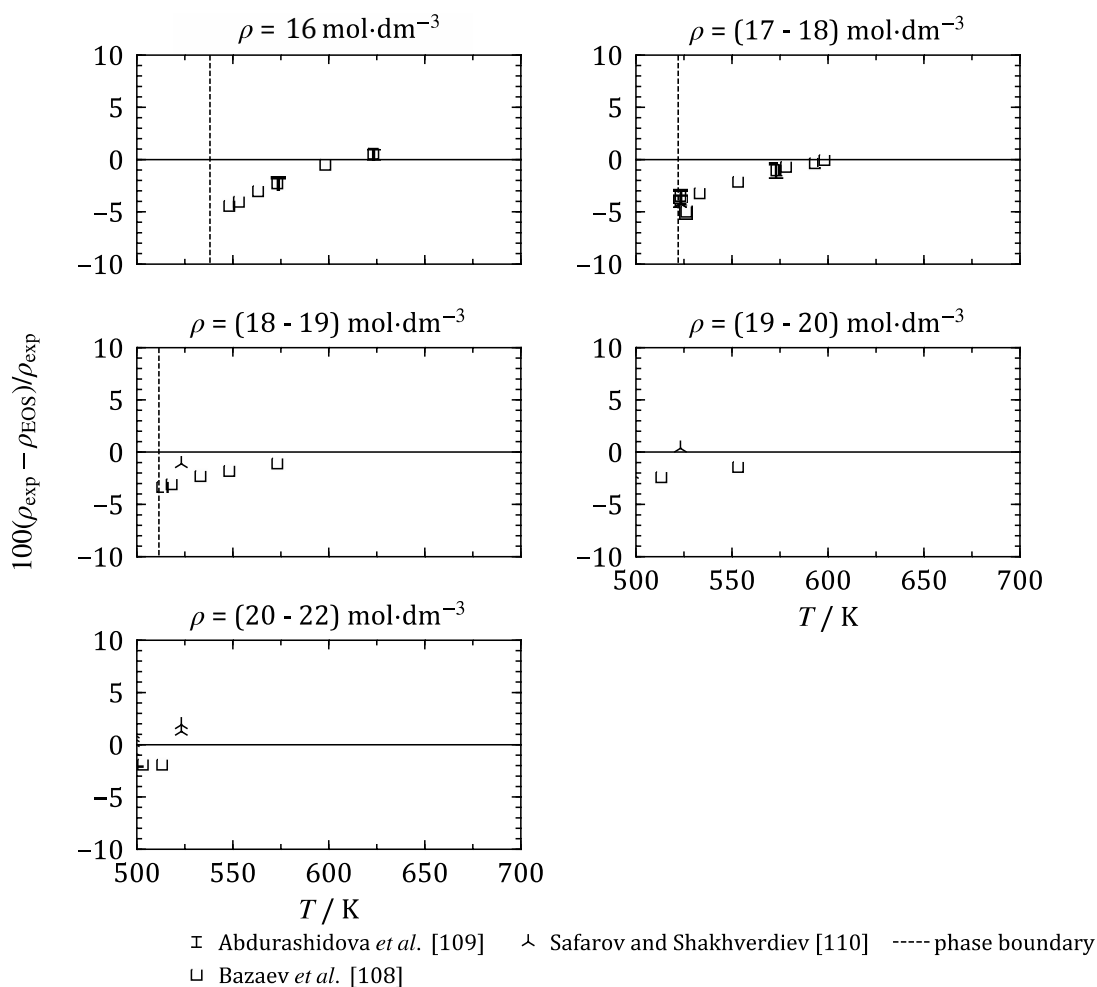


Figure 4.9 continued

Figure 4.9 presents good agreement of the new model with the data in the homogeneous phase at these high temperatures within $\pm 1\%$. However, the deviations increase significantly in the vicinity of the phase boundary. For all isochores and $T > (T_s + 50 \text{ K})$, the new model deviates by $\pm 5\%$ from the experimental data by up to $\pm 10\%$ directly at the phase boundary. For densities with $\rho > 18 \text{ mol/dm}^3$, the deviations are $\pm 3\%$ including the vicinity of the phase boundary.

The model of Lemmon [4] represents these data in a similar way. Nevertheless, the deviations in the homogeneous phases apart from the phase boundary, especially at high densities, are significantly larger with down to -5% .

The representation of the densities in the high temperature region was significantly improved by the new model and can be estimated with an uncertainty of $\pm 2\%$ away from the phase boundary.

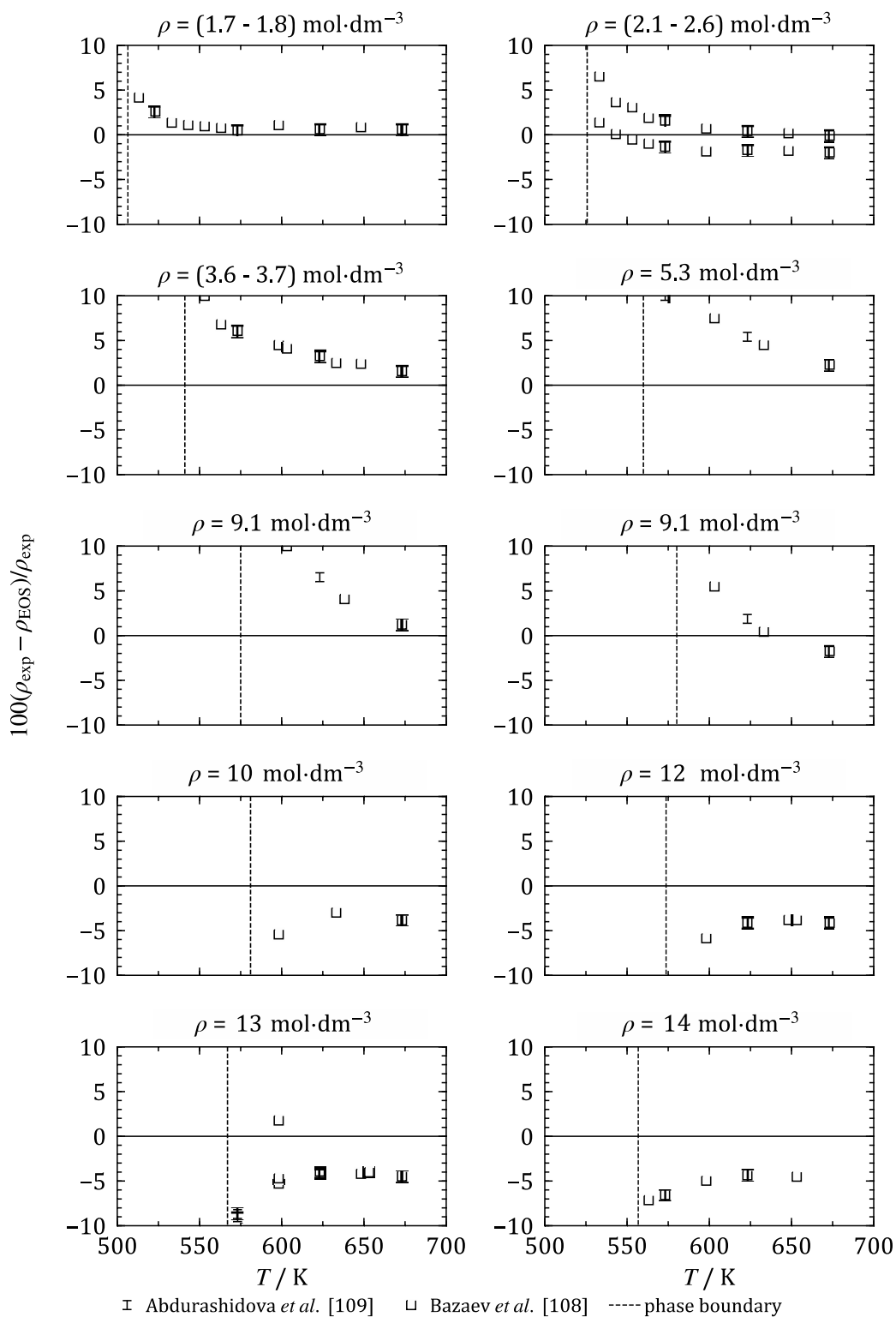


Figure 4.10: Relative deviations of the high temperature experimental densities along isochores over pressure from the model of Lemmon [4] with $x_{\text{Ethanol}} = 0.5$.

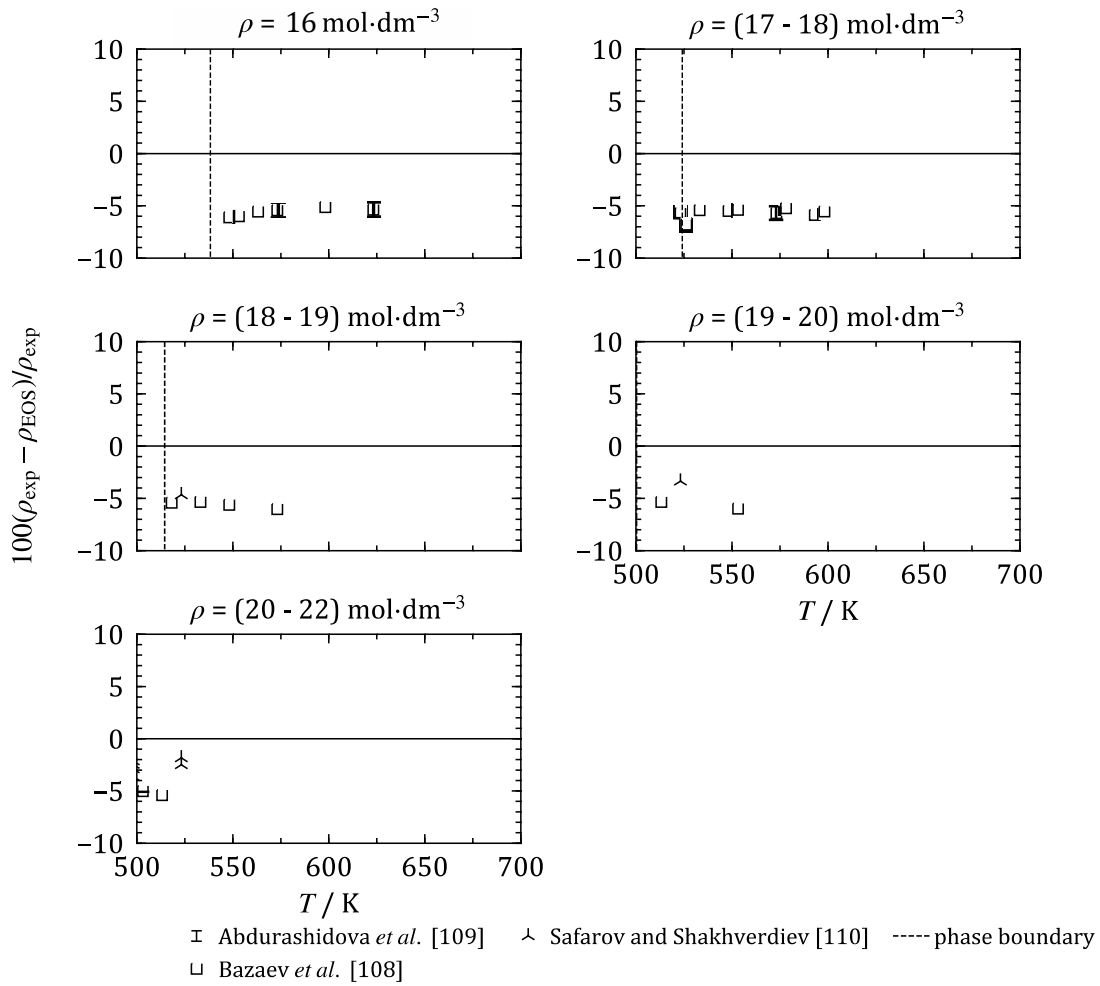


Figure 4.10 continued

Table 4.9 gives the average relative deviations of all experimental density data sets.

Table 4.9: Absolute average deviation of the new mixture model from the experimental density data.

| Author | Nr.-Pts | $(T_{\min} - T_{\max}) / K$ | $(p_{\min} - p_{\max}) / MPa$ | $x_{\min} - x_{\max}$ | AAD / % |
|-----------------------------------|---------|-----------------------------|-------------------------------|-----------------------|---------|
| Abdulagatovet <i>et al.</i> [198] | 124 | 292.95-448.15 | 2.45-40.14 | 0.0163-0.0946 | 0.245 |
| Abdurashidova <i>et al.</i> [109] | 87 | 523.15-673.15 | 5.38-50.36 | 0.2-0.8 | 35.197 |
| Arce <i>et al.</i> [199] | 28 | 298.15-298.15 | 0.1 | 0-1 | 0.263 |
| Arce <i>et al.</i> [200] | 21 | 298.15-298.15 | 0.1 | 0-1 | 0.253 |
| Arce <i>et al.</i> [201] | 7 | 298.15-298.15 | 0.1 | 0.2553-0.8988 | 0.268 |
| Arce <i>et al.</i> [202] | 8 | 298.15-298.15 | 0.1 | 0.2018-0.8959 | 0.241 |
| Arce <i>et al.</i> [203] | 15 | 298.15-298.15 | 0.1 | 0.0519-0.952 | 0.25 |
| Atik [204] | 13 | 298.15-298.15 | 0.1 | 0.1104-0.9468 | 12.608 |
| Bai <i>et al.</i> [205] | 28 | 298.15-298.15 | 0.1 | 0.0063-0.9732 | 0.206 |
| Bazaev <i>et al.</i> [108] | 290 | 456.15-673.15 | 4-51.76 | 0-0.8 | 2.58 |
| Belda Maximino [206] | 13 | 298.15-298.15 | 0.1 | 0-1 | 0.24 |
| Belda <i>et al.</i> [207] | 84 | 283.15-343.15 | 0.1 | 0-1 | 1.118 |
| Benson and Kiyohara [208] | 203 | 288.15-308.14 | 0.1 | 0.0229-0.9992 | 0.429 |
| Bruun <i>et al.</i> [209] | 14 | 298.14-298.14 | 0.1 | 0-1 | 0.181 |
| Chauhdry and Lamb [210] | 120 | 298.14-323.14 | 3-220.3 | 0.0226-0.862 | 0.209 |

Table 4.9 continued.

| Author | Nr.-Pts | ($T_{\min} - T_{\max}$) / K | ($p_{\min} - p_{\max}$) / MPa | $x_{\min} - x_{\max}$ | AAD / % |
|---|---------|-------------------------------|---------------------------------|-----------------------|---------|
| Dizechi and Marschall [211] | 80 | 283.15-323.14 | 0.1 | 0-1 | 0.2 |
| Dunstan and Thole [212] | 21 | 293-303 | 0.1 | 0-0.9798 | 0.162 |
| Ernst <i>et al.</i> [213] | 11 | 298.14-298.14 | 0.1 | 0-1 | 0.216 |
| Friedman <i>et al.</i> [214] | 20 | 274-323 | 0.1 | 0.002-1 | 0.071 |
| Galleguillos <i>et al.</i> [215] | 24 | 298.15-313.15 | 0.1 | 0.0454-0.4909 | 0.173 |
| Götze and Schneider [216] | 28 | 273.16-348.13 | 0.1-250 | 0.5-0.5 | 0.183 |
| Gonzalez <i>et al.</i> [217] | 37 | 293.15-303.15 | 0.1 | 0-1 | 0.233 |
| Grolier and Wilhelm [218] | 20 | 298.14-298.14 | 0.1 | 0.0128-0.9373 | 0.243 |
| Hafiz-ur-Rehman and Shahid Ansari [219] | 108 | 268.15-323.15 | 0.1 | 0.1-0.9 | 0.25 |
| Herraez and Belda [220] | 13 | 298.15-298.15 | 0.1 | 0-1 | 0.232 |
| Hervello and Sanchez [195] | 164 | 283.15-298.15 | 0.1 | 0-1 | 0.213 |
| Hurley <i>et al.</i> [221] | 33 | 283.15-303.15 | 0.1 | 0-1 | 0.196 |
| Hynčica <i>et al.</i> [222] | 189 | 298.15-573.15 | 0.39-30.3 | 0.0016-0.0184 | 0.044 |
| Ivanov [223] | 70 | 278.15-318.15 | 0.1 | 0.9634-0.999 | 0.071 |
| Kabir <i>et al.</i> [224] | 45 | 303.15-323.15 | 0.1 | 0-1 | 1.061 |
| Khattab <i>et al.</i> [225] | 77 | 293-323 | 0.1 | 0-1 | 0.334 |
| Kikuchi and Oikawa [226] | 88 | 288.16-323.17 | 0.1 | 0-1 | 0.188 |
| Konobeev and Lyapin [227] | 24 | 293.14-333.13 | 0.1 | 0-1 | 0.133 |
| Kubota <i>et al.</i> [228] | 180 | 298.15-323.15 | 0.1-348.6 | 0.2-0.8 | 0.252 |
| Kushare <i>et al.</i> [229] | 12 | 298.15-298.15 | 0.1 | 0.9552-1 | 0.125 |
| Marsh and Richards [230] | 306 | 278.15-338.13 | 0.1 | 0.0002-0.9978 | 0.175 |
| Mathews and Cooke [231] | 5 | 273.15-343.15 | 0.1 | 0.2424-0.2424 | 0.934 |
| Mori <i>et al.</i> [232] | 45 | 298.15-338.15 | 0.1 | 0.0937-0.8979 | 0.273 |
| Niazi <i>et al.</i> [233] | 8 | 298.15-298.15 | 0.1 | 0-0.4771 | 0.263 |
| Nikam and Hasan [234] | 20 | 298.15-313.15 | 0.1 | 0.0329-0.3155 | 0.229 |
| Noda <i>et al.</i> [235] | 11 | 298.15-298.15 | 0.1 | 0-1 | 0.206 |
| Ott <i>et al.</i> [236] | 239 | 298.15-348.15 | 0.4-15 | 0-1 | 0.236 |
| Pecar and Dolecek [196] | 810 | 298.15-348.15 | 0.1-40 | 0.003-1 | 0.164 |
| Pires <i>et al.</i> [237] | 18 | 298.15-318.15 | 0.1 | 0.0949-0.9002 | 0.293 |
| Romero and Rojas [238] | 5 | 298.15-298.15 | 0.1 | 0-0.1435 | 0.142 |
| Safarov and Shakhverdiev [110] | 217 | 298.15-523.15 | 0.1-60 | 0.1153-0.5398 | 1.577 |
| Spells [239] | 11 | 283.15-283.15 | 0.1 | 0-1 | 0.193 |
| Stahlberger and Guyer [240] | 11 | 298-298 | 0.1 | 0-0.8533 | 0.418 |
| Subnis <i>et al.</i> [241] | 24 | 303-323 | 0.1 | 0-1 | 2.089 |
| Takiguchi <i>et al.</i> [180] | 753 | 320-420 | 0.1-200 | 0.1002-0.8904 | 0.35 |
| Tanaka <i>et al.</i> [197] | 322 | 298-323 | 0.1-348.64 | 0-1 | 0.225 |
| Wang <i>et al.</i> [242] | 18 | 303.15-328.15 | 0.1 | 0.5398-0.6891 | 0.199 |
| Winnick and Kong [243] | 9 | 323.14-323.14 | 0.1 | 0.1-0.9 | 0.249 |
| Yang and Wang [244] | 15 | 293.15-313.15 | 0.1 | 0.0416-0.2811 | 0.183 |
| Zarei <i>et al.</i> [194] | 84 | 283.15-313.15 | 0.1 | 0.0395-0.9195 | 0.254 |
| Zhu [245] | 8 | 303-303 | 0.1 | 0.1361-0.7589 | 0.635 |

4.4.3 Excess Enthalpies

There are many data sets available for the excess enthalpy of ethanol-water mixtures that agree very well and can be directly used in the fitting process. Figure 4.11 illustrates the absolute experimental values and their representation by the newly developed mixture model. The mixture model of Lemmon [4] is included for comparison.

Up to $T = 323$ K, the curvature of the excess enthalpy changes twice with increasing ethanol composition. At $T = 273.15$ K, the excess enthalpy shows a drastically steep minimum at $x_{\text{Ethanol}} \approx 0.2$, which reduces fast with increasing temperature. A zero crossing occurs for temperatures higher than $T = 333$ K. For high water content, the excess enthalpy stays negative, whereas its value becomes positive for higher ethanol fractions. For temperatures $T > 380$ K, the mixture behavior is much simpler without any zero crossings or changes in curvature over composition.

A few representative publications are introduced briefly. Zhao and Tremaine [246] measured at $T = 298.15$ K from $p = 0.4$ MPa to $p = 10$ MPa with an estimated uncertainty of 2%. Ott *et al.* [247] investigated the excess enthalpy from $T = 323.14$ K to $T = 373.12$ K and from $p = 0.40$ MPa to $p = 15$ MPa. The authors claim an uncertainty of 1% for their experimental data. Wormald and Lloyd [248] measured from $T = 398$ K to $T = 548$ K at $p = 15$ MPa and claim an uncertainty of 3% in the excess enthalpy.

Figure 4.11 shows that both models struggle with the representation of the extreme shape of the excess enthalpy at low temperatures and low ethanol fractions. But even for the less complicated isotherms, the deviations of the models from the experimental data are of a magnitude of $\pm 10\%$. The model of Lemmon [4] is slightly superior in the low temperature region, whereas the new model follows the experimental data at higher temperatures more accurately. During the fitting process, the shape of the new model could be forced to the shape of the experimental data at low temperatures, but again at the cost of a significantly worse representation of other properties.

To assess the impact of the excess enthalpy and its deviation, Table 4.10 lists the AADs of all collected publications with respect to the “total” enthalpy, that was calculated as the sum of the excess enthalpy and the pure fluid enthalpies calculated from the respective pure fluid equations of state [3,20]. A constant of $h = 1000$ J/mol was added to all enthalpies in order to avoid zero crossings that cause excessively high relative deviations.

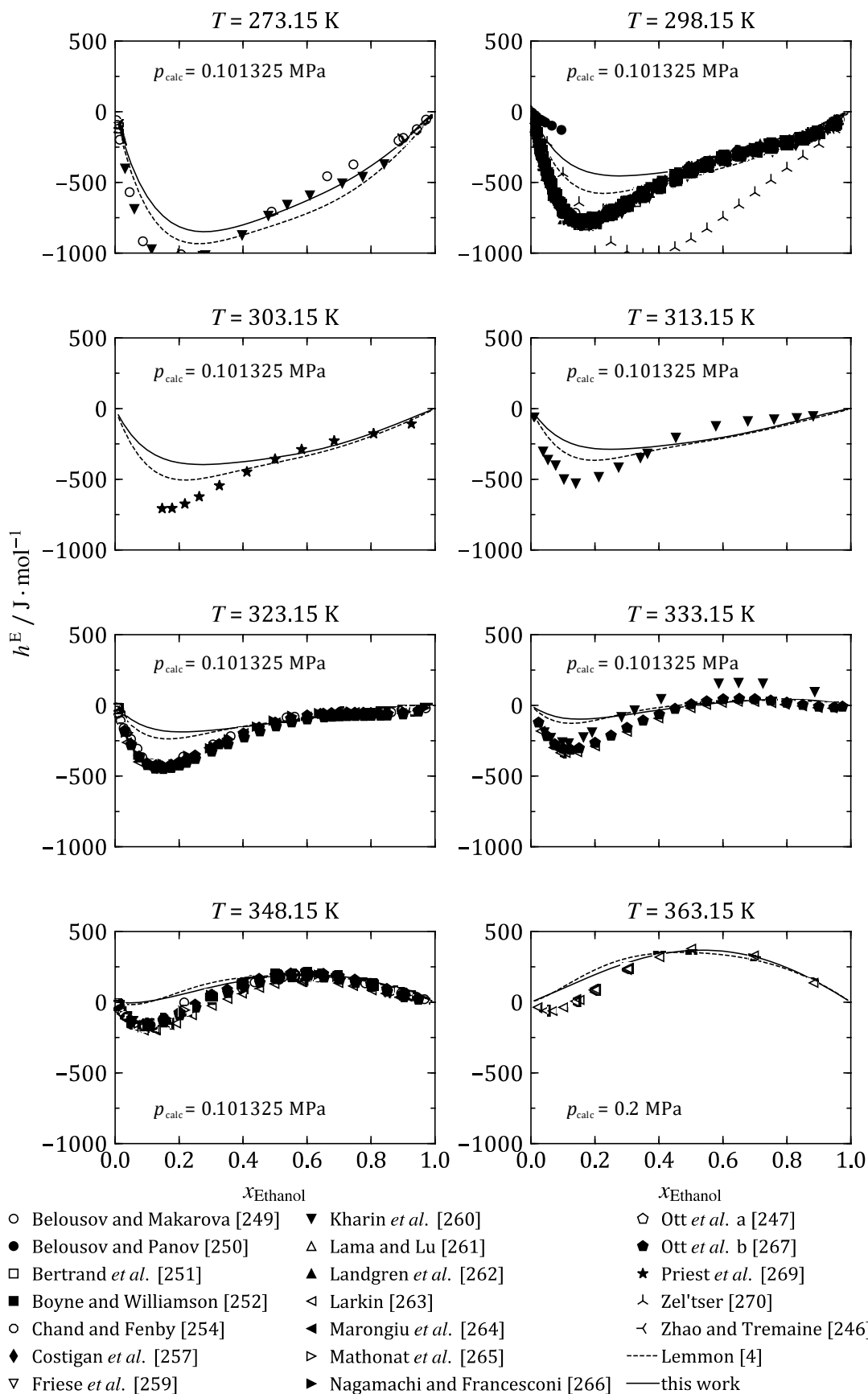


Figure 4.11: Experimental excess enthalpy data of the binary mixture ethanol-water over the ethanol fraction. Results from the presented new model and from the model of Lemmon [4] (dashed curve) are plotted for comparison.

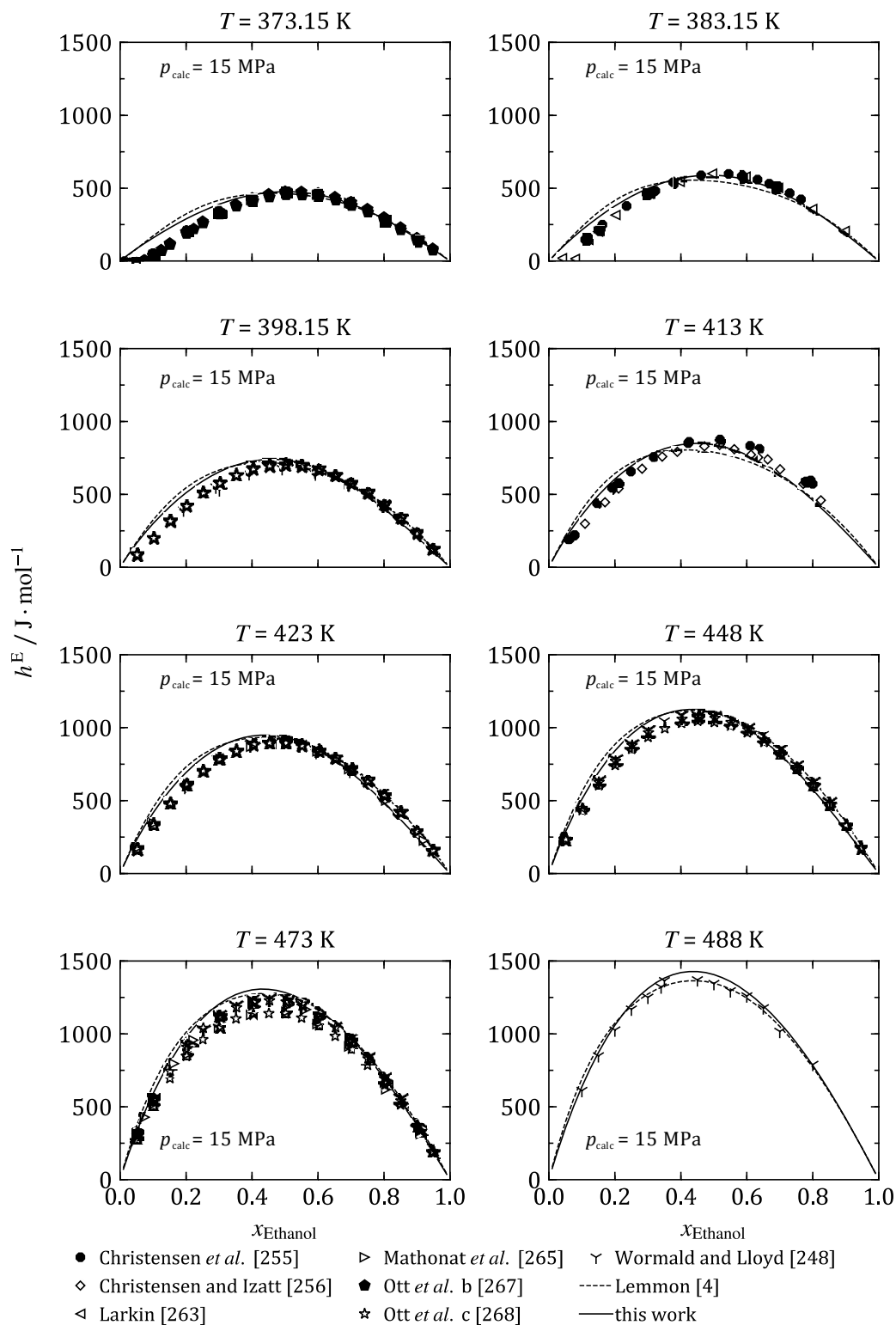


Figure 4.11 continued.

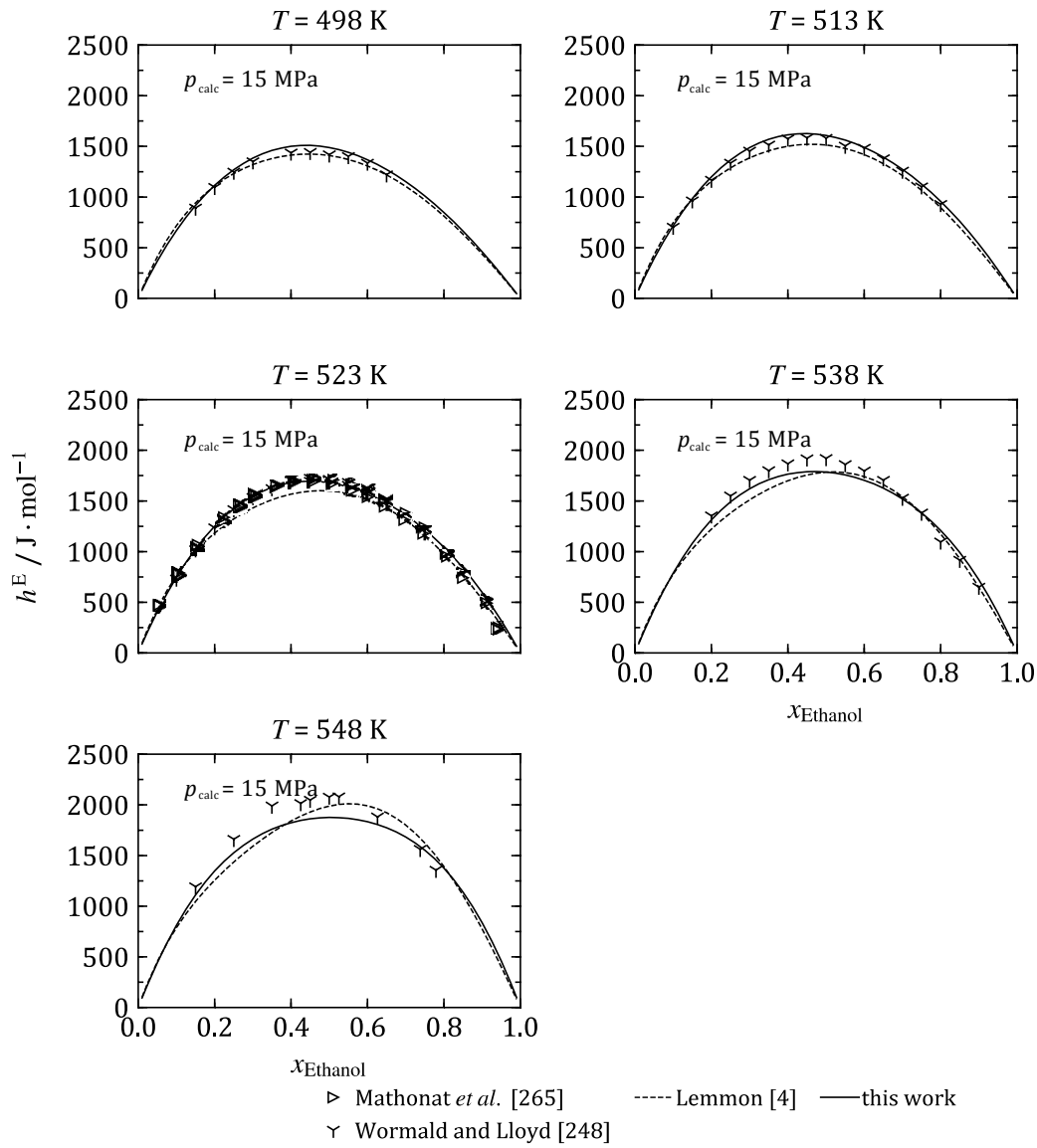


Figure 4.11 continued.

Table 4.10: Absolute average deviation of the new mixture model from the experimental excess enthalpy data converted to total enthalpies.

| Author | Nr.-Pts | $(T_{\min} - T_{\max}) / \text{K}$ | $(p_{\min} - p_{\max}) / \text{MPa}$ | $x_{\min} - x_{\max}$ | AAD / % |
|---------------------------------|---------|------------------------------------|--------------------------------------|-----------------------|---------|
| Belousov and Makarova [249] | 96 | 273.15 - 348.12 | 0.101325 | 0.0023 - 0.972 | 0.681 |
| Belousov and Panov [250] | 9 | 298.14 - 298.14 | 0.101325 | 0.001 - 0.095 | 0.655 |
| Bertrand <i>et al.</i> [251] | 11 | 298.13 - 298.13 | 0.101325 | 0.0335 - 0.875 | 1.304 |
| Boyne and Williamson [252] | 17 | 298.13 - 298.13 | 0.101325 | 0.077 - 0.894 | 1.683 |
| Brandt <i>et al.</i> [253] | 56 | 333.15 - 383.15 | | 0.0079 - 0.961 | 0.400 |
| Chand and Fenby [254] | 10 | 298.14 - 298.14 | 0.101325 | 0.0596 - 0.845 | 1.288 |
| Christensen <i>et al.</i> [255] | 41 | 382.97 - 412.96 | 1 | 0.0584 - 0.7994 | 0.220 |
| Christensen and Izatt [256] | 15 | 412.96 - 412.96 | 1 | 0.1092 - 0.8243 | 0.165 |
| Costigan <i>et al.</i> [257] | 100 | 298.14 - 298.14 | 0.101325 | 0.00015 - 0.962 | 1.177 |
| Fang <i>et al.</i> [258] | 30 | 423.2 - 523.2 | 5 - 15 | 0.0329 - 0.8534 | 0.139 |
| Friese <i>et al.</i> [259] | 19 | 298.15 - 298.15 | 0.101325 | 0.05 - 0.95 | 0.888 |
| Kharin <i>et al.</i> [260] | 58 | 273.15 - 333.15 | 0.101325 | 0.01 - 0.887 | 1.051 |
| Lama and Lu [261] | 19 | 298.13 - 298.13 | 0.101325 | 0.0132 - 0.959 | 0.775 |

Table 6.10 continued.

| Author | Nr.-Pts | $(T_{\min} - T_{\max}) / \text{K}$ | $(p_{\min} - p_{\max}) / \text{MPa}$ | $x_{\min} - x_{\max}$ | AAD / % |
|---------------------------------|---------|------------------------------------|--------------------------------------|-----------------------|---------|
| Landgren <i>et al.</i> [262] | 24 | 298.14 - 298.14 | 0.101325 | 0.005 - 0.95 | 0.941 |
| Larkin [263] | 83 | 298.14 - 383.12 | 0.101325 | 0.0206 - 0.945 | 0.477 |
| Marongiu <i>et al.</i> [264] | 21 | 298.15 - 298.15 | 0.101325 | 0.0201 - 0.928 | 0.921 |
| Mathonat <i>et al.</i> [265] | 104 | 348.15 - 523.15 | 5 - 20 | 0.0518 - 0.943 | 0.159 |
| Nagamachi and Francesconi [266] | 27 | 298.15 - 323.15 | 0.101325 | 0.033 - 0.968 | 0.881 |
| Ott <i>et al.</i> [247] | 179 | 323.13 - 373.12 | 0.4 - 15 | 0.01 - 0.9735 | 0.393 |
| Ott <i>et al.</i> [267] | 94 | 298.14 - 298.14 | 0.4 - 15 | 0.0249 - 0.948 | 1.157 |
| Ott <i>et al.</i> [268] | 152 | 398.11 - 473.11 | 5 - 15 | 0.0504 - 0.948 | 0.153 |
| Priest <i>et al.</i> [269] | 22 | 298.14 - 303.14 | 0.101325 | 0.147 - 0.926 | 1.039 |
| Wormald and Lloyd [248] | 131 | 398 - 548 | 15 - 15 | 0.1 - 0.9 | 0.130 |
| Zel'tser [270] | 19 | 293.13 - 293.13 | 0.101325 | 0.05 - 0.95 | 1.852 |
| Zhao and Tremaine [246] | 78 | 298.15 - 298.15 | 0.4 - 10 | 0.0126 - 0.945 | 1.333 |

4.4.4 Isobaric Heat Capacities

Figure 4.12 presents comparisons of the isobaric heat capacity calculated from the new mixture model to experimental data. The mixture model of Lemmon [4] is plotted for comparison. For experimental data that were published as excess heat capacities, the heat capacity was calculated with the equation of state for water of Wagner and Pruß [20] and the equation of state for ethanol by Schroeder *et al.* [3], and added to the excess value to obtain the full mixture property.

The experimental data of Westh and Hvidt [271] at low temperatures were in the end not included in the fitting. The experimental data at $T = 245.15 \text{ K}$ is represented by the new model with deviations higher than 40%. With increasing temperature, the deviations decrease significantly. There were preliminary equations during the fitting process that could describe these data better, at the cost of a worse description of other properties. Therefore, the focus was kept on the description of properties with $T > 273.15 \text{ K}$. Unfortunately, the publication of Westh and Hvidt [271] does not include a discussion of the experimental uncertainty.

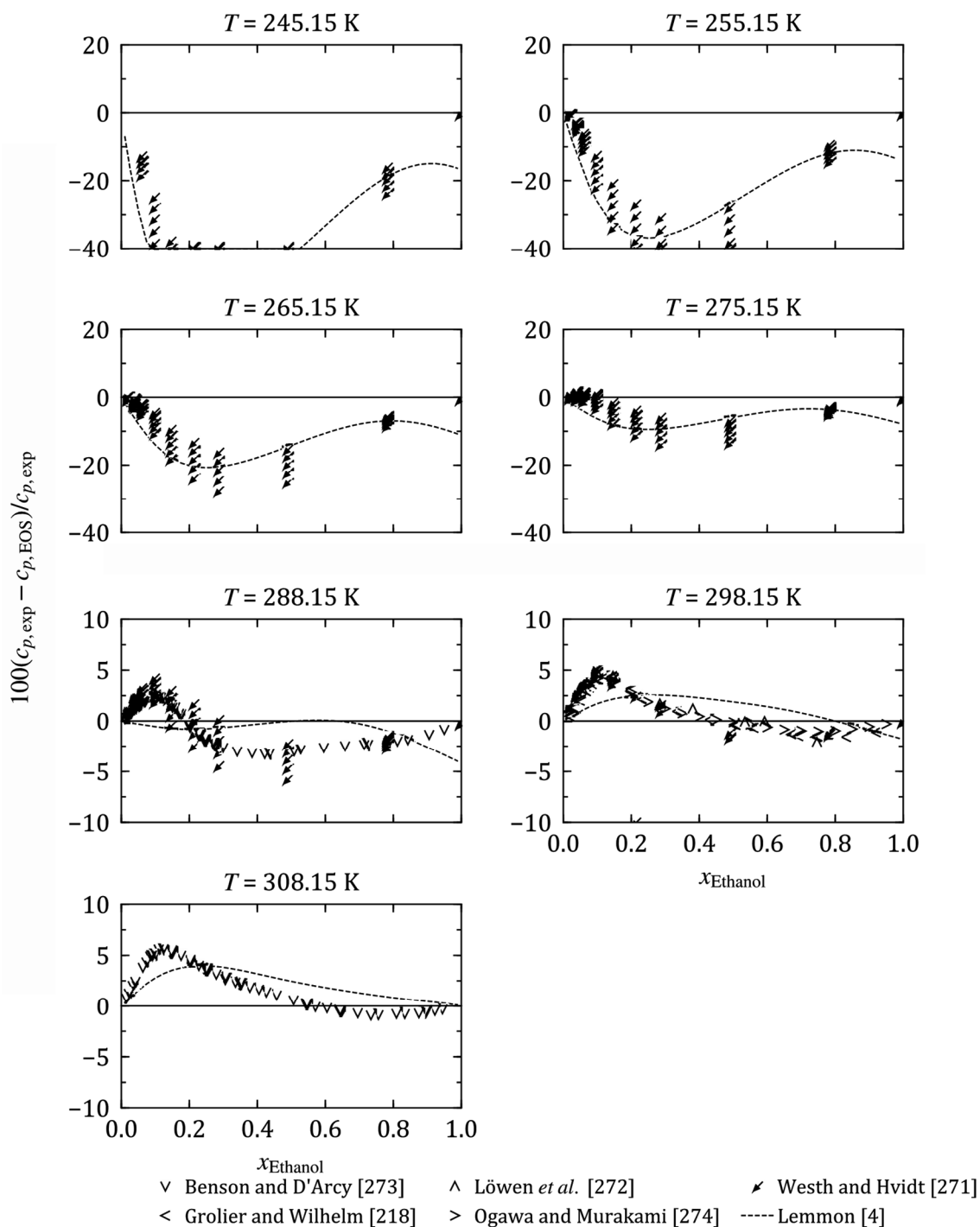


Figure 4.12: Relative deviations of the liquid experimental isobaric heat capacity data at atmospheric pressure from the new mixture model. Results from the model of Lemmon [4] (dashed curve) are plotted for comparison.

The mixture model of Lemmon [4] represents these data in a superior manner. However, the superiority of the new ethanol equation of state of Schroeder *et al.* [3] over the outdated equation of state of Dillon *et al.* [21], which is applied in the mixture model of Lemmon [4], becomes obvious. At these low temperatures, the equation of Dillon *et al.* [21] deviates by up to 20% from the experimental data for pure ethanol ($x_{Ethanol} = 1$), whereas the equation of Schroeder *et al.* [3] agrees very well.

For temperatures $T > 280$ K, the new model shows a systematical deviation from the experimental data with a maximum at a composition of $x_{\text{Ethanol}} \approx 0.1$. The new mixture model represents the experimental data in this temperature region within $\pm 5\%$, which corresponds to the claimed uncertainty of the experimental data of Löwen *et al.* [272]. Table 4.11 presents the average absolute relative deviations of the new mixture model from the experimental data. Leaving out the data in the low temperature region with $T < 280$ K, the data sets are represented with AADs of $\approx 2\%$.

Table 4.11: Absolute average deviation of the new mixture model from the experimental liquid isobaric-heat capacity data.

| Author | Nr of Pts | $(T_{\min} - T_{\max}) / \text{K}$ | p / MPa | $x_{\min} - x_{\max}$ | AAD / % |
|---------------------------|-----------|------------------------------------|------------------|-----------------------|---------|
| Benson and D'Arcy [273] | 98 | 288.15 - 308.14 | 0.1 | 0.0102 - 0.9498 | 2.088 |
| Grolier and Wilhelm [218] | 20 | 298.14 - 298.14 | 0.1 | 0.0189 - 0.9201 | 2.017 |
| Löwen <i>et al.</i> [272] | 8 | 298.16 - 298.16 | 0.1 | 0.056 - 0.746 | 2.18 |
| Ogawa and Murakami [274] | 22 | 298.14 - 298.14 | 0.1 | 0.025 - 0.95 | 1.483 |
| Westh and Hvidt [271] | 276 | 241.15 - 293.15 | 0.1 | 0.0218 - 1 | 11.394 |

4.4.5 Speed of Sound

There are only a few data sets with limited data points that published speed-of-sound data for ethanol-water mixtures. Figure 4.13 illustrates the course of the speed of sound of ethanol-water mixtures at $T = 298.15$ K and $p = 0.1$ MPa.

The new mixture model follows the data, whereas the model of Lemmon [4] deviates significantly and shows a different trend. In the beginning of the fitting process, the slope of the speed of sound at this temperature and pressure was constrained to follow the course of the experimental data. This constraint was no longer needed towards the end of the fitting process to ensure this behavior.

Figure 4.14 presents relative deviations of the experimental liquid speed-of-sound data at atmospheric pressure from the new mixture model. The mixture model of Lemmon [4] is again included for comparison. It deviates strongly from the experimental data with absolute deviations up to 25%. The new mixture model agrees well with the experimental data over the whole composition range.

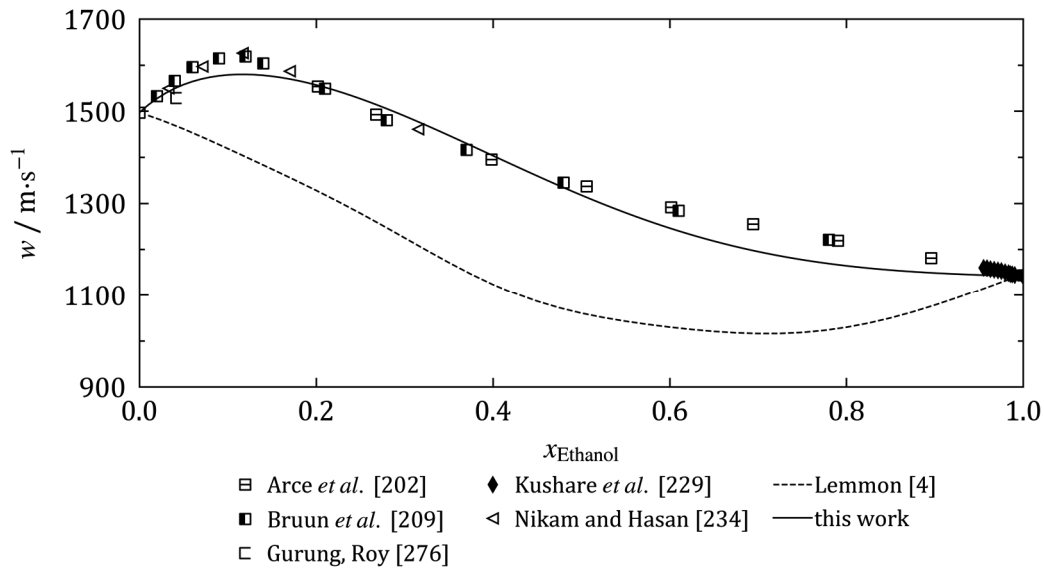


Figure 4.13: Experimental speed-of-sound data and values calculated from the new mixture model and from the model of Lemmon [4] at $T = 298.15 \text{ K}$ and $p = 0.1 \text{ MPa}$.

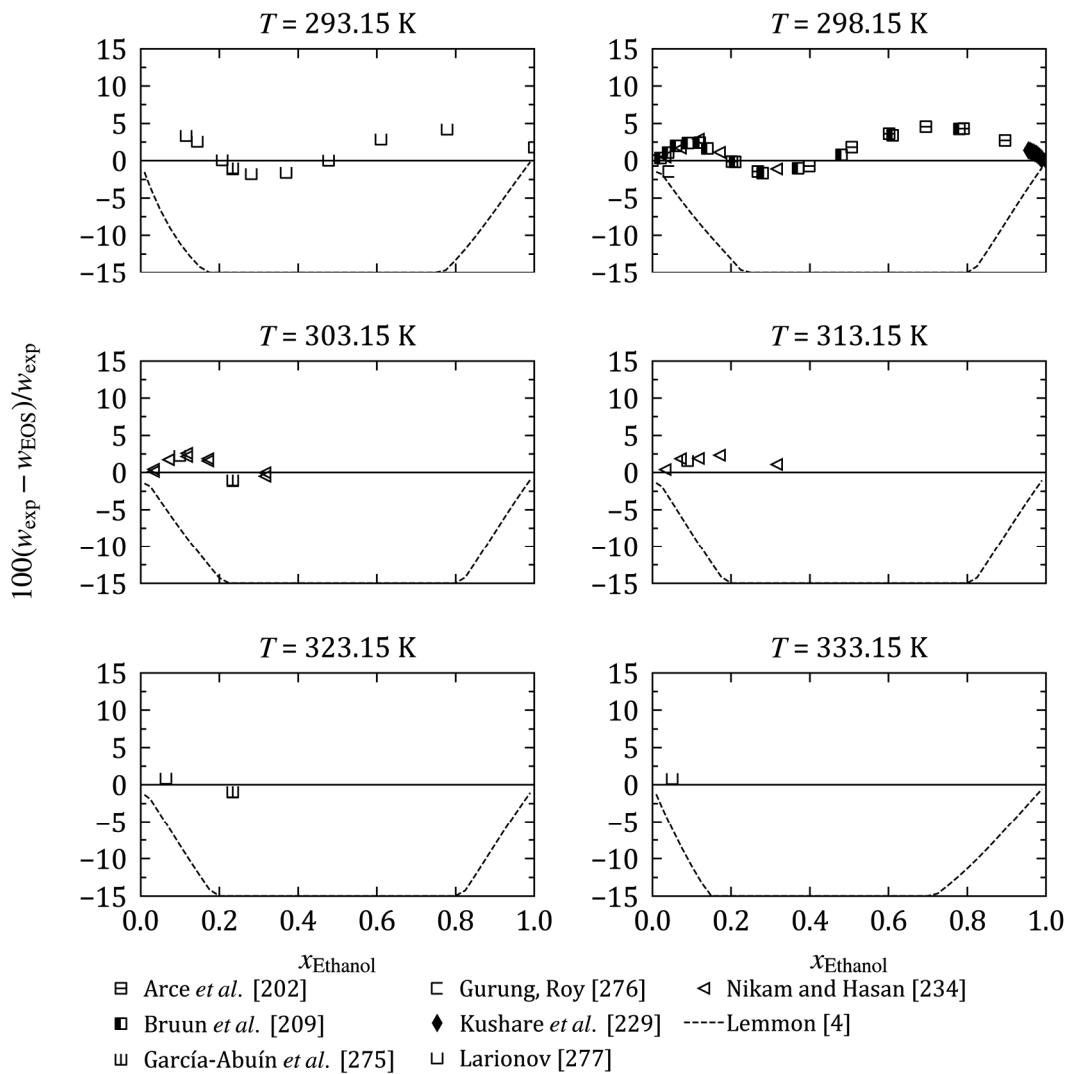


Figure 4.14: Relative deviations of the experimental liquid speed of sound data at atmospheric pressure from the new mixture model. Results from the model of Lemmon [4] (dashed curve) are plotted for comparison.

Arce *et al.* [202] claim only individual uncertainties for their experimental setup, which correspond to an approximated combined uncertainty of $\pm 0.29\%$. The remaining authors also claim an uncertainty of this magnitude, which cannot be maintained by the new model. Still, the new mixture model represents the experimental data within 4% and follows the data in a superior manner compared to the model of Lemmon [4]. Table 4.12 presents the average absolute relative deviations of the experimental data from the new mixture model. All AADs are below 2.5%.

Table 4.12: Absolute average deviation of the new mixture model from the experimental liquid speed-of-sound data.

| Author | Nr of Pts | $(T_{\min} - T_{\max}) / \text{K}$ | p / MPa | $x_{\min} - x_{\max}$ | AAD / % |
|----------------------------------|-----------|------------------------------------|------------------|-----------------------|---------|
| Arce <i>et al.</i> [202] | 8 | 298.15 - 298.15 | 0.1 | 0.2018 - 0.8959 | 2.408 |
| Bruun <i>et al.</i> [209] | 14 | 298.14 - 298.14 | 0.1 | 0 - 1 | 1.524 |
| García-Abuín <i>et al.</i> [275] | 8 | 288.15 - 323.15 | 0.1 | 0.2336 - 0.2336 | 1.023 |
| Gurung and Roy [276] | 1 | 298.15 - 298.15 | 0.1 | 0.0416 - 0.0416 | 1.442 |
| Kushare <i>et al.</i> [229] | 12 | 298.15 - 298.15 | 0.1 | 0.9552 - 1 | 0.764 |
| Larionov [277] | 13 | 293.14 - 333.13 | 0.1 | 0.0506 - 1 | 1.84 |
| Nikam and Hasan [234] | 20 | 298.15 - 313.15 | 0.1 | 0.0329 - 0.3155 | 1.372 |

4.5 Summary

A new model for ethanol-water mixtures was presented, which is superior to the model of Lemmon [4] with respect to the pressure dependence of the density, and, consequently, the description of the speed of sound. The representation of vapor-liquid equilibria at high temperatures could be improved as well. For a further improvement, supplementary measurements investigating high-temperature phase equilibria, density and speed-of-sound measurements in the gaseous phase, and isobaric heat capacity measurements at elevated pressures are required.

However, both mixture models exhibit shortcomings in the representation of the strong mixing effects for low ethanol fractions at low temperatures (see Figure 4.11). Systematical deviations were found for the excess enthalpy as well as for the isobaric heat capacity. A new functional form for the reducing functions considering a stronger impact of the mole fraction is assumed to be beneficial. In 1996, Lemmon proposed a different form of equation in his doctoral thesis [75] where the composition was considered with a power in the temperature reducing function. Since the historical

development of these mixture models concentrated on the description of natural gases (GERG-2004 [79], GERG-2008 [80]) and combustion-like gases (EOS-CG [81]), which behave considerably different than the ethanol-water system, there was no need to enhance this approach. Nevertheless, for non-ideal mixtures such as the ethanol-water system, this extended corresponding states approach might improve the description of mixing effects in the liquid phase.

5 A New Generalized EOS for a PAO Lubricant and its Mixture with Ethanol

In this chapter, the development of a pseudo-pure fluid equation of state for the PAO lubricant employed in the proposed EHR process is presented. Based on the given theoretical background in sections 3.3 and 3.5, the fitting process is briefly discussed, and results are presented.

Applying the new pure fluid equation of state for PAO and the equation of state for ethanol by Schroeder *et al.* [3], a mixture model based on the Helmholtz energy as presented in section 3.6 was developed and results are shown.

5.1 Pseudo Pure Fluid Equation for PAO

A property model for the newly designed lubricant of the family PAO is needed. Unfortunately, there is only very limited experimental data available. Furthermore, the lubricant is not a pure fluid but a mixture of different PAO base oils and further additives. Since there was no information provided about the composition of the lubricant, and, more importantly, there were no experimental data of these components and their binary combinations available, it was impossible to model this lubricant as an actual mixture. Therefore, the PAO is assumed to behave like a pure fluid. The molar mass is given with $M = 1773$ g/mol.

Experimental data

The company Fuchs Europe Schmierstoffe GmbH provided 13 density data points in a temperature interval from $T = 293$ K to $T = 353$ K. Furthermore, the isobaric heat capacity c_p was determined for 11 temperatures from $T = 293$ K to $T = 393$ K. Both data sets were measured at atmospheric pressure. [278]

Additionally, 15 experimental vapor pressures in the temperature range from $T = 283$ K to $T = 423$ K were provided by Fuchs Europe Schmierstoffe GmbH [279]. This data set was determined for a precursor lubricant in the development process. Since these lubricants are considered to be very similar, the dataset was applied to the final PAO as well. There was no information given about the uncertainty of any of the measurements.

Consequently, this limited data base is not sufficient to enable the development of a substance-specific Helmholtz energy equation of state as introduced in section 3.4. Therefore, a generalized approach is favored.

5.1.1 PAO: SRK

In a first approach, the SRK [34] equation was applied, which is widely accepted in industry. Section 3.3 contains a detailed description of this three-parameter corresponding states approach. Usually, the SRK is used predictively based on the critical temperature T_c , the critical pressure p_c , and the acentric factor ω . Since all these properties are unknown in case of the PAO, they are used as adjustable parameters here.

The software Excel was used as a simple fitting environment. The software tool TREND [280] was embedded in a VBA macro to make the thermodynamic property routines available. The Excel solver was then used to minimize the SSQ, which was calculated from the deviation of the experimental data from the calculated densities and vapor pressures. In order to calculate isobaric heat capacities, an equation describing the ideal gas behavior is needed. Since the molecular structure is unknown, a group contribution method cannot be applied to estimate the ideal gas heat capacity. Therefore, the experimental isobaric heat capacity data is not considered in the adjustment. Table 5.1 presents the results of the fitting process of the corresponding states parameters.

Table 5.1: Adjusted corresponding states parameters for the PAO described by the SRK [34].

| T_c / K | p_c / bar | $\omega / -$ |
|------------------|--------------------|--------------|
| 1821.5 | 6.45 | -0.175 |

A rather high critical temperature of $T_c = 1821.5 \text{ K}$ was found. It is important to keep in mind, that this temperature is used as an adjustable reducing parameter and therefore loses its physical meaning as the critical temperature of the fluid. However, complex molecules like those this lubricant consists of have a limited thermal stability, which is lower than the true critical temperature. Additionally, the adjusted acentric factor ω is unexpectedly small, but again, used as a freely adjustable parameter here.

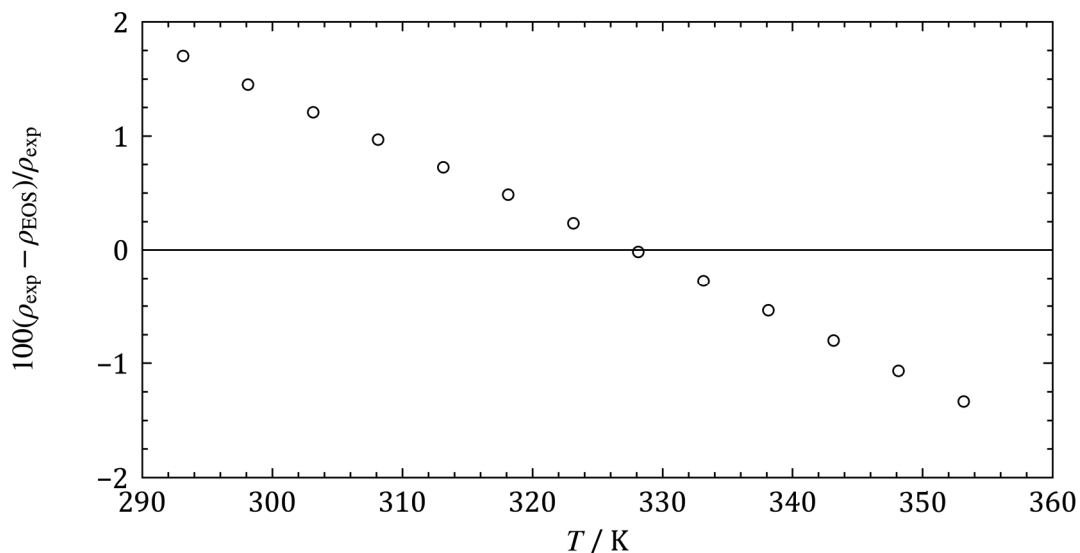


Figure 5.1: Relative deviations of the experimental density data [278] from the adjusted SRK equation for the PAO. The representation of the experimental density data by the adjusted SRK equation can be seen in Figure 5.1. The equation shows linear deviations in temperature from the experimental data which leads to a deviation of +2% to -1.5%.

Figure 5.2 presents the relative deviation of the calculated vapor pressure from the experimental data. The deviations range from -30% to +50%.

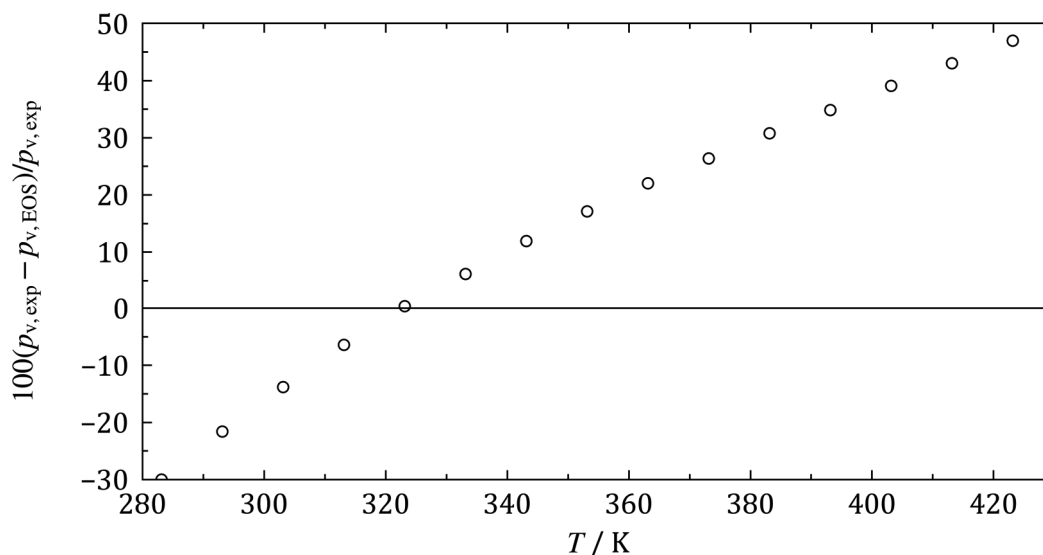


Figure 5.2: Relative deviations of the experimental vapor pressure data [279] from the adjusted SRK equation for the PAO.

Evidently, the SRK is not suitable to model this PAO. Therefore, a generalized Helmholtz energy equation of state was chosen next to describe the experimental data.

5.1.2 PAO: Generalized Helmholtz Equation

The generalized equation of state proposed by Alexandrov *et al.* [63] was chosen due to its development especially for long-chained hydrocarbons. For a description of the underlying model, see section 3.5.

The corresponding state parameters of this model have been adjusted using the fitter provided by NIST [55], which was presented in section 4.2. Table 5.2 shows the results of the adjustment.

Table 5.2: Adjusted corresponding states parameters for the PAO described by the generalized equation of Alexandrov *et al.* [63].

| T_c / K | $\rho_c / \text{mol} \cdot \text{m}^{-3}$ | $\omega / -$ |
|------------------|---|--------------|
| 1396.3 | 140.0 | 0.0207 |

The parameters according to equation (3.102) evaluated with the new adjusted corresponding states parameters can be taken from Appendix B.

The critical temperature found by the adjustment of this model is significantly lower than the one found for the SRK ($T_{c,\text{SRK}} = 1821.5 \text{ K}$). The acentric factor is again very small.

In order to use the isobaric heat capacity data in the adjustment, a c_p^0 -equation has been simultaneously fitted using the nonlinear fitting technique provided by NIST [55]. Table 5.3 shows the adjusted parameters according to equation (3.66).

Table 5.3: Parameters of the adjusted c_p^0 -equation for PAO with one polynomial and one Planck-Einstein term according to Eq. (3.66).

| $n_i / -$ | θ_i / K | Type |
|-----------|-----------------------|------|
| 414.79 | - | Pol |
| 878.39 | 2281.407 | PE |

Figure 5.3 presents the deviation of the model from the experimental density data. The experimental data can be represented within +0.15 % and -0.3%.

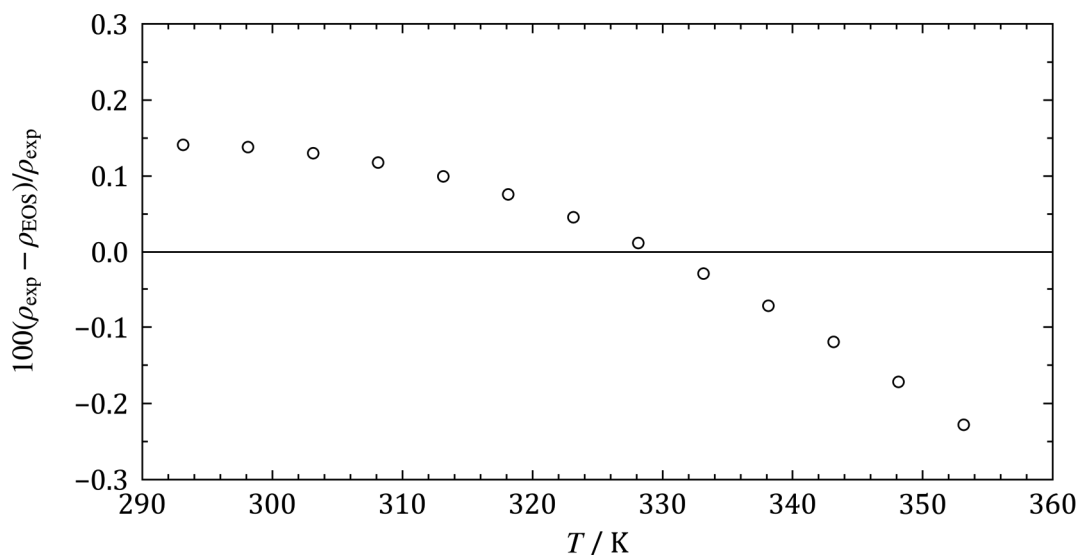


Figure 5.3: Relative deviations of the experimental density data [278] from the adjusted generalized Helmholtz equation for the PAO.

Figure 5.4 shows the relative deviation in terms of vapor pressure, which is significantly improved by this model. Now, the equation deviates from the experimental data within +4 % and -5%. Considering the very low vapor pressures of the PAO, this is a good representation. Absolute deviations are less than $2.1 \cdot 10^{-8}$ MPa.

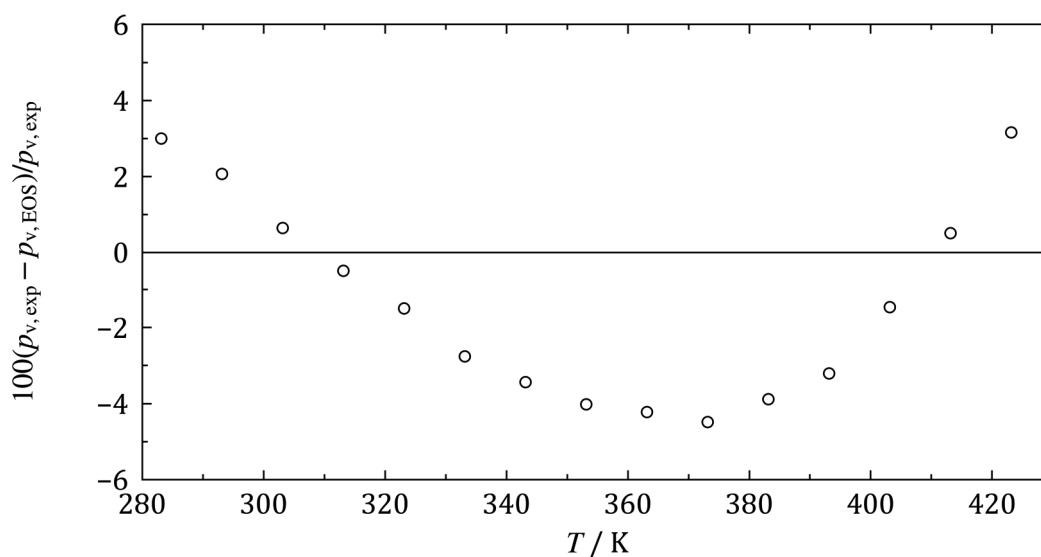


Figure 5.4: Relative deviations of the experimental vapor pressure data [279] from the adjusted generalized Helmholtz equation for the PAO.

Figure 5.5 illustrates the representation of the isobaric heat capacity data by the new generalized equation of state. The equation is in good agreement with the experimental data and deviates by only up to 2.4%.

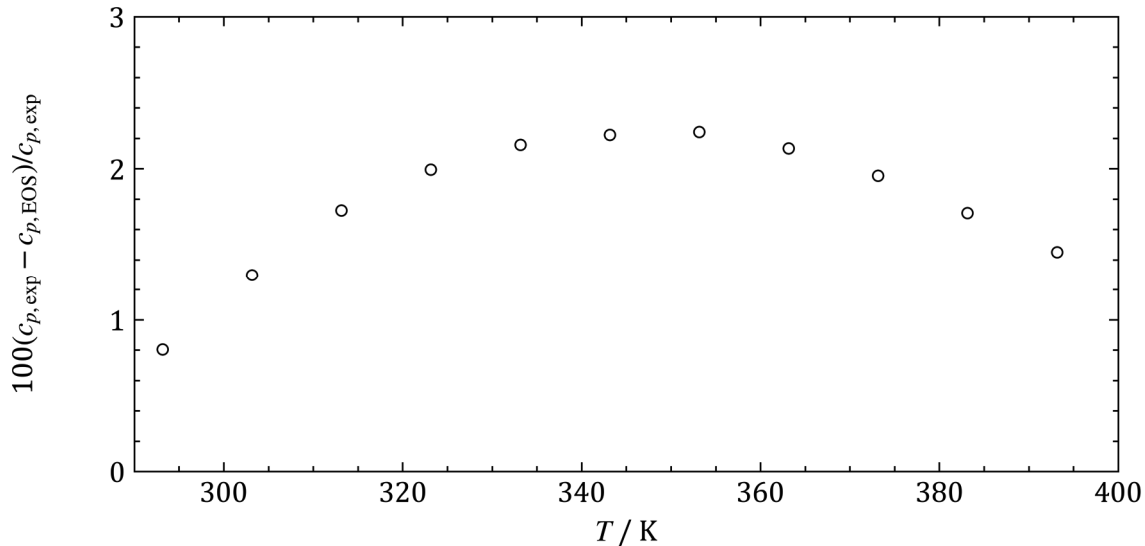


Figure 5.5: Relative deviations of the experimental isobaric heat capacity data [278] from the adjusted generalized equation for the PAO

Table 5.4 summarizes average absolute relative deviations of the presented experimental data from the new generalized equation of state.

Table 5.4: Average absolute relative deviations (AAD / %) of the experimental data from the generalized equation of state for PAO based on the model of Alexandrov *et al.* [63].

| Property | No. of data | Temperature range / K | Pressure / MPa | Average absolute relative deviations AAD / % |
|-----------|-------------|-----------------------|--|--|
| $p\rho T$ | 13 | 293 - 354 | 0.1 | 0.1 |
| p_v | 15 | 283 - 424 | $1.7 \cdot 10^{-11}$ - $6.6 \cdot 10^{-7}$ | 2.6 |
| c_p | 11 | 293 - 394 | 0.1 | 1.8 |

Applying the generalized equation of Alexandrov *et al.* [63] was beneficial for the representation of the experimental data.

5.2 Mixture Model for Ethanol-PAO

For the development of the mixture model, the pure fluid equation for ethanol by Schroeder *et al.* [3] was used as well as the generalized equation presented in section 5.1.2.

5.2.1 Experimental Data

There are no experimental data available in the literature describing this binary mixture. Therefore, it was decided by all project partners to investigate the densities, phase equilibrium, and rheological behavior in the framework of this research project. The

measurements were carried out by the Chair of Process Technology of RUB [281] and are not published, yet. Since the rheological behavior is not relevant to this work, these data will not be discussed here. Only densities and phase equilibria are considered for the adjustment of the new model.

As desired, ethanol and the new PAO form an emulsion under ambient conditions. The long-term stability of an emulsion consisting of 20 vol.-% PAO was investigated and results are presented in Figure 5.6. One sample was emulsified by applying ultrasound, the other sample was shaken. Pictures were taken after 24 hours, and after 7 days. Already after 24 hours, there are significant differences between the samples. The lighter ethanol-rich phase on top loses its milky appearance in case of the shaken sample. Consequently, the ultrasound-emulsified sample is more stable than the sample that had been shaken. This becomes even more distinct after seven days.

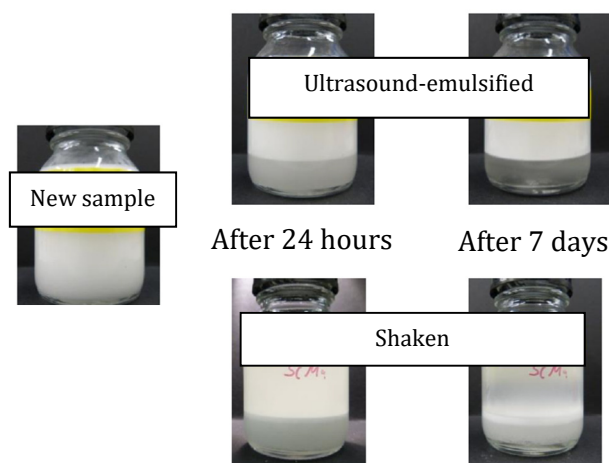


Figure 5.6: Investigation of the long-term stability of a shaken PAO-Ethanol emulsion and an ultrasound-emulsified sample, both with 20 vol.-% PAO [282].

The light microscope pictures presented in Figure 5.7 show that the diameter of the oil droplets in the ethanol-rich phase is significantly decreased in the ultrasound-emulsified sample. This characteristic leads to higher stability, which can be seen in Figure 5.6. Additionally, the light microscope pictures show that the oil-rich phase is an oil-ethanol-oil double emulsion, which means that the ethanol in the oil rich phase contains oil itself.

The emulsion of these two components is not a stable state, as was shown by the long-term stability investigation (Figure 5.6). It decomposed quickly into two phases, an ethanol-rich and an oil-rich phase. With time, the composition of the phases changed as the emulsion decomposed further. It is a challenge for the development of a mixture model to cope with this dynamic behavior, since by principle the model can only

describe equilibrium states. In contrast to emulsions, liquid-liquid equilibria can be represented by this model.

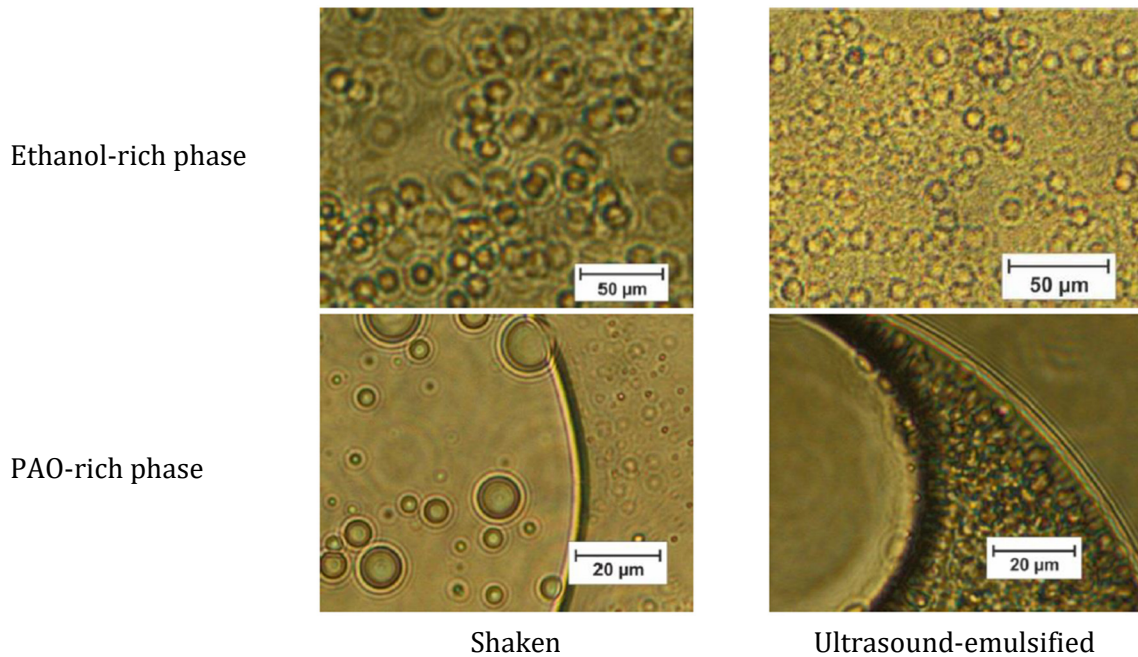


Figure 5.7: Light microscope investigation of an ethanol-rich and an oil-rich phase of a shaken sample and an ultrasound-emulsified sample [282].

Densities

Densities were measured in an autoclave mounted on a rocking rack with the help of a flexural resonator in form of a tuning fork. This experimental method determines a local density disregarding of a potential phase separation. For a homogeneous system, the overall density is measured, whereas for a heterogeneous system, only the density of one of the phases is determined. For details on this apparatus, see Brinkmann [283].

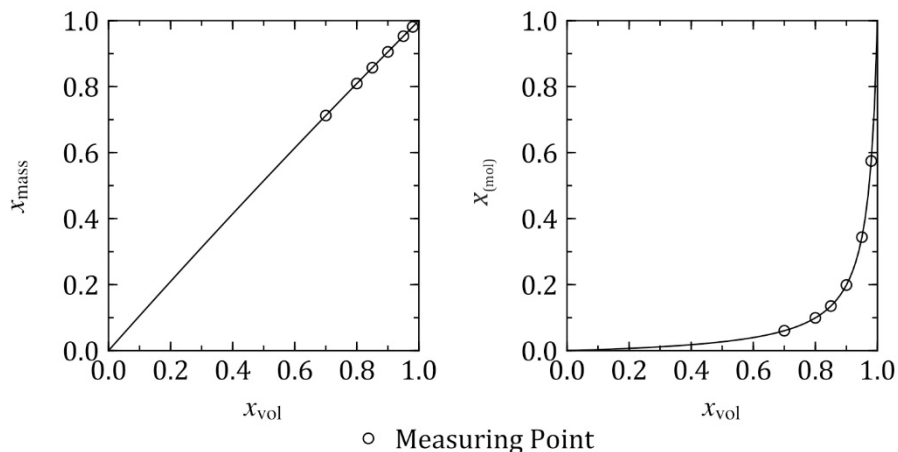


Figure 5.8: Relation between volumetric, mass, and mole fractions of the PAO in the mixture.

Only high volumetric concentrations of PAO have been measured in a temperature range from $T = 310$ K to $T = 410$ K. However, due to the very significant difference in the molar masses of the PAO ($M_{\text{PAO}} = 1173$ g/mol) and ethanol ($M_{\text{ETO}} = 46.07$ g/mol), the molar fraction deviates strongly from the respective volumetric or mass fractions. Figure 5.8 illustrates this effect and presents the compositions that have been investigated.

The samples were prepared under atmospheric conditions and filled in a sealed container, which was subsequently heated and shaken for 30 minutes. For higher temperatures, the samples were initially preheated before being sealed in the container. After shaking the sample for 30 minutes, the density was measured. Since the emulsion decomposes into two phases, and the composition of the phases change with the further decomposition of the emulsion, the measurement was repeated after 1, 2, 5, and 15 minutes to investigate the effect on the density and the simultaneously measured viscosity. In the case of two separated phases, the aim of the investigation was to measure the heavier oil-rich phase. The properties of the oil-rich phase were of special interest to the other project partners since this phase was to be used for the lubrication of the expander. For the adjustment of the new mixture model, only the initial measurement points were considered where the mixture was fully emulsified, and the measured density resembles the overall density of the emulsion.

Unfortunately, the pressure was not measured during the experiment. In order to be able to use this data, the pressure has been estimated to be slightly higher than the corresponding vapor pressure of the three-phase equilibrium, which means that a liquid-liquid equilibrium (LLE) is assumed for all measurement points. It is reasonable to assume that the effect of the error of the estimated pressure on the density is small, regarding the instability of the system. Evaluating the derivative of the density with respect to the pressure at constant temperature of the new model $(\partial\rho/\partial p)_T$, the error caused by an offset in the pressure estimation of for example 0.05 MPa can be approximated with 0.02% in molar density, which is reasonably small.

Phase equilibria

The measurements of the phase equilibrium were carried out in a high-pressure cell. The experimental setup has been described by Kukova *et al.* [284]. The samples were prepared and then filled in the initially evacuated measuring cell. The measuring points

were determined by the overall composition of the sample and the employed temperature. Figure 5.9 and Figure 5.10 illustrate different equilibria of systems with 5, 10 and 20 vol.-% PAO.

Depending on the overall composition and temperature, a three-phase vapor-liquid-liquid equilibrium (VLLE) could be observed, with an ethanol-rich vapor phase on top, an ethanol-rich liquid phase in the middle, and a PAO-rich liquid phase at the bottom.

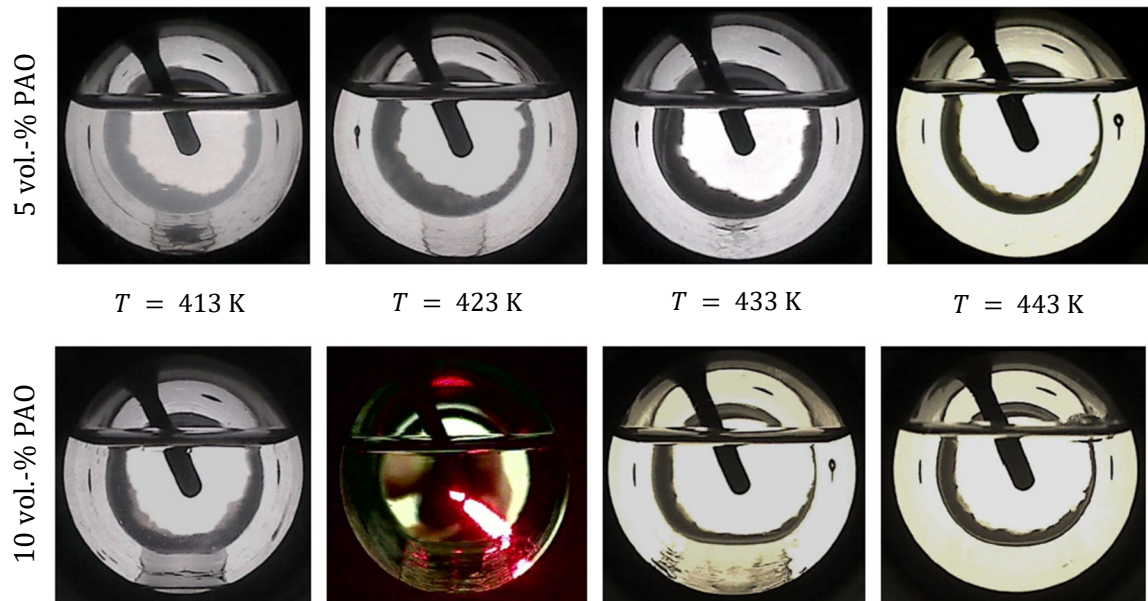


Figure 5.9: Phase equilibria of samples of 5 vol.-% and 10 vol.-% PAO at different temperatures [281].

The volume of the heavy liquid phase decreases with rising temperature until only a vapor-liquid equilibrium is left.

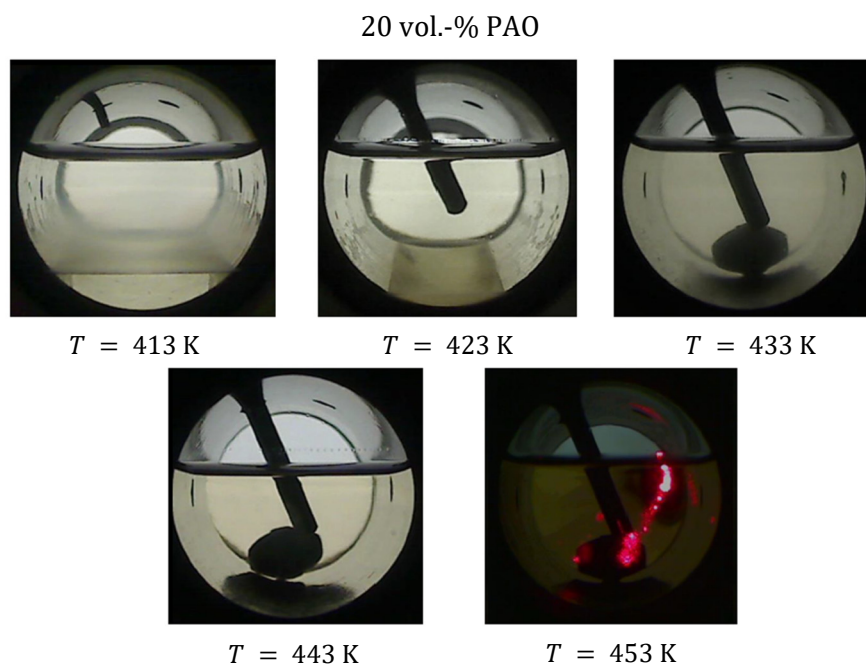


Figure 5.10: Phase equilibria of a sample of 20 vol.-% PAO at different temperatures [281].

Additionally, a relation between the overall composition and the phase fraction of the oil-rich phase can be observed. The more PAO is in the sample, the higher is the phase fraction of the PAO-rich phase.

During the experiment, a laser beam was used to examine the system for the occurrence of microemulsions. When a light beam passes through a colloidal system, the light is scattered at the microscopic particles or droplets and the beam is visible in the medium. This phenomenon is described by the Faraday-Tyndall effect [285]. Depending on the temperature and overall composition, a microemulsion could be determined in the ethanol-rich liquid phase, as can be seen in Figure 5.9 for $T = 423$ K and $z_{\text{PAO}} = 10$ vol.-%. Figure 5.10 illustrates that this effect vanishes for $T = 453$ K and the mixture is in solution in all phases. The possible formation of a microemulsion has no influence on the interpretation of the experimental data with respect to the adjustment of an equation of state for the mixture. For more information about microemulsions see Kahlweit *et al.* [286].

When the ethanol-PAO system reached its equilibrium, the composition of the vapor phase, and of the lighter ethanol-rich liquid phase were determined for the three presented overall compositions at the presented temperatures. The composition of the oil-rich liquid phase could only be determined for the highest overall PAO composition of 20 vol.-% at $T = 413$ K. Otherwise, the liquid level of this phase was too low to allow for sampling, as can be seen in Figure 5.9 and Figure 5.10.

As already discussed, the PAO incorporated here consists of several base PAOs and an emulsifier. Therefore, the mixture of this oil with ethanol is a multi-component system. However, since the PAO is modeled as a pure fluid, the mixture with ethanol is binary by definition. Gibbs' phase rule indicates that for a mixture of $N = 2$ components with $P = 3$ phases in equilibrium, there is only $F = 1$ degree of freedom:

$$F = N - P + 2. \quad (5.1)$$

Consequently, there is one three-phase line for a binary mixture, along which it decomposes into three phases. The compositions of the individual phases do not change with respect to a change in the overall composition of the mixture, given that the overall composition allows for the formation of three phases. However, the experimental results show a different behavior, which cannot be represented by the chosen binary model.

5.2.2 The New Mixture Model for Ethanol-PAO

Based on the new generalized equation for PAO and the ethanol equation of state of Schroeder *et al.* [3], a new mixture model was developed. The software tool TREND [280] was embedded in a VBA macro to make the thermodynamic property routines available in Excel. The Excel solver was used to minimize the SSQ, which was calculated from the deviation of the experimental data from the respective properties calculated from the new model. TREND [280] was used in order to be able to calculate liquid-liquid and vapor-liquid-liquid equilibria. Due to the limited data base, only the reducing parameters determining the pseudocritical temperature and pseudocritical density of the mixture (see equations (3.113) and (3.114)) were adjusted. The final parameters can be taken from Table 5.5.

Table 5.5: Adjusted parameters of the reducing functions for ethanol-PAO mixtures.

| | β | γ |
|----------|---------|----------|
| T_r | 1.578 | 0.5212 |
| ρ_r | 1.571 | 0.9833 |

Figure 5.11 presents relative deviations of densities calculated from the new mixture model for ethanol-PAO mixtures from the experimental values. As already discussed, the pressure was not measured and, therefore, estimated to be atmospheric or slightly above the corresponding vapor pressure. Thus, all calculated state points are in LLE, where the overall density is calculated as the sum of the phase densities weighed with the respective phase fraction as predicted by the new mixture model. As for the adjustment of the model, exclusively the initial measurements with the completely emulsified sample are considered for comparison. At temperatures from $T = 310$ K to $T = 330$ K, the deviations scatter and range from +6% to -3%. The new mixture model seems to overestimate the density by approximately 5% for temperatures above $T = 350$ K. The uncertainty in measurement of the density is claimed to be ± 1 kg/m³ [283] which corresponds to a maximum uncertainty of 0.14% in molar density with respect to this mixture. Nevertheless, the uncertainty in the composition of the mixture is not included. Since the boiling point of ethanol at atmospheric pressure is considerably low with $T_b \approx 350$ K, the preparation of the samples as conducted bears the risk of a significant evaporation of ethanol during the procedure at elevated temperatures. Assuming an overestimation of the ethanol fraction due to partial evaporation, the experimental

densities correspond to mixtures with less ethanol and are, therefore, lower than the “true” respective densities with respect to molar units. This effect might explain the change in the relative deviations of the experimental data from the new mixture model as discussed for temperatures above $T = 350$ K.

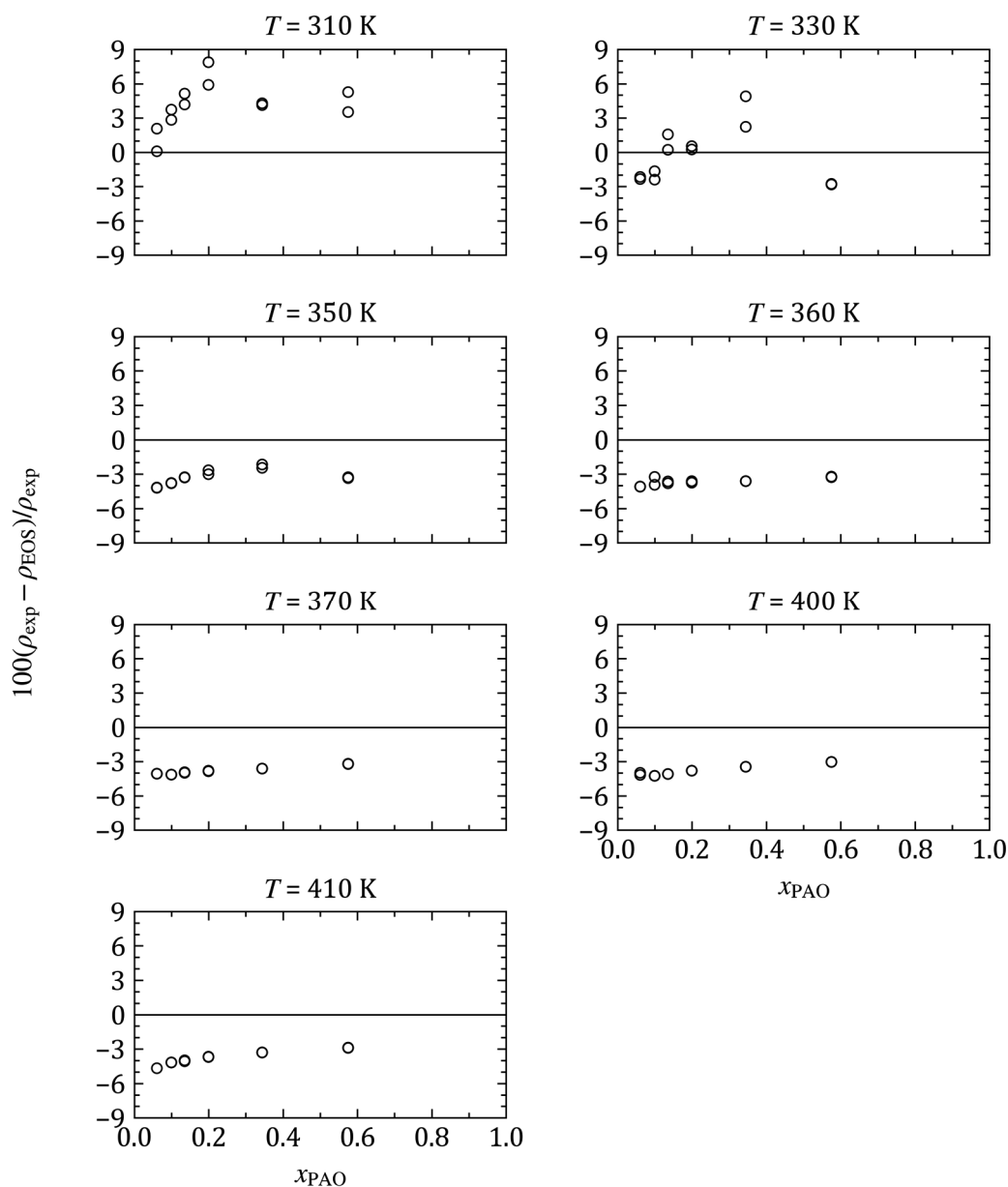


Figure 5.11: Relative deviations of the experimental densities [281] from the new mixture model for ethanol-PAO mixtures.

However, with respect to the challenge of modeling a multi-fluid mixture as a binary system, the new model is in good agreement with the experimental data with an overall average absolute relative deviation of $\text{AAD} = 3.5\%$.

Figure 5.12 presents the phase envelopes of several overall compositions of ethanol-PAO mixtures, calculated from the new model with TREND [280]. The left line (dashed) represents the three-phase line, whereas the right line depicts the dew line.

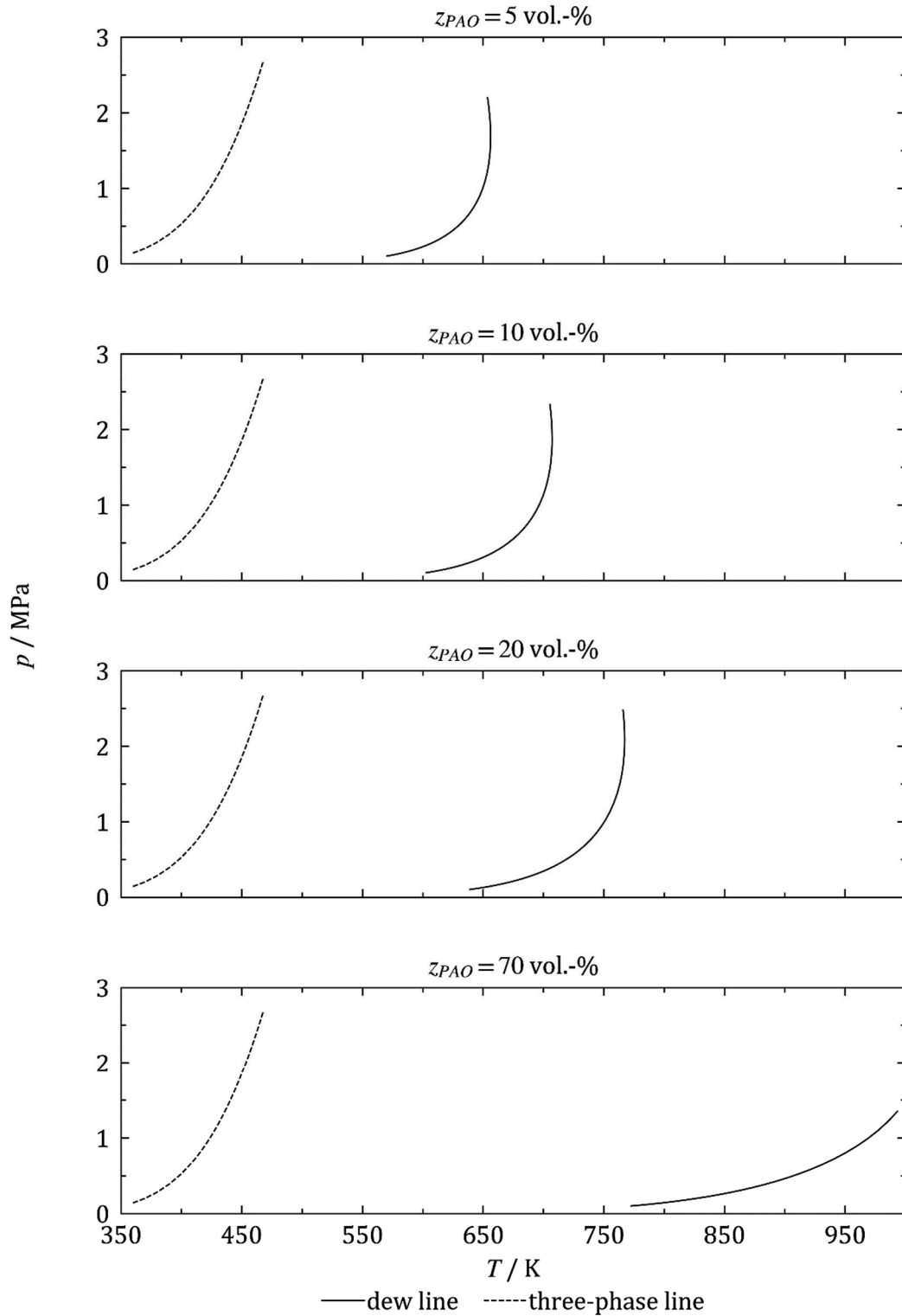


Figure 5.12: Phase envelopes of several ethanol-PAO systems in a p, T -diagram calculated from the new model with TREND [280].

As already discussed by means of the Gibbs phase rule, the location of the three-phase line does not depend on the overall composition. Left of this line, the mixture is in liquid-liquid equilibrium. At the three-phase line, the ethanol-rich vapor phase emerges, leading to the vapor-liquid region right of the three-phase line. Here, an ethanol-rich vapor phase is in equilibrium with an oil-rich liquid phase. Right of the dew line, the system is completely evaporated. Figure 5.12 also illustrates how the volumetric oil fraction influences the phase envelop. The vapor-liquid region expands with increasing overall oil fraction significantly. However, the corresponding mole fractions of the presented phase envelopes vary only from $x_{\text{PAO}} = 0.0014$ to $x_{\text{PAO}} = 0.0604$ (see Figure 5.8).

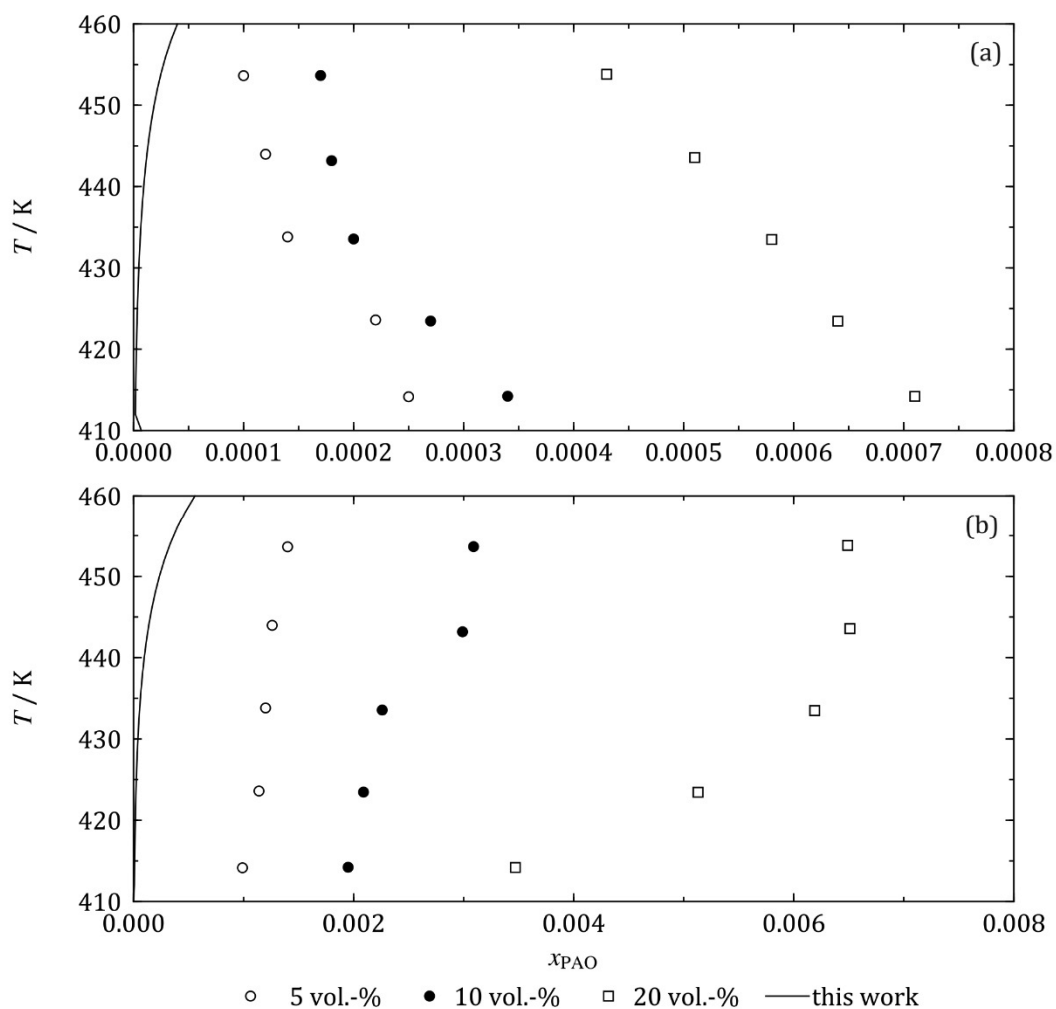


Figure 5.13: Phase equilibria of ethanol-PAO mixtures in a T, x -diagram. (a): Vapor phase composition for all overall compositions. (b): Liquid phase (ethanol-rich) composition for all overall compositions.

For the binary model, the compositions of three coexisting phases in equilibrium do not vary with the overall mixture composition. Consequently, one of the three investigated ethanol-PAO systems had to be chosen for the adjustment. Since the system with

$z_{\text{PAO}} = 5$ vol.-% contains least of the pseudo-pure fluid PAO, these experimental values are considered the most suitable for the adjustment of the model and therefore the most suitable for comparison here. Figure 5.13 presents the compositions of the ethanol-rich vapor and ethanol-rich liquid phase found by the experiment for the three overall compositions as well as the compositions calculated from the new model for these two phases. The new model predicts a three-phase equilibrium in the complete temperature range presented. The model underestimates the oil fraction in the ethanol-rich vapor and liquid phase significantly. Given that the PAO contains an emulsifier to increase the solubility and induce an emulsion, this was to be expected. The phase equilibrium of an emulsion, as presented here, is not a stable state in a thermodynamic sense. Therefore, it cannot be represented by the chosen model. As already discussed, there is only one experimental point describing the composition of the oil-rich phase, which was determined at $T = 414.2$ K for an overall composition of $z_{\text{PAO}} = 20$ vol.-% ($\approx z_{\text{PAO}} = 0.68$ mol.-%) to be $x_{\text{PAO}} = 0.047$. The value calculated by the new model deviates with $x_{\text{PAO}} = 0.911$ strongly.

During the fitting process, it became evident, that the model cannot reproduce the compositions of the coexisting phases of the three-phase equilibrium ($z_{\text{PAO}} = 5$ vol.-%) satisfactorily. Therefore, the heavy PAO-rich liquid phase was neglected and the ethanol-rich liquid phase used as input for a simple dew point calculation. In this manner, all three overall compositions could be considered for the adjustment. Figure 5.14 presents three T, x -diagrams containing the experimental data and the vapor phase compositions calculated with the new model using the liquid phase composition as input for a dew point calculation. The calculated vapor phase composition is in good agreement with the experimental data for all three overall compositions.

The representation of the VLLE did not change significantly with regard to the different fitting method of interpreting the experimental data as simple vapor-liquid equilibria.

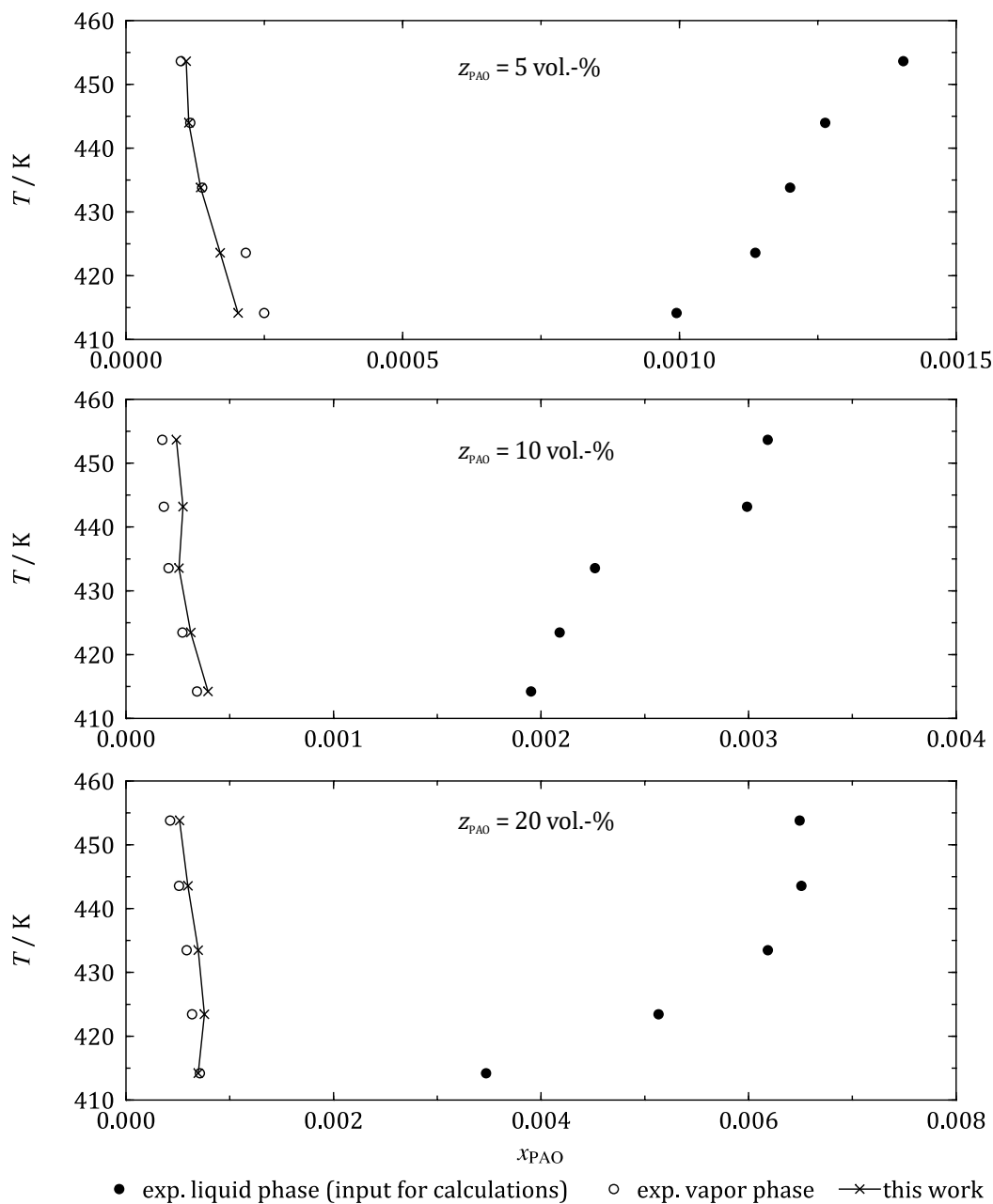


Figure 5.14: T, x' -flash calculation and experimental data of the vapor and ethanol-rich liquid phase.

Figure 5.15 illustrates the relative deviation of the new model from the experimentally found vapor pressures. The model is in good agreement with the data and deviates from -1% to $+2.3\%$.

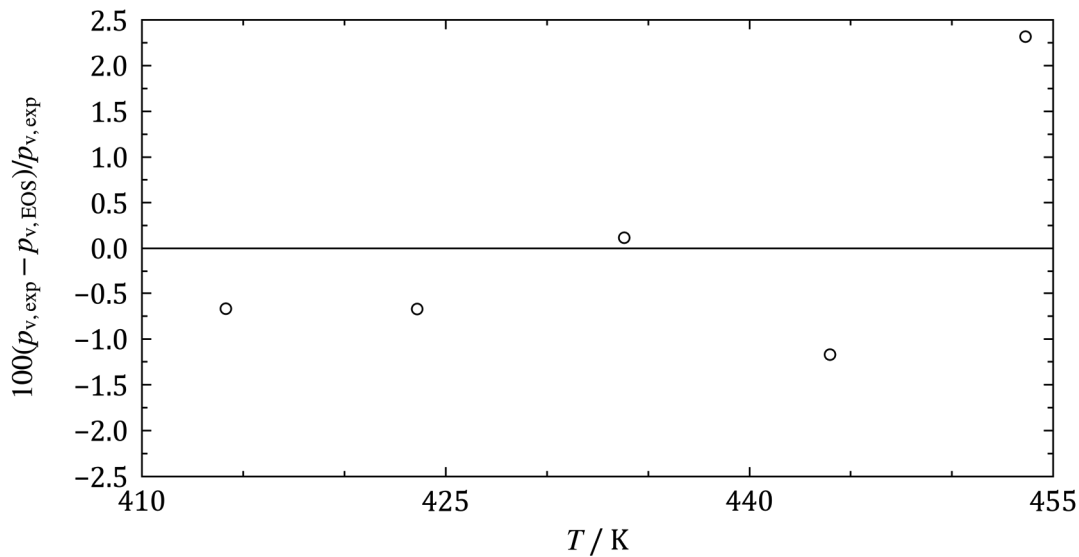


Figure 5.15: Relative deviations of the experimental vapor pressures from the new mixture model for ethanol-PAO.

5.2.3 Summary

A new model describing ethanol-PAO mixtures was found based on the new generalized equation of state for the PAO. The Helmholtz mixture approach was used for the description of this strongly asymmetric mixture. The new model reproduces the experimental densities satisfactorily. However, only the overall density of the emulsion or LLE could be compared because there were no experimental data available that describe the densities and compositions of the two coexisting liquid phases in equilibrium. The investigation of the long-term stability of the emulsion displayed in Figure 5.6 showed that the decomposition of the emulsion is a rather time-consuming process. Since the emulsifier increases the mutual solubility of ethanol and PAO significantly, it is assumed that the phase compositions predicted by the binary model would deviate rather strongly from the composition of the two stable phases of the fully decomposed emulsion. This theory is supported by the observation of the phase equilibrium calculations. When the model is used to freely predict the phases that a mixture of a given overall composition decomposes to, it finds three coexisting phases as found by experiment. However, the high solubility of both components due to the emulsifier cannot be represented. On the other hand, if the composition of the dominating ethanol-rich liquid phase is defined and the coexisting vapor phase is calculated, the model gives reliable results, as shown for the dew point calculations in Figure 5.14.

6 New Generalized EOS for two POE Lubricants and their Mixtures with CO₂

In this chapter, two generalized Helmholtz equations of state for two base stock POEs, PEC5 and PEC7, are presented. These equations were adjusted to the experimental data available in the literature, which comprise only densities and vapor pressures. They are compared to fluid-specific equations of state, which were developed by Lemmon and Eckermann and which are still to be published [23].

In order to develop the fluid-specific equations of state, experimental measurements were carried out at NIST including densities, vapor pressures, isobaric heat capacities, and speeds of sound. To evaluate the predictive representation of caloric properties by the generalized equations, which were exclusively adjusted to thermal property data, the new caloric data were not used for the adjustment of the generalized equations presented here. The thermal data measured at NIST was not yet available at the time of the development of the generalized equations.

Subsequently, a mixture model for PEC5-CO₂ was developed and transferred to the system PEC7-CO₂. The results are presented in sections 6.3 and 6.4.

6.1 Pure Fluid Equation for PEC5

Experimental data used for the adjustment

There are four publications in the literature dealing with the $p\rho T$ relationship of PEC5. Fandiño *et al.* [287], Fedele *et al.* [288], Wahlström and Vamling [289], and Shobha and Kishore [290] measured the homogeneous liquid density of this substance. Razzouk *et al.* [291] investigated vapor pressures of PEC5 and PEC7.

In addition to the vapor pressure data, Razzouk *et al.* [291] published PC-SAFT parameters, that were adjusted to their data set and are used for comparison here. The parameters are given in Table 6.1.

Table 6.1: PC-SAFT parameters for PEC5 [291].

| m | $\sigma / \text{Å}$ | $\epsilon \cdot k_{\text{B}}^{-1} / \text{K}$ |
|---------|---------------------|---|
| 10.5329 | 3.9721 | 261.81 |

6.1.1 The New Generalized Equation of State

The new generalized equation of state for PEC5 has been developed with the help of the fitter provided by NIST [4]. It is based on the generalized equation of Alexandrov *et al.* [63] presented in section 3.5 and uses the critical temperature T_c , the critical density ρ_c , and the acentric factor ω as adjustable parameters. Table 6.2 presents the results of the adjustment.

Table 6.2: The corresponding states parameters for PEC5 adjusted in this work based on the generalized equation of Alexandrov *et al.* [63] and the corresponding states parameters found by Lemmon and Eckermann [23].

| | This work | Lemmon and Eckermann [23] |
|---|-----------|---------------------------|
| T_c / K | 875.19 | 890.00 |
| $\rho_c / \text{mol} \cdot \text{m}^{-3}$ | 549.69 | 556.00 |
| $\omega / -$ | 0.98689 | 0.89 |

The critical parameters found in this work are compared to the critical parameters used in the equation of Lemmon and Eckermann [23]. The adjusted acentric factor is compared to the value calculated from the equation of Lemmon and Eckermann [23]. The agreement with the critical parameters and the acentric factor found by Lemmon and Eckermann [23] validates their order of magnitude. However, PEC5 molecules are thermally stable only up to $T \approx 600$ K. For higher temperatures, the molecules begin to decompose significantly [292]. Therefore, these parameters are treated as mathematically adjustable parameters and their meaning is basically reduced to their function as reducing parameters in the respective equations.

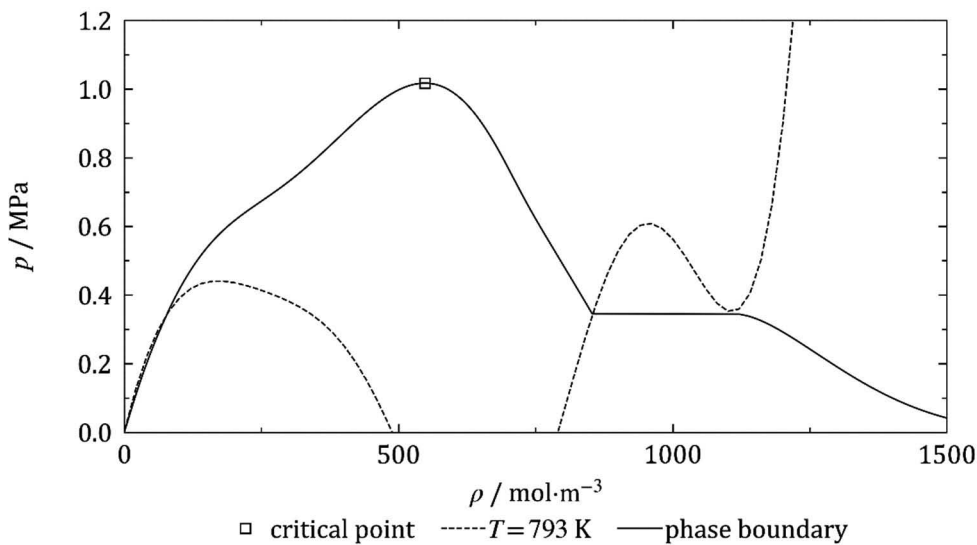


Figure 6.1: p, ρ -diagram of PEC5 with the isotherm $T = 793$ K calculated from the new generalized equation of state with $T_c = 875.19$ K.

Figure 6.1 shows a p, ρ -diagram of PEC5 with the isotherm $T = 793$ K calculated from the new generalized equation of state. This isotherm illustrates an unfavorable course and placement of the outer minimum. With increasing temperature, the outer extrema no longer overlap with respect to pressure. As a result, the flash calculation fails finding a vapor pressure by combining the outer extrema, leading to a discontinuity in the saturated vapor line at this temperature. This effect was also found for other fluids with comparable acentric factors as shown and discussed in section 3.5. However, this issue is not crucial for the description of the pure fluid PEC5, since the molecules already decompose in this temperature region [292]. Nevertheless, it might affect the application of the equation in a mixture model.

Since there was no data that could have been used for the adjustment of a c_p^0 -equation, the isobaric heat capacity of the ideal gas has been estimated with the group contribution method by Joback and Reid [293]:

$$\frac{c_p^0}{\text{J} \cdot \text{mol}^{-1} \cdot \text{K}^{-1}} = \sum_{i=0}^3 n_i \cdot T^{t_i} = \left(\sum \Delta_A - 37.93 \right) + \left(\sum \Delta_B - 0.21 \right) \cdot (T/K) \quad (6.1)$$

$$+ \left(\sum \Delta_C - 3.91 \cdot 10^{-4} \right) \cdot (T/K)^2 + \left(\sum \Delta_D - 2.06 \cdot 10^{-7} \right) \cdot (T/K)^3.$$

The coefficients of this classical polynomial form are determined by the structure of the molecule, which is presented in Figure 6.2. The individual contributions of the functional groups to the constants Δ_A , Δ_B , Δ_C , and Δ_D can be taken from Joback and Reid [293]. The resulting coefficients for the c_p^0 -equation (3.66) are listed in Table 6.3.

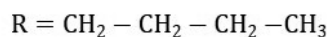
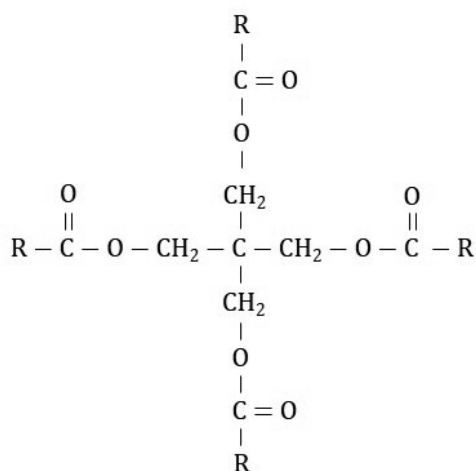


Table 6.3: Parameters in form of the c_p^0 -equation (3.66) determined by the group contribution method of Joback and Reid [293] for PEC5, reduced with $R = 8.3144598 \text{ J} \cdot \text{mol}^{-1} \cdot \text{K}^{-1}$.

| n_i | t_i |
|--------------------------|-------|
| 10.47885 | 0 |
| 0.257368 | 1 |
| $-1.18973 \cdot 10^{-4}$ | 2 |
| $1.236881 \cdot 10^{-8}$ | 3 |

Figure 6.2: Chemical structure of a PEC5 molecule.

6.1.2 Comparison to $p\rho T$ Data

Figure 6.3 presents relative deviations of the experimental density data from the new generalized equation of state. The deviations from the fluid-specific equation of state of Lemmon and Eckermann [23] and from the PC-SAFT equation of state [91,291] are also included in all figures of this section. The experimental data points in red were exclusively used for the adjustment of the fluid-specific equation of state [23]. The data sets of Fandiño *et al.* [287], and Fedele *et al.* [288] deviate from each other by approximately 0.5% in the overlapping temperature range. Since the data of Fortin [294] and Outcalt [295] were not yet available, the data of Fandiño *et al.* [287] were preferred in the fitting process of the generalized equation due to the lower estimated uncertainty of 0.14 kg/m³ compared to the uncertainty of the data set of Fedele *et al.* [288], which is estimated to be 0.6 kg/m³. Nevertheless, the data of these authors can be reproduced within 0.5% by the new generalized equation of state. The data of Fandiño *et al.* [287] are represented with an AAD of 0.14%, the data of Fandiño *et al.* [287] with an AAD of 0.35%. The generalized equation reproduces the experimental data of Outcalt [295], which agree very well with the data of Fedele *et al.* [288], with -0.5% to $+0\%$ in the whole temperature and pressure range (AAD = 0.29%). Only for temperatures lower than $T = 290$ K, the deviations enlarge to -0.7% .

The deviation of the PC-SAFT equation of state [91,291] increases rapidly with increasing pressure, always overestimating the density. The density predicted by Lemmon and Eckermann [23] is lower than the predicted density of the new generalized equation of state in the whole temperature and pressure range presented and follows the data of Outcalt [295] and Fedele *et al.* [288] accurately with an AAD of 0.061% and 0.078%, respectively.

The representation of the ambient pressure data of Wahlström and Vamling [289], Shobha and Kishore [290], and Fortin [294] is illustrated in Figure 6.4. The new generalized equation of state deviates by -0.5% to $+1\%$ from the experimental data of Wahlström and Vamling [289] (AAD = 0.18%), and Shobha and Kishore [290] (AAD = 0.39%). The equation of Lemmon and Eckermann [23] deviates by up to -0.5% from the new generalized equation following the data of Fortin [294] accurately (AAD = 0.049%). The PC-SAFT equation of state [91,291] is in agreement with the new generalized equation exhibiting only a small constant offset from the new equation.

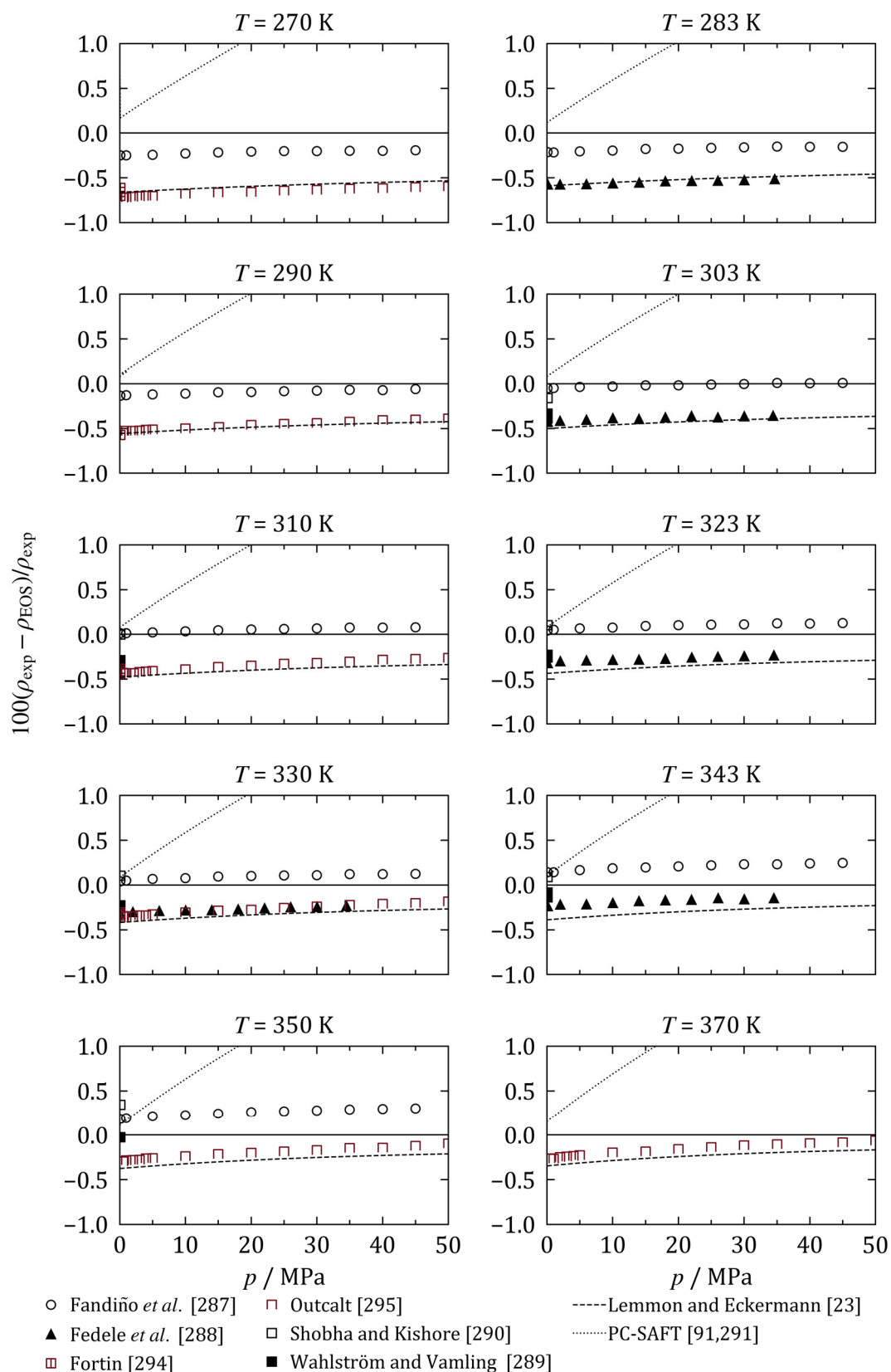


Figure 6.3: Relative deviations of experimental liquid densities from the new generalized equation of state for PEC5. Deviations from the PC-SAFT equation of state [91,291] (dotted curve), and from the equation of Lemmon and Eckermann [23] (dashed curve) are plotted for comparison.

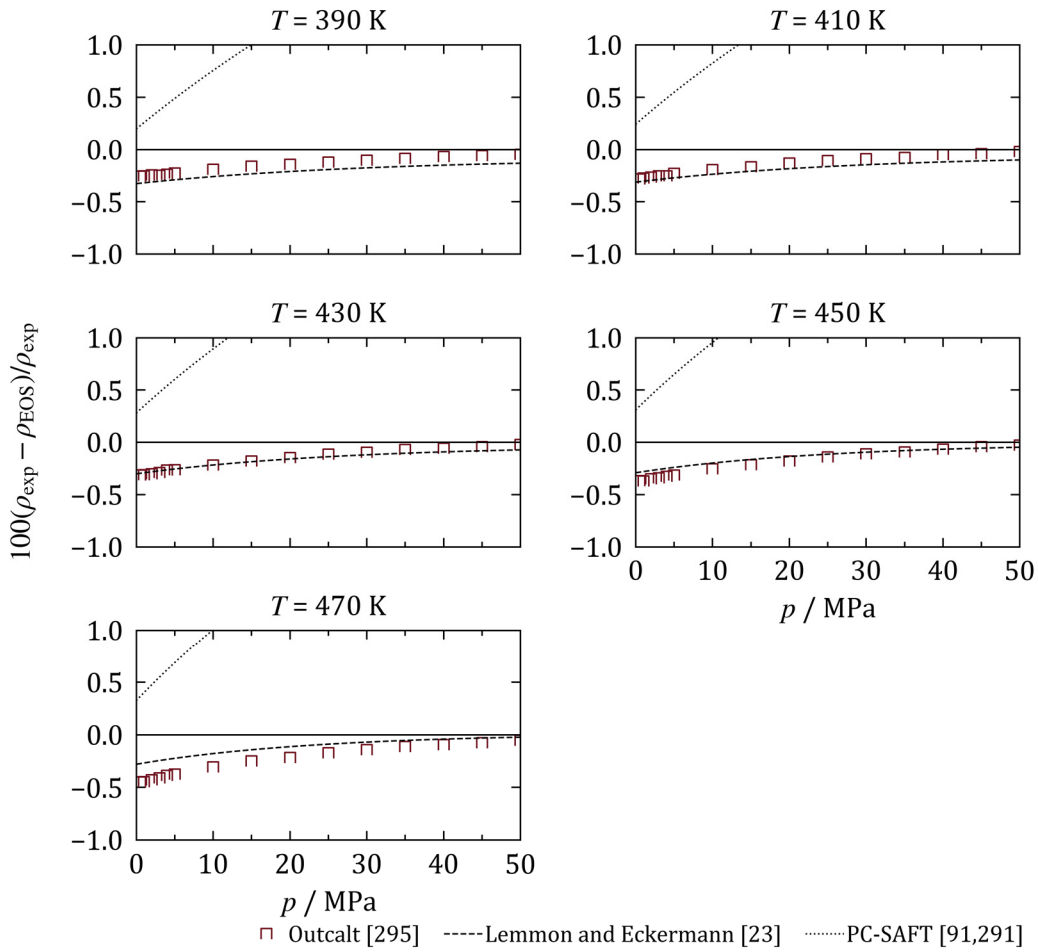


Figure 6.3 continued.

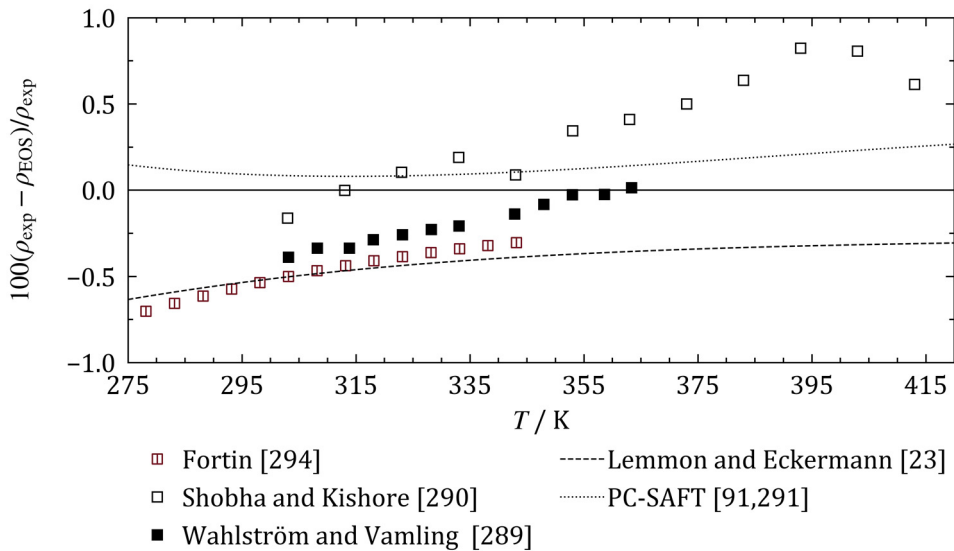


Figure 6.4: Relative deviations of experimental liquid densities at ambient pressure from the new generalized equation of state for PEC5. Deviations from the PC-SAFT equation of state [91,291] (dotted curve), and from the equation of Lemmon and Eckermann [23] (dashed curve) are plotted for comparison.

Table 6.4 summarizes the average absolute relative deviations of the three compared equations of state from the experimental density data. The fluid-specific equation of

state has the lowest AADs except for the data sets of Fandiño *et al.* [287], Wahlström and Vamling [289], and Shobha and Kishore [290], which do not agree accurately with the data of Fortin [294] and Outcalt [295], which were measured at NIST and used for the adjustment of this equation [23]. These data sets are represented best by the new generalized equation of state. The PC-SAFT equation of state [91,291] shows the highest AADs.

Table 6.4: Average absolute relative deviations of the experimental densities from the new generalized equation of state for PEC5, from the PC-SAFT equation of state [91,291], and from the equation of Lemmon and Eckermann [23].

| Author | No. of data | Temperature range / K | Pressure range / MPa | Average absolute relative deviations AAD / % | | |
|-----------------------------|-------------|-----------------------|----------------------|--|------------------|---------------------------|
| | | | | This work | PC-SAFT [91,291] | Lemmon and Eckermann [23] |
| Fandiño <i>et al.</i> [287] | 99 | 278 - 354 | 0.1 - 46 | 0.14 | 1.2 | 0.45 |
| Fedele <i>et al.</i> [288] | 40 | 283 - 344 | 0.1 - 35 | 0.35 | 1.0 | 0.078 |
| Wahlström and Vamling [289] | 13 | 303 - 364 | 0.101325 | 0.18 | 0.28 | 0.24 |
| Shobha and Kishore [290] | 12 | 303 - 414 | 0.101325 | 0.39 | 0.28 | 0.74 |
| Fortin [294] | 14 | 278 - 344 | 0.083 | 0.47 | 0.57 | 0.049 |
| Outcalt [295] | 165 | 269 - 471 | <0.1 - 51 | 0.29 | 1.4 | 0.061 |

6.1.3 Comparison to Vapor Pressure Data

There is only one data set describing the vapor pressures of PEC5 published in the literature so far. Razzouk *et al.* [291] measured five state points in a temperature range from $T = 334$ K to $T = 414$ K. Relative deviations of these experimental data points and the data measured at NIST by Widegren [296] from the new generalized equation of state are illustrated in Figure 6.5. The new generalized equation of state reproduces the data of Razzouk *et al.* [291] within -8% to $+3\%$ (AAD = 3.5%). The model of Lemmon and Eckermann [23] shows a different course over the temperature by following the data of Widegren [296], which it was adjusted to. The PC-SAFT parameters used here were adjusted to the experimental data of Razzouk *et al.* [291]. Therefore, the PC-SAFT equation of state [91,291] reproduces these data with deviations similar to those observed for the new generalized equation of state (AAD = 3.1%). The new generalized equation of state has an offset of approximately -30% from the experimental data of Widegren [296], since these data differ significantly from the vapor pressures investigated by Razzouk *et al.* [291] that were used for the development of the new equation. Despite this discrepancy, both data sets agree with respect to the estimated uncertainty

of both measurements acknowledging the effect of very small absolute values of the vapor pressure ($2.55 \cdot 10^{-10}$ MPa to $9.35 \cdot 10^{-7}$ MPa). Razzouk *et al.* [291] claim an uncertainty of $\pm 4\%$, whereas Widegren [296] proposes $\pm 24\%$.

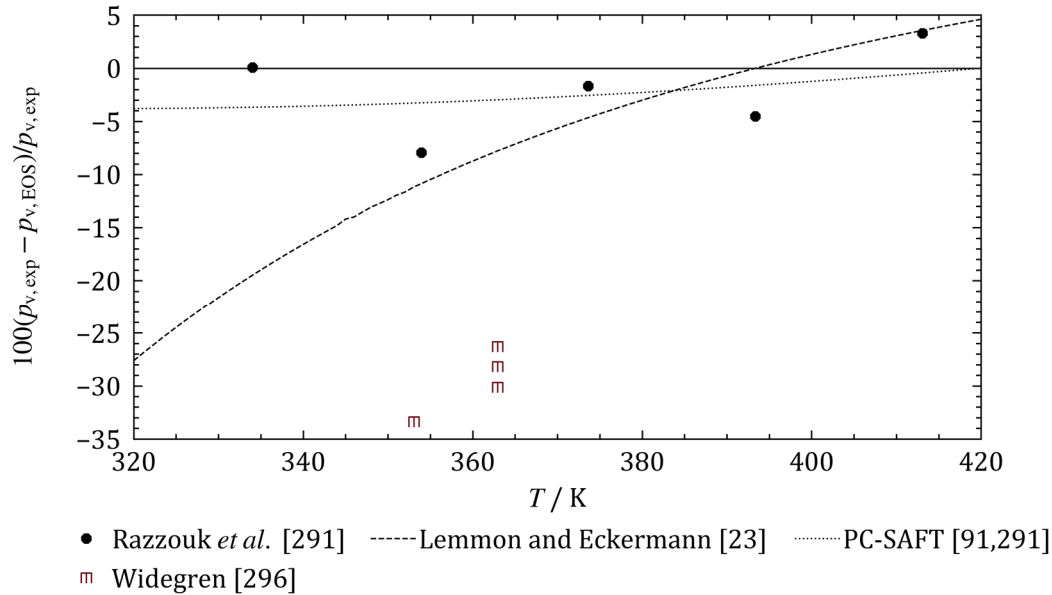


Figure 6.5: Relative deviations of the experimental vapor pressure data used for the development of the present generalized equation of state for PEC5 from the new equation of state. Results from the PC-SAFT equation of state [91,291] (dotted curve), and from the equation of Lemmon and Eckermann [23] (dashed curve) are plotted for comparison.

Table 6.5 presents the average absolute relative deviations of the experimental vapor pressures from the new generalized equation of state for PEC5, from the PC-SAFT equation of state [91,291], and from the equation of Lemmon and Eckermann [23].

Table 6.5: Average absolute relative deviations of the experimental vapor pressures used for the development of the present generalized equation of state for PEC5 from the present generalized equation of state, from the PC-SAFT equation of state [91,291], and from the equation of Lemmon and Eckermann [23].

| Author | No. of data | Temperature range / K | Average absolute relative deviations AAD / % | | |
|-----------------------------|-------------|-----------------------|--|------------------|---------------------------|
| | | | This work | PC-SAFT [91,291] | Lemmon and Eckermann [23] |
| Razzouk <i>et al.</i> [291] | 5 | 334 - 414 | 3.5 | 3.1 | 5.3 |
| Widegren [296] | 5 | 353 - 363 | 29 | 25 | 19 |

In Figure 6.6, the vapor pressure curves calculated from the three equations of state as well as both experimental data sets for the vapor pressure are presented in a p, T -diagram. For temperatures above $T = 370$ K, all models agree rather well with respect to the very low vapor pressures of PEC5. For lower temperatures, the course of the curve calculated from the equation of Lemmon and Eckermann [23] deviates from the others

following the data of Widegren [296]. It predicts lower vapor pressures than the new generalized equation of state and the PC-SAFT equation of state [91,291].

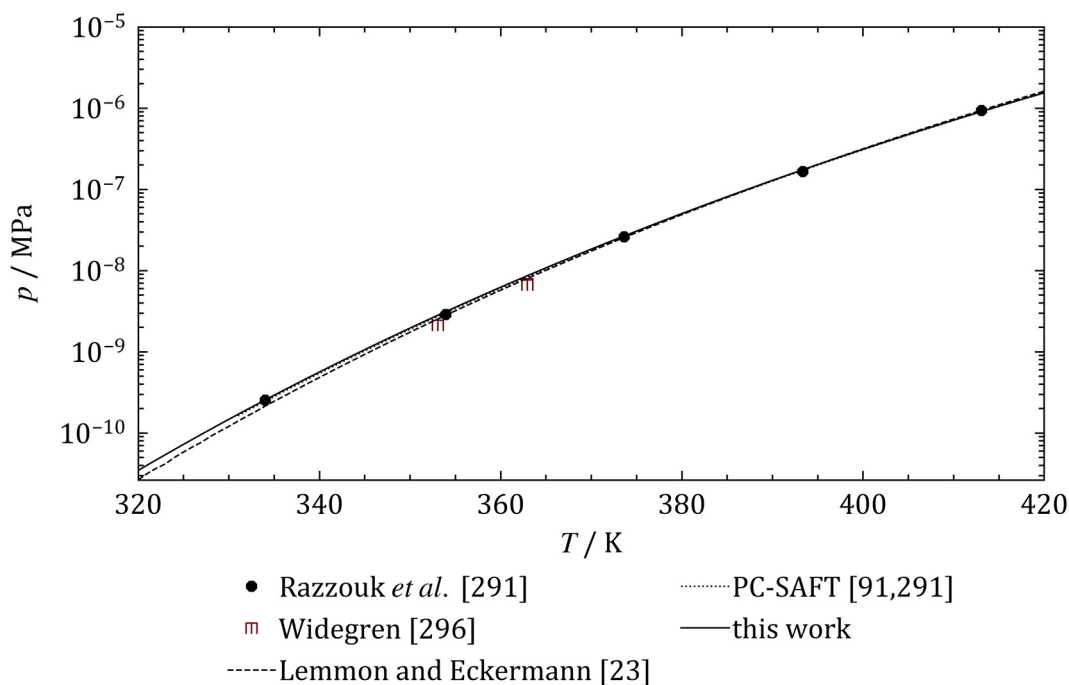


Figure 6.6: p, T -diagram of PEC5 with the vapor pressure curve calculated from the new generalized equation of state, from the PC-SAFT equation of state [91,291] (dotted curve), and from the equation of Lemmon and Eckermann [23] (dashed curve).

6.1.4 Comparison to Caloric Data

There were no experimental data sets containing caloric properties published in the literature. Therefore, no such data was used for the adjustment of the generalized equation of state. However, the investigation at NIST included isobaric heat-capacity measurements in the liquid phase, which were conducted with a commercial differential scanning calorimeter, as well as speed-of-sound measurements in the liquid phase, which were conducted with a dual-path, pulse-echo-type instrument. These data sets have not yet been published, but were used for the development of the fluid-specific equation of state of Lemmon and Eckermann [23]. In order to analyze the ability of the generalized equation of state to predict caloric properties, the group contribution method of Joback and Reid [293] has been used to provide a c_p^0 -equation, which is required for such calculations. For comparison, the PC-SAFT equation of state [91,291] is also combined with this c_p^0 -equation.

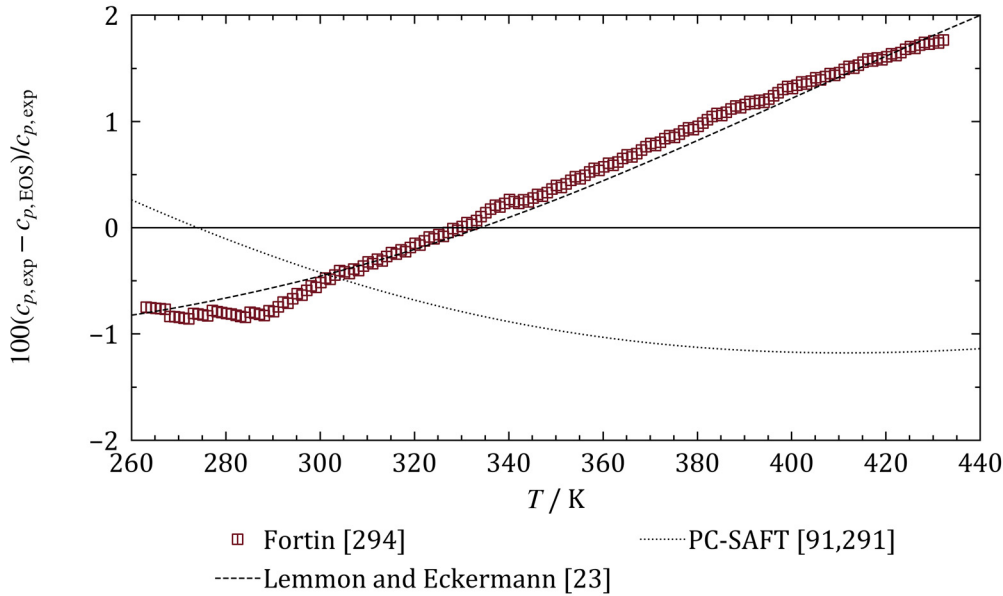


Figure 6.7: Relative deviations of the experimental liquid isobaric heat capacities at $p = 0.083$ MPa used for the development of the fluid-specific equation of state for PEC5 [23] from the new generalized equation of state. Results from the PC-SAFT equation of state [91,291] (dotted curve), and from the equation of Lemmon and Eckermann [23] (dashed curve) are plotted for comparison.

Relative deviations of the experimental liquid isobaric heat capacities at $p = 0.083$ MPa used for the development of the fluid-specific equation of state for PEC5 [23] from the new generalized equation of state, from the PC-SAFT equation of state [91,291], and from the equation of Lemmon and Eckermann [23] are presented in Figure 6.7. The new generalized equation of state is able to predict the experimental data within -1% to $+1.8\%$.

Table 6.6: Average absolute relative deviations of the experimental isobaric heat capacity data used for the development of the fluid-specific Helmholtz equation of state for PEC5 of Lemmon and Eckermann [23] from the present generalized equation of state, from the PC-SAFT equation of state [91,291], and from the equation of Lemmon and Eckermann [23].

| Author | No. of data | Temperature range / K | Pressure range / MPa | Average absolute relative deviations AAD / % | | |
|--------------|-------------|-----------------------|----------------------|--|------------------|---------------------------|
| | | | | This work | PC-SAFT [91,291] | Lemmon and Eckermann [23] |
| Fortin [294] | 170 | 263 - 433 | 0.083 | 0.79 | 1.4 | 0.096 |

Table 6.6 lists the AAD of the new equation as 0.79%. This is a remarkably good agreement considering the application of a group contribution c_p^0 -equation and the missing adjustment to any caloric property data. The PC-SAFT equation of state [91,291] reproduces the data within $+1\%$ to -3% (AAD = 1.4%). The fluid-specific Helmholtz equation of state by Lemmon and Eckermann [23] represents the data with an AAD of 0.096%.

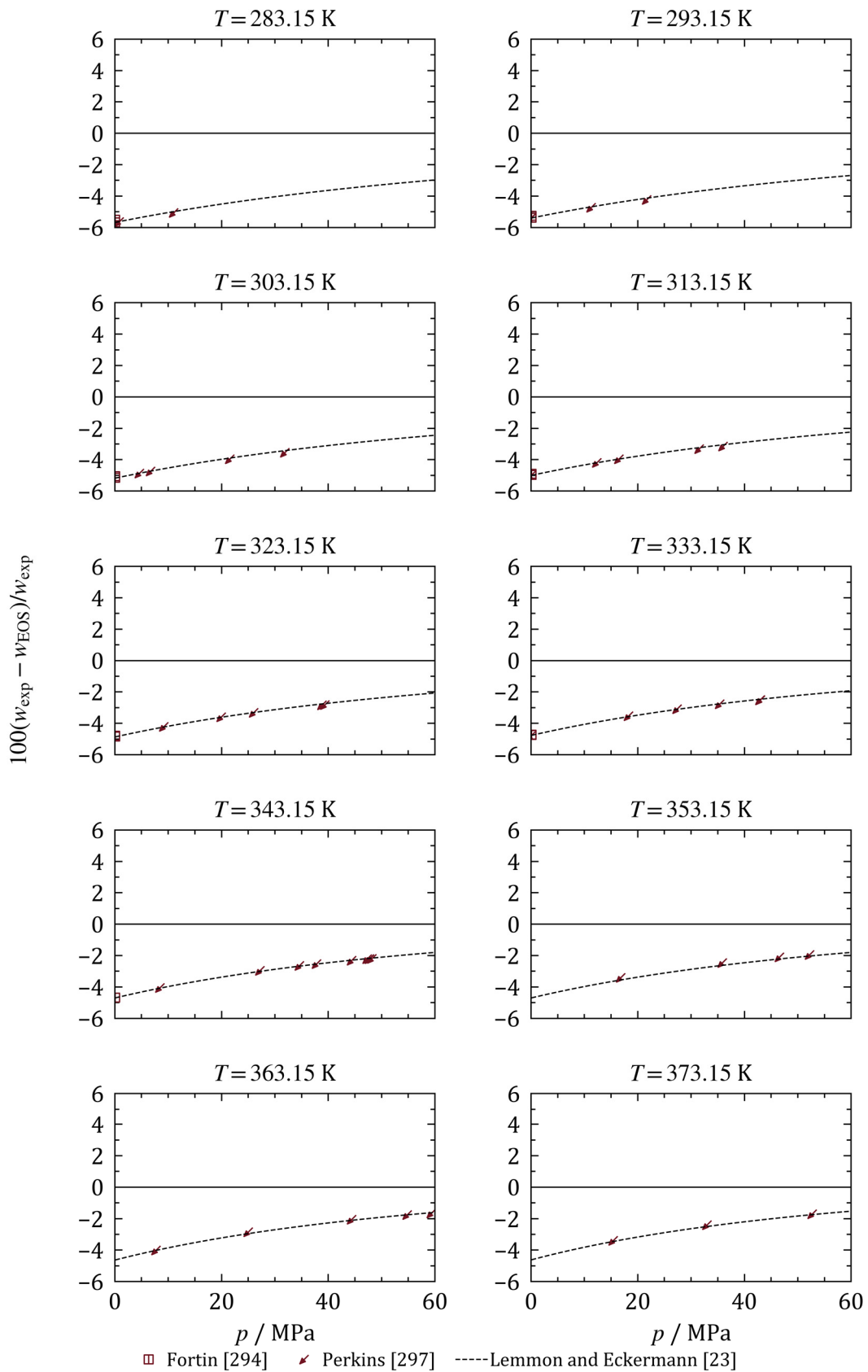


Figure 6.8: Relative deviations of the experimental liquid speed-of-sound data used for the development of the fluid-specific equation of state for PEC5 [23] from the new generalized equation of state. Results from the equation of Lemmon and Eckermann [23] (dashed curve) are plotted for comparison.

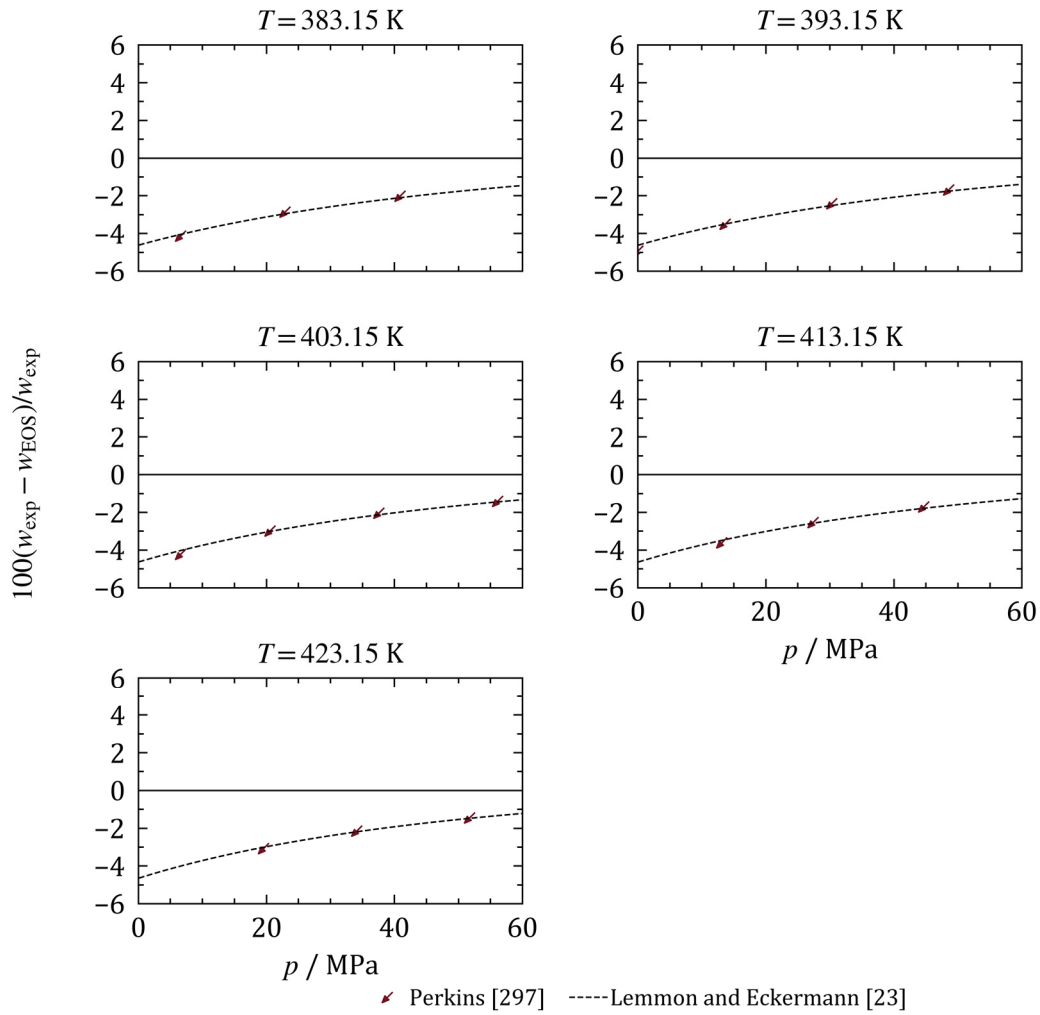


Figure 6.8 continued.

Table 6.7: Average absolute relative deviations of the experimental speed-of-sound data used for the development of the fluid-specific Helmholtz equation of state for PEC5 of Lemmon and Eckermann [23] from the present generalized equation of state, from the PC-SAFT equation of state [91,291], and from the equation of Lemmon and Eckermann [23].

| Author | No. of data | Temperature range / K | Pressure range / MPa | Average absolute relative deviations AAD / % | | |
|---------------|-------------|-----------------------|----------------------|--|------------------|---------------------------|
| | | | | This work | PC-SAFT [91,291] | Lemmon and Eckermann [23] |
| Fortin [294] | 14 | 278 - 344 | 0.083 | 5.1 | 25 | 0.027 |
| Perkins [297] | 66 | 283 - 424 | 0.0 - 63 | 3.1 | 23 | 0.050 |

In Figure 6.8, the experimental speed-of-sound data used for the development of the fluid-specific equation of state [23] and their reproduction by the fluid-specific and generalized equation of state are shown. The PC-SAFT equation of state [91,291] is not included here, since the relative deviations of this model lie outside the plotted range. The deviations of the new generalized equation are almost independent of

temperature. They decrease with increasing pressure, starting from -5% at atmospheric pressures, ending at -1% for $p = 60$ MPa in the complete temperature range. The equation of Lemmon and Eckermann [23] follows the data in all presented regions. Table 6.7 lists the average absolute relative deviations of the experimental speed-of-sound data from the three equations of state. The AAD of the PC-SAFT equation of state [91,291] is 23% with respect to the experimental speed-of-sound data of Perkins [297]. Significantly higher deviations compared to the generalized equation were expected due to the unfavorable pressure dependency of the model which could already be observed in the representation of densities at increasing pressures (Figure 6.3). As expected, all thermodynamic properties are best described by the fluid-specific Helmholtz equation of state, which has numerous fluid-specific adjustable parameters. In contrast to the PC-SAFT equation of state [91,291], which is based on a three-parameter corresponding states approach as well, the new generalized equation of state shows a correct pressure dependence of densities in the liquid. Thereby, the new equation satisfactorily predicts liquid heat capacities and liquid speeds of sound more than. All AADs of the new equation are within the range stated by Alexandrov *et al.* [63] (see section 3.5).

6.2 Pure Fluid Equation for PEC7

Experimental data used for the adjustment

There are three publications in the literature dealing with the $p\rho T$ relationship of PEC7. Fandiño *et al.* [18], Fedele *et al.* [288], as well as Shobha and Kishore [290] measured the liquid density of this substance. Razzouk *et al.* [291] investigated vapor pressures of PEC5 and PEC7. There are PC-SAFT parameters published by Razzouk *et al.* [291], which are used for comparison.

Table 6.8: PC-SAFT parameters for PEC7 [291].

| m | $\sigma / \text{\AA}$ | $\epsilon \cdot k_{\text{B}}^{-1} / \text{K}$ |
|---------|-----------------------|---|
| 12.1041 | 4.1405 | 269.99 |

6.2.1 The New Generalized Equation of State

Like PEC5, the new generalized equation of state for PEC7 has been developed using of the fitter provided by NIST, and is based on the generalized equation of state of Alexandrov *et al.* [63], which is presented in section 3.5. The critical temperature T_c , the critical density ρ_c , and the acentric factor ω are again used as adjustable parameters. Table 6.9 gives the results of the adjustment.

Table 6.9: The corresponding states parameters for PEC7 adjusted in this work based on the generalized equation of Alexandrov *et al.* [63], and the corresponding states parameters found by Lemmon and Eckermann [23].

| | This work | Lemmon and Eckermann [23] |
|---|-----------|---------------------------|
| T_c / K | 916.03 | 940.00 |
| $\rho_c / \text{mol} \cdot \text{m}^{-3}$ | 408.99 | 412.00 |
| $\omega / -$ | 1.2011 | 1.06 |

The critical parameters found in this work are compared to the critical parameters used in the equation of Lemmon and Eckermann [23]. The adjusted acentric factor is compared to the acentric factor calculated from the equation of Lemmon and Eckermann [23] according to its definition (see equation (3.7)). Again, the good agreement with the corresponding states parameters found by Lemmon and Eckermann [23] validates their order of magnitude. Like PEC5, PEC7 molecules are thermally stable until $T = 600 \text{ K}$. For higher temperatures, the molecules begin to decompose significantly [292]. Consequently, the meaning of the critical parameters is basically reduced to their function as reducing parameters in the respective equations.

Figure 6.9 shows a p, ρ -diagram of PEC7 with the isotherm $T = 805 \text{ K}$ calculated from the generalized equation of state. Again, this isotherm features an unfavorable course and placement of the outer minimum. Consequently, the flash calculation cannot find a correct solution, which leads to a discontinuity in the saturated vapor line at this temperature. This effect was also found for PEC5 and for other fluids with comparable acentric factors calculated with the model of Alexandrov *et al.* [63] as shown and discussed in section 3.5.

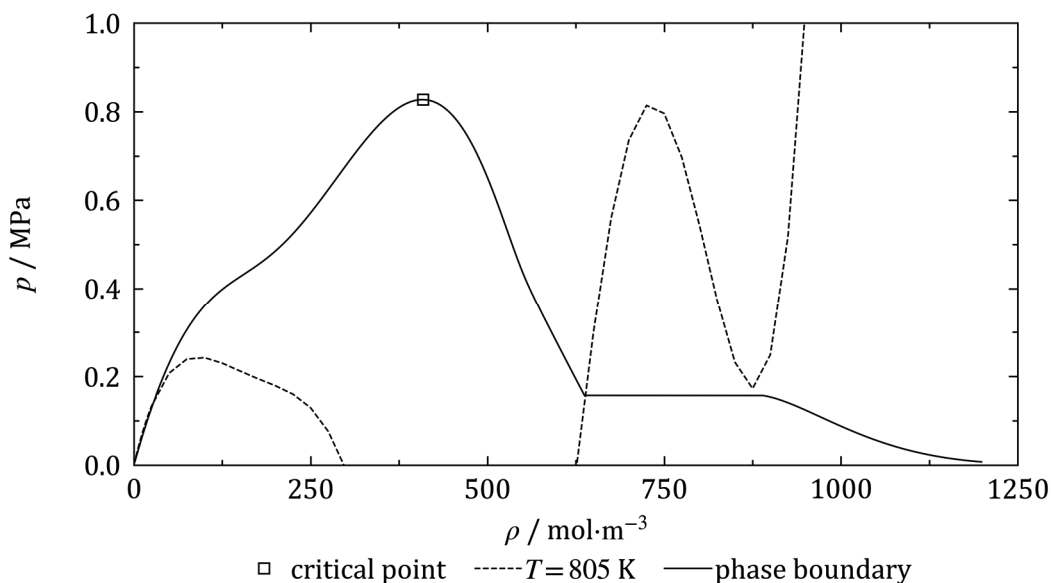


Figure 6.9: p, ρ -diagram of PEC7 with the isotherm $T = 805 \text{ K}$ calculated from the new generalized equation of state.

Again, this effect is not crucial for the description of the pure fluid PEC7, since the molecules already decompose in this temperature region [292]. However, it might affect the use of this equation in a mixture model.

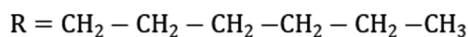
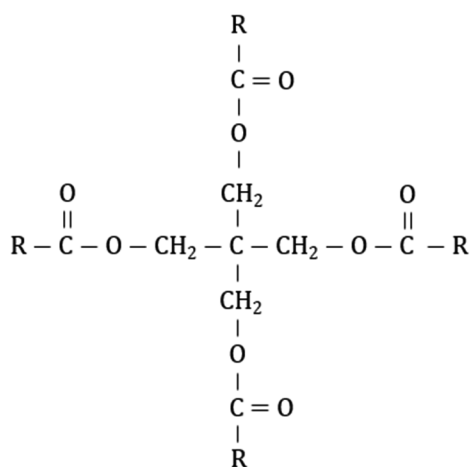


Figure 6.10: Chemical structure of a PEC7 molecule.

Table 6.10: Parameters in form of the c_p^0 -equation (3.66) determined by the group contribution method of Joback and Reid [293] for PEC7, reduced with $R = 8.3144598 \text{ J}/(\text{mol} \cdot \text{K})$.

| n_i | t_i |
|--------------------------|-------|
| 9.60423 | 0 |
| 0.348775 | 1 |
| $-1.71316 \cdot 10^{-4}$ | 2 |
| $2.381874 \cdot 10^{-8}$ | 3 |

As with PEC5, the isobaric heat capacity has been estimated for PEC7 with the group contribution method by Joback and Reid [293]. In Figure 6.10, the structure of a PEC7 molecule is illustrated. The resulting coefficients according to the c_p^0 -equation (3.66) are given in Table 6.10.

6.2.2 Comparison to $p\rho T$ Data

Relative deviations of the experimental density data from the new generalized equation of state are illustrated in Figure 6.11. The data sets of Fandiño *et al.* [18] and Fedele *et al.* [288] deviate from each other by approximately 0.5% in the overlapping temperature range, as they did for PEC5. Again, the data set of Fandiño *et al.* [18] was favored in the adjustment due to a lower estimated uncertainty (0.14 kg/m^3) compared to the data set of Fedele *et al.* [288]. The new generalized equation reproduces the data of these authors within -1% to $+0.25\%$, representing the data of Fandiño *et al.* [18] with an AAD of 0.19% and the data of Fedele *et al.* [288] with an AAD of 0.69%. The equation of Lemmon and Eckermann [23] follows the data of Fedele *et al.* [288] and Outcalt [295], which agree very well, accurately with an AAD of 0.58% and 0.63%, respectively. The offset between the new generalized equation of state and the fluid-specific equation of state is 1% for low temperatures and decreases to 0.5% for elevated temperatures. The experimental data of Outcalt [295] cover a broader temperature range than the data available in the literature. The offset between the new generalized equation and the fluid-specific Helmholtz equation [23] as well as the offset between the new generalized equation and the data of Outcalt [295] almost vanishes at $T = 450 \text{ K}$. Deviations of the PC-SAFT equation of state [91,291] from the new model and from the experimental data increase rapidly with increasing pressure.

Figure 6.12 illustrates relative deviations of the experimental values at ambient pressure from the new generalized equation of state for PEC7. The course of the data of Shoba and Kishore [290] is discontinuous with a sudden jump at $T = 360 \text{ K}$. Up to that temperature, the offset of the new equation increases with increasing temperature from approximately $+0.3\%$ to $+1\%$. The deviations do not exceed $+0.2\%$ for elevated temperatures (AAD = 0.39%). At ambient pressure, the PC-SAFT equation of state [91,291] is in good agreement with the experimental data of Shoba and Kishore [290] as well (AAD = 0.49%). The fluid-specific equation of Lemmon and Eckermann [23] follows the data of Fortin [294] closely. The offset of the new generalized equation of state from this data set decreases from -1% to -0.5% with increasing temperature (AAD = 0.75%).

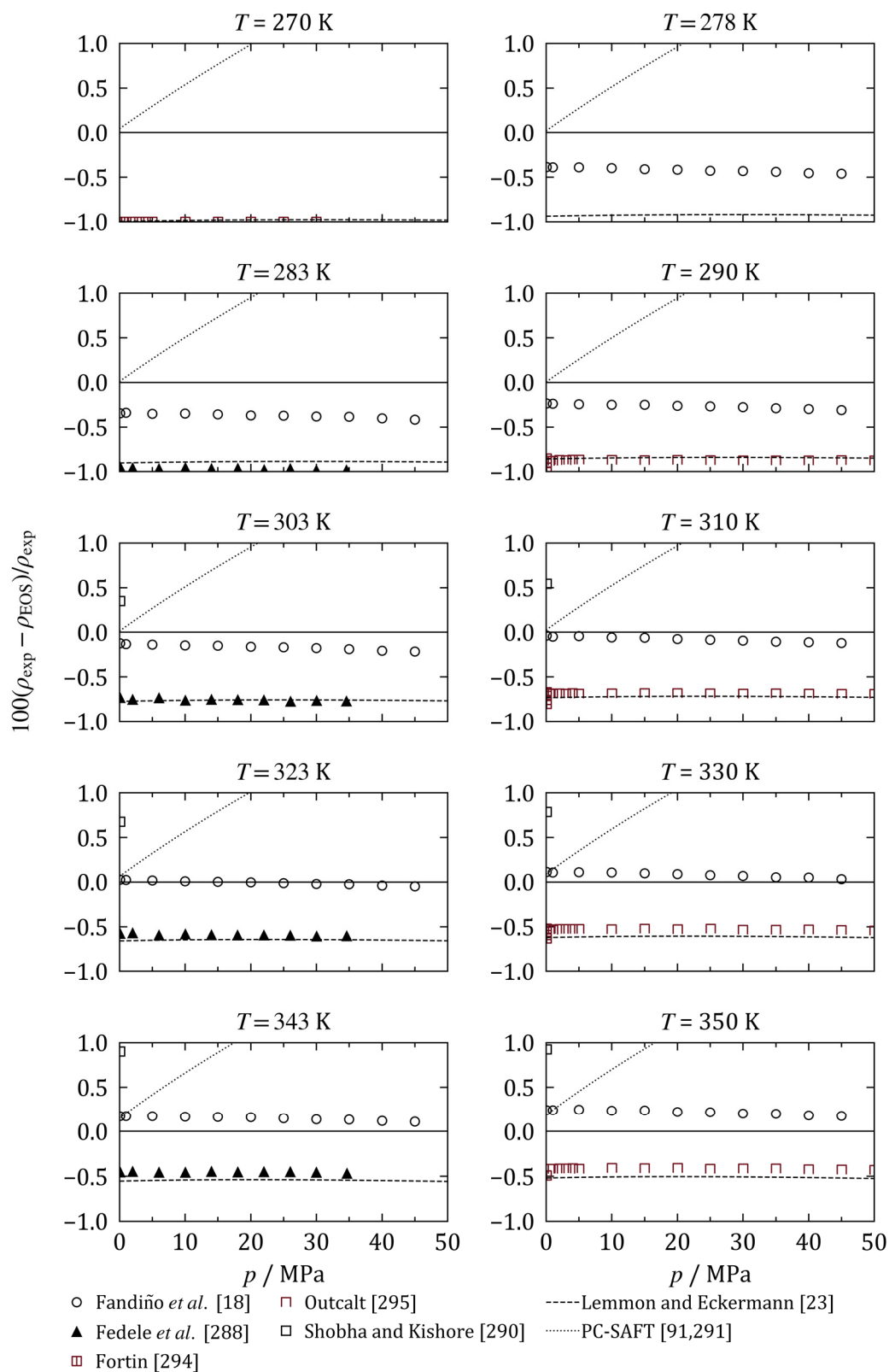


Figure 6.11: Relative deviations of the experimental liquid density data from the new generalized equation of state for PEC7. Results from the PC-SAFT equation of state [91,291] (dotted curve) and from the equation of Lemmon and Eckermann [239] (dashed curve) are plotted for comparison.

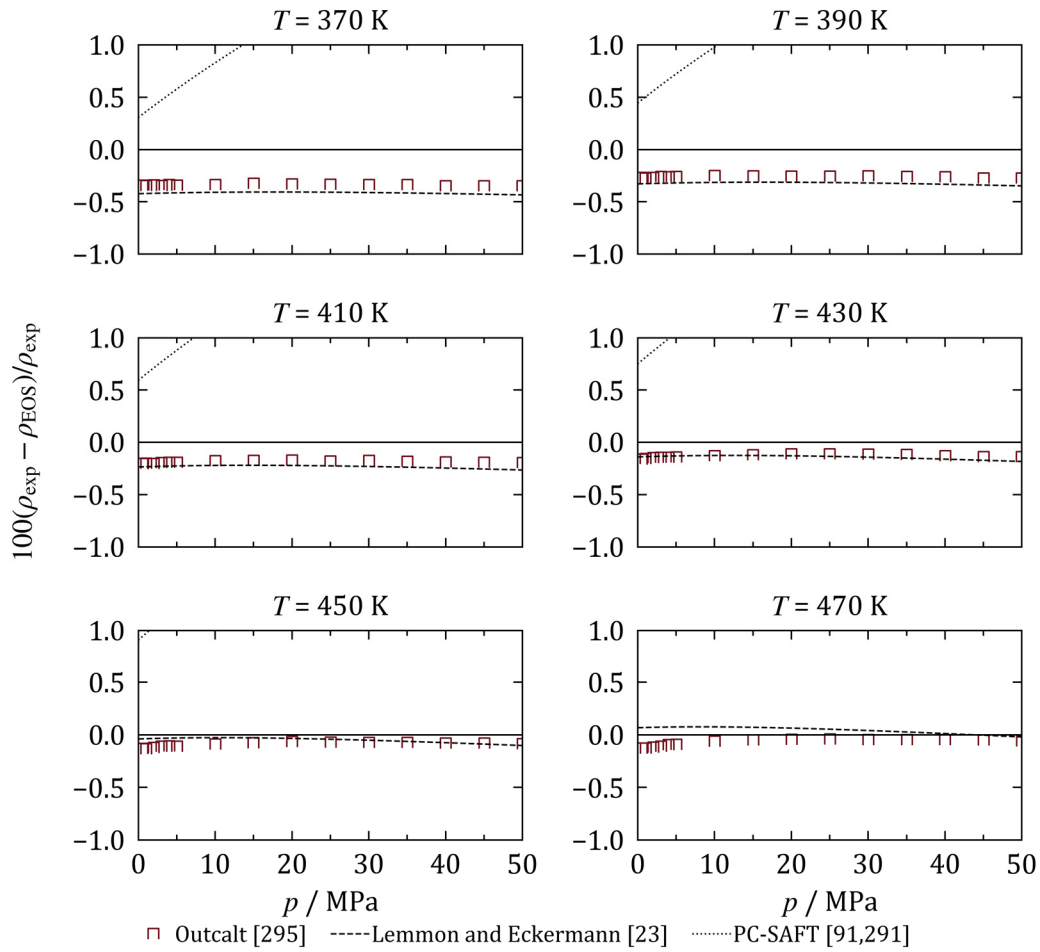


Figure 6.11 continued.

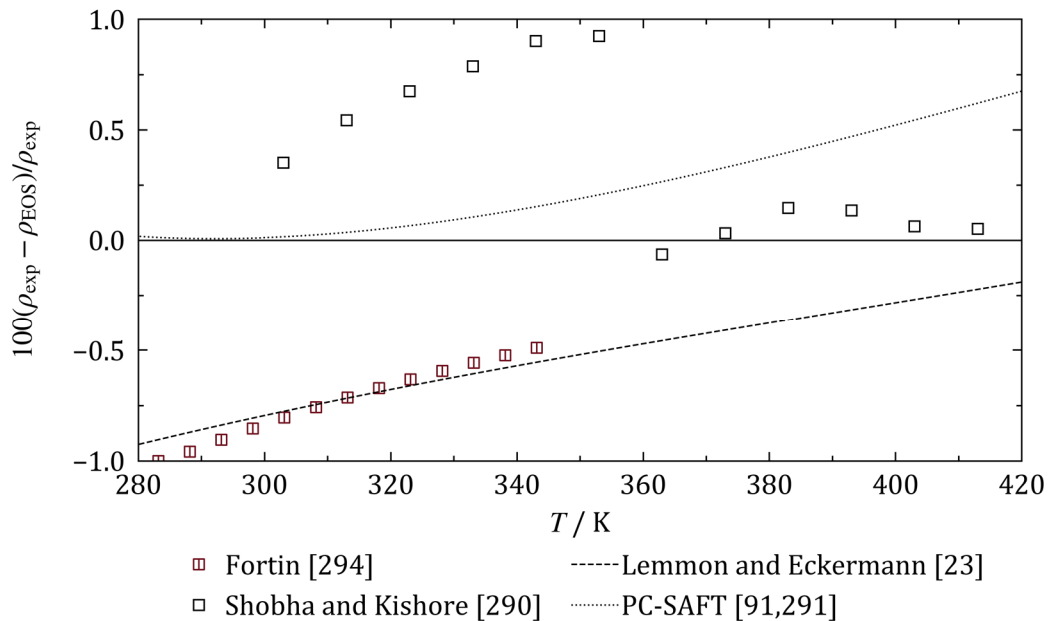


Figure 6.12: Relative deviations of the experimental densities at ambient pressure from the new generalized equation of state for PEC7. Results from the PC-SAFT equation of state [91,291] (dotted curve), and from the equation of Lemmon and Eckermann [239] (dashed curve) are plotted for comparison.

Table 6.11 gives the average absolute relative deviations of the experimental densities from the three compared equations of state. All density data sets can be represented by the new generalized equation of state with an AAD lower than 0.75%.

Table 6.11: Average absolute relative deviations of the experimental densities from the new generalized equation of state for PEC7, from the PC-SAFT equation of state [91,291], and from the model of Lemmon and Eckermann [23].

| Author | No. of data | Temperature range / K | Pressure range / MPa | Average absolute relative deviations AAD / % | | |
|----------------------------|-------------|-----------------------|----------------------|--|------------------|---------------------------|
| | | | | This work | PC-SAFT [91,291] | Lemmon and Eckermann [23] |
| Fandiño <i>et al.</i> [18] | 98 | 278 - 354 | <0.1 - 46 | 0.19 | 1.1 | 0.61 |
| Fedele <i>et al.</i> [288] | 40 | 283 - 344 | 0.1 - 35 | 0.69 | 1.5 | 0.058 |
| Shobha and Kishore [290] | 12 | 303 - 414 | 0.101325 | 0.39 | 0.49 | 0.86 |
| Fortin [294] | 14 | 278 - 344 | 0.083 | 0.75 | 0.81 | 0.053 |
| Outcalt [295] | 161 | 269 - 471 | 0.5 - 51 | 0.41 | 1.691 | 0.063 |

6.2.3 Comparison to Vapor Pressure Data

Figure 6.13 illustrates relative deviations of the experimental vapor pressures used for the adjustment of the new generalized equation of state for PEC7 from the new equation, from the PC-SAFT equation of state [91,291], and from the equation of Lemmon

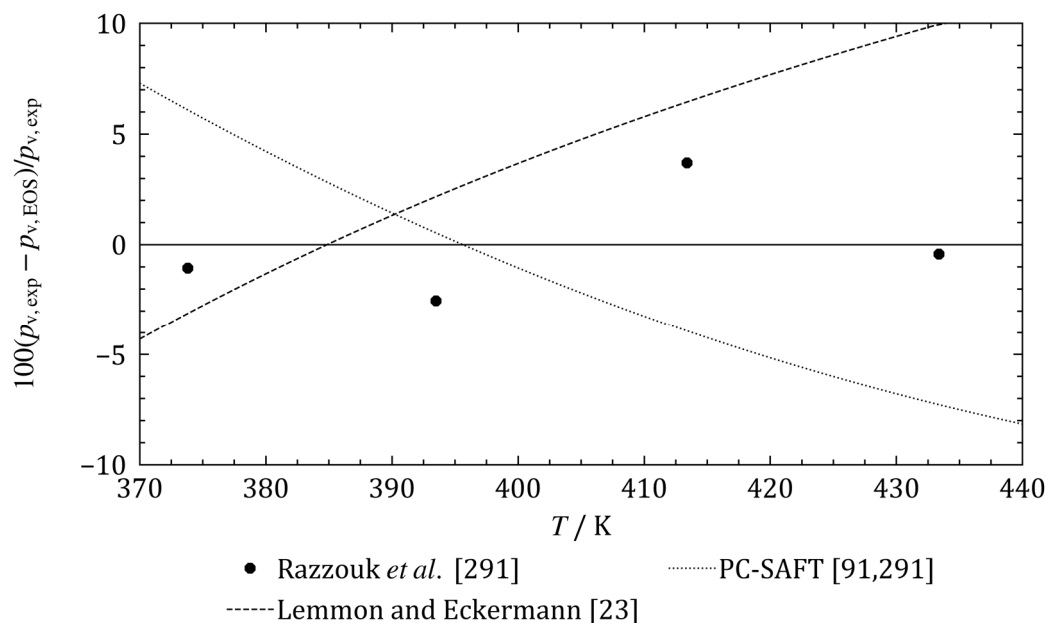


Figure 6.13: Relative deviations of the experimental vapor pressure data from the new generalized equation of state for PEC7. Results from the PC-SAFT equation of state [91,291] (dotted curve), and from the equation of Lemmon and Eckermann [239] (dashed curve) are plotted for comparison.

and Eckermann [239]. The average absolute relative deviations of the experimental vapor pressures presented in Figure 6.13 from the three equations of state are given in Table 6.12.

The data scatter between -3% and $+4\%$ around the generalized equation of state. With an AAD of 1.9% , the new equation represents the data best, although the PC-SAFT parameters were adjusted to these data. The PC-SAFT equation of state [91,291] (AAD = 6.1%) and the equation of state of Lemmon and Eckermann [23] (AAD = 5.7%) exhibit opposite trends.

Table 6.12: Average absolute relative deviations of the experimental vapor pressures used for the development of the present generalized equation of state for PEC7 from the present generalized equation, from the PC-SAFT equation of state [91,291], and from the equation of Lemmon and Eckermann [23].

| Author | No. of data | Temperature range / K | Average absolute relative deviations AAD / % | | |
|-----------------------------|-------------|-----------------------|--|------------------|---------------------------|
| | | | This work | PC-SAFT [91,291] | Lemmon and Eckermann [23] |
| Razzouk <i>et al.</i> [291] | 5 | 373 - 434 | 1.925 | 6.114 | 5.679 |

6.2.4 Comparison to Caloric Data

Since there are no experimental data sets containing caloric properties published in the literature, no such data were used for the adjustment of the generalized equation of state. However, the investigation at NIST included isobaric heat-capacity measurements in the liquid phase, which were conducted with a commercial differential scanning calorimeter, as well as speed-of-sound measurements in the liquid phase, which were conducted with a dual-path, pulse-echo-type instrument. These data sets were used for the adjustment of the fluid-specific equation of state of Lemmon and Eckermann [23] and are still to be published. In order to see how the new generalized equation of state for PEC7 reproduces these data sets without being adjusted to any caloric property, the group contribution method of Joback and Reid [293] has been used to develop a c_p^0 -equation, which is required for such calculations. For comparison, the PC-SAFT equation of state [91,291] is also combined with this c_p^0 -equation.

Relative deviations of the experimental isobaric heat capacities at $p = 0.083$ MPa from the new generalized equation of state are presented in Figure 6.14. Deviations of the PC-SAFT equation of state [91,291] and of the equation of Lemmon and Eckermann [23], which was fitted to these data, are included for comparison. The fluid-specific

Helmholtz equation of state follows the data of Fortin [294] closely (AAD = 0.088%). The new generalized equation of state deviates by -2% from the experimental data at the lowest investigated temperature. This deviation decreases with increasing temperature to -0.5% (AAD = 1.3%).

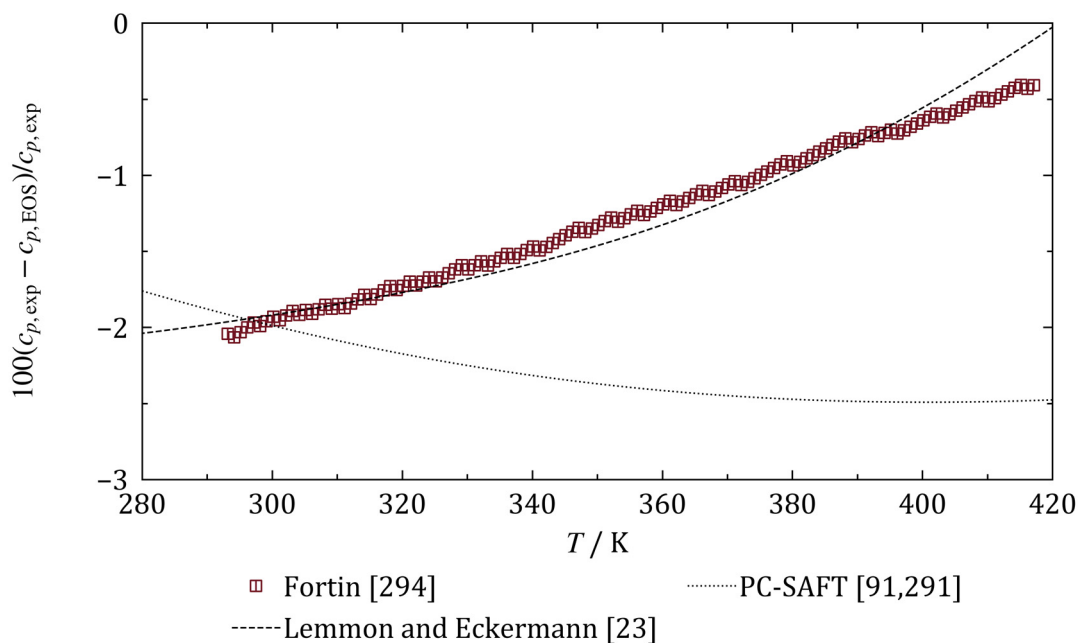


Figure 6.14: Relative deviations of the experimental liquid isobaric heat capacity data at $p = 0.083$ MPa used for the development of the fluid-specific equation of state for PEC7 [239] from the new generalized equation of state. Results from the PC-SAFT equation of state [91,291] (dotted curve), and from the equation of Lemmon and Eckermann [23] (dashed curve) are plotted for comparison.

The PC-SAFT equation of state [91,291] shows an opposite trend reproducing the experimental data better at low temperatures with increasing deviations at elevated temperatures (AAD = 1.1%).

Table 6.13 contains the average absolute relative deviations of the experimental isobaric heat capacities used for the development of the fluid-specific Helmholtz equation of state for PEC7 of Lemmon and Eckermann [23] from the present generalized equation, from the PC-SAFT equation of state [91,291], and from the equation of Lemmon and Eckermann [23].

Table 6.13: Average absolute relative deviations of the experimental liquid isobaric heat capacity data at $p = 0.083$ MPa used for the development of the fluid-specific Helmholtz equation of state for PEC7 of Lemmon and Eckermann [23] from the present generalized equation of state, from the PC-SAFT equation of state [91,291], and from the equation of Lemmon and Eckermann [23].

| Author | No. of data | Temperature range / K | Pressure / MPa | Average absolute relative deviations AAD / % | | |
|--------------|-------------|-----------------------|----------------|--|------------------|---------------------------|
| | | | | This work | PC-SAFT [91,291] | Lemmon and Eckermann [23] |
| Fortin [294] | 170 | 263 - 433 | 0.083 | 1.3 | 1.1 | 0.088 |

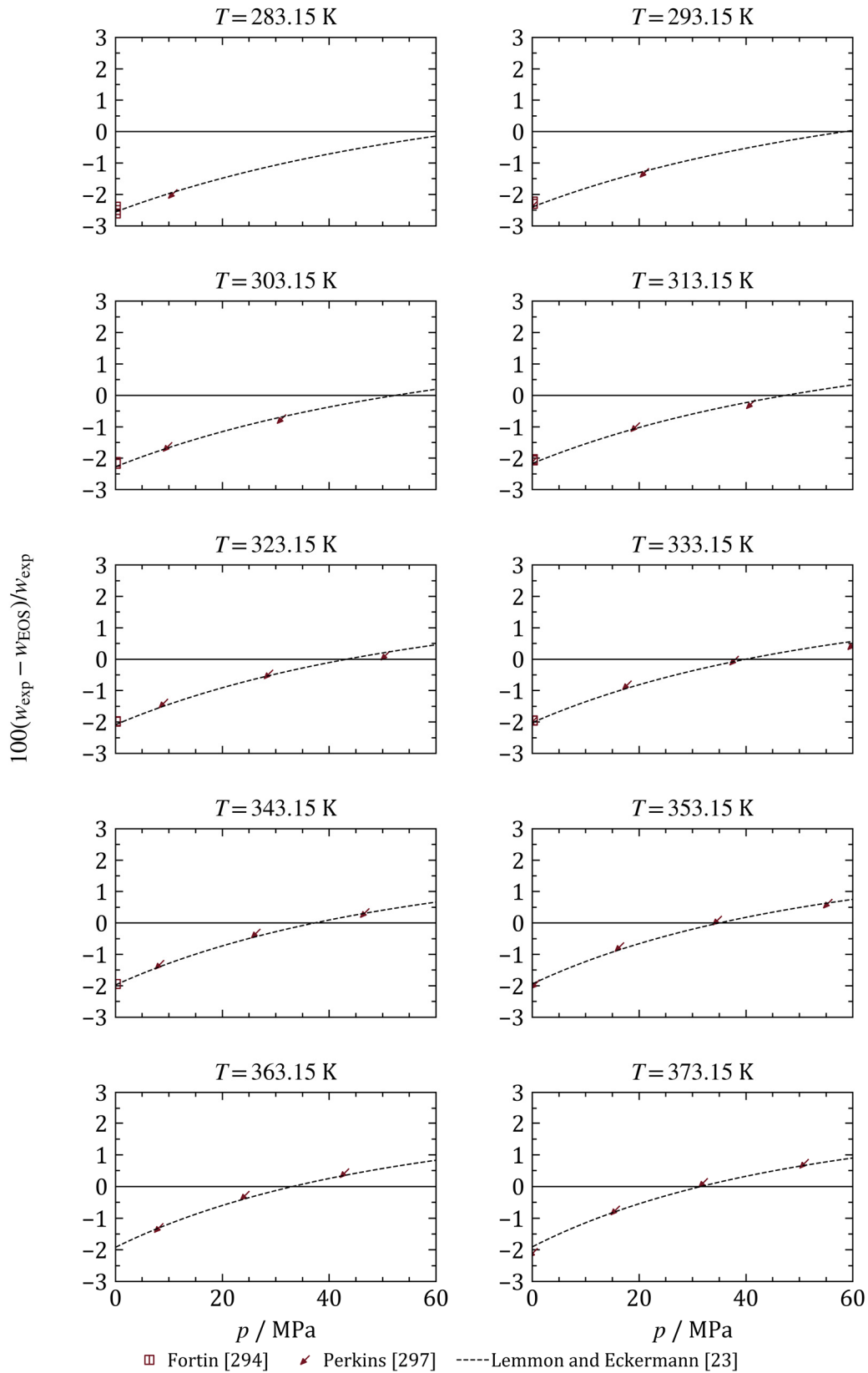


Figure 6.15: Relative deviations of the experimental liquid speed-of-sound data used for the development of the fluid-specific equation of state for PEC7 [239] from the new generalized equation of state. Results from the equation of Lemmon and Eckermann [239] (dashed curve) are plotted for comparison.

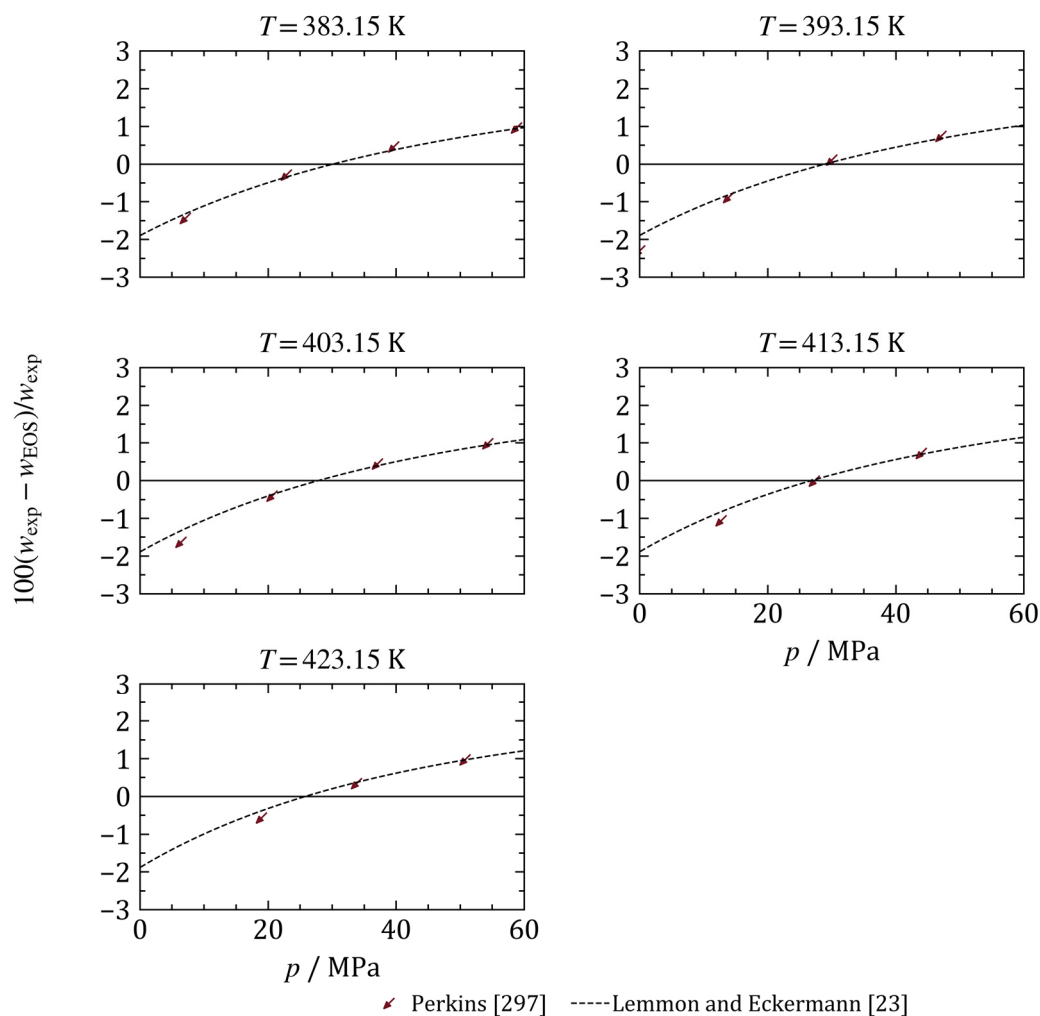


Figure 6.15 continued.

Table 6.14: Average absolute relative deviations of the experimental sound speeds used for the development of the fluid-specific Helmholtz equation of state for PEC7 [23] from the present generalized equation, from the PC-SAFT equation of state [91,291], and from the equation of Lemmon and Eckermann [23]

| Author | No. of data | Temperature range / K | Pressure range / MPa | Average absolute relative deviations AAD / % | | |
|---------------|-------------|-----------------------|----------------------|--|------------------|---------------------------|
| | | | | This work | PC-SAFT [91,291] | Lemmon and Eckermann [23] |
| Fortin [294] | 14 | 278 - 344 | 0.083 | 2.2 | 27 | 0.077 |
| Perkins [297] | 66 | 283 - 424 | 0.1 - 70 | 2.1 | 23 | 0.081 |

In Figure 6.15, the relative deviations of the experimental liquid speed-of-sound data used for the development of the fluid-specific equation of state for PEC7 [239] from the new generalized equation of state are illustrated. Only the equation of state of Lemmon and Eckermann [23] is plotted for comparison, since the deviations of the PC-SAFT equation of state [91,291] exceed the limits of the presented graph (AAD > 23%). The fluid-specific Helmholtz equation of state [23] follows the experimental data closely,

whereas the generalized equation shows a linear offset in the whole presented temperature range. This offset starts at low temperatures from -2.5% at the lowest pressure going to -0.5% with increasing pressure, shifting to -2% going to $+1\%$ at higher temperatures.

Table 6.14 shows the average absolute relative deviations of the experimental speed-of-sound data from the present generalized equation, and from the equation of Lemmon and Eckermann [23]. The new generalized equation of state reproduces both experimental data sets with an AAD of about 2%. This result is remarkably positive considering the strictly predictive character of the new equation with respect to the speed of sound.

As shown for PEC5 in section 6.1, the experimental data of all thermodynamic properties except for the vapor pressure is best described by the fluid-specific Helmholtz equation of state [23] with numerous fluid-specific adjustable parameters. In contrast to the PC-SAFT equation of state [91,291], which is based on a three-parameter corresponding states approach as well, the new generalized equation of state for PEC7 presents a correct pressure dependence. Thereby, the model predicts liquid speeds of sound more than satisfactorily. All presented AADs of the new equation for PEC7 are within the stated range of Alexandrov *et al.* [63] (see section 3.5).

6.3 Mixture Model for CO₂-PEC5

A new mixture model incorporating the reference equation of state for CO₂ of Span and Wagner [22] and the new generalized equation of state for PEC5 introduced in section 6.1 is presented here.

In total, there are three data sets available, which contain experimental data of CO₂-PEC5 mixtures. Pensado *et al.* [26] measured liquid densities for two compositions with a very low lubricant content, $x_{\text{PEC5}} = 8 \text{ mass-\%}$ and $x_{\text{PEC5}} = 15 \text{ mass-\%}$, in the temperature range from $T = 303.15 \text{ K}$ to $T = 353.15 \text{ K}$ and pressures from $p = 10 \text{ MPa}$ to $p = 60 \text{ MPa}$. Bobbo *et al.* [24] published VLE data ($pT\mathbf{x}'$) for the isotherm $T = 283.15 \text{ K}$. Fandiño *et al.* [25] reported VLE data ($pT\mathbf{x}'$) between $T = 283.15 \text{ K}$ and $T = 333.15 \text{ K}$.

A binary interaction parameter for the PC-SAFT equation of state adjusted to the experimental data presented in [25] was proposed by Fandiño *et al.* [298], which is used for comparison here.

Due to the limited data base, only the reducing parameters have been fitted. The results are listed in Table 6.15.

Table 6.15: Adjusted reducing parameters for CO₂-PEC5 mixtures.

| β_T | γ_T | β_v | γ_v |
|-----------|------------|-----------|------------|
| 0.90106 | 1.6247 | 2.4339 | 3.1587 |

The values of the binary parameters of the density reducing function have a rather high value compared to typical values of reducing parameters of the GERG-2008 [80]. This is probably caused by the large difference in molecular weight and critical density of the two mixture components.

In order to investigate the effect of the numerical problems found for near-critical temperatures for PEC5 (see section 6.1.1), Figure 6.16 displays the temperatures at which the pure fluid equations are evaluated for an exemplary mixture calculation at $T_{\text{mix}} = 293$ K with the new mixture model.

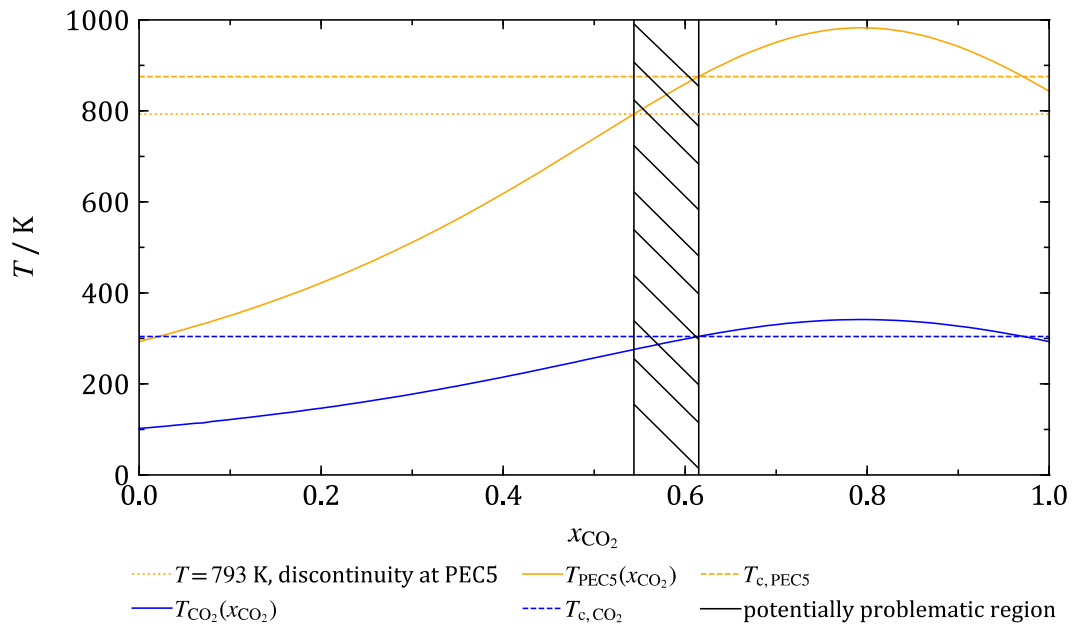


Figure 6.16: Temperatures at which the pure fluid equations are evaluated for an exemplary mixture calculation with $T = 293$ K with the new mixture model.

The pure fluid temperatures are calculated as shown for PEC5:

$$T_{\text{PEC5}} = \frac{T_{c,\text{PEC5}}}{\tau_{\text{mix}}}, \text{ with } \tau_{\text{mix}} = \frac{T_r(\mathbf{x})}{T_{\text{mix}}}. \quad (6.2)$$

For $T = 293$, the PEC5 equation is evaluated in the problematic region in the composition range with $0.54 < x_{\text{CO}_2} < 0.61$. At $T = 313.15$ K, this region is shifted to $0.47 < x_{\text{CO}_2} < 0.53$. The following discussion of the experimental data shows that the shortcomings of the pure fluid equation do not cause a failure in the iterative mixture calculations.

Figure 6.17 illustrates the experimental phase equilibrium data as well as calculated values from the new model, and from the PC-SAFT equation of state [91,291,298]. The solubility of CO₂ in PEC5 increases with pressure and decreases with temperature. The PC-SAFT equation of state [91,291,298] follows the experimental data closely throughout the entire presented range. Since the bubble line calculated from the new model oscillates slightly, the new model presented here follows the data but deviates significantly more than the PC-SAFT equation of state [91,291,298]. The deviations between the new model and the experimental data increase with increasing temperature. The oscillation does not result from unphysical contributions from the generalized pure fluid equation. Figure 6.18 exemplarily illustrates the bubble line of the isotherm $T = 313.15$ K calculated from the original setup of the new mixture model and calculated from the new mixture model using the fluid-specific equation of state of Lemmon and Eckermann [23]. The bubble line calculated with the fluid-specific equation features an even more pronounced bump at high CO₂ fractions. Therefore, the mixture model itself seems responsible for the oscillations.

For temperatures above the critical temperature of CO₂ ($T_{c,\text{CO}_2} = 304.13$ K), both models predict liquid-liquid equilibria at high CO₂ fractions. The vicinity of the change from VLE to LLE is marked in the respective plots. The slope of the “bubble” line (LLE) predicted with the PC-SAFT equation of state [91,291,298] is much steeper than the slope predicted by the new model. Consequently, the two-phase region predicted by the PC-SAFT equation of state [91,291,298] extends to significantly higher pressures.

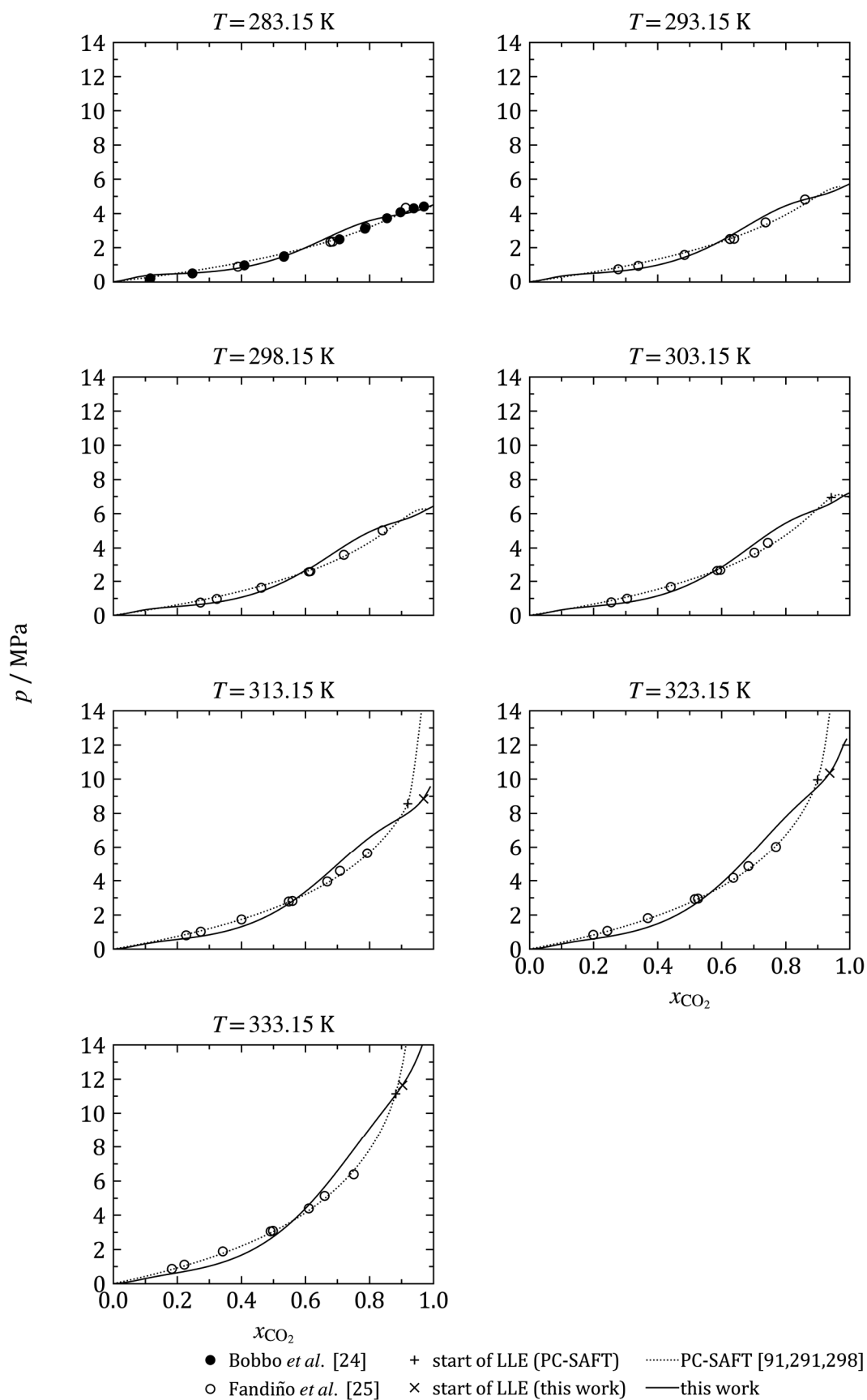


Figure 6.17: Experimental and calculated values for the pressure on the bubble line of CO₂-PEC5 mixtures for several isotherms. The PC-SAFT equation of state [91,291,298] (dotted curve) is plotted for comparison.

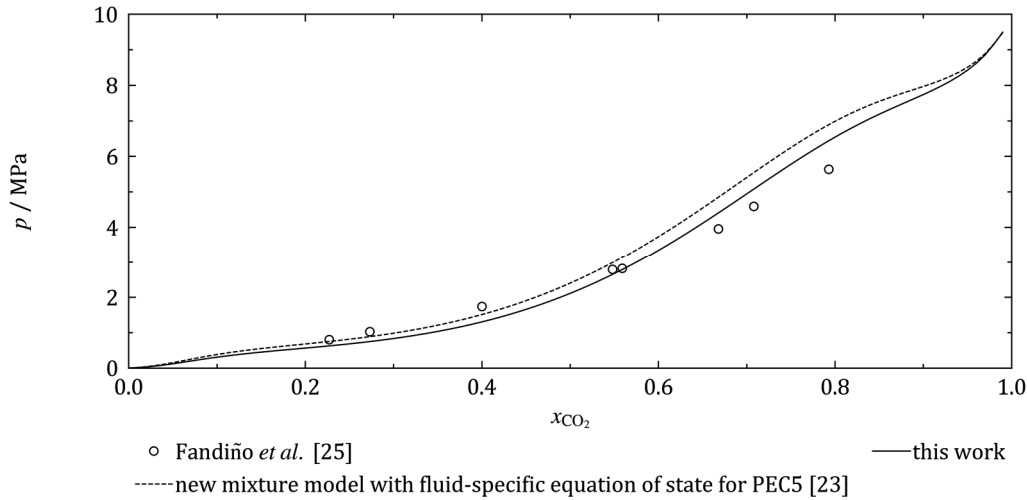


Figure 6.18: Experimental and calculated values for the pressure on the bubble line of CO₂-PEC5 mixtures for $T = 313.15$ K. The new mixture model was additionally evaluated based on the fluid-specific equation of state of Lemmon and Eckermann [23] for PEC5.

Table 6.16: Average absolute relative deviations of the experimental bubble line data with respect to the CO₂ fraction, and with respect to pressure from the present mixture model for CO₂-PEC5, and from the PC-SAFT equation of state [91,291,298].

| Author | No. of data | Temperature range / K | Pressure range / MPa | Average absolute relative deviations AAD / % | | | |
|----------------------------|-------------|-----------------------|----------------------|--|-----|----------------------|-----|
| | | | | This work | | PC-SAFT [91,291,298] | |
| | | | | x_{CO_2} | p | x_{CO_2} | p |
| Bobbo <i>et al.</i> [24] | 9 | 283.16 | 0.50 - 4.41 | 8.9 | 14 | 7.2 | 10 |
| Fandiño <i>et al.</i> [25] | 51 | 283.12 - 333.16 | 0.74 - 6.39 | 11 | 14 | 3.4 | 5.0 |

In Table 6.16, the average absolute relative deviations of the experimental phase equilibrium data from the new mixture model for CO₂-PEC5, and from the PC-SAFT equation of state [91,291,298] are given. It is calculated as a deviation in the composition of CO₂ in the liquid phase as function of temperature and pressure, and as a deviation in bubble pressure as a function of temperature and composition. Fandiño *et al.* [25] claim an uncertainty of 4% in the CO₂ fraction. The new mixture model represents this data set with an AAD of 11%. The data of Fandiño *et al.* [25] is best reproduced by the PC-SAFT equation of state [91,291,298] (AAD = 3.4%). The new model represents the data of Bobbo *et al.* [24] [24] with an AAD of 8.9%, the PC-SAFT equation of state [91,291,298] with an AAD of 7.2%. The authors did not discuss the experimental uncertainty.

Relative deviations of the experimental liquid densities of a CO₂-PEC5 mixture consisting of $x_{\text{CO}_2} = 0.9831$ from the present mixture model are presented in Figure 6.19. Results from the PC-SAFT equation of state [91,291,298] are plotted for comparison. The average absolute relative deviations of the experimental density data from the new mixture model for CO₂-PEC5, and from the PC-SAFT equation of state [91,291,298] are presented in Table 6.17. Pensado *et al.* [26] estimate the uncertainty of their experimental data to be $\pm 0.4\%$.

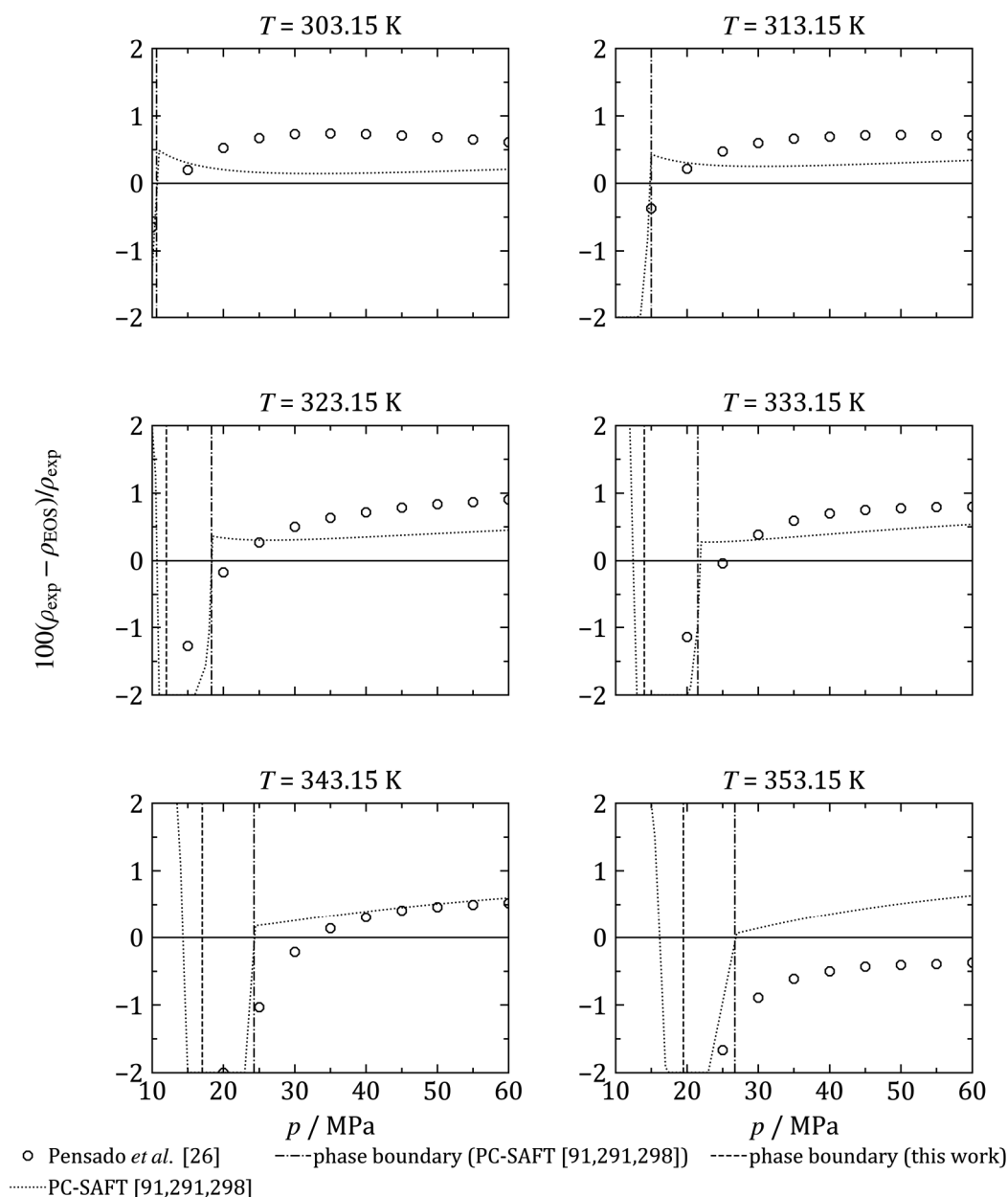


Figure 6.19: Relative deviations of the experimental liquid densities of a CO₂-PEC5 mixture consisting of $x_{\text{CO}_2} = 0.9831$ from the present mixture model. The PC-SAFT equation of state [91,291,298] (dotted curve) is plotted for comparison. The dashed line represents the pressure below which LLE occur calculated from the new model, the dashed-dotted line indicates the pressure below which LLE occur calculated from the PC-SAFT equation of state [91,291,298].

Except for the isotherm $T = 353.15$ K, the data of Pensado *et al.* [26] have a negative offset from the new model for low pressures, turning into a positive offset for high pressures. The deviations range from -1% to $+1\%$ with an AAD of 0.67% . Close to the phase boundary, the deviations go up to -2% . For lower temperatures, the PC-SAFT equation of state [91,291,298] describes the data better (AAD = 0.47%). The rapid change in course of the PC-SAFT equation of state [91,291,298] is caused by a shift of the liquid-liquid equilibrium of the two models, which results in a change of the calculated densities and consequently a jump in the calculated relative deviations. In contrast to the new equation and except for the two lowest isotherms, the PC-SAFT equation of state [91,291,298] describes the single-phase experimental data points at the lowest pressure as two-phase states.

Table 6.17: Average absolute relative deviations of the experimental phase equilibrium data from the present mixture model for CO₂-PEC5, and from the PC-SAFT equation of state [91,291,298].

| Author | No. of data | Temperature range / K | Pressure range / MPa | x_{CO_2} | Average absolute relative deviations AAD / % | |
|----------------------------|-------------|-----------------------|----------------------|-------------------|--|----------------------|
| | | | | | This work | PC-SAFT [91,291,298] |
| Pensado <i>et al.</i> [26] | 57 | 303 - 353 | 10 - 60 | 0.9831 | 0.67 | 0.47 |
| Pensado <i>et al.</i> [26] | 55 | 303 - 353 | 10 - 60 | 0.9919 | 0.28 | 0.45 |
| Pensado <i>et al.</i> [26] | 112 | 303 - 353 | 10 - 60 | 0.9831 - 0.9919 | 0.477 | 0.473 |

Figure 6.20 shows relative deviations of experimental density data for a CO₂-PEC5 mixture consisting of $x_{\text{CO}_2} = 0.9919$ from the present mixture model. The PC-SAFT equation of state [91,291,298] is plotted for comparison. The new model represents these data well within the estimated uncertainty ($\pm 0.4\%$). Only the points near the phase boundary or at high temperatures and high pressures deviate stronger. Again, the effect of the shifted LLE of this model and the PC-SAFT equation of state [91,291,298] is distinct. At this composition, the experimental data are better described by the new model (AAD = 0.28%), than by the PC-SAFT equation of state [91,291,298] (AAD = 0.45%). Again, the PC-SAFT equation of state [91,291,298] describes some of the single-phase experimental data points at the lowest pressure as two-phase states.

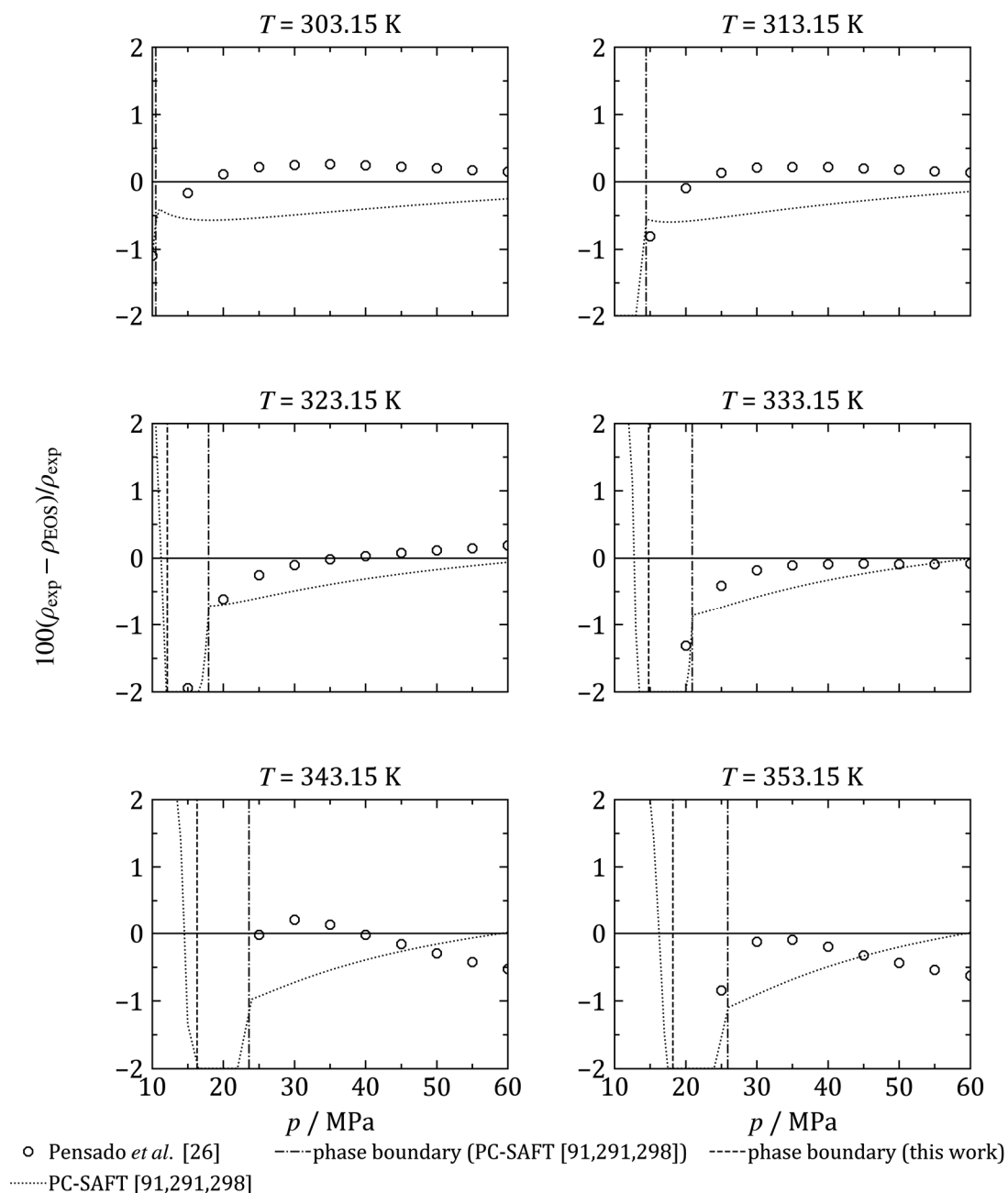


Figure 6.20: Relative deviations of the experimental liquid densities of a CO₂-PEC5 mixture consisting of $x_{\text{CO}_2} = 0.9919$ from the present mixture model. Results from the PC-SAFT equation of state [86,244,249] (dotted curve) are plotted for comparison. The dashed line represents the pressure below which LLE occur calculated from the new model, the dashed-dotted line indicates the pressure below which LLE occur calculated from the PC-SAFT equation of state [91,291,298].

6.4 Mixture Model for CO₂-PEC7

A new mixture model based on the reference equation of state for CO₂ of Span and Wagner [22] and the new generalized equation of state for PEC7 introduced in section 6.2 is presented here.

As for CO₂-PEC5, three data sets are available in the literature for the CO₂-PEC7 system, which are published by the same authors. Bobbo *et al.* [24] published phase equilibrium data ($pT\mathbf{x}'$) for the isotherm $T = 283.15$ K, whereas Fandiño *et al.* [298] reported phase equilibrium data ($pT\mathbf{x}'$) from $T = 283.15$ K to $T = 343.15$ K. Pensado *et al.* [26] investigated the density for two overall compositions with a very low lubricant content ($x_{\text{PEC7}} = 8$ mass-% and $x_{\text{PEC7}} = 15$ mass-%), in the temperature range from $T = 303.15$ K to $T = 353.15$ K with pressures from $p = 10$ MPa to $p = 60$ MPa.

A binary interaction parameter for the PC-SAFT equation of state adjusted to the experimental data presented in [298] was proposed by Fandiño *et al.* [298], which is used for comparison here.

The mixture model for CO₂-PEC7 developed in this work was not adjusted to the experimental data but was found by scaling of the mixture model for CO₂-PEC5. Thus, the experimental data is used only for the validation of this method. The aim was to show the applicability of this principle, in order to gain mixture models for CO₂ with similar POEs without any adjustment. The binary parameters of the functions describing the reducing temperature are scaled with the ratio of the critical temperatures of the two POEs:

$$\beta_{T,\text{CO}_2\text{PEC7}} = \beta_{T,\text{CO}_2\text{PEC5}} \cdot \frac{T_{c,\text{PEC5}}}{T_{c,\text{PEC7}}}, \text{ and} \quad (6.3)$$

$$\gamma_{T,\text{CO}_2\text{PEC7}} = \gamma_{T,\text{CO}_2\text{PEC5}} \cdot \frac{T_{c,\text{PEC7}}}{T_{c,\text{PEC5}}}. \quad (6.4)$$

The binary parameters of the functions describing the reducing density are scaled with the ratio of the critical densities of the two POEs:

$$\beta_{v,\text{CO}_2\text{PEC7}} = \beta_{v,\text{CO}_2\text{PEC5}} \cdot \frac{\rho_{c,\text{PEC7}}}{\rho_{c,\text{PEC5}}}, \text{ and} \quad (6.5)$$

$$\gamma_{v,\text{CO}_2\text{PEC7}} = \gamma_{v,\text{CO}_2\text{PEC5}} \cdot \frac{\rho_{c,\text{PEC7}}}{\rho_{c,\text{PEC5}}}. \quad (6.6)$$

Different approaches for the conversion of the reducing parameters were investigated and these relations were found to be most beneficial.

Table 6.18 gives the reducing parameters for CO₂-PEC7 mixtures found by this method.

Table 6.18: Scaled reducing parameters for CO₂-PEC7 mixtures.

| β_T | γ_T | β_v | γ_v |
|-----------|------------|-----------|------------|
| 0.8621 | 1.6981 | 3.2724 | 4.2468 |

Experimental and calculated values for the phase equilibrium of CO₂-PEC7 mixtures are presented in Figure 6.21. The scaled model shows reliable results for compositions with CO₂ contents of $x_{\text{CO}_2} > 0.4$. At lower CO₂ fractions, the model shows an unphysical negative slope of the bubble line. This behavior was observed during the fitting process of the CO₂-PEC5 system as well. The numerical stability of such asymmetric models is very sensitive with respect to the values of the reducing parameters. For very high CO₂ contents, the new model predicts liquid-liquid equilibria for temperatures above the critical temperature of CO₂ ($T_{c,\text{CO}_2} = 304.13$ K). With the PC-SAFT equation of state [91,291,298], liquid-liquid equilibria can already be found at $T = 298.15$ K. Although the bubble line calculated from the new model oscillates slightly, there is no significant difference in the description of the experimental data by both models for CO₂ fractions of $x_{\text{CO}_2} > 0.4$.

Table 6.19: Average absolute relative deviations of the experimental bubble-line data with respect to the CO₂ fraction, and with respect to pressure from the present mixture model for CO₂-PEC7, and from the PC-SAFT equation of state [91,291,298].

| Author | No. of data | Temperature range / K | Pressure range / MPa | Average absolute relative deviations AAD / % | | | |
|-----------------------------|-------------|-----------------------|----------------------|--|-----|----------------------|-----|
| | | | | This work | | PC-SAFT [91,291,298] | |
| | | | | x_{CO_2} | p | x_{CO_2} | p |
| Bobbo <i>et al.</i> [24] | 9 | 283 | 0.50 - 4.41 | 7.5 | 14 | 5.8 | 10 |
| Fandiño <i>et al.</i> [298] | 51 | 283 - 333 | 0.74 - 6.39 | 18(4.6)* | 14 | 6.8 | 5.0 |

*: For $x_{\text{CO}_2} > 0.4$.

Figure 6.22 illustrates relative deviations of experimental densities of a CO₂-PEC7 mixture consisting of $x_{\text{CO}_2} = 0.9872$ from the present mixture model. The PC-SAFT equation of state [91,291,298] is again plotted for comparison. The new model reproduces the experimental data with a maximum offset of -2% to $+1.5\%$. A deviation of -4.5% is reached only for the lowest pressure of the highest isotherm. For temperatures $T < 333.15$ K, the experimental data is best described by the new model within -0.5% to $+1\%$. For higher temperatures, the PC-SAFT equation of state [91,291,298] follows the trend of the experimental data better. The new model reproduces the data with an average absolute relative deviation of $\text{AAD} = 0.69\%$, whereas the PC-SAFT equation of

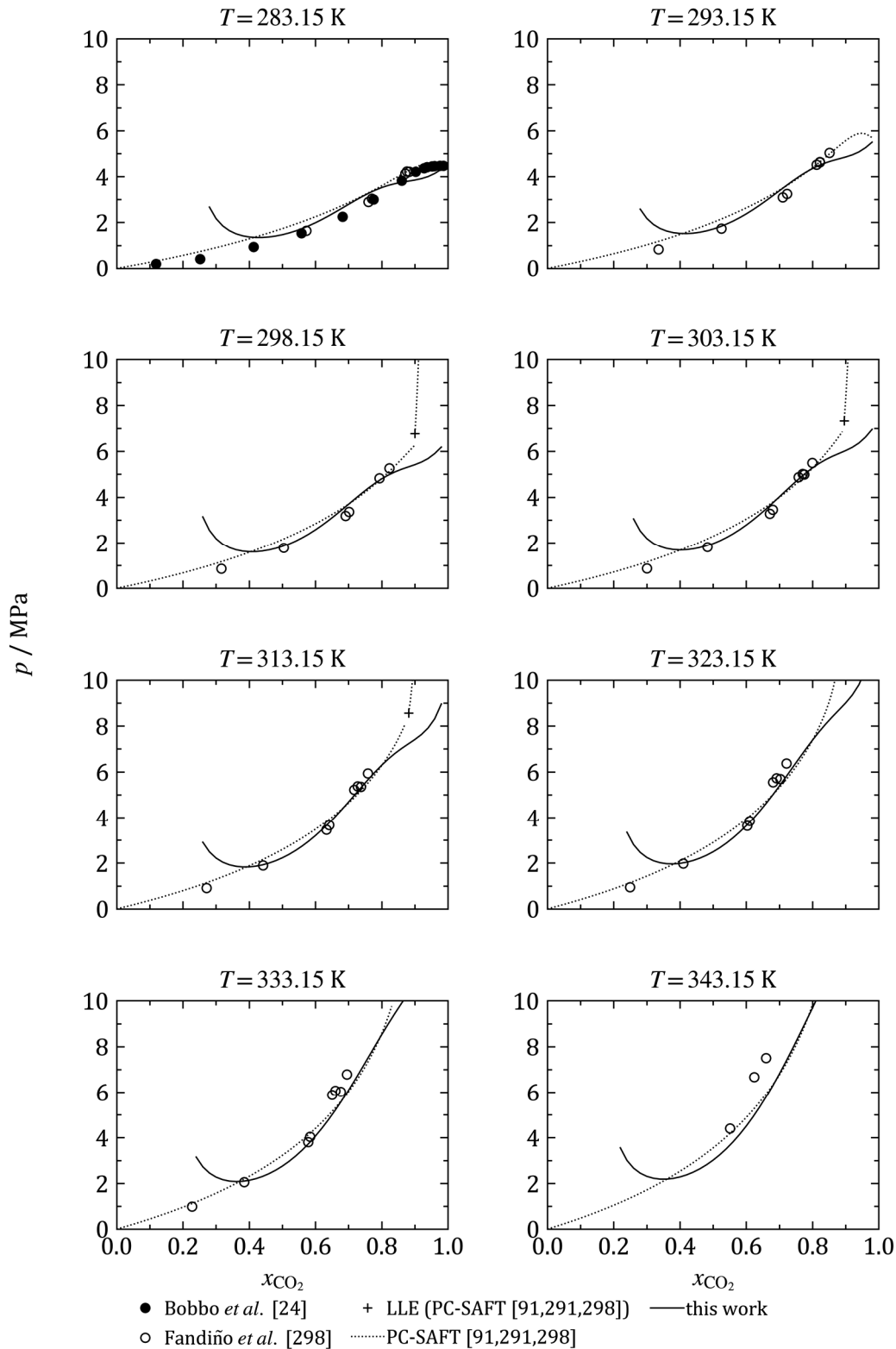


Figure 6.21: Experimental and calculated values for the bubble-line pressure of CO₂-PEC7 mixtures for several isotherms. The PC-SAFT equation of state [91,291,298] (dotted curve) is plotted for comparison.

state [91,291,298] reproduces the data with an AAD of 1.7%. Density calculations from the PC-SAFT equation of state did not converge for all pressures at this composition, resulting in an “edgy” appearance in the plot.

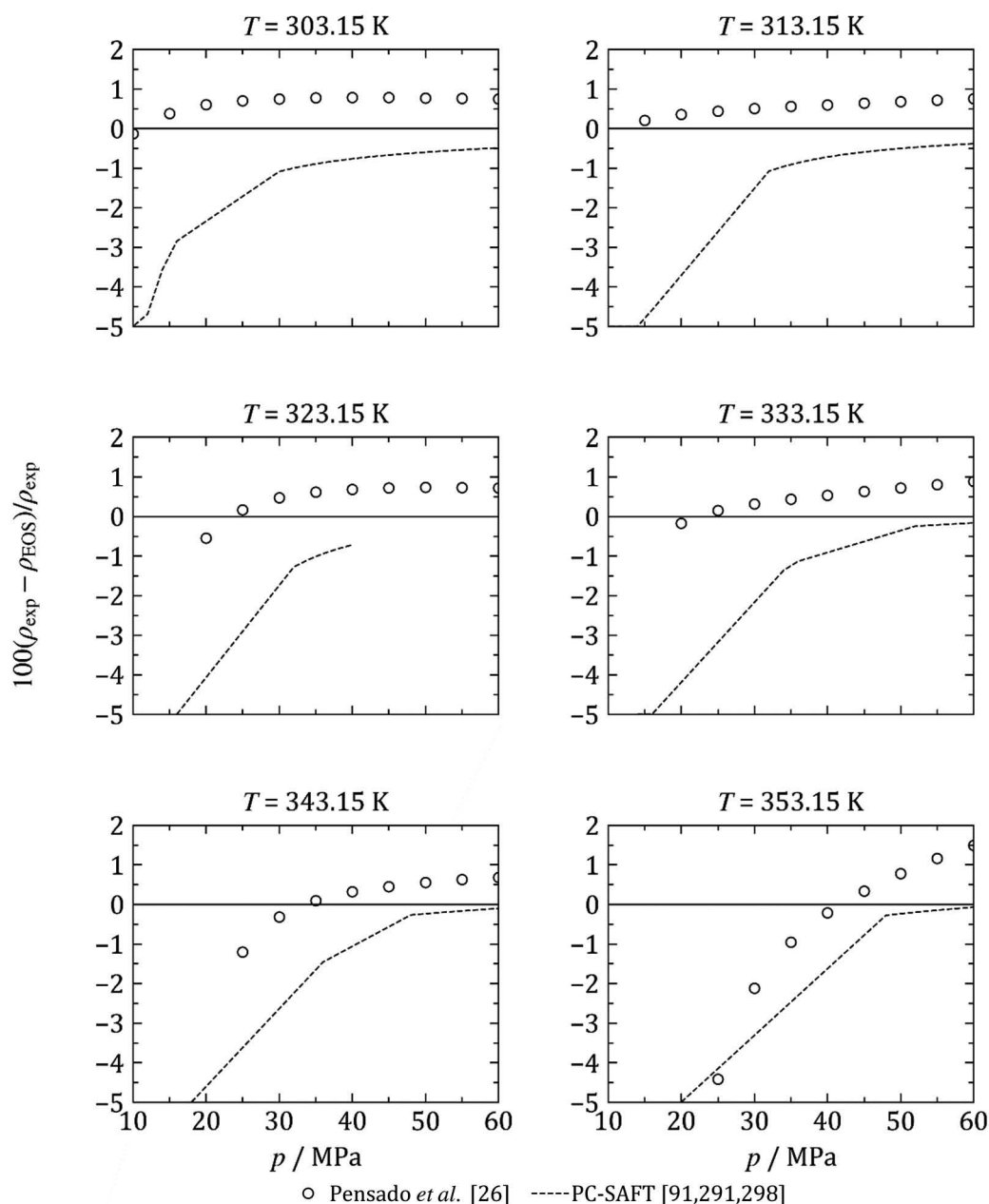


Figure 6.22: Relative deviations of the experimental liquid density data of a CO₂-PEC7 mixture consisting of $x_{\text{CO}_2} = 0.9872$ from the present mixture model. Results from the PC-SAFT equation of state [91,291,298] (dotted curve) are plotted for comparison.

Relative deviations of the experimental densities of a CO₂-PEC7 mixture consisting of $x_{\text{CO}_2} = 0.9934$ from the present mixture model are shown in Figure 6.23. For temperatures $T < 323.15$ K, the new mixture model deviates from the data by -1% to 0% . For higher temperatures, the PC-SAFT equation of state [91,291,298] follows the trend of the data more closely. The average absolute relative deviation of the new model from these data is $\text{AAD} = 0.59\%$, whereas the PC-SAFT equation of state [91,291,298] reproduces the data with $\text{AAD} = 0.83\%$.

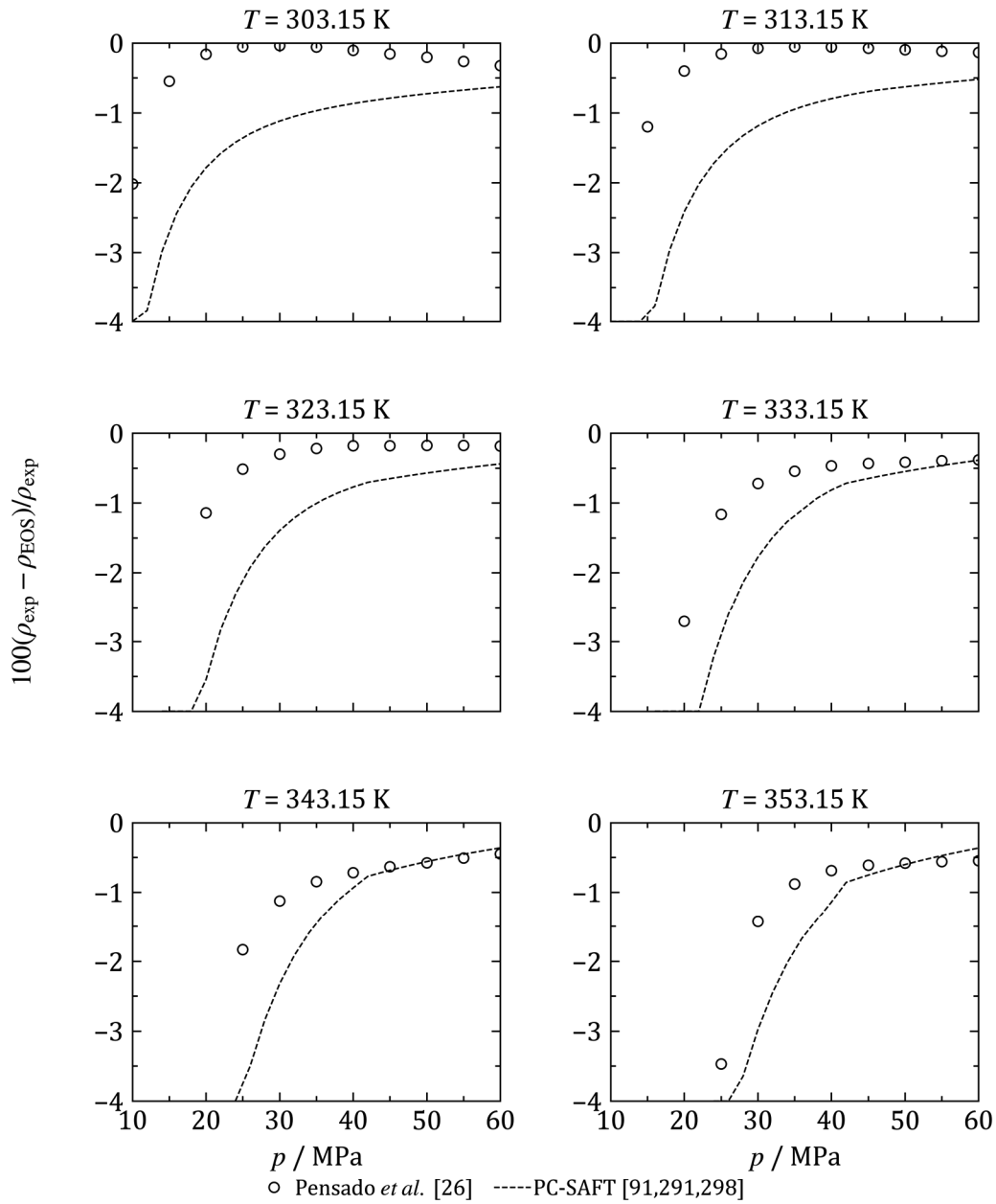


Figure 6.23: Relative deviations of the experimental liquid density data of a CO₂-PEC7 mixture consisting of $x_{\text{CO}_2} = 0.9934$ from the present mixture model. Results from the PC-SAFT equation of state [91,291,298] (dotted curve) are plotted for comparison.

Table 6.20: Average absolute relative deviations of the experimental phase equilibrium data from the present mixture model for CO₂-PEC7, and from the PC-SAFT equation of state [91,291,298].

| Author | No. of data | Temperature range / K | Pressure range / MPa | x_{CO_2} | Average absolute relative deviations AAD / % | |
|----------------------------|-------------|-----------------------|----------------------|-------------------|--|----------------------|
| | | | | | This work | PC-SAFT [91,291,298] |
| Pensado <i>et al.</i> [26] | 55 | 303 - 353 | 10 - 60 | 0.9872 | 0.69 | 1.7 |
| Pensado <i>et al.</i> [26] | 55 | 303 - 353 | 10 - 60 | 0.9934 | 0.59 | 0.83 |
| Pensado <i>et al.</i> [26] | 110 | 303 - 353 | 10 - 60 | 0.9872 - 0.9934 | 0.64 | 1.27 |

6.5 Summary

Generalized equations of state for the synthetic lubricants PEC5 and PEC7 were developed, which were exclusively adjusted to thermal property data. Nevertheless, caloric properties such as the isobaric heat capacity and speed of sound are remarkably well predicted by the present equations. The new data measured at NIST [294,297] as well as the fluid-specific equations of Lemmon and Eckermann [23] were used to validate this feature. In contrast, the PC-SAFT equation of state [91,291] deviates strongly from the fluid-specific equation [23] and from experimental data with respect to the caloric properties. In particular, speeds of sound in the liquid phase are not well represented. Subsequently, the new generalized equation of state for PEC5 was applied to establish a new Helmholtz mixture model for the system CO₂-PEC5, which is based on the extended corresponding states approach. It was compared to the PC-SAFT equation of state [91,291,298] which yields better results in the context of such an asymmetric mixture, especially with regard to the description of the phase behavior. Figure 6.18 shows that these shortcomings are not caused by the generalized equation of state developed in this work. It rather seems that the extended corresponding states approach is limited in the description of such asymmetric mixtures. Consequently, different mixture models are required for future improvements. However, the new model is capable of a reasonable estimation of phase equilibria and homogeneous liquid densities of CO₂-PEC5 mixtures and is still slightly superior with regard to the representation of liquid densities.

Finally, a converted CO₂-PEC7 mixture model based on the new mixture model for the system CO₂-PEC5 was developed. It was shown that the model predicts the available experimental data with a similar accuracy as the base model for CO₂-PEC5, except for some issues in the representation of the phase behavior for low CO₂ fractions. Although the new model was not adjusted to these data, the experimental densities are better described by the new scaled equation than by the PC-SAFT equation of state [91,291,298]. Thus, general applicability of the proposed conversion approach is assumed, with limitations for the prediction of phase equilibria at low CO₂ fractions.

7 Conclusions

In a joint research project, the potential of (Organic) Rankine Cycles for Exhaust Heat Recovery (EHR) in heavy-duty diesel engines for mobile applications was investigated. For a safe process design, the knowledge of thermophysical properties of the involved fluids or fluid mixtures is crucial. The EHR process design features ethanol as working fluid. The potential benefit of ethanol-water mixtures as working fluid was to be investigated based on a parameter study. A preliminary ethanol-water mixture model is available in REFPROP [4], which is based on an outdated ethanol pure fluid equation [21]. In order to incorporate the more current ethanol equation of Schroeder *et al.* [3], which is based on a broader experimental data base, a new Helmholtz mixture model was developed in this work.

The uncertainty of the new mixture model for ethanol-water with respect to the speed of sound is estimated to be $\pm 4\%$, which is a significant improvement in contrast to the model of Lemmon [4], which deviates by up to 25% from the experimental data. For temperatures $T > 280$ K, the isobaric heat capacity is represented within 5%. The uncertainty in terms of density is estimated to be 0.5% for temperatures $T < 450$ K, increasing to 1% for elevated pressures. For higher temperatures, the uncertainty is estimated to be 2% in the homogeneous phase up to 5% approaching the phase boundary. The relative deviations in bubble and dew pressure increase from 1% at $T = 313$ K to 3% at $T = 623$ K.

The design of the ORC application includes direct lubricant injection into the expansion machine. Hence, the knowledge of the thermodynamic properties of the lubricant, and the thermodynamic properties of its mixture with ethanol are required. A poly-alpha-olefin (PAO)-based synthetic lubricant containing several PAO base oils and an emulsifier was specially designed for this EHR process and is commercially available [278]. Despite the different compounds, the lubricant is treated as a pure fluid in the models developed in this work. Due to an insufficient data base, a generalized equation of state was developed for the PAO, which is based on the model of Alexandrov *et al* [63]. For the adjustment of such a three-parameter corresponding states model, less experimental data are required than for a fully optimized equation of state. With the new generalized equation of state, the experimental data describing the PAO can be reproduced reasonably well.

A new Helmholtz model describing ethanol-PAO mixtures was subsequently developed, which is based on the new generalized pure fluid equation of state for the PAO and the current ethanol equation of state of Schroeder *et al.* [3]. General application of this method for the estimation of fluid properties was shown. The mixture model developed in this work reproduces the experimental densities reasonably and predicts a three-phase equilibrium as found by experiment in the investigated temperature range. In flash calculations, the compositions of the phases deviate strongly from experimentally determined compositions. However, the vapor composition can be reproduced, if the lubricant-rich liquid phase is neglected and the ethanol-rich liquid phase composition is used as input for a flash calculation.

To validate the new approach of using a generalized equation of a state in a mixture model with challenging, asymmetric components, the systems CO₂-PEC5 and CO₂-PEC7 were investigated. Therefore, new generalized equations for the POE base lubricants PEC5 and PEC7 were fitted and mixture models for these lubricants with CO₂, a promising refrigerant in ORC processes, were developed. For the new generalized equations of state, exclusively the thermal property data available in the literature were included in the adjustment. In a collaborative work with NIST, which is not part of this thesis, two substance-specific Helmholtz equations of state for PEC5 and PEC7 were adjusted to new experimental data measured at NIST containing thermal and caloric properties. The intention was to use these fluid-specific equations for the validation of the new generalized equations of state, especially with regard to the prediction of caloric properties that were not included in the adjustment of the generalized equation of state. It was shown that the generalized equations of state reproduce the available experimental data within the AAD uncertainties range claimed by Alexandrov *et al.* [63]. Comparisons with the PC-SAFT equation of state [91,291] showed that although both models are three-parameter corresponding states approaches, the generalized equations adjusted in this work predict the caloric properties in a superior manner.

The new mixture model for CO₂-PEC5 represents the available phase-equilibrium and density data reasonably. Nevertheless, bubble lines calculated from the new model exhibit an unphysical oscillation that is not caused by the shortcomings of the generalized equation of state but by the mixture model itself. New mixture models are required for a better description of such asymmetric mixtures.

The new mixture model for CO₂-PEC5 was converted to the CO₂-PEC7 system by a simple empirical conversion developed in this work. This conversion was accomplished through the use of the critical pure-fluid parameters and the molar masses only. General applicability was shown with the restriction of $x_{\text{CO}_2} > 0.4$. For smaller CO₂ fractions, the bubble lines calculated from this model show an unphysical negative slope.

In this work, the extended corresponding states-based mixture approach was challenged by the strongly non-ideal ethanol-water system as well as by mixtures of significantly different molecular size and weight. Shortcomings were found that demand for a further development of new mixture approaches. The current status of mixture models is based on a development for natural gases and for mixtures of refrigerants, which contain mostly similar components with significantly less intermolecular forces. Therefore, future research should be focused on the investigation of new mixture models that improve the description of complex mixtures.

References

- [1] Umweltbundesamt, Nationale Inventarberichte zum Deutschen Treibhausgasinventar 1990 bis 2016 (Stand 03/2018), Zeitnauschätzung 2017, Deutscher Projektionsbericht 2017 zur Entwicklung der Treibhausgasemissionen in Deutschland gemäß Verordnung 525/2013/EU.
- [2] Bundesministerium für Umwelt, Naturschutz, Bau und Reaktorsicherheit, Klimaschutz in Zahlen: Der Sektor Verkehr, https://www.bmu.de/fileadmin/Daten_BMU/Download_PDF/Klimaschutz/klimaschutz_in_zahlen_verkehr_bf.pdf (accessed 7.08.2018).
- [3] J.A. Schroeder, S.G. Penoncello, J.S. Schroeder, A Fundamental Equation of State for Ethanol, *J. Phys. Chem. Ref. Data* 43 (2014) 43102.
- [4] E.W. Lemmon, I.H. Bell, M.L. Huber, M.O. McLinden, REFPROP 10.0: NIST Standard Reference Database 23, National Institute of Standards and Technology, Thermophysical Properties Division, 2018.
- [5] Antriebsenergie aus Abwärme: Clausius-Rankine-Prozess (ORC); Möglichkeiten von Expansionsprozessen zur Umwandlung von Abwärme in mechanische Energie, VDI-Verl., Düsseldorf, 1980.
- [6] J. Ringler, M. Seifert, V. Guyotot, W. Hübner, Rankine Cycle for Waste Heat Recovery of IC Engines, *SAE Int. J. Engines* 2 (2009) 67–76.
- [7] M. Jung, Auslegung eines Clausius-Rankine-Zyklus mit Kolbenexpansionsmaschine für die Anwendung im schweren Nutzfahrzeug. Doctoralthesis, Bochum, 2015.
- [8] R. Span, W. Eifler, R. Struzyna, Nutzung der Motorabwärme durch Kreisprozesse, Bad Neuenahr, 2011.
- [9] G. Qiu, H. Liu, S. Riffat, Expanders for Micro-CHP Systems with Organic Rankine Cycle, *Applied Thermal Engineering* 31 (2011) 3301–3307.
- [10] B. Saleh, G. Koglbauer, M. Wendland, J. Fischer, Working Fluids for Low-Temperature Organic Rankine Cycles, *Energy* 32 (2007) 1210–1221.
- [11] N.A. Lai, M. Wendland, J. Fischer, Working Fluids for High-Temperature Organic Rankine Cycles, *Energy* 36 (2011) 199–211.

- [12] J. Bao, L. Zhao, A Review of Working Fluid and Expander Selections for Organic Rankine Cycle, *Renewable and Sustainable Energy Reviews* 24 (2013) 325–342.
- [13] J. Wiedemann, Simulation of an Exhaust Heat Driven Rankine Cycle for Heavy-Duty Diesel Engines in Mobile Applications. Doctoralthesis, 2017.
- [14] M. Grieb, A. Bruemmer, Application-Oriented Design and Theoretical Investigation of a Screw-Type Steam Expander, *International Compressor Engineering Conference* 1449 (2014) 1-10.
- [15] A. Brümmer, Energieeffizienz – Abwärmenutzung durch Schraubenexpander, Pumpen, Kompressoren und prozesstechnische Komponenten (2012) 120–126.
- [16] K.N. Marsh, M.E. Kandil, Review of Thermodynamic Properties of Refrigerants + Lubricant Oils, *Fluid Phase Equilib.* 199 (2002) 319–334.
- [17] S. Bobbo, L. Fedele, R. Stryjek, Oil Structure Influence on the Solubility of Carbon Dioxide in POE Lubricants, in: Purdue University (Ed.), *International Refrigeration and Air Conditioning Conference*, 2006.
- [18] O. Fandiño, A.S. Pensado, L. Lugo, E.R. López, J. Fernández, Volumetric Behaviour of the Environmentally Compatible Lubricants Pentaerythritol Tetraheptanoate and Pentaerythritol Tetranonanoate at High Pressures, *Green Chem.* 7 (2005) 775–783.
- [19] T. Matsumoto, Y. Kawaguchi, Development of PVE Refrigeration Lubricants for R32, in: Purdue University (Ed.), *International Refrigeration and Air Conditioning 15th Conference*, July 14-17, 2014, pp. 1–9.
- [20] W. Wagner, A. Pruß, The IAPWS Formulation 1995 for the Thermodynamic Properties of Ordinary Water Substance for General and Scientific Use, *J. Phys. Chem. Ref. Data* 31 (2002) 387–535.
- [21] H.E. Dillon, S.G. Penoncello, A Fundamental Equation for Calculation of the Thermodynamic Properties of Ethanol, *Int. J. Thermophys.* 25 (2004) 321–335.
- [22] R. Span, W. Wagner, A New Equation of State for Carbon Dioxide Covering the Fluid Region from the Triple-Point Temperature to 1100 K at Pressures up to 800 MPa, *Journal of Physical and Chemical Reference Data* 25 (1996) 1509–1596.
- [23] E.W. Lemmon, T. Eckermann, *J. Phys. Chem. Ref. Data* (2018) to be published.

- [24] S. Bobbo, M. Scattolini, R. Camporese, L. Fedele, R. Stryjek, Solubility of carbon dioxide in pentaerythritol esters., in: IIF/IIR (Ed.), Commercial Refrigeration. Thermophysical Properties and Transfer Processes of Refrigerants. Proceedings of the IIR International Conferences., France, 2005.
- [25] O. Fandiño, E.R. López, L. Lugo, M. Teodorescu, A.M. Mainar, J. Fernández, Solubility of Carbon Dioxide in Two Pentaerythritol Ester Oils between (283 and 333) K, J. Chem. Eng. Data 53 (2008) 1854–1861.
- [26] A.S. Pensado, A.A.H. Pádua, M.J.P. Comuñas, J. Fernández, Viscosity and Density Measurements for Carbon Dioxide + Pentaerythritol Ester Lubricant Mixtures at Low Lubricant Concentration, J. Supercrit. Fluids 44 (2008) 172–185.
- [27] É. Clapeyron, Mémoire sur la Puissance Motrice de la Chaleur, Journal de l'Ecole Royale Polytechnique 14 (1834) 153–190.
- [28] J.D. van der Waals, Over De Continuïteit Van Den Gas: En Vloeistofoestand. Doctoralthesis, Leiden, 1873.
- [29] J.D. van der Waals, The Law of Corresponding States for Different Substances, Proceedings of the Koninklijke Nederlandse Akademie van Wetenschappen 15 (1913) 971–981.
- [30] K.S. Pitzer, Corresponding States for Perfect Liquids, J. Chem. Phys. 7 (1939) 583–590.
- [31] E.A. Guggenheim, The Principle of Corresponding States, J. Chem. Phys. 13 (1945) 253–261.
- [32] O. Redlich, J.N.S. Kwong, On the Thermodynamics of Solutions. V. An Equation of State. Fugacities of Gaseous Solutions, Chem. Rev. 44 (1949) 233–244.
- [33] K.S. Pitzer, D.Z. Lippmann, R.F. Curl, C.M. Huggins, D.E. Petersen, The Volumetric and Thermodynamic Properties of Fluids. II. Compressibility Factor, Vapor Pressure and Entropy of Vaporization 1, J. Am. Chem. Soc. 77 (1955) 3433–3440.
- [34] G. Soave, Equilibrium constants from a modified Redlich-Kwong equation of state, Chem. Eng. Sci. 27 (1972) 1197–1203.
- [35] D.-Y. Peng, D.B. Robinson, A New Two-Constant Equation of State, Ind. Eng. Chem. Fund. 15 (1976) 59–64.

- [36] H. Kamerlingh Onnes, Expression of the Equation of State of Gases and Liquids by Means of Series, Proc. KNAW 4 (1901-1902) 125–147.
- [37] J.A. Beattie, O.C. Bridgeman, A New Equation of State for Fluids, Proc. Am. Acad. Arts Sci. 63 (1928) 229–308.
- [38] M. Benedict, G.B. Webb, L.C. Rubin, An Empirical Equation for Thermodynamic Properties of Light Hydrocarbons and Their Mixtures I. Methane, Ethane, Propane and n -Butane, J. Chem. Phys. 8 (1940) 334–345.
- [39] N.F. Carnahan, K.E. Starling, Equation of State for Nonattracting Rigid Spheres, J. Chem. Phys. 51 (1969) 635–636.
- [40] K.E. Starling, Fluid Thermodynamic Properties for Light Petroleum Systems, Gulf publishing Co., Houston, 1973.
- [41] E. Bender, Equations of State Exactly Representing the Phase Behavior of Pure Substances, in: Amer. Soc. Mech. Eng. (Ed.), Proceedings of the Fifth Symposium on Thermophys. Prop., 1970, pp. 227–235.
- [42] W. Wagner, Eine thermische Zustandsgleichung zur Berechnung der Phasengleichgewichte flüssig-gasförmig für Stickstoff. Doctoralthesis, Braunschweig, 1970.
- [43] R.T. Jacobsen, R.B. Stewart, Thermodynamic Properties of Nitrogen Including Liquid and Vapor Phases from 63K to 2000K with Pressures to 10,000 Bar, J. Phys. Chem. Ref. Data 2 (1973) 757–922.
- [44] B.I. Lee, M.G. Kesler, A Generalized Thermodynamic Correlation Based on three-parameter Corresponding States, AIChE J. 21 (1975) 510–527.
- [45] B. Platzner, G. Maurer, A Generalized Equation of State for Pure Polar and Nonpolar Fluids, Fluid Phase Equilib. 51 (1989) 223–236.
- [46] R.L. Halm, L.I. Stiel, A Fourth Parameter for the Vapor Pressure and Entropy of Vaporization of Polar Fluids, AIChE J. 13 (1967) 351–355.
- [47] G.K. Stipp, S.D. Bai, L.I. Stiel, Compressibility Factor of Polar Fluids in the Gaseous and Liquid Regions, AIChE J. 19 (1973) 1227–1233.
- [48] J.H. Keenan, F.G. Keyes, P.G. Hill, J.G. Moore, Steam Tables: Thermodynamic Properties of Water Including Vapor, Liquid, and Solid Phases, John Wiley & Sons, New York, 1969.

- [49] R. Pollak, Die thermodynamischen Eigenschaften von Wasser: dargestellt durch eine kanonische Zustandsgleichung für die fluiden homogenen und heterogenen Zustände bis 1200 Kelvin und 3000 bar. Doctoralthesis, Bochum, 1974.
- [50] R. Schmidt, W. Wagner, A New Form of the Equation of State for Pure Substances and its Application to Oxygen, *Fluid Phase Equilib.* 19 (1985) 175–200.
- [51] W. Wagner, Eine mathematisch statistische Methode zum Aufstellen thermodynamischer Gleichungen - gezeigt am Beispiel der Dampfdruckkurve reiner fluider Stoffe, VDI-Verlag, Düsseldorf, 1974.
- [52] J. Ewers, W. Wagner, Eine Methode zur Optimierung der Struktur von Zustandsgleichungen und ihre Anwendung zur Aufstellung einer Fundamentalgleichung für Sauerstoff, *VDI-Forsch.-Heft* 609 (1982) 27–34.
- [53] J. Ewers, W. Wagner, in: ASME (Ed.), *Proceedings of the Eighth Symposium on Thermophysical Properties: Vol. 1: Thermophysical Properties of Fluids*, 1982, pp. 78–87.
- [54] U. Setzmann, W. Wagner, A New Method for Optimizing the Structure of Thermodynamic Correlation Equations, *Int. J. Thermophys.* 10 (1989) 1103–1126.
- [55] E.W. Lemmon, R.T. Jacobsen, A New Functional Form and New Fitting Techniques for Equations of State with Application to Pentafluoroethane (HFC-125), *J. Phys. Chem. Ref. Data* 34 (2005) 69–108.
- [56] R. Span, W. Wagner, Equations of State for Technical Applications., *Int. J. Thermophys.* 24 (2003) 1–39.
- [57] R. Span, W. Wagner, Equations of State for Technical Applications., *Int. J. Thermophys.* 24 (2003) 41–109.
- [58] R. Span, W. Wagner, Equations of State for Technical Applications., *Int. J. Thermophys.* 24 (2003) 111–162.
- [59] R. Span, *Multiparameter Equations of State: An Accurate Source of Thermodynamic Property Data*, Springer, Berlin, Heidelberg, 2000.
- [60] L. Sun, J.F. Ely, Universal Equation of State for Engineering Application: Algorithm and Application to Non-Polar and Polar Fluids, *Fluid Phase Equilib.* 222-223 (2004) 107–118.

- [61] R. Lustig, G. Rutkai, J. Vrabec, Thermodynamic Correlation of Molecular Simulation Data, *Molecular Physics* 113 (2015) 910–931.
- [62] L. Sun, J.F. Ely, A Corresponding States Model for Generalized Engineering Equations of State, *Int. J. Thermophys.* 26 (2005) 705–728.
- [63] I. Alexandrov, A. Gerasimov, B. Grigor'ev, Generalized Fundamental Equation of State for the Normal Alkanes (C5–C50), *Int. J. Thermophys.* 34 (2013) 1865–1905.
- [64] J.D. van der Waals, *Die Kontinuität des gasförmigen und flüssigen Zustandes*, Barth, Leipzig, 1899.
- [65] T.W. Leland, P.S. Chapple, B.W. Gamson, Prediction of Vapor-Liquid Equilibria from the Corresponding States Principle, *AIChE J.* 8 (1962) 482–489.
- [66] T.W. Leland, J.S. Rowlinson, G.A. Sather, Statistical Thermodynamics of Mixtures of Molecules of Different Sizes, *Trans. Faraday Soc.* 64 (1968) 1447.
- [67] T.W. Leland, P.S. Chapple, The Corresponding States Principle - A Review of Current Theory and Practice, *Ind. Eng. Chem.* 60 (1968) 15–43.
- [68] T.Y. Kwak, G.A. Mansoori, Van der Waals Mixing Rules for Cubic Equations of State. Applications for Supercritical Fluid Extraction Modelling, *Chem. Eng. Sci.* 41 (1986) 1303–1309.
- [69] D. Zudkevitch, J. Joffe, Correlation and Prediction of Vapor-Liquid Equilibria with the Redlich-Kwong Equation of State, *AIChE J.* 16 (1970) 112–119.
- [70] P.R. Bishnoi, D.B. Robinson, New Mixing Rules for the BWR Parameters to Predict Mixture Properties, *Can. J. Chem. Eng.* 50 (1972) 101–107.
- [71] U. Plöcker, H. Knapp, J. Prausnitz, Calculation of High-Pressure Vapor-Liquid Equilibria from a Corresponding-States Correlation with Emphasis on Asymmetric Mixtures, *Ind. Eng. Chem. Proc. Des. Dev.* 17 (1978) 324–332.
- [72] B. Platzner, G. Maurer, Application of a Generalized Bender Equation of State to the Description of Vapour-Liquid Equilibria in Binary Systems, *Fluid Phase Equilib.* 84 (1993) 79–110.
- [73] M.L. Huber, J.F. Ely, A Predictive Extended Corresponding States Model for Pure and Mixed Refrigerants Including an Equation of State for R134a, *Int. J. Refrig.* 17 (1994) 18–31.

- [74] R. Tillner-Roth, Die thermodynamischen Eigenschaften von R152a, R134a und ihren Gemischen, Hannover, 1993.
- [75] E.W. Lemmon, A Generalized Model for the Prediction of the Thermodynamic Properties of Mixtures Including Vapor-Liquid Equilibrium. Ph.D. Dissertation, Moscow, 1996.
- [76] E.W. Lemmon, R. Tillner-Roth, A Helmholtz Energy Equation of State for Calculating the Thermodynamic Properties of Fluid Mixtures, *Fluid Phase Equilib.* 165 (1999) 1–21.
- [77] E.W. Lemmon, R.T. Jacobsen, S.G. Penoncello, D.G. Friend, Thermodynamic Properties of Air and Mixtures of Nitrogen, Argon, and Oxygen From 60 to 2000 K at Pressures to 2000 MPa, *J. Phys. Chem. Ref. Data* 29 (2000) 331–385.
- [78] R. Klimeck, Entwicklung einer Fundamentalgleichung für Erdgase für das Gas- und Flüssigkeitsgebiet sowie das Phasengleichgewicht. Dissertation, Bochum, 2000.
- [79] O. Kunz, R. Klimeck, W. Wagner, M. Jaeschke, The GERG-2004 Wide-Range Equation of State for Natural Gases and Other Mixtures, VDI-Verl., Düsseldorf, 2007.
- [80] O. Kunz, W. Wagner, The GERG-2008 Wide-Range Equation of State for Natural Gases and Other Mixtures, *J. Chem. Eng. Data* 57 (2012) 3032–3091.
- [81] J. Gernert, R. Span, EOS-CG, *J. Chem. Thermodyn.* 93 (2016) 274–293.
- [82] W.G. Chapman, K.E. Gubbins, G. Jackson, M. Radosz, SAFT, *Fluid Phase Equilib.* 52 (1989) 31–38.
- [83] W.G. Chapman, K.E. Gubbins, G. Jackson, M. Radosz, New Reference Equation of State for Associating Liquids, *Ind. Eng. Chem. Res.* 29 (1990) 1709–1721.
- [84] M.S. Wertheim, Fluids with Highly Directional Attractive Forces. II. Thermodynamic Perturbation Theory and Integral Equations, *J Stat Phys* 35 (1984) 35–47.
- [85] M.S. Wertheim, Fluids with Highly Directional Attractive Forces. I. Statistical Thermodynamics, *J Stat Phys* 35 (1984) 19–34.
- [86] M.S. Wertheim, Fluids with Highly Directional Attractive Forces. III. Multiple Attraction Sites, *J Stat Phys* 42 (1986) 459–476.
- [87] M.S. Wertheim, Fluids with Highly Directional Attractive Forces. IV. Equilibrium Polymerization, *J Stat Phys* 42 (1986) 477–492.

- [88] S.H. Huang, M. Radosz, Equation of State for Small, Large, Polydisperse, and Associating Molecules, *Ind. Eng. Chem. Res.* 29 (1990) 2284–2294.
- [89] S.H. Huang, M. Radosz, Equation of State for Small, Large, Polydisperse, and Associating Molecules, *Ind. Eng. Chem. Res.* 30 (1991) 1994–2005.
- [90] S.S. Chen, A. Kreglewski, Applications of the Augmented van der Waals Theory of Fluids, *Berichte der Bunsengesellschaft für physikalische Chemie* 81 (1977) 1048–1052.
- [91] J. Gross, G. Sadowski, Perturbed-Chain SAFT, *Ind. Eng. Chem. Res.* 40 (2001) 1244–1260.
- [92] B. Saager, R. Hennenberg, J. Fischer, Construction and Application of Physically Based Equations of State, *Fluid Phase Equilib.* 72 (1992) 41–66.
- [93] B. Saager, J. Fischer, Construction and Application of Physically Based Equations of State, *Fluid Phase Equilib.* 72 (1992) 67–88.
- [94] A. Müller, J. Winkelmann, J. Fischer, Backbone Family of Equations of State, *AIChE J.* 42 (1996) 1116–1126.
- [95] U. Weingerl, M. Wendland, J. Fischer, A. Müller, J. Winkelmann, Backbone family of equations of state, *AIChE J.* 47 (2001) 705–717.
- [96] W.A. Fouad, A Systematic Study of Short and Long Range Interactions in Associating Fluids Using Molecular Theory. Doctoralthesis, 2015.
- [97] G.A. Mansoori, N.F. Carnahan, K.E. Starling, T.W. Leland, Equilibrium Thermodynamic Properties of the Mixture of Hard Spheres, *J. Chem. Phys.* 54 (1971) 1523–1525.
- [98] T. Boublík, Hard-Sphere Equation of State, *J. Chem. Phys.* 53 (1970) 471–472.
- [99] J.A. Barker, D. Henderson, Perturbation Theory and Equation of State for Fluids, *J. Chem. Phys.* 47 (1967) 2856–2861.
- [100] J.A. Barker, D. Henderson, Perturbation Theory and Equation of State for Fluids. II. A Successful Theory of Liquids, *J. Chem. Phys.* 47 (1967) 4714–4721.
- [101] J.P. Wolbach, S.I. Sandler, Using Molecular Orbital Calculations To Describe the Phase Behavior of Cross-associating Mixtures, *Ind. Eng. Chem. Res.* 37 (1998) 2917–2928.

- [102] G.M. Kontogeorgis, G.K. Folas, *Thermodynamic Models for Industrial Applications: From Classical and Advanced Mixing Rules to Association Theories*, Wiley, Chichester, 2010.
- [103] U. Setzmann, W. Wagner, A New Equation of State and Tables of Thermodynamic Properties for Methane Covering the Range from the Melting Line to 625 K at Pressures up to 100 MPa, *J. Phys. Chem. Ref. Data* 20 (1991) 1061–1155.
- [104] L. Haar, J.S. Gallagher, G.S. Kell, in: *Proc. 8th Symp. Thermophys. Prop.*, 1982, pp. 298–302.
- [105] E.W. Lemmon, M.O. McLinden, W. Wagner, Thermodynamic Properties of Propane. III. A Reference Equation of State for Temperatures from the Melting Line to 650 K and Pressures up to 1000 MPa, *J. Chem. Eng. Data* 54 (2009) 3141–3180.
- [106] E.W. Lemmon, R.T. Jacobsen, A Generalized Model for the Thermodynamic Properties of Mixtures, *Int. J. Thermophys.* 20 (1999) 825–835.
- [107] I.H. Bell, K. Gao, E.W. Lemmon, *J. Phys. Chem. Ref. Data* (2018) to be published.
- [108] A.R. Bazaev, I.M. Abdulagatov, E.A. Bazaev, A. Abdurashidova, (p,v,T,x) Measurements of $\{(1-x)\text{H}_2\text{O}+x\text{C}_2\text{H}_5\text{OH}\}$ Mixtures in the Near-Critical and Supercritical Regions, *J. Chem. Thermodyn.* 39 (2007) 385–411.
- [109] A.A. Abdurashidova, A.R. Bazaev, E.A. Bazaev, I.M. Abdulagatov, The Thermal Properties of Water-Ethanol System in the Near-Critical and Supercritical States, *High Temp.* 45 (2007) 178–186.
- [110] D.T. Safarov, A.N. Shakhverdiev, Investigation of the Thermophysical Properties of Ethyl Alcohol + Water Solutions, *High Temp.* 39 (2001) 395–400.
- [111] J. Gernert, A new Helmholtz Energy Model for Humid Gases and CCS Mixtures. Doctoralthesis, Bochum, 2013.
- [112] K. Gao, J. Wu, P. Zhang, E.W. Lemmon, A Helmholtz Energy Equation of State for Sulfur Dioxide, *J. Chem. Eng. Data* 61 (2016) 2859–2872.
- [113] M. Thol, E.W. Lemmon, Equation of State for the Thermodynamic Properties of trans-1,3,3,3-Tetrafluoropropene [R-1234ze(E)], *Int. J. Thermophys.* 37 (2016) 3710.

- [114] S. Herrig, M. Thol, A.H. Harvey, E.W. Lemmon, A Reference Equation of State for Heavy Water, *J. Phys. Chem. Ref. Data* (2018) accepted for publication.
- [115] R.C. Pemberton, C.J. Mash, Thermodynamic Properties of Aqueous Non-Electrolyte Mixtures II. Vapour Pressures and Excess Gibbs Energies for Water + Ethanol at 303.15 to 363.15 K Determined by an Accurate Static Method, *J. Chem. Thermodyn.* 10 (1978) 867–888.
- [116] K. Kurihara, T. Minoura, K. Takeda, K. Kojima, Isothermal Vapor-Liquid Equilibria for Methanol + Ethanol + Water, Methanol + Water, and Ethanol + Water, *J. Chem. Eng. Data* 40 (1995) 679–684.
- [117] F. Barr-David, B.F. Dodge, Vapor-Liquid Equilibrium at High Pressures. The Systems Ethanol-Water and 2-Propanol-Water, *J. Chem. Eng. Data* 4 (1959) 107–121.
- [118] F.A. Abu Al-Rub, F.A. Banat, R. Jumah, Vapor-Liquid Equilibrium of Ethanol-Water System in the Presence of Molecular Sieves, *Sep. Sci. Technol.* 34 (1999) 2355–2368.
- [119] E.W. Aldrich, D.W. Querfeld, Freezing and Boiling Points of the Ternary System Ethanol-Methanol-Water, *Ind. Eng. Chem.* 23 (1931) 708–711.
- [120] A. Arce, J. Martínez-Ageitos, A. Soto, VLE for Water + Ethanol + 1-Octanol Mixtures. Experimental Measurements and Correlations, *Fluid Phase Equilib.* 122 (1996) 117–129.
- [121] D.M. Babinets, A.G. Polischuk, I.N. Tsiparis, Dependence of Calcium-Chloride Salting Out Action On the Composition of Aqueous-Solutions of the Lowest Aliphatic-Alcohols, *Izv. Vyssh. Uchebn. Zaved. Khim. Khim. Tekhnol.* 24 (1981) 1394–1396.
- [122] A.M. Balcazar-Ortiz, R.B. Patel, M.M. Abbott, H.C. van Ness, Excess Thermodynamic Functions for Ternary Systems. 5. Total-Pressure Data and GE for 1,4-Dioxane-Ethanol-Water at 50°C, *J. Chem. Eng. Data* 24 (1979) 133–136.
- [123] A.H. Beebe, K.E. Coulter, R.A. Lindsay, E.M. Baker, Equilibria in Ethanol-Water System at Pressures Less Than Atmospheric, *Ind. Eng. Chem.* 34 (1942) 1501–1504.

- [124] C.H. Bloom, C.W. Clump, A.H. Koeckert, Simultaneous Measurement of Vapor-Liquid Equilibria and Latent Heats of Vaporization, *Ind. Eng. Chem.* 53 (1961) 829–832.
- [125] J.S. Carey, W.K. Lewis, Studies in Distillation, *Ind. Eng. Chem.* 24 (1932) 882–883.
- [126] B.H. Carroll, J.H. Mathews, A Calorimeter for Heats of Mixing at Elevated Temperatures, *J. Am. Chem. Soc.* 46 (1924) 30–36.
- [127] M.M. Chaudhry, H.C. van Ness, M.M. Abbott, Excess Thermodynamic Functions for Ternary Systems. 6. Total-Pressure Data and GE for Acetone-Ethanol-Water at 50 °C, *J. Chem. Eng. Data* 25 (1980) 254–257.
- [128] M.K. Dutta Choudhury, Excess Free Energy Of Binary Mixtures of n-Butylamine with Ethyl Alcohol & n-Propyl Alcohol, *Indian J. Chem., Sect A* 14 (1976) 553–556.
- [129] S.P. Christensen, Measurement of Dilute Mixture Vapor-Liquid Equilibrium Data for Aqueous Solutions of Methanol and Ethanol with a Recirculating Still, *Fluid Phase Equilib.* 150-151 (1998) 763–773.
- [130] A.F. Cristino, S. Rosa, P. Morgado, A. Galindo, E.J.M. Filipe, A.M.F. Palavra, C.A. Nieto de Castro, High-Temperature Vapour-Liquid Equilibrium for the Water-Alcohol Systems and Modeling with SAFT-VR: 1. Water-Ethanol, *Fluid Phase Equilib.* 341 (2013) 48–53.
- [131] P. Dalager, Vapor-Liquid Equilibriums of Binary Systems of Water with Methanol and Ethanol at Extreme Dilution of the Alcohols, *J. Chem. Eng. Data* 14 (1969) 298–301.
- [132] I. Dalmolin, E. Skovroinski, A. Biasi, M.L. Corazza, C. Dariva, J.V. Oliveira, M. Corazza, J. Oliveira, Solubility of Carbon Dioxide in Binary and Ternary Mixtures with Ethanol and Water, *Fluid Phase Equilib.* 245 (2006) 193–200.
- [133] S.G. D'Avila, M.L. Cotrim, Prediction of Isothermal Vapour Liquid Equilibrium Data of Nonideal Ternary Mixtures from Binary Data System, *Rev. Bras. Tecnol.* 4 (1973) 191–197.
- [134] S.G. D'Avila, R.S.F. Silva, Isothermal Vapor-Liquid Equilibrium Data by Total Pressure Method. Systems Acetaldehyde-Ethanol, Acetaldehyde-Water, and Ethanol-Water, *J. Chem. Eng. Data* 15 (1970) 421–424.

- [135] H.J.E. Dobson, CCCXCVII.-The Partial Pressures of Aqueous Ethyl Alcohol, J. Chem. Soc. Trans. 127 (1925) 2866–2873.
- [136] R.W. Dornte, Partial Pressures of Binary Solutions, J. Phys. Chem. 33 (1928) 1309–1331.
- [137] K.A. Dulitskaya, Vapor Pressure of Binary System: I, Zh. Obshch. Khim. 15 (1945).
- [138] V.G. Garbarenko, V.N. Stabnikov, On Phase Equilibria in the System Ethanol-Water-Gas, Izv. Vyssh. Uchebn. Zaved., Pishch. Tekhnol. 4 (1960) 112–120.
- [139] S. Ghosh, A.B. Ghosal, Salt Effect in Vapour-Liquid Equilibrium Under Reduced Pressures. Part I, Indian Chem. Eng. 6 (1964) 70–74.
- [140] C. Gonzalez, H.C. van Ness, Excess Thermodynamic Functions for Ternary Systems. 9. Total-Pressure Data and GE for Water/Ethylene Glycol/ Ethanol at 50°C, J. Chem. Eng. Data 28 (1983) 410–412.
- [141] J. Griswold, J.D. Haney, V.A. Klein, Ethanol-Water System - Vapor-Liquid Properties at High Pressure, Ind. Eng. Chem. 35 (1943) 701–704.
- [142] D.J. Hall, C.J. Mash, R.C. Pemberton, Vapour-Liquid Equilibria for the Systems Water + Methanol, Water + Ethanol, Methanol + Ethanol and Water + Methanol + Ethanol at 298.15 K Determined by a Rapid Transpiration Method, NPL Rep. Chem., Nat. Phys. Lab, UK,, 1979.
- [143] J.E. Heitz, Measurement of Vapor-Liquid Equilibria for Acetaldehyde-Ethanol-Water Mixtures, Am. J. Enol. Vitic. 11 (1960) 19–29.
- [144] J. Herraiz, S. Shen, A. Coronas, Vapor-Liquid Equilibria for Methanol + Poly(ethylene glycol) 250 Dimethyl Ether, J. Chem. Eng. Data 43 (1998) 191–195.
- [145] J. Hong, M.R. Ladisch, G.T. Tsao, Vapor-Liquid Equilibriums of the Water-Ethanol System at Low Alcohol Concentrations, J. Chem. Eng. Data 26 (1981) 305–307.
- [146] F. Hrnčirik, Vypočty Binarnich Rektifikacnich Rovnovah Pomoci Kalkulatoru TI-59, Chem. Prum. 29 (1979) 539–544.
- [147] H.E. Hughes, J.O. Maloney, The Application of Radioactive Tracers to Diffusional Operations, Chem. Eng. Prog. 48 (1952) 192–200.

- [148] K. Iwakabe, H. Kosuge, Isobaric Vapor-Liquid-Liquid Equilibria With a Newly Developed Still, *Fluid Phase Equilib.* 192 (2001) 171–186.
- [149] A.I. Johnson, W.F. Furter, Salt Effect in Vapor-Liquid Equilibrium Part I, *Can. J. Chem. Eng.* 34 (1957) 413–424.
- [150] C.A. Jones, E.M. Schoenborn, A.P. Colburn, Equilibrium Still for Miscible Liquids, *Ind. Eng. Chem.* 35 (1943) 666–672.
- [151] E. Kauer, H.-J. Bittrich, The Simultaneous Determination of Liquid-Vapor Equilibrium and the Vaporization Enthalpy of Liquid Mixtures, *Wiss. Z. Tech. Hochsch. Carl Schorlemmer Leuna-Merseburg* 5 (1963) 329.
- [152] E. Kirschbaum, F. Gerstner, Gleichgewichtskurven, Siede- und Taulinien von Äthylalkohol-Wasser-Gemischen bei Unterdrücken, VDI, 1939.
- [153] K. Kojima, M. Kato, Measurements of Isobaric Boiling Point Curves at High and Low Pressures, *Kagaku Kogaku* 33 (1969) 769–775.
- [154] K. Kojima, K. Ochi, Y. Nakazawa, Relationship Between Liquid Activity Coefficient and Composition for Ternary Systems, *Int. Chem. Eng.* 9 (1969) 342–347.
- [155] K. Kojima, K. Tochigi, H. Seki, K. Watase, Determination of Vapor-Liquid Equilibrium from Boiling Point Curve, *Kagaku Kogaku* 32 (1968) 149–153.
- [156] B. Kolbe, J. Gmehling, Thermodynamic Properties of Ethanol + Water. I. Vapour-Liquid Equilibria Measurements from 90 to 150°C by the Static Method, *Fluid Phase Equilib.* 23 (1985) 213–226.
- [157] K. Kurihara, M. Nakamichi, K. Kojima, Isobaric Vapor-Liquid Equilibria for Methanol + Ethanol + Water and the Three Constituent Binary Systems, *J. Chem. Eng. Data* 38 (1993) 446–449.
- [158] C.U. Linderstroem-Lang, F. Vaslow, The Isotope Effect on the Vapor Pressures of H₂O-C₂H₅OH and D₂O-C₂H₅OD Mixtures, *J. Phys. Chem.* 72 (1968) 2645–2650.
- [159] X. Liu, Z. Lei, T. Wang, Q. Li, J. Zhu, Isobaric Vapor-Liquid Equilibrium for the Ethanol + Water + 2-Aminoethanol Tetrafluoroborate System at 101.3 kPa, *J. Chem. Eng. Data* 57 (2012) 3532–3537.

- [160] A.S. Lozovoi, Z.M. Zyangareev, V.M. Brednev, Improved Apparatus for Study of the Liquid-Gas Equilibria, *Izv. Vyssh. Uchebn. Zaved., Pishch. Tekhnol.* 16 (1973) 142–143.
- [161] A. Macarron, Determination of Liquid-Vapor Equilibrium Diagrams in Binary Systems with Chemical Reactions, *Rev. Real Acad. Cienc. Exact. Fís. Natur. Madrid* 53 (1959) 607–647.
- [162] J. Manczinger, K. Tettaman, Phase Equilibria of System Caprolactam/Water, *Period. Polytech. Chem. Eng.* 10 (1966) 183–195.
- [163] I. Mertl, Liquid-Vapor Equilibrium .49. Phase Equilibria in Ternary-System Ethyl Acetate Ethanol-Water, *Collect. Czech. Chem. Commun.* 37 (1972) 366–374.
- [164] V. Niesen, A. Palavra, A.J. Kidnay, V.F. Yesavage, An Apparatus for Vapor-Liquid Equilibrium at Elevated Temperatures and Pressures and Selected Results for the Water-Ethanol and Methanol-Ethanol Systems, *Fluid Phase Equilib.* 31 (1986) 283–298.
- [165] A.V. Nikolskaya, Vapor-pressure of Ternary Immisibility Systems. Water-Alcohol Solutions of K_2CO_3 and $MgSO_4$, *Zh. Fiz. Khim.* 20 (1946) 421–431.
- [166] E.C. Novella, J.M. Tarraso, Modified Distillation of Binary Liquid Mixtures: I Experimental Technique for the Determination of Vapor-Liquid Equilibrium, *An. R. Soc. Esp. Fis. Quim., B* 48 (1952) 397–408.
- [167] A.A. Novitskiy, E. Pérez, W. Wu, J. Ke, M. Poliakoff, A New Continuous Method for Performing Rapid Phase Equilibrium Measurements on Binary Mixtures Containing CO_2 or H_2O at High Pressures and Temperatures †, *J. Chem. Eng. Data* 54 (2009) 1580–1584.
- [168] W.A. Noyes, R.R. Warfel, The Boiling-Point Curve for Mixtures of Ethyl Alcohol and Water, *J. Am. Chem. Soc.* 23 (1901) 463–468.
- [169] D.F. Othmer, W.P. Moeller, S.W. Englund, R.G. Christopher, Composition of Vapors from Boiling Binary Solutions - Recirculation-type Still and Equilibria under Pressure for Ethyl Alcohol-Water System, *Ind. Eng. Chem.* 43 (1951) 707–711.
- [170] H. Otsuki, F.C. Williams, Effect of Pressure on Vapor-Liquid Equilibria for the System Ethyl Alcohol-Water, *Chem. Eng. Prog. Symp. Ser.* 49 (1953) 55–67.
- [171] R.N. Paul, Study of Liquid-Vapor Equilibrium in Improved Equilibrium Still, *J. Chem. Eng. Data* 21 (1976) 165–169.

- [172] R.C. Phutela, Z.S. Kooner, D.V. Fenby, Vapour Pressure Study of Deuterium Exchange Reactions in Water-Ethanol Systems: Equilibrium Constant Determination, *Aust. J. Chem.* 32 (1979) 2353–2359.
- [173] T.B. Protsyuk, V.I. Devyatko, Analytical Correlations in the Ethanol + Water System at Atmospheric Pressure, *Pishch. Prom-st.* 10 (1969) 72–76.
- [174] J.R. Rarey, J. Gmehling, Computer-Operated Differential Static Apparatus for the Measurement of Vapor-Liquid Equilibrium Data, *Fluid Phase Equilib.* 83 (1993) 279–287.
- [175] R.M. Rieder, A.R. Thompson, Vapor-Liquid Equilibria Measured by a Gillespie Still - Ethyl Alcohol - Water System, *Ind. Eng. Chem.* 41 (1949) 2905–2908.
- [176] A. Rius, J.L. Otero, A. Macarron, Errata: Equilibres liquide-vapeur de mélanges binaires donnant une réaction chimique: systèmes méthanol-acide acétique ; éthanol-acide acétique ; n-propanol-acide acétique ; n-butanol-acide acétique, *Chem. Eng. Sci.* 10 (1959) 288–290.
- [177] V.N. Stabnikov, B.Z. Matyushev, T.B. Protsyuk, N.M. Yushchenko, Equilibrium in the Ethyl Alcohol + Water System at Atmospheric Pressure, *Pishch. Prom-st.* 15 (1972) 49–56.
- [178] V.N. Stabnikov, T.B. Protsyuk, N.M. Yushchenko, Study of Liquid-Vapour Equilibrium in the System Ethanol-Water with Various Pressures, *Izv. Vyssh. Uchebn. Zaved., Pishch. Tekhnol.* 3 (1972) 149–151.
- [179] V. Svoboda, V. Hynek, J. Pick, Liquid-Vapour Equilibrium .XXXXVII. Simultaneous Determination of Vapour-Liquid Equilibrium and Integral Isobaric Evaporation Heat of a Mixture, *Collect. Czech. Chem. Commun.* 33 (1968) 2584–2597.
- [180] Y. Takiguchi, O. Osada, M. Uematsu, Thermodynamic Properties of $\{x\text{C}_2\text{H}_5\text{OH}+(1-x)\text{H}_2\text{O}\}$ in the Temperature Range from 320 K to 420 K at Pressures up to 200 MPa, *J. Chem. Thermodyn.* 28 (1996) 1375–1385.
- [181] K. Tochigi, H. Inoue, K. Kojima, Determination of Azeotropes in Binary Systems at Reduced Pressures, *Fluid Phase Equilib.* 22 (1985) 343–352.
- [182] D.S. Tsiklis, A.I. Kulikova, L.I. Shenderei, Phase Equilibria in the System Ethanol + Ethylene + Water at High Pressures and Temperatures, *Khim. Prom-st.* 5 (1960) 401–406.

- [183] V.V. Udoenko, L.G. Fatkulina, Vapor Pressure of Three-Component Systems II The System Ethyl Alcohol - 1,2 -Dichloroethane - Water, *Zh. Fiz. Khim.* 26 (1952) 1438–1447.
- [184] F. Van Zandijcke, F. Verhoeye, The Vapor-Liquid Equilibrium of Ternary Systems with Limited Miscibility at Atmospheric Pressure, *J. Appl. Chem. Biotechnol.* 24 (1974) 709–729.
- [185] V.N. Vostrikova, M.E. Aerov, R.E. Gurovich, R.M. Solomatina, Investigation of Liquid-Vapor Equilibrium in the System Ethyl Alcohol - Water in the Region of Low Water Concentrations, *Zh. Prikl. Khim.* 40 (1967) 683–686.
- [186] E.C. Voutsas, C. Pamouktsis, D. Argyris, G.D. Pappa, Measurements and Thermodynamic Modeling of the Ethanol–Water System with Emphasis to the Azeotropic Region, *Fluid Phase Equilib.* 308 (2011) 135–141.
- [187] D.T. Vu, C.T. Lira, N.S. Asthana, A.K. Kolah, D.J. Miller, Vapor–Liquid Equilibria in the Systems Ethyl Lactate + Ethanol and Ethyl Lactate + Water, *J. Chem. Eng. Data* 51 (2006) 1220–1225.
- [188] S.R. Wilson, R.B. Patel, M.M. Abbott, H.C. van Ness, Excess Thermodynamic Function for Ternary Systems. 4. Total-Pressure Data and GE for Acetonitrile-Ethanol-Water at 50°C, *J. Chem. Eng. Data* 24 (1979) 130–132.
- [189] C.J. Wormald, M.D. Vine, Molar enthalpy increments for (0.5 H₂O+0.5C₂H₅OH) at temperatures up to 573.2 K and pressures up to 11.3 MPa, *J. Chem. Thermodyn.* 32 (2000) 439–449.
- [190] M. Wrewsky, On the Composition and Tension of Binary Vapor-Liquid Mixtures, *Z. Phys. Chem., Stöchiom. Verwandtschaftsl.* 81 (1913) 81–113.
- [191] H. Yamamoto, T. Terano, Y. Nishi, J. Tokunaga, Vapor-Liquid Equilibria for Methanol + Ethanol + Calcium Chloride, + Ammonium Iodide, and + Sodium Iodide at 298.15 K, *J. Chem. Eng. Data* 40 (1995) 472–477.
- [192] B. Yang, H. Wang, Vapor–Liquid Equilibrium for Mixtures of Water, Alcohols, and Ethers, *J. Chem. Eng. Data* 47 (2002) 1324–1329.
- [193] J. Zielkiewicz, A. Konitz, Vapour-liquid Equilibrium in Ternary System N, N-Dimethyl-Formide + Water + Ethanol at 313.15 K, *Fluid Phase Equilib.* 63 (1991) 129–139.

- [194] H.A. Zarei, F. Jalili, S. Assadi, Temperature Dependence of the Volumetric Properties of Binary and Ternary Mixtures of Water (1) + Methanol (2) + Ethanol (3) at Ambient Pressure (81.5 kPa), *J. Chem. Eng. Data* 52 (2007) 2517–2526.
- [195] M.F. Hervello, A. Sánchez, Densities of Univalent Cation Sulfates in Ethanol + Water Solutions, *J. Chem. Eng. Data* 52 (2007) 752–756.
- [196] D. Pečar, V. Doleček, Volumetric Properties of Ethanol-Water Mixtures Under High Temperatures and Pressures, *Fluid Phase Equilib.* 230 (2005) 36–44.
- [197] Y. Tanaka, T. Yamamoto, Y. Satomi, H. Kubota, T. Makita, Specific Volume and Viscosity of Ethanol-Water Mixtures Under High-Pressure, *Rev. Phys. Chem. Jpn.* 47 (1977) 12–24.
- [198] I.M. Abdulagatov, L.A. Akhmedova-Azizova, N.D. Azizov, Experimental study of the density and derived (excess, apparent, and partial molar volumes) properties of binary water+ethanol and ternary water+ethanol+lithium nitrate mixtures at temperatures from 298K to 448K and pressures up to 40MPa, *Fluid Phase Equilib.* 376 (2014) 1–21.
- [199] A. Arce, A. Blanco, A. Soto, I. Vidal, Densities, Refractive Indices, and Excess Molar Volumes of the Ternary Systems Water + Methanol + 1-Octanol and Water + Ethanol + 1-Octanol and Their Binary Mixtures at 298.15 K, *J. Chem. Eng. Data* 38 (1993) 336–340.
- [200] A. Arce, A. Blanco, A. Soto, P. Souza, I. Vidal, Excess volumes and refractions and liquid-liquid equilibria of the ternary system water + ethanol + hexyl acetate, *Fluid Phase Equilib.* 87 (1993) 347–364.
- [201] A. Arce, A. Blanco, J. Mendoza, A. Soto, Densities, Refractive Indices, and Excess Molar Volumes of Water + Ethanol + 2-Methoxy-2-Methylpropane at 298.15 K, *J. Chem. Eng. Data* 40 (1995) 1285–1287.
- [202] A. Arce, J. Martínez-Ageitos, J. Mendoza, A. Soto, Water + Ethanol + 2-Methoxy-2-Methylbutane: Properties of Mixing at 298.15 K and Isobaric Vapour-Liquid Equilibria at 101.32 kPa, *Fluid Phase Equilib.* 141 (1997) 207–220.
- [203] A. Arce, A. Soto, J. Ortega, G. Sabater, Viscosities and Volumetric Properties of Binary and Ternary Mixtures of Tris(2-hydroxyethyl) Methylammonium Methylsulfate + Water + Ethanol at 298.15 K, *J. Chem. Eng. Data* 53 (2008) 770–775.

- [204] Z. Atik, Densities and Excess Molar Volumes of Binary and Ternary Mixtures of Aqueous Solutions of 2,2,2-Trifluoroethanol with Acetone and Alcohols at the Temperature of 298.15 K and Pressure of 101 kPa, *J. Solution Chem.* 33 (2004) 1447–1466.
- [205] T.-C. Bai, J. Yao, S.-J. Han, Excess Molar Volumes for Binary and Ternary Mixtures of (N,N-Dimethylformamide+Ethanol+Water) at the Temperature 298.15 K, *J. Chem. Thermodyn.* 30 (1998) 1347–1361.
- [206] R. Belda Maximino, Surface tension and density of binary mixtures of monoalcohols, water and acetonitrile, *Phys. Chem. Liq.* 47 (2009) 475–486.
- [207] R. Belda, J.V. Herraéz, O. Diez, Rheological Study and Thermodynamic Analysis of the Binary System (Water/Ethanol): Influence of Concentration, *Phys. Chem. Liq.* 42 (2004) 467–479.
- [208] G.C. Benson, O. Kiyohara, Thermodynamics of aqueous mixtures of nonelectrolytes. I. Excess volumes of water - n-alcohol mixtures at several temperatures, *J. Solution Chem.* 9 (1980) 791–804.
- [209] S.G. Bruun, P.G. Sørensen, A. Hvidt, A. Kjekshus, B. Klewe, D.L. Powell, Ultrasonic Properties of Ethanol-Water Mixtures, *Acta Chem. Scand.* 28a (1974) 1047–1054.
- [210] M.S. Chauhdry, J.A. Lamb, Excess Volumes of Ethanol + Water at 298.15 and 323.15 K at Pressures up to 220 MPa, *J. Chem. Eng. Data* 32 (1987) 431–434.
- [211] M. Dizechi, E. Marschall, Viscosity of Some Binary and Ternary Liquid Mixtures, *J. Chem. Eng. Data* 27 (1982) 358–363.
- [212] A.E. Dunstan, F.B. Thole, CLXXV.-The Relation Between Viscosity and Chemical Constitution. Part IV. Viscosity and Hydration in Solution, *J. Chem. Soc. Trans.* 95 (1909) 1556–1561.
- [213] R.C. Ernst, C.H. Watkins, H.H. Ruwe, The Physical Properties of the Ternary System Ethyl Alcohol–Glycerin–Water, *J. Phys. Chem.* 40 (1935) 627–635.
- [214] M.E. Friedman, H.A. Scheraga, Volume Changes in Hydrocarbon--Water Systems. Partial Molal Volumes of Alcohol--Water Solutions, *J. Phys. Chem.* 69 (1965) 3795–3800.
- [215] H.R. Galleguillos, M.E. Taboada, T.A. Graber, S. Bolado, Compositions, Densities, and Refractive Indices of Potassium Chloride + Ethanol + Water and Sodium

- Chloride + Ethanol + Water Solutions at (298.15 and 313.15) K, *J. Chem. Eng. Data* 48 (2003) 405–410.
- [216] G. Götze, G.M. Schneider, Excess volumes of liquid mixtures at high pressures IV. Pressure dependence of excess Gibbs energies, excess entropies, and excess enthalpies of aqueous non-electrolyte mixtures up to 250 MPa, *J. Chem. Thermodyn.* 12 (1980) 661–672.
- [217] B. González, N. Calvar, E. Gómez, Á. Domínguez, Density, dynamic viscosity, and derived properties of binary mixtures of methanol or ethanol with water, ethyl acetate, and methyl acetate at $T=(293.15, 298.15, \text{ and } 303.15)\text{K}$, *J. Chem. Thermodyn.* 39 (2007) 1578–1588.
- [218] J.-P.E. Grolier, E. Wilhelm, Excess Volumes and Excess Heat Capacities of Water + Ethanol at 298.15 K, *Fluid Phase Equilib.* 6 (1981) 283–287.
- [219] Hafiz-ur-Rehman, M. Shahid Ansari, Density, Viscosity, and Electrical Conductivity Measurements on the Ternary System $\text{H}_2\text{O} + \text{C}_2\text{H}_5\text{OH} + \text{LiCl}$ over the Entire Ranges of Solvent Composition and LiCl Solubility from $(-5 \text{ to } +50)^\circ\text{C}$, *J. Chem. Eng. Data* 53 (2008) 2072–2088.
- [220] J.V. Herráez, R. Belda, Refractive Indices, Densities and Excess Molar Volumes of Monoalcohols + Water, *J. Solution Chem.* 35 (2006) 1315–1328.
- [221] L.A. Hurley, A.G. Jones, J.N. Drummond, Solubility and Density for Cyanazine + Ethanol + Water, *J. Chem. Eng. Data* 40 (1995) 277–279.
- [222] P. Hynčica, L. Hnědkovský, I. Cibulka, Partial molar volumes of organic solutes in water. XII. Methanol(aq), ethanol(aq), 1-propanol(aq), and 2-propanol(aq) at $T=(298 \text{ to } 573)\text{K}$ and at pressures up to 30 MPa, *J. Chem. Thermodyn.* 36 (2004) 1095–1103.
- [223] E.V. Ivanov, Volumetric properties of dilute solutions of water in ethanol and water-d₂ in ethanol-d₁ between $T=(278.15 \text{ and } 318.15)\text{K}$, *J. Chem. Thermodyn.* 47 (2012) 162–170.
- [224] M.H. Kabir, M.A. Motin, M.E. Huque, Densities and excess molar volumes of Methanol, Ethanol and N- Propanol in pure Water and in Water + Surf Excel solutions at different temperatures, *Phys. Chem. Liq.* 42 (2004) 279–290.

- [225] I.S. Khattab, F. Bandarkar, M.A.A. Fakhree, A. Jouyban, Density, viscosity, and surface tension of water+ethanol mixtures from 293 to 323K, *Korean J. Chem. Eng.* 29 (2012) 812–817.
- [226] M. Kikuchi, E. Oikawa, Viscosities of Aqueous Solutions of Alcohols, *Nippon Kagaku Zasshi* 88 (1967) 1259–1267.
- [227] B.I. Konobeev, V.V. Lyapin, Density, Viscosity and Surface Tension on Certain Binary Systems, *Zh. Prikl. Khim.* 43 (1970) 803.
- [228] H. Kubota, Y. Tanaka, T. Makita, Volumetric Behavior of Pure Alcohols and Their Water Mixtures Under High Pressure, *Int. J. Thermophys.* 8 (1987) 47–70.
- [229] S.K. Kushare, R.R. Kolhapurkar, D.H. Dagade, K.J. Patil, Compressibility Studies of Binary Solutions Involving Water as a Solute in Nonaqueous Solvents at T = 298.15 K, *J. Chem. Eng. Data* 51 (2006) 1617–1623.
- [230] K.N. Marsh, A.E. Richards, Excess volumes for ethanol + water mixtures at 10-K intervals from 278.15 to 338.15, *Aust. J. Chem.* 33 (1980) 2121–2132.
- [231] J.H. Mathews, R.D. Cook, On the Existence of Compounds in Binary Liquid Mixtures, *J. Phys. Chem.* 18 (1914) 559–585.
- [232] H. Mori, S. Iwata, T. Kawachi, T. Matsubara, Y. Nobuoka, T. Aragaki, Practical Correlation of Excess Molar Volumes of Binary, Ternary and Quaternary Mixtures of Water, Methanol, Ethanol and 1-Propanol by an NRTL-Type Equation, *J. Chem. Eng. Japan* 37 (2004) 850–857.
- [233] M.S.K. Niazi, S.S. Shah, J. Ali, M.Z.I. Khan, Thermodynamic dissociation constants of benzoic and nitrobenzoic acids in mixtures of ethanol and 1-propanol with water at 25C, *J. Solution Chem.* 19 (1990) 623–638.
- [234] P.S. Nikam, M. Hasan, Ultrasonic Velocity and Adiabatic Compressibility of Monochloroacetic Acid in Aqueous Ethanol at Various Temperatures, *J. Chem. Eng. Data* 33 (1988) 165–169.
- [235] K. Noda, Y. Aono, K. Ishida, Viscosity and Density of Ethanol-Acetic Acid-Water Mixtures, *Kagaku Kogaku Ronbunshu* 9 (1983) 237–240.
- [236] J.B. Ott, J.T. Sipowska, M.S. Gruszkiewicz, A.T. Woolley, Excess Volumes for (Ethanol+Water) at the Temperatures (298.15 and 348.15) K and Pressures (0.4, 5, and 15) MPa and at the Temperature 323.15 K and Pressures (5 and 15) MPa, *J. Chem. Thermodyn.* 25 (1993) 307–318.

- [237] R.M. Pires, H.F. Costa, A.G.M. Ferreira, I.M.A. Fonseca, Viscosity and Density of Water + Ethyl Acetate + Ethanol Mixtures at 298.15 and 318.15 K and Atmospheric Pressure, *J. Chem. Eng. Data* 52 (2007) 1240–1245.
- [238] C.M. Romero, J.L. Rojas, Apparent Molar Volumes and Viscosities of Dl- α -Alanine in Water-Ethanol Mixtures, *Phys. Chem. Liq.* 38 (2000) 237–243.
- [239] K.E. Spells, The viscosities of liquid mixtures, *Trans. Faraday Soc.* 32 (1936) 530–540.
- [240] B. Stahlberger, A. Guyer, Die Messung von Oberflächenspannungen nach der Ringmethode mit neuen apparativen Hilfsmitteln, *Helv. Chim. Acta* 33 (1950) 243–249.
- [241] S.W. Subnis, W.V. Bhagwat, R.B. Kanugo, Application of Mixture Law to Rheochor .2., *J. Indian Chem. Soc.* 25 (1948) 575–578.
- [242] Y. Wang, H.-L. Lian, T.-L. Luo, G.-J. Liu, Densities and Viscosities of (1,6-Hexanediamine + Ethanol) and (1,6-Hexanediamine + Ethanol + Water) Mixtures at T = (303.15 to 328.15) K, *J. Chem. Eng. Data* 54 (2009) 1158–1162.
- [243] J. Winnick, J. Kong, Excess Volumes of Mixtures Containing Polar Liquids, *Ind. Eng. Chem. Fund.* 13 (1974) 292–293.
- [244] X.-Z. Yang, J. Wang, Densities and Viscosities of 1,1'-(Pentane-1,5-diyl)-bis(pyridinium) Dibromide in Ethanol + Water from (293.15 to 344.15) K, *J. Chem. Eng. Data* 55 (2010) 2322–2325.
- [245] M. Zhu, Solubility and Density of the Disodium Salt Hemiheptahydrate of Ceftriaxone in Water + Ethanol Mixtures, *J. Chem. Eng. Data* 46 (2001) 175–176.
- [246] J.P. Zhao, P.R. Tremaine, Excess Enthalpies of (Carbon Dioxide + Propylene Carbonate or N-Methyl-e-Caprolactam or 1-Formyl Piperidine) at the Temperatures 298.15 K and 308.15 K and Pressures from 7.5 MPa to 12.5 MPa, *J. Chem. Thermodyn.* 27 (1995) 1169–1185.
- [247] J.B. Ott, G.V. Cornett, C.E. Stouffer, B.F. Woodfield, C. Guanquan, J.J. Christensen, Excess enthalpies of (ethanol+water) at 323.15, 333.15, 348.15, and 373.15 K and from 0.4 to 15 MPa, *J. Chem. Thermodyn.* 18 (1986) 867–875.
- [248] C.J. Wormald, M.J. Lloyd, Excess Enthalpies for (Water + Ethanol) at T= 398 K to T= 548 K and p= 15 MPa, *J. Chem. Thermodyn.* 28 (1996) 615–626.

- [249] V.P. Belousov, N.L. Makarova, Heats of Mixing of Liquids: VIII. Heats of Mixing in Ethyl Alcohol-Water, Dioxane-Water, and Dioxane-Ethyl Alcohol Binary Systems, *Zh. Fiz. Khim.* 4 (1970) 101–107.
- [250] V.P. Belousov, M.Y. Panov, Heats of Mixing of Liquids: XI. Enthalpies of Solution of Water in Alcohols, *Zh. Fiz. Khim.* 2 (1976) 149–150.
- [251] G.L. Bertrand, F.J. Millero, C.-h. Wu, L.G. Hepler, Thermochemical Investigations of the Water-Ethanol and Water-Methanol Solvent Systems. I. Heats of Mixing, Heats of Solution, and Heats of Ionization of Water, *J. Phys. Chem.* 70 (1966) 699–705.
- [252] J.A. Boyne, A.G. Williamson, Enthalpies of Mixing of Ethanol and Water at 25 °C, *J. Chem. Eng. Data* 12 (1967) 318.
- [253] S. Brandt, S. Horstmann, S. Steinigeweg, J. Gmehling, Phase Equilibria and Excess Properties for Binary Systems in Reactive Distillation Processes. Part II. Ethyl Acetate Synthesis, *Fluid Phase Equilib.* 376 (2014) 48–54.
- [254] A. Chand, D.V. Fenby, Enthalpy of Deuterium Exchange Reactions in Water + Ethanol and Methanol + Ethanol, *J. Chem. Thermodyn.* 10 (1978) 997–1001.
- [255] J.J. Christensen, L.D. Hansen, R.M. Izatt, D.J. Eatough, R.M. Hart, Isothermal, Iso-baric, Elevated Temperature, High-Pressure, Flow Calorimeter, *Rev. Sci. Instrum* 52 (1981) 1226–1231.
- [256] J.J. Christensen, R.M. Izatt, An Isothermal Flow Calorimeter Designed for High Temperature, High Pressure Operation, *Thermochim. Acta* 73 (1984) 117–129.
- [257] M.J. Costigan, L.J. Hodges, K.N. Marsh, R.H. Stokes, C.W. Tuxford, The Isothermal Displacement Calorimeter: Design Modifications for Measuring Exothermic Enthalpies of Mixing, *Aust. J. Chem.* 33 (1980) 2103–2119.
- [258] G.S. Fang, K. Tsukamoto, M. Maebayashi, M. Ohba, H. Ogawa, Excess Enthalpy for the (Benzene+Cyclohexane) Mixture Over a Wide Range of Temperature and Pressure, *J. Chem. Thermodyn.* 78 (2014) 204–214.
- [259] T. Friese, S. Schulz, P. Ulbig, K. Wagner, Effect of NaCl on the Excess Enthalpies of Binary Liquid Systems, *Thermochim. Acta* 310 (1998) 87–94.
- [260] S.E.V. Kharin, Y.A. Byval'tsev, V.M. Perelygin, Heat of Mixing of Ethanol and Water, *Izv. Vyssh. Uchebn. Zaved., Pishch. Tekhnol.* 4 (1970) 115–120.

- [261] R.F. Lama, B.C.-Y. Lu, Excess Thermodynamic Properties of Aqueous Alcohol Solutions, *J. Chem. Eng. Data* 10 (1965) 216–219.
- [262] M. Landgren, D. McEachern, G. Olofsson, S. Randzio, S. Sunner, Evaluation of Excess Enthalpies from Flow-Calorimetric Measurements of Enthalpies of Dilution Using Local Approximation by Polynomials, *J. Chem. Thermodyn.* 10 (1978) 847–854.
- [263] J.A. Larkin, Thermodynamic Properties of Aqueous Non-Electrolyte Mixtures I. Excess Enthalpy for Water + Ethanol at 298.15 to 383.15 K, *J. Chem. Thermodyn.* 7 (1975) 137–148.
- [264] B. Marongiu, I. Ferino, R. Monaci, V. Solinas, S. Torrazza, Thermodynamic Properties of Aqueous Non-Electrolyte Mixtures. Alkanols + + Water Systems, *J. Mol. Liq.* 28 (1984) 229–247.
- [265] C. Mathonat, V. Hynek, V. Majer, J.-P.E. Grolier, Measurements of Excess Enthalpies at High Temperature and Pressure Using a New Type of Mixing Unit, *J. Solution Chem.* 23 (1994) 1161–1182.
- [266] M.Y. Nagamachi, A.Z. Francesconi, Measurement and Correlation of Excess Molar Enthalpy for (1,2-Propanediol, or 1,3-Propanediol, or 1,4-Butanediol + Water) at the Temperatures (298.15, 323.15, and 343.15) K, *J. Chem. Thermodyn.* 38 (2006) 461–466.
- [267] J.B. Ott, C.E. Stouffer, G.V. Cornett, B.F. Woodfield, R.C. Wirthlin, J.J. Christensen, U.K. Deiters, Excess Enthalpies for (Ethanol + Water) at 298.15 K and Pressures of 0.4, 5, 10, and 15 MPa, *J. Chem. Thermodyn.* 18 (1986) 1–12.
- [268] J.B. Ott, C.E. Stouffer, G.V. Cornett, B.F. Woodfield, C. Guanquan, J.J. Christensen, Excess Enthalpies for (Ethanol + Water) at 398.15, 423.15, 448.15, and 473.15 K and at Pressures of 5 and 15 MPa. Recommendations for Choosing (Ethanol + Water) as an HmE Reference Mixture, *J. Chem. Thermodyn.* 19 (1987) 337–348.
- [269] J.G. Priest, E.M. Woolley, J.B. Ott, J.R. Goates, Solid + Liquid Phase Equilibria, Excess Enthalpies, and Enthalpies of Fusion in (2,3-Dimethyl-2,3-Butanediol + Water), *J. Chem. Thermodyn.* 15 (1983) 357–366.
- [270] Y.V. Zel'tser, Heat of Mixing of Ethanol + Water Solutions, *Fermentn. Spirt. Prom-st.* 32 (1966) 11–14.

- [271] P. Westh, A. Hvidt, Heat Capacity of Aqueous Solutions of Monohydric Alcohols at Subzero Temperatures, *Biophys. Chem.* 46 (1993) 27–35.
- [272] B. Löwen, U. Peukert, S. Schulz, Heat Capacity Measurement With a Heat Flow Calorimeter, *Thermochim. Acta* 255 (1995) 1–8.
- [273] G.C. Benson, P.J. D'Arcy, Excess Isobaric Heat Capacities of Water-n-Alcohol Mixtures, *J. Chem. Eng. Data* 27 (1982) 439–442.
- [274] H. Ogawa, S. Murakami, Excess Isobaric Heat Capacities for Water + Alkanol Mixtures at 298.15 K, *Thermochim. Acta* 109 (1986) 145–154.
- [275] A. García-Abuín, D. Gómez-Díaz, M.D. La Rubia, J.M. Navaza, R. Pacheco, Density, Speed of Sound, and Isentropic Compressibility of Triethanolamine (or N-Methyldiethanolamine) + Water + Ethanol Solutions from $t = (15 \text{ to } 50) \text{ }^\circ\text{C}$, *J. Chem. Eng. Data* 54 (2009) 3114–3117.
- [276] B.B. Gurung, M.N. Roy, Study of Densities, Viscosity Deviations, and Isentropic Compressibilities of Ternary Liquid Mixtures of Water and Ethane-1,2-Diol with Some Monoalcohols at Various Temperatures, *Phys. Chem. Liq.* 45 (2007) 331–343.
- [277] N.I. Larionov, Investigation of the Speed of Ultrasonic Waves in Mixtures with Components Which Associate, *Zh. Fiz. Khim.* 27 (1953) 1002–1012.
- [278] Fuchs Europe Schmierstoffe GmbH, RENOLIN ORC 135: Special Lubricant for Expanders in Organic Rankine Cycles, 2013.
- [279] Fuchs Europe Schmierstoffe GmbH, Experimental Vapor Pressures for a Synthetic PAO Lubricant Similar to RENOLIN ORC 135.
- [280] R. Span, T. Eckermann, S. Herrig, S. Hielscher, A. Jäger, M. Thol, TREND 3.0: Thermodynamic Reference & Engineering Data, Lehrstuhl für Thermodynamik, Ruhr-Universität Bochum, 2016.
- [281] M. Schild, Personal communication, 2014.
- [282] R. Span, J. Wiedemann, T. Eckermann, S. Kareth, M. Schild, Schlussbericht – Verbundprojekt EHR – Ruhr-Universität Bochum, June 9th, 2015.
- [283] J. Brinkmann, Aufbau und Validierung von In-Situ-Messmethoden für den Hochdruckbereich - Phasenverhalten, Dichten Viskositäten und Grenzflächen

- Spannungen des Modellsystems Polyethylenglycol, Wasser und Kohlenstoffdioxid. Dissertation, Bochum, 2013.
- [284] E. Kukova, M. Petermann, E. Weidner, Phasenverhalten (S-L-G) und Transporteigenschaften binärer Systeme aus hochviskosen Polyethylenglykolen und komprimiertem Kohlendioxid, *Chem. Ing. Tech.* 76 (2004) 280–284.
- [285] A.F. Holleman, E. Wiberg, *Lehrbuch der anorganischen Chemie*, de Gruyter, 1971.
- [286] M. Kahlweit, R. Strey, G. Busse, Weakly to Strongly Structured Mixtures, *Phys. Rev. E* 47 (1993) 4197–4209.
- [287] O. Fandiño, J. García, M.J.P. Comuñas, E.R. López, J. Fernández, P ρ T Measurements and Equation of State (EoS) Predictions of Ester Lubricants up to 45 MPa, *Ind. Eng. Chem. Res.* 45 (2006) 1172–1182.
- [288] L. Fedele, S. Marinetti, S. Bobbo, M. Scattolini, P ρ T Experimental Measurements and Data Correlation of Pentaerythritol Esters, *J. Chem. Eng. Data* 52 (2007) 108–115.
- [289] Å. Wahlström, L. Vamling, Solubility of HFC32, HFC125, HFC134a, HFC143a, and HFC152a in a Pentaerythritol Tetrapentanoate Ester, *J. Chem. Eng. Data* 44 (1999) 823–828.
- [290] H.K. Shobha, K. Kishore, Structural Dependence of Density in High Molecular Weight Esters, *J. Chem. Eng. Data* 37 (1992) 371–376.
- [291] A. Razzouk, I. Mokbel, J. Fernández, N. Msakni, J. Jose, Vapor Pressure Measurements in the Range 10⁻⁵ Pa to 1 Pa of Four Pentaerythritol Esters, *Fluid Phase Equilib.* 260 (2007) 248–261.
- [292] K.N. Urness, R.V. Gough, J.A. Widegren, T.J. Bruno, Thermal Decomposition Kinetics of Polyol Ester Lubricants, *Energy Fuels* 30 (2016) 10161–10170.
- [293] K.G. Joback, R.C. Reid, Estimation of Pure-Component Properties From Group Contributions, *Chem. Eng. Commun.* 57 (1987) 233–243.
- [294] T. Fortin, Personal communication, 2018.
- [295] S. Outcalt, Personal communication, 2018.
- [296] J.A. Widegren, Personal communication, 2018.
- [297] R. Perkins, Personal communication, 2018.

-
- [298] O. Fandiño, E.R. López, L. Lugo, J. García, J. Fernández, Solubility of Carbon Dioxide in Pentaerythritol Ester Oils. New Data and Modeling Using the PC-SAFT Model, *J. Supercrit. Fluids* 55 (2010) 62–70.

Appendix A – Parameters of the Basic Generalized Equation of State

Table A 1: Temperature and density exponents of the generalized model by Alexandrov *et al.* [63].

| i | t_i | d_i | p_i | γ_i |
|-----|--------|-------|-------|------------|
| 1 | 0.686 | 1 | 0 | 0 |
| 2 | 1.118 | 1 | 0 | 0 |
| 3 | 0.857 | 1 | 0 | 0 |
| 4 | 0.559 | 3 | 0 | 0 |
| 5 | 0.442 | 7 | 0 | 0 |
| 6 | 0.831 | 2 | 0 | 0 |
| 7 | 0.484 | 1 | 1 | 1 |
| 8 | 2.527 | 1 | 1 | 1 |
| 9 | 1.549 | 2 | 1 | 1 |
| 10 | 0.757 | 5 | 1 | 1 |
| 11 | 3.355 | 1 | 2 | 1 |
| 12 | 1.905 | 1 | 2 | 1 |
| 13 | 4.941 | 4 | 2 | 1 |
| 14 | 12.805 | 2 | 3 | 1 |

Table A 2: Values of the parameters for the determination of the generalized coefficients.

| i | $c_{i,1}$ | $c_{i,2}$ | $c_{i,3}$ | $c_{i,4}$ |
|-----|-----------------------------|-----------------------------|-----------------------------|----------------------------|
| 1 | $0.53410734 \cdot 10^{+1}$ | $0.66819473 \cdot 10^{+1}$ | $0.16692414 \cdot 10^{+1}$ | $0.29446922 \cdot 10^{+1}$ |
| 2 | $-0.22778189 \cdot 10^{+1}$ | $-0.12846893 \cdot 10^{+1}$ | $0.13795302 \cdot 10^{+1}$ | $0.23284396 \cdot 10^{+1}$ |
| 3 | $-0.38785499 \cdot 10^{+1}$ | $-0.86095696 \cdot 10^{+1}$ | $-0.26707821 \cdot 10^{+1}$ | $0.27960114 \cdot 10^{+1}$ |
| 4 | $-0.12190959 \cdot 10^{-1}$ | $0.36869492 \cdot 10^{+0}$ | $-0.20627285 \cdot 10^{+0}$ | $0.63731470 \cdot 10^{+0}$ |
| 5 | $0.92942159 \cdot 10^{-3}$ | $0.80731074 \cdot 10^{-1}$ | $-0.81358186 \cdot 10^{-1}$ | $0.99619992 \cdot 10^{+0}$ |
| 6 | $-0.16631229 \cdot 10^{-1}$ | $-0.80314182 \cdot 10^{-1}$ | $-0.35343719 \cdot 10^{+0}$ | $0.11870929 \cdot 10^{+1}$ |
| 7 | $-0.16572887 \cdot 10^{+1}$ | $0.21646346 \cdot 10^{+2}$ | $-0.1618967 \cdot 10^{+2}$ | $0.10375103 \cdot 10^{+1}$ |
| 8 | $0.12642606 \cdot 10^{+1}$ | $0.21645843 \cdot 10^{+1}$ | $-0.25726222 \cdot 10^{+1}$ | $0.13733437 \cdot 10^{+1}$ |
| 9 | $0.96008662 \cdot 10^{-1}$ | $0.44221976 \cdot 10^{+1}$ | $0.11591367 \cdot 10^{+1}$ | $0.11168557 \cdot 10^{+1}$ |
| 10 | $0.92950830 \cdot 10^{-1}$ | $-0.57463893 \cdot 10^{-1}$ | $0.44419682 \cdot 10^{+0}$ | $0.76390402 \cdot 10^{+0}$ |
| 11 | $-0.38271299 \cdot 10^{+0}$ | $-0.20429713 \cdot 10^{+1}$ | $0.11751452 \cdot 10^{+1}$ | $0.14829049 \cdot 10^{+1}$ |
| 12 | $0.34936066 \cdot 10^{+0}$ | $0.6455642 \cdot 10^{+1}$ | $-0.83598749 \cdot 10^{+1}$ | $0.10080516 \cdot 10^{+1}$ |
| 13 | $0.4171879 \cdot 10^{-1}$ | $-0.90287649 \cdot 10^{+0}$ | $0.23069811 \cdot 10^{+0}$ | $0.13320474 \cdot 10^{+1}$ |
| 14 | $-0.12149915 \cdot 10^{-1}$ | $-0.15474203 \cdot 10^{+0}$ | $0.23233099 \cdot 10^{+0}$ | $0.12062411 \cdot 10^{+1}$ |

Appendix B – Parameters of the adjusted generalized equation of state

Table B 1: Generalized equation parameters for PAO with coefficients evaluated from the adjusted corresponding states parameters.

| i | N_i | t_i | d_i | p_i |
|-----|---------------------------------|--------|-------|-------|
| 1 | 5.479408056325 | 0.686 | 1 | 0 |
| 2 | -2.304246555419 | 1.118 | 1 | 0 |
| 3 | -4.056820239042 | 0.857 | 1 | 0 |
| 4 | $-2.198447281716 \cdot 10^{-2}$ | 0.559 | 3 | 0 |
| 5 | $8.914407509800 \cdot 10^{-4}$ | 0.442 | 7 | 0 |
| 6 | $-2.183543931921 \cdot 10^{-2}$ | 0.831 | 2 | 0 |
| 7 | -1.495915082277 | 0.484 | 1 | 1 |
| 8 | 1.296546913602 | 2.527 | 1 | 1 |
| 9 | $2.027997920456 \cdot 10^{-1}$ | 1.549 | 2 | 1 |
| 10 | $1.147301175206 \cdot 10^{-1}$ | 0.757 | 5 | 1 |
| 11 | $-4.212628050360 \cdot 10^{-1}$ | 3.355 | 1 | 2 |
| 12 | $3.142257447543 \cdot 10^{-1}$ | 1.905 | 1 | 2 |
| 13 | $2.434692684979 \cdot 10^{-2}$ | 4.941 | 4 | 2 |
| 14 | $-1.319154456018 \cdot 10^{-2}$ | 12.805 | 2 | 3 |

Appendix C – Density Deviations (Ethanol-Water)

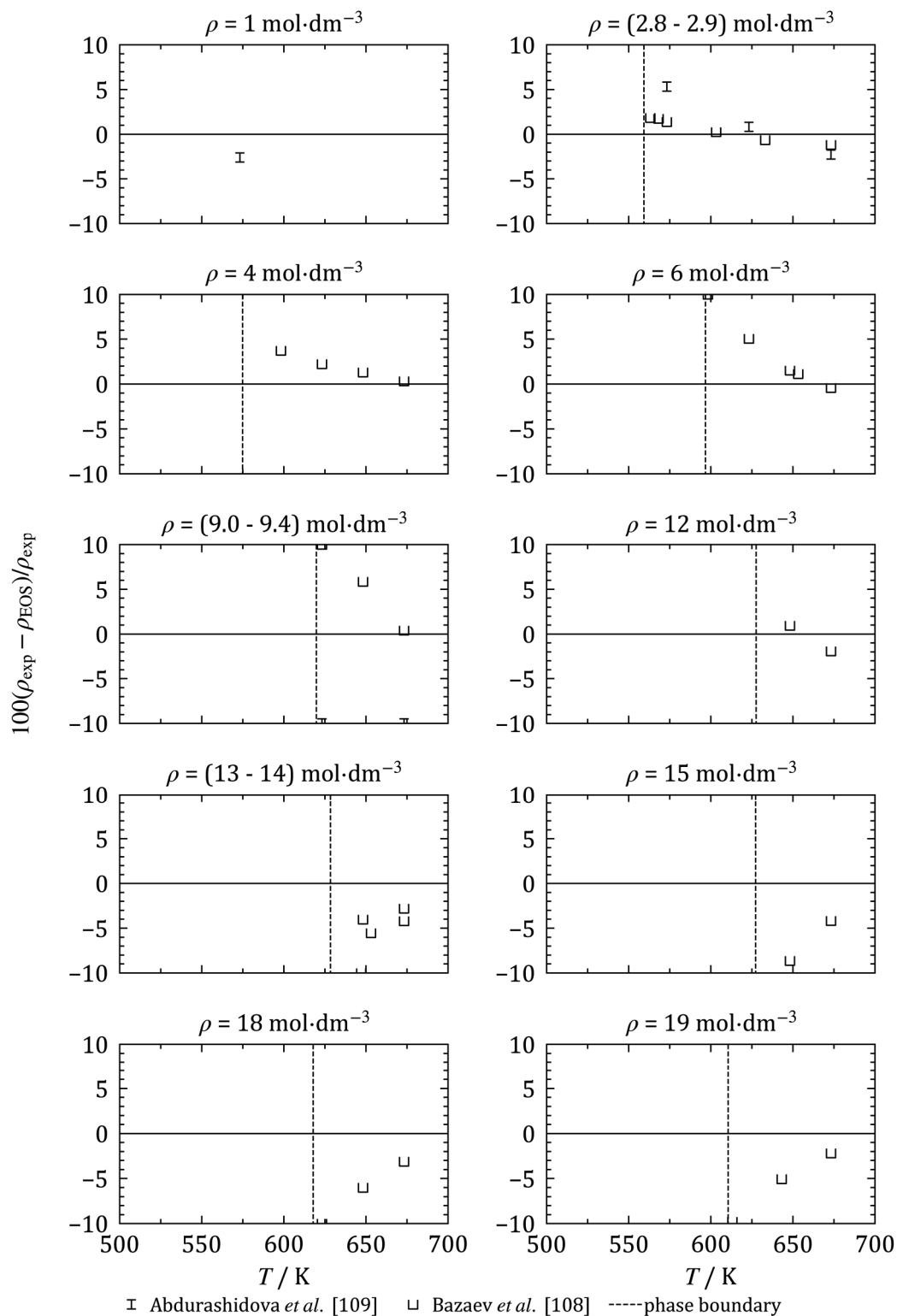


Figure C 1: Relative deviations of the high temperature experimental densities along isochores over pressure from the new mixture model with $x_{\text{Ethanol}} = 0.2$.

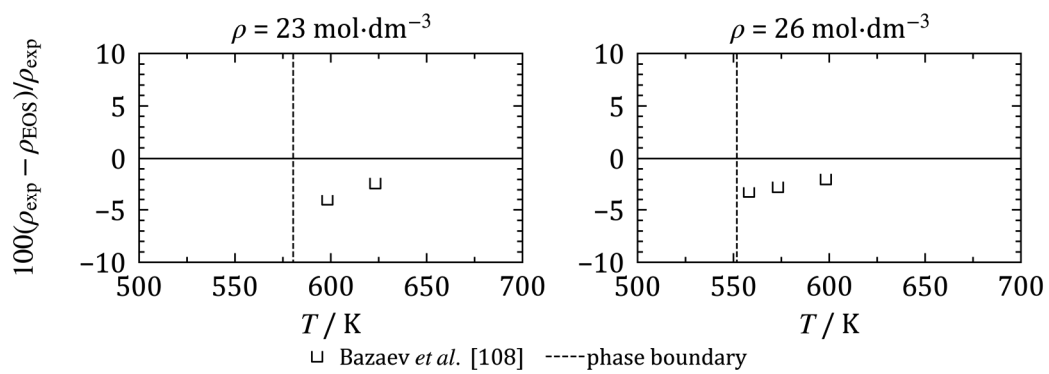


Figure C 1 continued.

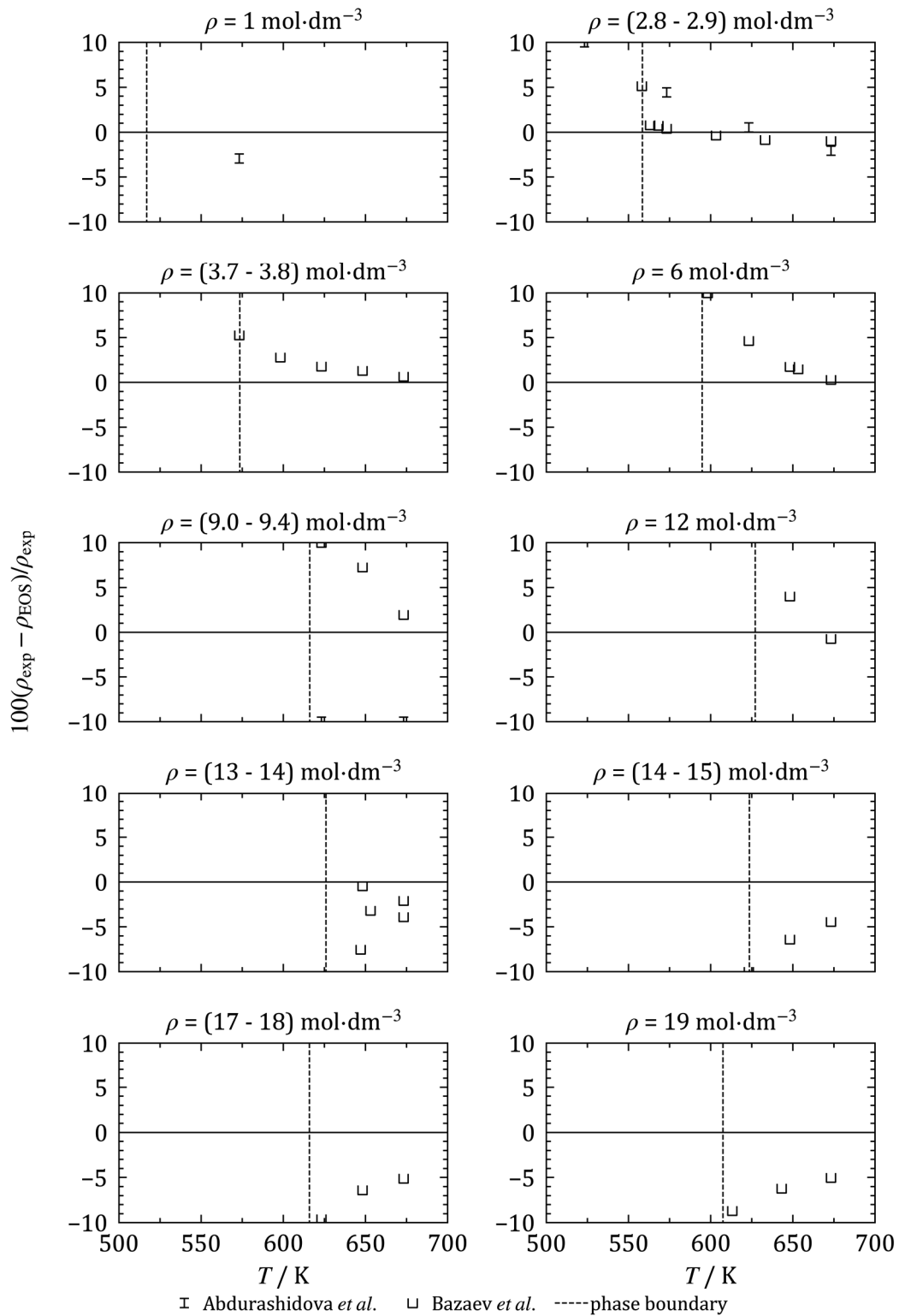


Figure C 2: Relative deviations of the high temperature experimental densities along isochores over pressure from the mixture model of Lemmon [4] with $x_{\text{Ethanol}} = 0.2$.

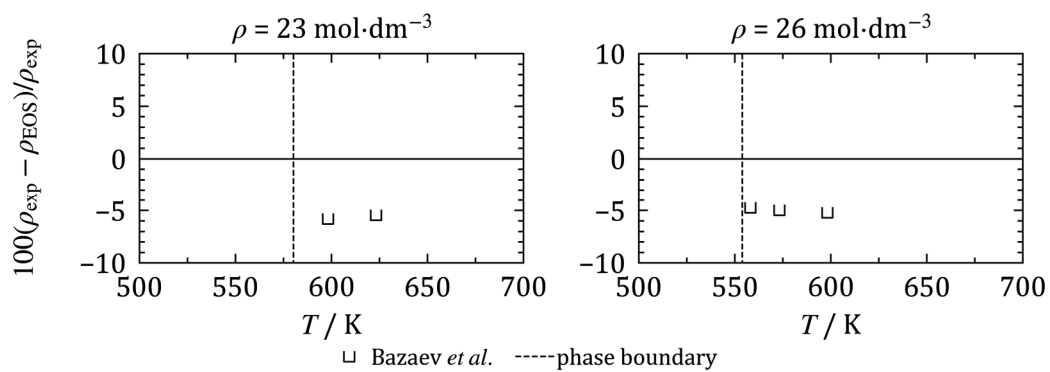


Figure C 2 continued.

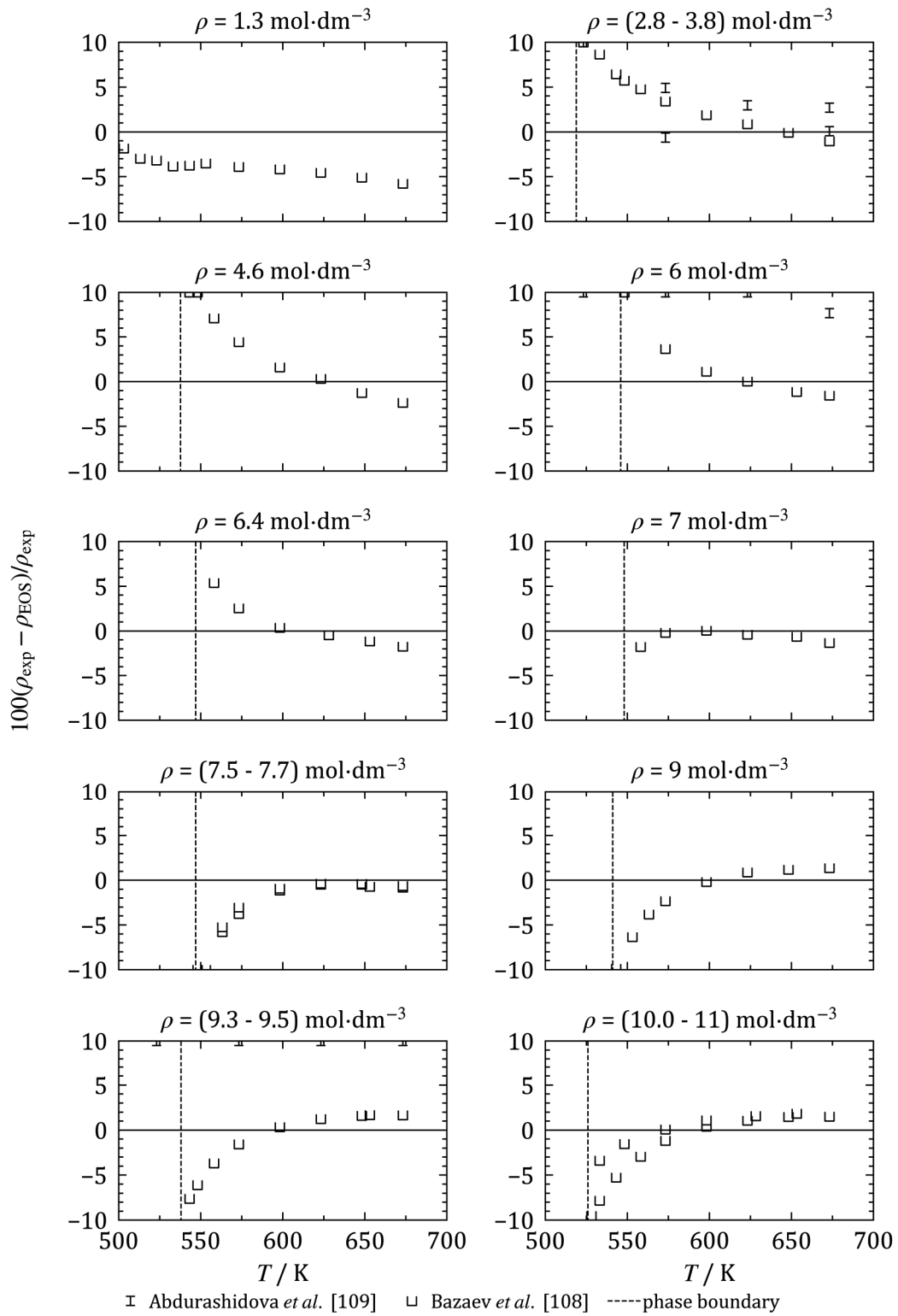


Figure C 3: Relative deviations of the high temperature experimental densities along isochores over pressure from the new mixture model with $x_{\text{Ethanol}} = 0.8$.

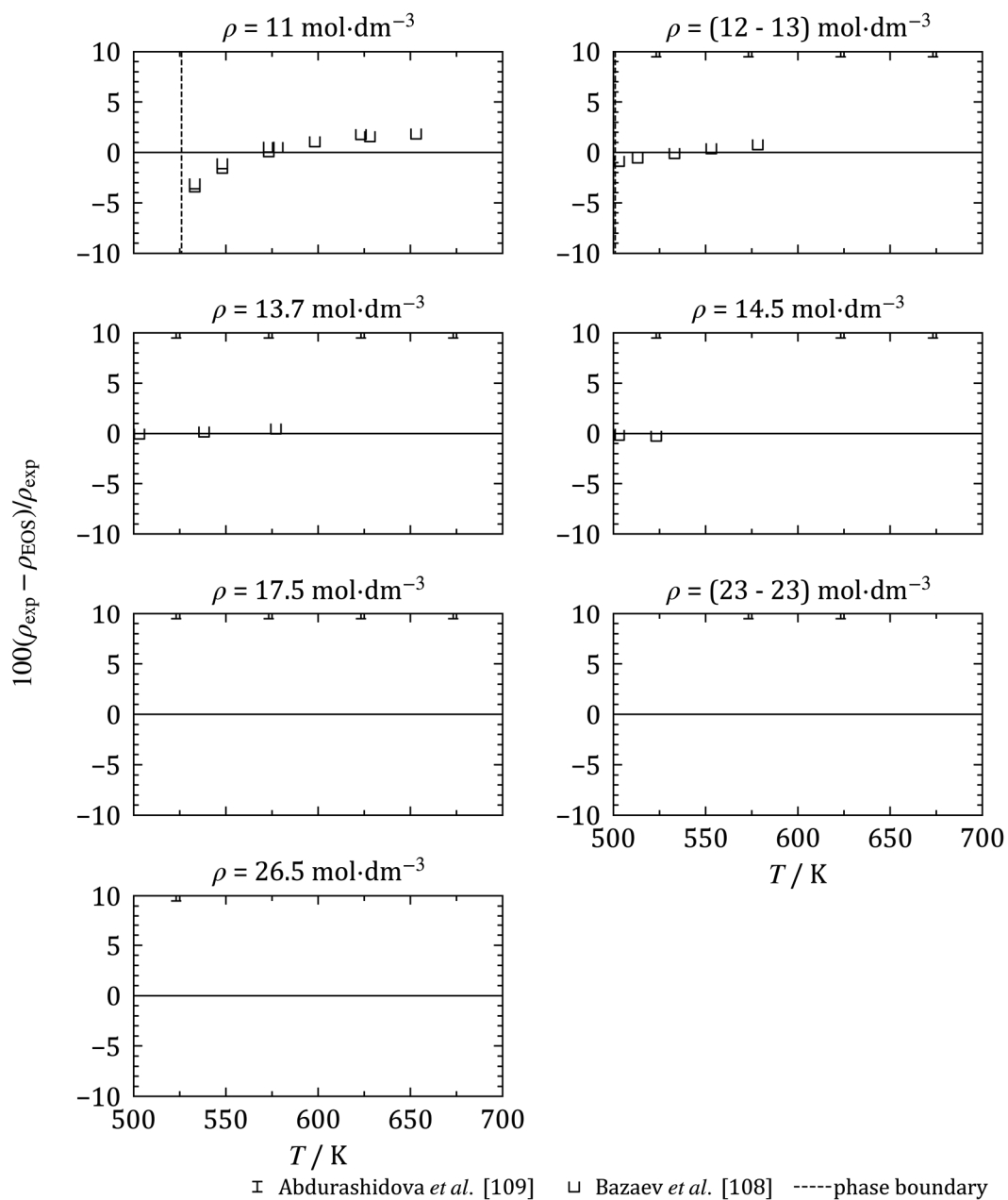


Figure C 3 continued.

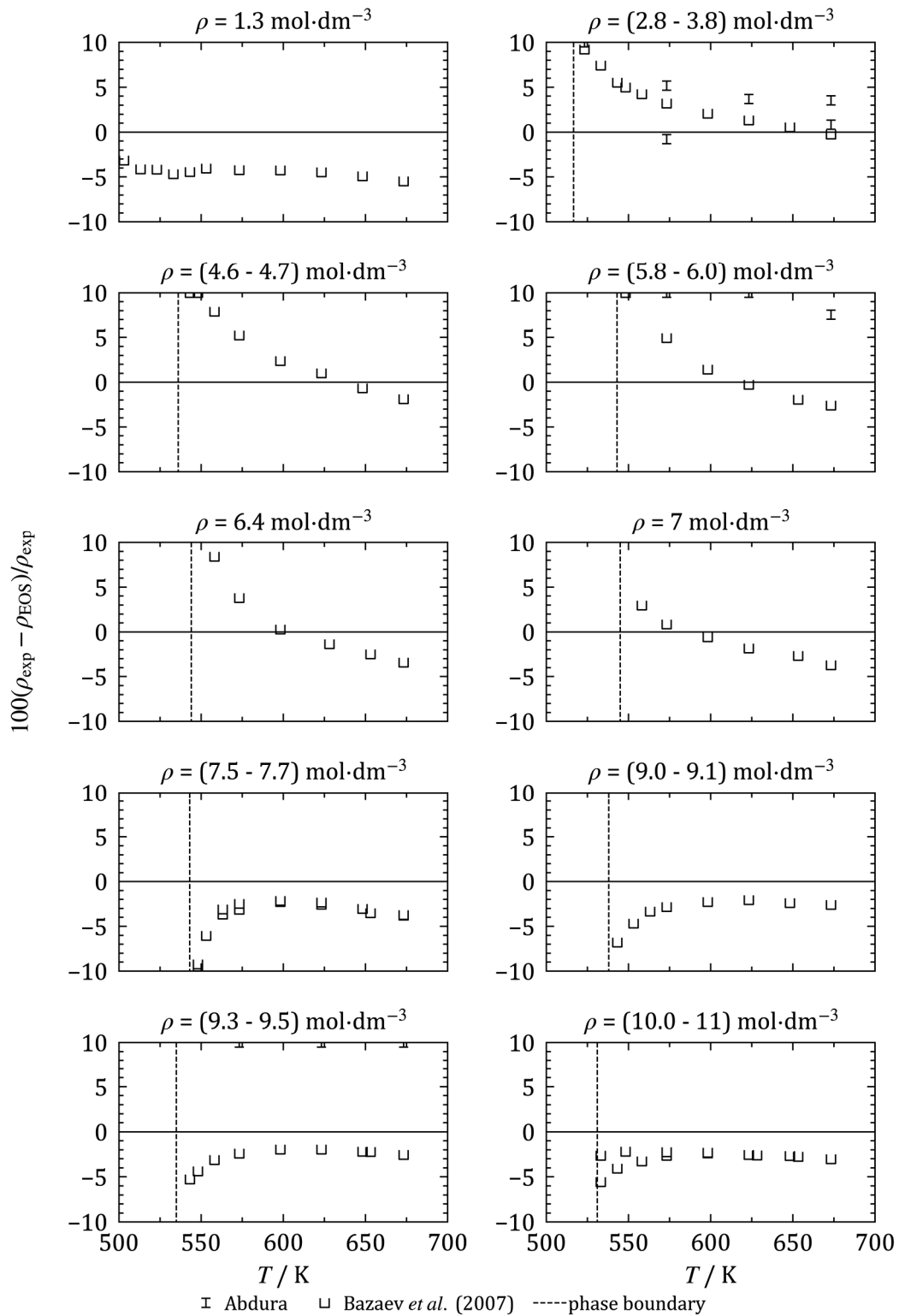


Figure C 4: Relative deviations of the high temperature experimental densities along isochores over pressure from the mixture model of Lemmon [4] with $x_{\text{Ethanol}} = 0.8$.

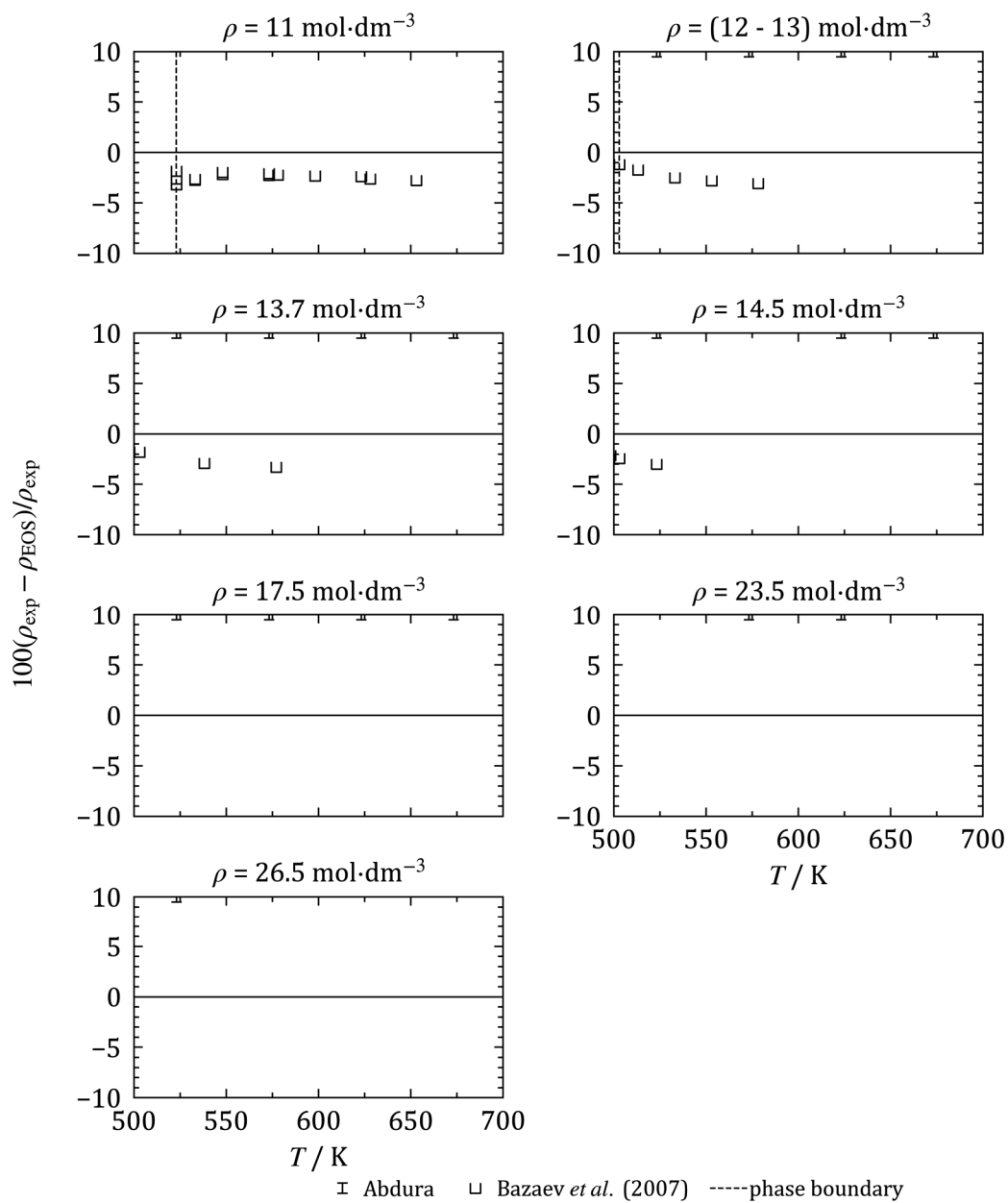


Figure C 4 continued.

Lebenslauf

Theresa Eckermann, geb. Wiens
Geboren am 29.08.1985 in Witten
Verheiratet, 2 Kinder

Berufliche Tätigkeit

05/2011 – 08/2018 Ruhr-Universität Bochum
Wissenschaftliche Mitarbeiterin am Lehrstuhl für
Thermodynamik
Prof. Dr.-Ing. Roland Span

Nebentätigkeiten und Praktika

11/2008 – 04/2011 Ruhr-Universität Bochum, Lehrstuhl für Thermodynamik
Studentische Hilfskraft
04/2009 – 03/2011 E.ON New Build and Technology, Gelsenkirchen
Studentische Hilfskraft
04/2007 – 03/2009 SimPlan Integrations GmbH, Witten
Studentische Hilfskraft
02/2007 – 04/2007 Degussa GmbH, Herne
Grundpraktikum
09/2006 – 03/2007 Nolte Consult GmbH, Witten
Studentische Hilfskraft
05/2006 – 06/2006 MEVA Umwelttechnologie GmbH, Dortmund
Grundpraktikum
12/2005 – 04/2006 Sanitop-Wingenroth, Remscheid
Studentische Hilfskraft

Ausbildung

10/2006 – 03/2012 Ruhr-Universität Bochum
Umwelttechnik und Ressourcenmanagement
Studienschwerpunkt: Nachhaltige Prozess- und Umwelt-
technik
Abschluss: Diplom-Ingenieur
08/1996 – 06/2005 Albert-Martmöller-Gymnasium, Witten
Abschluss: Abitur